Role of acetylation in TDP-43 pathophysiology

Dissertation

zur Erlangung des Grades eines

Doktors der Naturwissenschaften

der Mathematisch-Naturwissenschaftlichen Fakultät

und

der Medizinischen Fakultät

der Eberhard-Karls-Universität Tübingen

vorgelegt

von

Jorge Garcia Morato

aus Madrid, Spanien

2022

Tag der mündlichen Prüfung: 20.04.2022

Dekan der Math.-Nat. Fakultät: Prof. Dr. Thilo Stehle

Dekan der Medizinischen Fakultät: Prof. Dr. Bernd Pichler

1. Berichterstatter: Prof. Dr. Philipp J. Kahle

2. Berichterstatter: Prof. Dr. Dirk Schwarzer

Prüfungskommission: Prof. Dr. Philipp J. Kahle

Prof. Dr. Dirk Schwarzer

Prof. Dr. Manuela Neumann

Prof. Dr. Ralf-Peter Jansen

Erklärung / Declaration:

Ich erkläre, dass ich die zur Promotion eingereichte Arbeit mit dem Titel:

„Role of acetylation in TDP-43 pathophysiology “

selbständig verfasst, nur die angegebenen Quellen und Hilfsmittel benutzt und wörtlich oder inhaltlich übernommene Stellen als solche gekennzeichnet habe. Ich versichere an Eides statt, dass diese Angaben wahr sind und dass ich nichts verschwiegen habe. Mir ist bekannt, dass die falsche Abgabe einer Versicherung an Eides statt mit Freiheitsstrafe bis zu drei Jahren oder mit Geldstrafe bestraft wird.

*I hereby declare that I have produced the work entitled “*Role of acetylation in TDP-43 pathophysiology*”, submitted for the award of a doctorate, on my own (without external help), have used only the sources and aids indicated and have marked passages included from other works, whether verbatim or in content, as such. I swear upon oath that these statements are true and that I have not concealed anything. I am aware that making a false declaration under oath is punishable by a term of imprisonment of up to three years or by a fine.*

Tübingen, den 5. November .....

Unterschrift /Signature

„ Man's mind cannot grasp the causes of events in their completeness, but the desire to find those causes is implanted in man's soul.”

Leo Tolstoy, War and Peace

Contents

1.- Summary

The TAR DNA binding protein 43kDa (TDP-43) is a predominantly nuclear protein that is involved mainly in mRNA splicing, processing and transport. TDP-43 is also the main component of the insoluble inclusions found in neurons in both in amyotrophic lateral sclerosis (ALS) and a subset of fronto-temporal lobar degeneration cases (FTLD-TDP). Within these inclusions, TDP-43 is hyperphosphorylated, ubiquitinated, acetylated and fragmented. The regulation of these modifications and their impact in the physiology and aggregation process of TDP-43 is not fully understood yet.

The objective of the following study was to identify new acetylation sites in TDP-43 and characterize their impact in TDP-43's pathophysiology. In order to do this, wild type TDP-43 was expressed in HEK293E cells, purified and analysed via mass spectrometry. Four novel acetylation targets were identified, two of which were around the nuclear localisation signal while the other two were at the RNA recognition domain. The impact of these acetylation sites was assessed by generating lysine-to-arginine and lysine-to-glutamine substitutions, which showed the impact of acetylation-mimic mutations at lysines 84 and 136 in nuclear-cytoplasmic trafficking and RNA-binding of TDP-43, respectively.

The effect of K136Q substitution in RNA binding was examined via RNA-protein pulldown, RNA-binding filter assays and by looking at its effect on CFTR splicing. K136Q causes a reduction in RNA-binding and a subsequent loss in RNA-splicing capabilities. In addition, K136Q TDP-43 is found in nuclear phase-separated bodies, with reduced recovery rate after photobleaching. K136Q TDP-43 eventually loses solubility and coalescences into solid, phosphorylated aggregates, similar to those found in ALS and FTLD patients.

To validate all these results, an amber suppressed TDP-43 model which introduces acetylated lysine at either K84 or K136, was devised. Acetylated TDP-43 behaved in a similar manner to the K-to-Q mutants characterised, validating the previous results. To further characterise TDP-43 acetylation, antibodies against acetylated K84 TDP-43 and K136 TDP-43 were developed and tested against full length, amber suppressed TDP-43. With this new tool, Sirt1 was identified as the responsible enzyme deacetylating K136, disengaging the phase-separated TDP-43 and preventing its further aggregation.

The identification of acetylation as a modulator of TDP-43 cytoplasmic mislocalisation and RNA-binding offers a powerful tool to modulate TDP-43 activity. Furthermore, this study describes

how acetylation at K136 can trigger TDP-43 phase separation and eventual pathological aggregation, identifying the responsible enzymes that can mitigate this process. Future research into this specific mechanism could be pivotal for ALS and FTLD early diagnosis and treatment.

2.- Introduction

In 1824 Charles Bell, a Scottish neurosurgeon and anatomist, described for the first time the symptoms of amyotrophic lateral sclerosis (ALS) (1,2). At a time where neuroanatomy was still in its infancy it took several years and contributions (from Duchenne and Cruveilhier, among others) until in 1874 Jean Martin Charcot linked the muscle wasting to the atrophy in the anterior horn cells of the spinal cord, the motor neurons (1). He developed his work at the Hospital of Salpêtrière which at the time was one of the largest hospitals in the world. The diagnosis of the disease is only starting to be improved in the last years (3).

20 years after Charcot's description of ALS, a Czech neurologist, described for the first time what would be later called frontotemporal lobar degeneration (FTLD) (4). He noted a progressive degeneration of language in one of his patients at the Charles University of Prague, where he taught psychiatry. The post-mortem study showed temporal lobe atrophy, and subsequent histological examination of the same cases by Alois Alzheimer revealed cytoplasmic inclusions in neurons (5). Unlike ALS, FTLD research went through a series of paradigm shifts in the past century (6,7) and recent advances in genetics, molecular biology and neuroimaging are helping dissect the disease.

However, these two diseases are not separate entities, we see them now as the two extremes of a spectrum disorder. While in the past 130 years much research has been done, we still lack a deep understanding of the disease and therefore, a reliable treatment or diagnosis. Thus, further research needs to be done.

2. 1.- Amyotrophic lateral sclerosis

2. 1. 1.- Clinical manifestation and epidemiology

ALS is a heterogeneous fatal disorder that comprises most of the motor neuron disease (MND) cases. The disease (ALS) causes the loss of upper and lower motor neurons, which leads to somatic muscle spasticity, weakness and eventually muscle atrophy (Fig. 2. 1A) (8,9). As the disease progresses respiratory muscles weaken, making respiratory failure the eventual cause of death in most patients (10). The mean survival time is 3 years after diagnosis, unfortunately not very different from the survival time in the times of Charcot. Depending on the area first

affected, the initial symptoms can vary, and cases are usually divided into spinal-onset and bulbar-onset (11). Spinal-onset accounts for around 60% of the cases and is characterised by limb weakness, while bulbar-onset patients present dysarthria (speech difficulty) that eventually evolves into dysphagia (difficulty swallowing). Bulbar-onset accounts for 30% of the ALS cases (12). A small percentage (5%) of patients at the beginning of the disease have difficulty breathing, and in these cases, patients are usually sent first to respiratory and cardiovascular specialists before being examined by a neurologist (Fig. 2.1B). In addition to the motor and respiratory symptoms 50% of the patients develop some cognitive impairment during the progression of the disease, and 13% of the total numbers of patients can be classified as ALS-FTD (11,13).

In Europe the incidence of ALS is 2-3 cases per 100.000 people per year, that is the number of new cases reported every year, with a slightly higher proportion of males than females affected, 1.2-1.5 men for every woman (12). These data combined result in a lifetime risk of contracting ALS of 1:350 and 1:400 for men and women, respectively. Unfortunately, not enough studies have been done in populations of non-European ascendancy to make a robust comparison, except for Guam and areas of Japan where high frequency of ALS has been reported (14). Due to the lack of evidence supporting the role of environmental factors, bottlenecks in the genetic background seem to be more relevant for these specific cases (15).

2. 1. 2.- Neuropathology

The genesis of the pathophysiology, the question this thesis is trying to answer, is not fully understood yet. The most definitive characteristic is the degeneration of upper and/or lower motor neurons, which causes a reduction in size of the anterior horn of the spinal cord (9,16). Upper motor neuron degeneration can be best observed at the pyramidal tract where Betz cells are lost and there is a loss of myelin staining (17). As with other neurodegenerative disorders, astrocytic gliosis can be observed in the affected areas (18). Patients with cognitive decline also present degeneration at the frontotemporal lobes.

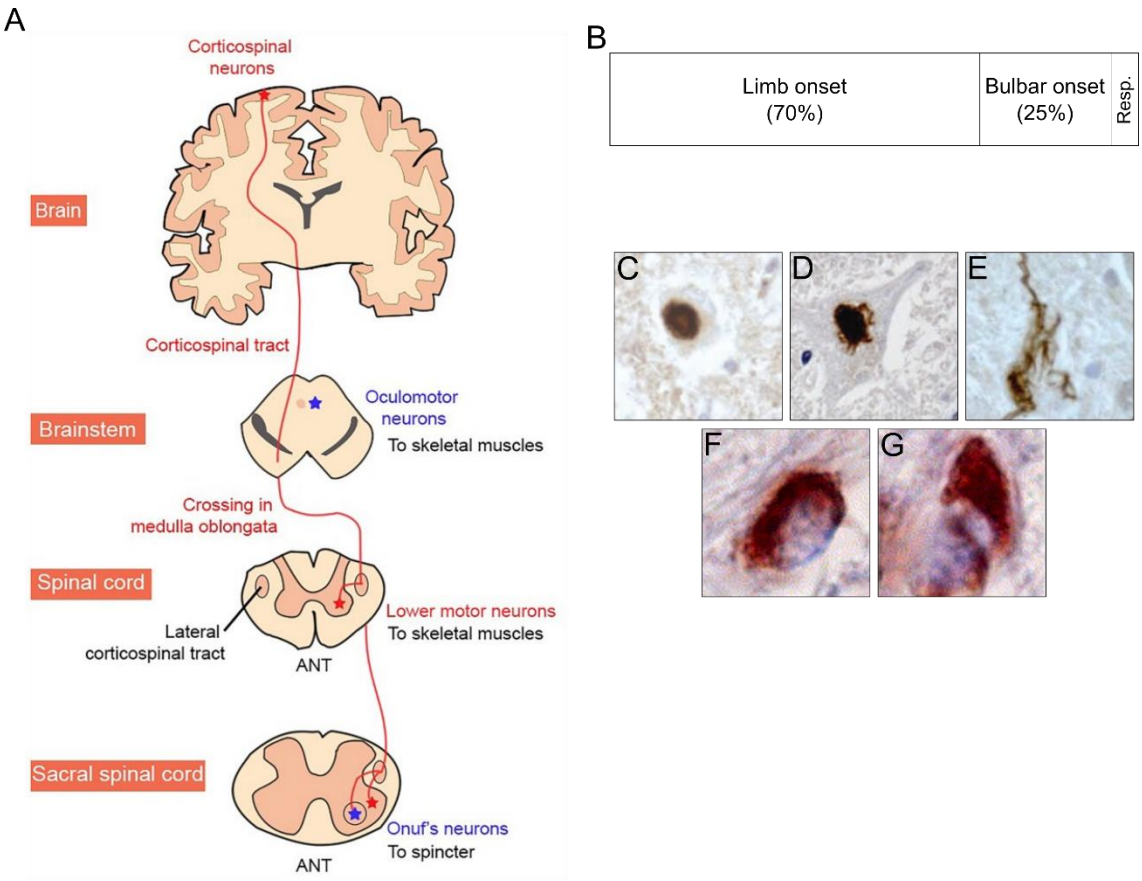

Figure 2. 1.- Cortico-spinal tract and ALS neuropathology. A) Schematic of spinocortical tract portraying both upper (labelled corticospinal neurons) and lower motor neurons. In blue are the tracts spared in ALS. From Ragagnin et al. 2019. B) Classification of ALS pathology based on the onset: Respiratory (5%), bulbar, or limb onset. C-E) Different TDP-43 aggregates in motor neurons of ALS patients. Adapted from Neumann et al. 2006. F-G) TDP-43 glial inclusions from spinal cord in ALS. Adapted from Arai et al. 2006.

At a cellular level there are two types of intracellular inclusions characteristic of ALS, Bunina inclusions and ubiquitin-positive inclusions. Bunina bodies are small inclusions (1-5µm) found in the cytoplasm of motor neurons that are positive for cystatin C and transferrin (19). Their involvement in the disease and their cause are still unclear. Ubiquitin-positive inclusions can be cytoplasmic and intranuclear and they are present mostly in motor neurons but also in glial cells (Fig. 2. 1C-G) (20,21). In addition, they can also be found in the brainstem, striatum and thalamus. Their presence in these areas, however, does not correlate with neurodegeneration, as it does in motor neurons (22). In patients with cognitive decline aggregates can also be observed in the orbitofrontal and frontotemporal cortices. The main components of the ubiquitin-positive inclusions are ubiquitin and TDP-43 in 97% of the patients (23,24). The remaining 3% are patients carrying mutations in the *SOD1* or in the *FUS* genes and have ubiquitin-positive aggregates with the respective mutated protein (25).

2. 2.- Frontotemporal dementia

2 .2 .1.- Clinical manifestation and epidemiology

Frontotemporal dementia (FTD) is the second most common form of early onset dementia after Alzheimer's disease. FTD is the clinical syndrome of FTLD. It has an incidence of up to 2.7-4.1 cases per 100000 people per year with strong regional variations, without any clear gender bias. The survival after diagnosis is between 6 and 11 years (26).

At its core, it is characterized by degeneration at the frontotemporal lobes, which are involved in a variety of higher cognitive tasks (Figure 2.2A). The most prominent of them are decision making, social cognition, reward processing and, at their temporal end, movement. FTD is a heterogeneous disease comprising a set of syndromes, which are classified in three categories: behavioural variant (bvFTD), nonfluent progressive aphasia (nfvPPA) and the semantic variant progressive aphasia (svPPA) (4). In addition, up to 10-15% of FTD patients develop MND (9).

To understand the complexity and variability of symptoms, it is crucial to examine in detail the frontotemporal cortex architecture. The frontotemporal cortex receives information from the neocortex and subcortical areas. While the dorsolateral area of the frontotemporal cortex is involved in executive functions (planning, working memory), the ventrolateral area is more related to language processing and behaviour (27). Taking all its functions together, progressive degeneration, localised or at a more general level, can trigger a wide variety of clinical manifestations.

While bvFTD patients suffer from loss of empathy and apathy (28) and nfvPPA patients have difficulty in language comprehension and speech initiation (29), both types of FTD share a motor phenotype that can evolve to ALS. On the other hand, svPPA patients usually do not develop motor symptoms until later in the disease, if at all (30). Currently, as with ALS, there is no pharmaceutical approach to treat the disease. Serotonin reuptake inhibitors are used to treat behavioural symptoms with moderate success (31), as well as antipsychotics (32). Given the lack of clear pharmaceutical treatments, a strong emphasis is put in care and non-pharmaceutical interventions, such as speech therapy for the semantic variants (33).

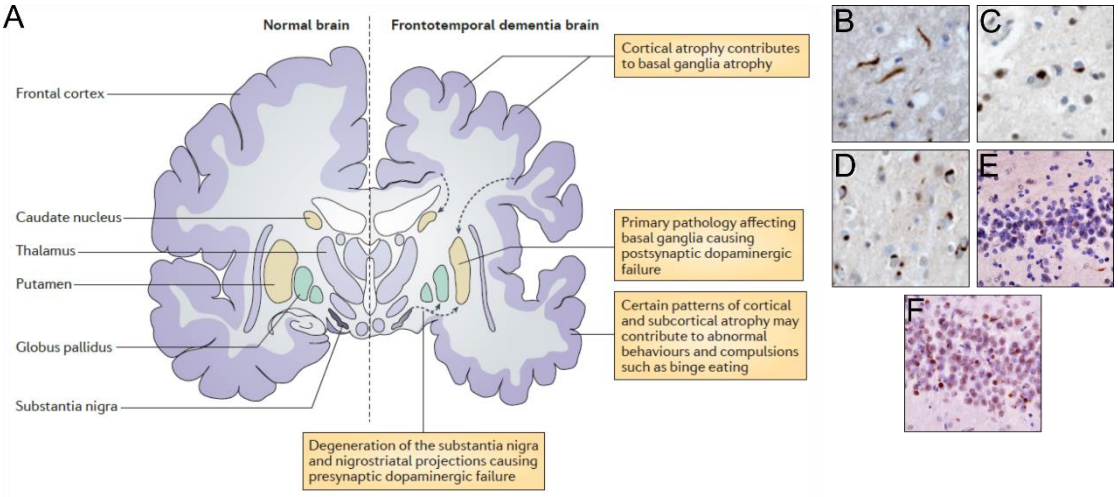

Figure 2. 2.- Frontotemporal dementia neuropathology. A) Comparison of healthy vs FTD brain, with areas prone to neurodegeneration labelled. From Baizabal-Carvallo and Jankovic, 2016. B-D) TDP-43 inclusions in FTLD cortex from patients with type A (B), type B (C) or type C (D). Adapted from Neumann et al. 2006. E-F) TDP-43 cytoplasmic aggregates in FTLD dentate gyrus. Adapted from Arai et al. 2006

2. 2. 2.- Neuropathology

Analogous to the extension of the symptoms, the neuropathology of FTD can greatly vary. In general terms FTD is diagnosed by the selective degeneration and gliosis in the frontotemporal cortical area of the brain (34). However, the stratification of cases is done by the different protein inclusions that patients present in neurons. Depending on histological staining, cases are classified as FTLD-tau, FTLD-TDP, FTLD-FET and FTLD-UPS (34,35).

The most common types are FTD-tau and FTD-TDP (Fig 2.2 B-F), each accounting for 45% of the FTD cases. FTD-tau patients present inclusions of Tau protein, a microtubule assembly protein (36). It has two splice variants depending on the inclusion of exon 10, giving rise to 3R and 4R tau. Both forms can form aggregates and this further splits FTD-tau into 3R and 4R (37). FTD-TDP-43 is characterised by the presence of ubiquitinated and phosphorylated TDP-43 aggregates. It can be further classified in four subtypes, A, B, C and D (38). Type A presents cytoplasmic round or crescent and less frequently intranuclear TDP-43 aggregates. Type B has granular cytoplasmic aggregates, and it is linked to FTD-MND. Type C cases present cytoplasmic inclusions to a lesser extent than the previous subtypes and, in addition, dystrophic neurites. 90% of svPPA patients develop FTD-TDP-43 type C (Fig. 2.2 B-D). Type D is characterised by lentiform intranuclear TDP-43 aggregates and few cytoplasmic inclusions (38–40).

FTD-FET represents around 9% of the cases, while FTD-UPS is the rarest variant, accounting for less than 1% of FTD patients. FET protein family is composed of FUS (fused in sarcoma), EWS

(Ewing's sarcoma) and TAF15 (TATA-binding protein-associated factor) (41). They are ubiquitously expressed in the body, and, in general terms, their primary function is DNA/RNA binding metabolism and RNA transport and processing (42). They are mostly nuclear but form ubiquitin-positive cytoplasmic inclusions in patient neurons. The rarest FTLD-UPS is characterised by inclusions containing ubiquitin and p62 (43). It is unclear if these aggregates are composed only by ubiquitin and p62 or if there is a core protein not yet identified.

2. 3.- Genetics of ALS and FTD

ALS cases are classified in familial (fALS) and sporadic cases (sALS), symptomatically indistinguishable from one another (44). Familial ALS accounts for 5-10% of the total cases and this distinction is based on the presence of reported ALS cases in the family. In fALS, 50-70% of the cases can be traced to mutations in either *C9orf72*, *TARDBP* (encoding for TDP-43), *FUS/TLS* or *SOD1 (45)*. The remaining ~90% of the total cases are classified as sporadic, where no family history of the disease can be found. In most of these cases, there is not a clear genetic cause, although 6-7% of sALS cases carry mutations in *C9orf72* and around ~5% of patients carry mutations in *SOD1 (46)*. It is worth noting that the proportions aforementioned are representative for the western population; for instance, in Asian populations *SOD1* accounts for 30% of fALS cases, in contrast with 14.8% of western fALS (47).

On the other hand, FTD has a stronger genetic component than ALS, with up to 30% of the cases presenting previous cases in their ascendency (familial FTD, fFTD) (48). Mutations in three genes account together for 30% of the cases: *C9orf72*, *GRN* and *FUS*. Each of the genes can be linked to ~10% of the total FTD cases, respectively (45,49–52). These percentages can vary depending on the geographical area, for example in Northern Italy and in the Basque country *GRN* mutations are overrepresented, while American fFTD cohorts can be linked monstly to C9orf72 mutations (53).

The overlap in the clinical manifestation of FTD and ALS mentioned before can also be seen in the genetics of both diseases (44). In a similar manner, the neuropathology, previously described, is remarkably similar in both disorders, with TDP-43 as the main component of ALS and half of the FTD aggregates (23,24,54). This reinforces the idea that we are looking not at two separate maladies, but at a continuum of disorders. The relevant genes identified do not belong to a single pathway or function, although RNA-processing and RNA-mediated toxicity seem to

have a critical role in both diseases (55). The roles and functions of the most represented genes are discussed now.

2. 3. 1.- *C9ORF72*

The *C9orf72* locus was first associated with ALS-FTD causing gene in a GWAS study in the Finish population (49,56). The hexanucleotide expansion GGGGCC in the first intron of C*9orf72* was found to be the most common cause of ALS (57). After the initial identification, the expansion has been found in 50% of fALS, 80% of fALS-FTD and 10-30% of FTD patients, bridging FTD and ALS (58). Although a high number of GGGGCC copies are positively linked with ALS/FTD, there is no clear cut off in the number of copies linked to the development of ALS or FTD. 95% of neurologically healthy controls have less than 11 copies of the repeat and, in most studies, the chosen cut-off is 30 copies, although hundreds or even thousands of copies can be found in patients (59). An additional difficulty is the fact that the number of copies found in the brain do not match the copies found in blood, possibly due to somatic instability in the neurons, hinting at somatic mosaicism as a relevant dynamic in ALS and FTD (60).

All *C9orf72* patients present TDP-43 inclusions and, in addition, RNA foci, and dipeptide repeat proteins (DPRs) inclusions (61,62). These last two are unique features of *C9orf72* repeat carriers. RNA foci contain sense and antisense transcripts of the *C9orf72* repeat transcript, arranged in RNA G-quadruplex structures, a stable RNA-configuration (63). They are nuclear and can be found in motor and frontal cortex, as well as in spinal cord of patients (64). These transcripts can be translated via repeat-associated non-ATG translation (RAN), which give rise to different DPR depending on the frame and sense (65).

The pathogenesis of *C9orf72* cases seems to involve gain and loss of function mechanisms, which current hypotheses divide in three parts. The first proposed mechanism is a loss of function, supported by the reduced levels of *C9orf72* transcripts in lymphocytes, cortex and spinal cord of C*9orf72* repeat carriers (57,66). The function of *C9orf72* in healthy tissue is still being delineated, but the protein has been found to interact with Rab proteins and to localise in the presynaptic area, suggesting a role in synaptic vesicle trafficking (67–69). Most interesting are the effects of *C9orf72* knock down: disrupted autophagy and axonal trafficking (70,71). Given the prominent role of autophagy in other neurodegenerative disorders, this is an interesting model for *C9orf72* loss of function. The second hypothesis for pathogenesis is a toxic gain of function of the RNA foci. The secondary structures formed by RNA repeats (G-quadruplex) have been found to

sequester RNA-binding proteins (RBPs) *in vivo*, depleting them from their respective targets and functions (72,73). The third and last mechanism is a toxic gain of function of the different DPRs. This third mechanism seems to be more controversial, since DPR pathology does not colocalize with areas of neurodegeneration in the brain (65). However, DPRs seem to disrupt the ubiquitin proteasome system and stress granule formation and cause nucleolar stress.

These three mechanisms are by no means exclusive, and it is most probable that a mix of gain and loss of function is responsible for the neuronal stress and degeneration observed in patients.

2. 3. 2.- *SOD1*

Mutations in *SOD1*, the gene encoding for superoxide dismutase 1 (SOD1) were linked to ALS patients, marking it as the first gene to be directly linked with ALS (74). SOD1 is a metalloprotein widely expressed in the body which catalyses the conversion of free radicals to prevent ROS damage (75). More than 180 mutations in SOD1 have been reported and, due to its function and the presence of misfolded proteins in ALS, a toxic loss of function has been proposed (76). It is worth noting that ubiquitinated inclusions in SOD1 patients are not TDP-43 positive, which sets these ALS cases apart (77).

2. 3. 3.- *GRN*

GRN encodes for progranulin in both neurons and microglia. Progranulin is cleaved and secreted to the intercellular space where it is further cleaved into active granulin. It plays a role in inflammation, development and tissue repair (78,79). 70 mutations in *GRN* have been reported and in all cases patients present TDP-43 positive inclusions in cortex. Most of the mutations are causing a loss of function due to reduced levels of progranulin (premature ending and mRNA decay, unstable protein) or result in a non-functional protein (80,81). The interplay between granulin and TDP-43 is unclear but recent studies suggest that progranulin expression reduces insolubility of mutant TDP-43 in one ALS mouse model, while a progranulin-deficient mouse model develop TDP-43 aggregates (82,83). Further confirmation in the specific context of FTD is needed.

2. 3. 4.- *MAPT*

Up to 45% of FTD patients present ubiquitin-positive, TDP-43-negative inclusions which have tau, the product of *MAPT*, as the main component (84). Tau, or microtubule associated protein tau, is involved in microtubule stabilisation and it is expressed at high levels in neurons (85,86). In FTD patients it forms filamentous aggregates in the cytoplasm of neurons and glia cells. Tau aggregates are not only confined to FTD, but they can also appear in Alzheimer's patients. Over 50 mutations have been linked to tau malfunction and tauopathies and, in addition, posttranslational modifications (PTMs) such as acetylation and phosphorylation also seem to play a role in disease (87–91). Aggregated tau is hyperphosphorylated when compared to diffuse tau, drawing a link with pathology. Acetylation seems to play a more ambivalent role depending on the residue, promoting or inhibiting degradation, probably in an interplay with ubiquitination. The effect of tau aggregation in cells is not clear, but research suggests loss of function due to caspase cleavage is more relevant for tau pathology (92).

2. 3. 5.- *FUS*

FUS present mutations in 5% of fALS and 1% of FTD cases (93). In those ALS patients carrying *FUS* mutations, FUS aggregate in the cytoplasm of cells, while FTD-FET cases (see Frontotemporal dementia - Neuropathology) do not always carry mutations. FUS and TDP-43 both have RNA processing functions, which puts RNA dysregulation at the centre of the ALS-FTD spectrum (94). Just like TDP-43, FUS has a non-structured glycine-rich domain, a C-terminal PY-nuclear localisation signal (NLS) and an RNA recognition motif (RRM) and, in addition, it has a Zinc finger domain and arginine-glycine and glutamine-glycine-serine-tyrosine (QGSY) prion-like domain (95). These features allow the mostly nuclear FUS to form RNA/DNA-protein and protein-protein interactions. Importantly, most of the identified mutations cluster at the NLS, promoting FUS mislocalisation to the cytoplasm. Since FUS autoregulates itself via nonsense mediated decay of its own RNA, mislocalisation of FUS impacts the total levels of FUS in the cell (96). FUS is also involved in transcription initiation, RNA polymerase II regulation, DNA damage response and RNA processing (transport, splicing, miRNA processing). FUS interacts with a vast number of RNA targets in the nucleus, but it is also involved in transport and local translation of targets in neurons (94). In response to DNA damage, it interacts with PAR and HDAC1 directly to repair double strand breaks and in addition binds to CBP and p300, repressing their activity (97,98). The involvement of FUS ith p300/CBP goes both ways, since FUS K315/316 acetylation is regulated by p300/CBP (99). In ALS and FTD patients, the cytoplasmic mislocalisation and

aggregation interferes directly with its nuclear functions, suggesting a toxic loss of function as a pathological mechanism (100–102). In addition, aggregates act as a protein sink, sequestering other FET proteins (TAF15 and EWS) (41). Another hypothesis for the FUS pathology puts the aggregation at the end of the process, an epiphenomenon of unknown trigger.

2. 3. 6.- *TARDBP*

Mutations in *TARDBP,* the gene encoding for TDP-43, are only present in 9% of fALS cases and in very rare instances in FTLD patients. Despite this, 97% of all ALS and 45% of FTD patients present intracellular TDP-43 inclusions in cortex and/or motor neurons, both upper and lower ones. Most of the mutations cluster in the C-terminal region of the protein, involved in protein-protein interaction (103). The widespread presence of TDP-43 aggregates along the ALS-FTD spectrum puts TDP-43 at the centre of the pathogenesis.

2. 4.- TDP-43 physiology and pathophysiology

After describing the neuropathology of both ALS and FTD, TDP-43 appears as a central piece in the pathogenesis of both diseases. The encoding human gene, *TARDBP*, is located on locus 1p36.22 and contains 6 exons and 5 introns, resulting in a 414aa protein with a predicted size of 45kDa. It is ubiquitously expressed in the body, mostly in the nucleus of cells. A member of the heterogeneous nuclear ribonucleoprotein family (hnRNP), it is mostly associated with RNA metabolism. It is evolutionarily highly conserved, from *C. elegans* to humans only with some minor changes in its structure.

2. 4. 1.- Protein structure

TDP-43 is composed of two RRMs and a NLS in the N-terminal half, and an unstructured, glycine-rich domain at the C-terminal part (Fig. 2. 3). The domain composition is remarkably close to the domain composition of FUS, but also to other hnRNP proteins.

The nuclear shuttling is mediated via the bipartite NLS, located between residues 82 and 98 (104). As mentioned before, TDP-43 is mostly nuclear with a small fraction of it cytoplasmic. The import of TDP-43 into the nucleus is mediated by a karyopherin-dependent mechanism (105). Previously a predicted nuclear export signal (NES) was considered but recent studies suggest

that the nuclear-cytoplasmic distribution of TDP-43 is balanced via active nuclear import and passive, XPO-1 independent, size-dependent nuclear export (106,107). The apparent loss of toxicity in NES deleted TDP-43 is now considered to be caused by a loss of splicing activity. Recently, 6 mitochondrial localisation signals have been predicted and from those 3 have been validated in TDP-43 (108). Structurally, those 3 are the most accessible ones.

The binding to RNA is mediated via the two RNA binding motifs. RRMs are among the most abundant domains and, canonically, they are composed of four β-sheets and two α-helixes. This is the case for RRM1 of TDP-43, however RRM2 has an additional β-sheet that seems to add

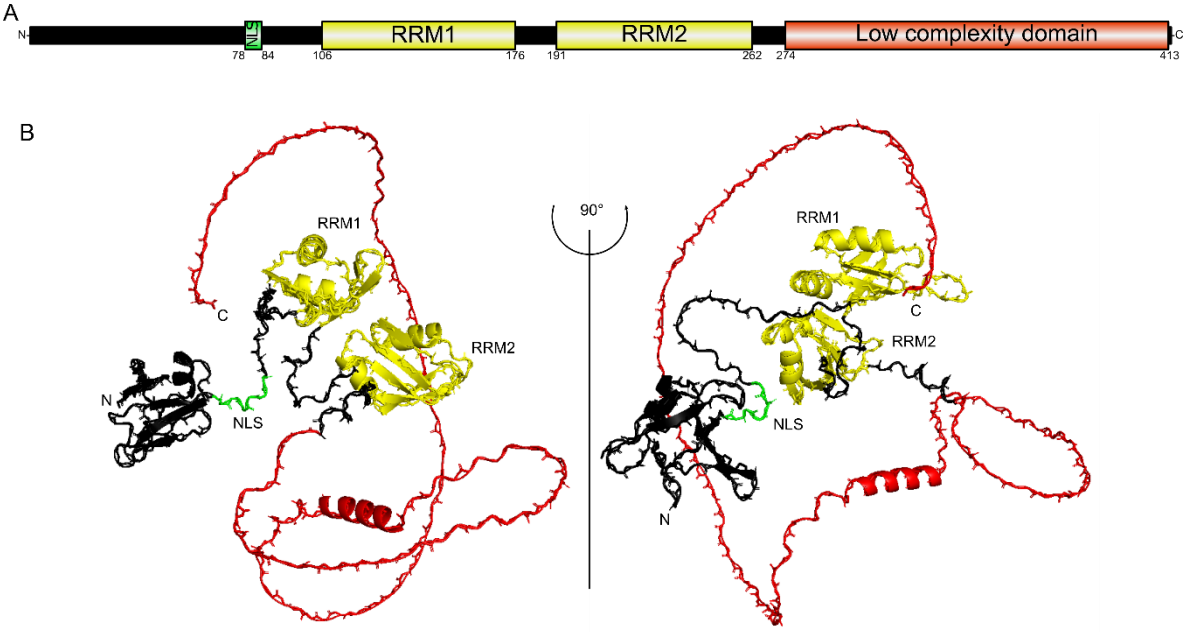

Figure 2. 3.- TDP-43 domain structure. A) Schematic graph of TDP-43 domains: NLS (Nuclear Localisation Signal), RRM1 and 2 (RNA Recognition Motif 1 and 2) and low complexity domain. **B)** TDP-43 Structural prediction (From AlphaFold) with labelled domains. The model confidence of the C-terminal domain (red) is very low, while RRMs and N-terminal domain have a high confidence.

protein-protein binding capabilities to the domain (109). The characterisation of TDP-43 targets *in vivo* has shown that it binds specifically to UG repeats, between 30 and 100 nucleotides. More in detail studies have shown that both RRMs can independently bind to UG and TG rich regions. This specificity is given by an intricate network of hydrogen bonds, creating RNA binding pockets. Even though both domains can bind to RNA or DNA, it is the interaction of both of them which increases both the specificity and the strength of the RNA-protein binding (110). For sequences longer than 100 bases, TDP-43 homo oligomerizes, creating a continuous surface of RNA-binding (111). In addition, a RGG motif in the C-terminal part of the protein seems to be capable of binding to RNA as well, although it is unclear the relevance of this finding. Lastly, there is a weak nucleotide binding site at the N-terminal domain (aa81-102) (112). Other studies have failed in

showing nucleotide binding capabilities of N-terminal fragments, but the presence of these seems to enhance the specificity of TDP-43 to its RNA targets (113).

In the context of protein-protein interactions, several domains have been identified as crucial for self-interaction as well as binding to other proteins. The N-terminal domain has been found to form homodimers and oligomers (114,115). More interestingly, the N-terminal part of TDP-43 forms a DIX-like domain with 6 β-strands and one α-helix like the one found in disheveled, axin and ubiquitin (112). Thanks to it, N-terminal fragments of TDP-43 can form oligomers assemble in a head-to-tail fashion, giving rise to helical structures *in vitro*. In these oligomers, the interface between the components is composed of polar and charged amino acids (114). One specific serine in this part of the protein has been found to be phosphorylated in several cell lines: serine 48 (116). While this residue is hidden in the oligomers, phosphomimic substitution impairs TDP-43 oligomerisation (117). However, the *in vivo* conditions where this phosphorylation might take place have not been described yet.

While the structure of the C-terminal domain is not as well defined as the N-terminal one, its relevance for protein-protein interaction and aggregation is well established. It has been found to be crucial for TDP-43 interaction with several partners, such as UBQLN (118), FMRP (119) and hnRNP (120). It contains two Glycine-Aromatic-Serine-Rich domains (GaRoS) at positions 273-317 and 368-414, and one amyloidogenic core (112). The GaRoS have been suggested to play a role in RNA granule formation and phase separation (112,121). Finally, an Ω-loop helix has been identified at aa320-343 that can form Low Aromatic-Rich Structures (LARKS) that create reversible velcro-like structures which may play a role in protein-protein interaction and aggregation (122).

2. 4. 2.- Subcellular localisation determinants

In physiological conditions, TDP-43 is located mostly in the nucleus and only partially in the cytoplasm of cells. The cytoplasmic fraction has been found to colocalize with stress granules (SGs), dendrites and, recently, mitochondria and myo-granules as well. In the nucleus TDP-43 is homogeneously distributed in fine punctae, with slightly different sizes, colocalising with perinuclear fibrils, where active transcription takes place (123). It is not found in the nucleolus, Gemini or Cajal bodies (GEM) or telomeric regions but shows a small degree of colocalization with nuclear speckles. However, a shorter variant of 27kDa found in mouse is distributed in nuclear aggregates of up to 2.6μm (124). Nuclear bodies formed by this variant can overlap with

Cajal bodies, GEMs, PML gene product oncogene domains (PODs) and speckles, suggesting that alternative splice variants of TDP-43 might be at the interphase of different nuclear granules (124). Splice variants with similar functions, however, are yet to be found in humans.

2. 4. 3.- Physiological functions of TDP-43

miRNA regulation and processing

One of the least studied functions of TDP-43 is its role in the biogenesis and modulation of miRNA. Drosha and DGCR8, main players in the processing of miRNA primary transcripts, interact with TDP-43 (125,126). Despite being a mainly nuclear protein, the cytoplasmic portion of TDP-43 is also involved in miRNA activity, as a partner of Dicer and modulating its binding to the RISC complex (125,127). Therefore, the regulation does not happen only at the biogenesis or even processing of miRNA, but at every step of the miRNA activity. Through the silencing and overexpression of TDP-43 a network of interacting miRNA has been unveiled, such as miR-132, miR-143, miR- 558, miR-663, miR-206 or let-7b, among others (125,127,128). Some of these targets might be of special relevance for neurodegeneration due to their targets, such as miR-132 or let-7b. The interaction goes even further, with a crosstalk between miR-27b-3p, miR-181c-5p and TDP-43 regulating each other's expression level (129). All this data is now translating in the investigation of circulating miRNA in patients as a biomarker or even as a possible treatment (130,131). Circulating RNA is transported in exosomes and therefore it is out of reach for the RNAses in the media. However, despite the efforts, no single miRNA has been clearly linked with FTD or ALS, suggesting perhaps that a signature or combination of targets is more representative of disease, or that there are still technical pitfalls reducing the sensitivity and specificity of this method.

mRNA transport and processing

The main and most studied role of TDP-43 in the cell is its involvement in mRNA processing and transport. A considerable number of transcripts are regulated by TDP-43 at the splicing level via alternative splicing(132–134). It mediates the exclusion of exon 9 of the *CFTR* gene(135) and of exon 18 in *SORT1* (136). It can also mediate exon inclusion, as in *SKAR/POLDIP3* (133,137). Other pre-mRNA targets include *SKAR, MADD, STAG2, BRD8, FNIP1, SMN, SC35* and *ApoA II* (132,137–139). High throughput studies have found TDP-43 bound to many more transcripts, like *Sirt2,*

FUS, Grn, Mapt or *Snca* (140,141), mostly at their 3'UTRs. As previously mentioned, TDP-43 preferentially binds to poly-UG sequences. These high throughput studies found a bias towards 3'UTRs and distal introns, at least in mouse models (133,140,142). It is worth noting that brain-specific proteins seem to have longer introns in average, which reinforce the nervous system role of TDP-43 (133). An intriguing paper on a mouse KO model suggested that cryptic exons from non-conserved regions were upregulated upon TDP-43 knockout (134). While the relevance of specific cryptic exons found in mice is questionable, *GPSM2* and *ATG4B* were found to include cryptic exons in FTD patients' samples (134). To further support this crucial role in pre-mRNA splicing, TDP-43 has been found to interact directly with spliceosome components and mRNA proteins like *MECP2* and *hnRNPA2/b1* (142). Of special relevance is the interaction of TDP-43 with its own mRNA (140,143). TDP-43 is able to bind to its own 3'UTR and trigger the degradation of its own transcript (143), resulting in a tightly controlled expression level. The same effect has been found in mouse models (144). Mislocalization of TDP-43 to the cytoplasm in disease might disrupt these negative feedback loop, resulting in abnormal levels of TDP-43.

The regulation of TDP-43 targets occurs not only via alternative splicing but also by changing the stability of the transcripts. *Nefl* and *HDAC6* transcripts are stabilised via TDP-43 interaction and its silencing causes a reduction in mRNA and protein levels (145,146). In a similar manner, *NEAT*, *MALAT1* and *XIST* mRNA levels go down upon TDP-43 depletion (133). While all these targets have increased stability of mRNA when interacting with TDP-43, this interaction can also cause the opposite effect and destabilise mRNA transcripts. This effect is observed in *Vegfa*, *Grn* or *Tau* (142,147).

As mentioned earlier, the interaction of TDP-43 with RNA-processing proteins suggests a role in pre-mRNA splicing. In a similar way, interactions with transport proteins, such as Staufen, FMRP and SMN, have been reported (148). This prompted the investigation of the TDP-43 role in mRNA trafficking, which is especially important in neurons, and critical in motorneurons. Axonal transport of Nefl mRNA to neurites is regulated by TDP-43(149). This transport is microtubule-dependent, and it can be altered by ALS mutations in TDP-43. Furthermore, the TDP-43-RNA complexes that are transported form a phase separated entity, which modulate its fluidity along the axon (150). In addition, ribosomal proteins (RPs) are reduced in neurites after TDP-43 depletion in cortical neurons (151). TDP-43 interacts with 5'UTR of their transcripts, regulating its transport to neurites and by doing so, regulating indirectly the local translation there. In addition to its role in neurons, Vogler et al. have identified cytoplasmic structures composed of TDP-43 bound to mRNA in fibroblasts (152). While more research is needed into the role of TDP-43 in fibroblasts, these structures seem to be involved in mRNA transport and local translation

of sarcomere elements during muscle repair. These results reinforce the role of TDP-43 in mRNA transport of proteins required at very specific subcellular locations.

Lastly, there is some evidence that TDP-43 is involved in translation itself, by regulating the transport of RPs to neurites (151). In agreement with this, ALS patients' pyramidal tracts contain less RPs. More specifically, it can repress the translation of Rac1, GluA1 and Map1b in hippocampal neurons (119,153).

Mitochondrial transport and regulation

An aspect of TDP-43 physiology that has been gaining attention in recent years is its involvement with mitochondria, both in healthy and disease conditions. Several groups have found that TDP-43 colocalises with mitochondria (154,155) and it does so via 3 different mitochondrial targeting sequences (108). There, it interacts with and regulates the stability of ND3 and ND6 transcripts, and, more intriguingly, mitochondrial tRNA (108,156). The effects on ND3 and 6, however, have not been found in other studies (157,158). Similarly, several groups have reported that overexpression of TDP-43 can induce mitochondrial fission (155,159), reduction in mitochondrial complex I activity (108,160,161), defects of mitochondrial transport along the axon (155,162) and disruption of ER-mitochondrial interactions and Ca^{2+} homeostasis (163). Again, there is some controversy regarding the direct effects of TDP-43 in the respiratory chain. Some groups have reported no detectable changes in complex I and OXPHOS levels after TDP-43 overexpression (164,165). The characterization of TDP-43's mitochondrial functions seem to be especially tough. Much of the work was done in HEK or NSC34 cells, which are derived from tumours or immortalised. The bioenergetic parameters of such cells might be very different from ageing neurons in the cortex or the spinal horn. Other papers on the field rely on mouse models, which given their shorter lifespan might not reflect the conditions in the human brain. Further research in the topic looking at endogenous conditions is needed.

mRNA transcription

The first identified function of TDP-43 was DNA binding and transcriptional regulator of the HIV-1 protein(166). In later years it has also been found in mouse testis repressing the transcription of SP-10(167). More comprehensive studies have uncovered the widespread effect on transcription (168,169). Alu elements, a class of short interspersed nuclear elements (SINEs), and specifically AluS seem to be regulated by TDP-43 (169). The specific nature of this regulation

has not been described yet but Morera et al. suggest that since TDP-43 does not bind directly to Alu sequences, the transcriptional regulation must happen indirectly.

Stress granule dynamics

Stress granules (SGs) are short lived cytoplasmic membranelles organelles that can form in every cell type (170–172). They assemble in response to environmental stressors, such as heat shock, osmotic stress, oxidative stress or viral infection. The general function of SGs is to sequester mRNA-ribosomal complexes and minimize the cellular energy demands during the environmental stress (173). The components of SGs encompass both mRNA and proteins, some of them are stalled preinitiation complexes, small ribosomal subunits, eiF3, eiF4g, eiF4e, PABP, Staufen, p54/rck, TIA-1 or G3BP1 (170). As mentioned before, some of these proteins are regulated at a transcript level by TDP-43 or are interactors of it.

In general terms, upon stress eiF2α gets phosphorylated, which triggers ribosomal stalling and starts the formation of SGs. An alternative pathway independent of eiF2α phosphorylation can lead to the formation of SGs via the inactivation of the RNA helicase eiF4a (170). The assembly occurs in two stages: a core forms in an ATP-dependent manner first and this core nucleates the outer shell of the SG (174). The core is composed of G3BP1 and a network of protein-protein, mRNA-protein interactions. After the core is formed, RBPs such as hnRPP2, TIA-1 or TDP-43 are recruited to the shell of the SG (175–177). The disassembly of SG occurs after the environmental stress has ceased and it follows the inverse path than the nucleation: the RBPs from the shell leave first the SG and the core disengages last (174).

As mentioned before, TDP-43 interacts with several RBPs and mRNA, and it is not surprising that it also plays a role in SG dynamics. TDP-43 is present in SG but not in processing bodies, another cytoplasmic membraneless organelle associated with mRNA decay (176). When mammalian cells are treated with sodium arsenite (a substance capable of triggering an oxidative stress response in cells) TDP-43 is recruited to SGs. If TDP-43 is knocked down, the SG core protein G3BP1 transcript and protein levels are reduced, while TIA-1 mRNA and protein levels are increased. However, eiF2α phosphorylation is not decreased (176,177). These results put TDP-43 upstream of both G3BP1 and TIA-1 in the SG assembly pathway. The reduction of TDP-43 has also a measurable impact on stress granules dynamics. TDP-43 depleted mammalian cells present less and smaller SGs upon stress that disassembly faster than SGs in cells with TDP-43, with an impaired secondary aggregation of TIA-1 to the shell of the granule (175,178). The

reduction of TDP-43 in turn affects the polyadenylated RNA stored in stress granules, which is less preserved than under wild type conditions (178). To reinforce the idea that TDP-43 is upstream of G3BP1, the alterations in SGs dynamics can be rescued by overexpression of G3BP1 in KD TDP-43 cells (175).

The interaction of TDP-43 with stress granules depends on its C-terminal domain as well as on its RNA binding capabilities (176,179). In addition, TDP-43 gets PARylated at its NLS and this modification seems to be crucial for its recruitment into SGs (180). Additionally, recent studies have developed an ingenious light-dependent system to nucleate G3BP1 (181). This system has showed that nucleation of G3BP1 is sufficient to recruit TDP-43, independently of eiF2α.

Finally, SGs are temporary organelles that arrest translation as long as there is an environmental stress present. However, if the stressor prolongs long enough SGs might become less soluble and eventually turn into insoluble, solid aggregates (182). The ability to cope with alterations in the SGs dynamics is different in cells with higher turnover compared to long lived cells, such as neurons, which seem to be highly sensitive to SG-related toxicity (175). Together all this data hints that TDP-43 is a strong modulator of SG dynamics, directly or via a target of TDP-43 itself. Any malfunction of SGs might lead to the formation of toxic aggregates, which might cause even cell death in neurons or other long lived cell types.

2. 4. 4.- TDP-43 in disease

As previously mentioned, TDP-43 is present in nuclear and cytoplasmic aggregates in both ALS and FTD patients. The mechanism that links pathological aggregation and neuronal toxicity has been studied in great detail. Alas, it is still not clear how these two are linked, or if the aggregation is an epiphenomenon of disease, with a trigger further up the pathological pathway. The large volume of literature looking at TDP-43 pathology seems to agree on a mixture of toxic gain of function combined with a loss of function of some of the functions that have been previously covered.

Role of identified mutations

While mutations are only present in <5% of ALS cases they are the first and most accessible way to study the proteinopathy. However, one of the caveats of this approach is the lack of consistency in the models used to examine the role of the reported mutations. This is something worth keeping in mind when looking at the existing literature on the topic.

Most of the reported mutations are located in the C-terminal glycine rich domain and only a few are located in the N-terminal half of the protein. A90V TDP-43 increases the cytoplasmic fraction of TDP-43 slightly when expressed in QBI-293 cells, possibly by disturbing the NLS, which is only a couple amino acids away (183,184). The other well studied N-terminal mutation, D169G, is located is in the RRM1 and has an impact in UBQLN and Oxr1 binding (185,186). In addition, D169G TDP-43 has a longer half-life and it is more prone to be cleaved by caspase 3 than the wildtype molecule, giving rise to stable 35kDa fragments (187). This is probably behind the reported increase in the aggregation potential of D169G TDP-43 in SH-SY5Y cells (188).

As mentioned, the C-terminal domain harbours the majority of the identified mutations, importantly the most studied ones: G298S, A315T, Q331K, M337V and A382T. While mutations are not present in all ALS/FTD cases, these 5 mutations have been linked to earlier disease onset and increased aggregation potential (189,190). In addition, G298S, A315T and M337V have been shown to have a deleterious effect on *Drosophila* eye development, causing thinner retina and exacerbating its degeneration (191). A315T TDP-43 has enhanced fibril formation potential, generating more stable fibrils than wild-type TDP-43 (122,192). At the same time, this particular mutation seems to enhance the cleavage of TDP-43 by Calpain (193). Interestingly, even when A315T TDP-43 interactome is indistinguishable from wtTDP-43's, it indirectly induces a HO-1 stress response and causes a decreases in AMPK release in mice models (103,194). Recently, a A135T mouse model has been used to examine metabolic changes in specific brain areas during the presymtomatic phase, showing a decrease in glucose uptake in the prefrontal motor cortex happening before the motor phenotype appears (195). Q331K TDP-43 has been found to form toxic aggregates in yeast and SH-SY5Y cells(188,196). The balance between mitochondrial fission and fusion seems to be disturbed in rat cortical neurons expressing Q331K TDP-43 (155). This effect seems to be mediated by an abnormal interaction of mutant TDP-43 with its targets. The effect of this mutation however is not constrained only to mitochondrial fission and fusion proteins, but it is affecting hundreds of TDP-43 RNA targets (197). Mice expressing Q331K TDP-43 develop a motor deficit that worsens in an age dependent manner. Several rat models expressing M337V TDP-43 develop extensive neurodegeneration that progresses with age (198,199). The exact mechanism is unclear but M337V TDP-43 induces a reduction in the unfolded protein response and a depletion on XBP1 (200). In addition, when expressed in rat astrocytes in can lead to motor neuron degeneration and to an upregulation of Lnc2 and Chi3L1 (201). While rat models expressing M337V TDP-43 model some aspects of disease, data from mouse model studies is unfortunately less consistent (103). More in-depth studies have shown that this particular amino acid substitution can lead to cytoplasmic mislocalisation both in

neurons and astrocytes and an altered RNA splicing signature (197,202,203). Finally, even though A382T is one of the most common mutations found in patients, it has not been as widely studied as the other mutants already mentioned in this section. Besides being more stable than the wild-type TDP-43, its expression in HEK293E cells lead to cytoplasmic mislocalisation of the mutant construct, together with elevated levels of Bcl-2 and impaired Ca^{2+} release (204,205). In addition, the presence of A382T TDP-43 in fibroblasts impairs the stress granule response and sensitizes cell to arsenite treatment (206). As with other pathological mutants, the mRNA splicing of several targets is affected by A382T mutation (207). Lastly, a recent study has linked TDP-43 with R-loop modulation, with mutations at A382 leading to an impairment of this mechanism which can lead eventually to DNA damage (208).

The effect of the mutations discussed here are only representative of the five most studied missense mutations. While the literature goes back to some effects, such as RNA splicing changes or modulation of stress granule dynamics, the link between these mutations and human disease is still unclear.

Nuclear depletion and cytoplasmic mislocalisation

Cytoplasmic mislocalisation of TDP-43 is a hallmark of ALS and several types of TDP-43-FTD (21,24). There is an important distinction to be made between nuclear depletion and cytoplasmic mislocalisation. Nuclear depletion seems to be an early event in TDP-43 pathology (209), with cytoplasmic mislocalisation following it. As mentioned before, some mutations can trigger this mislocalization but the bare nuclear depletion seems to be enough to trigger TDP-43 related toxicity, probably via a loss of function (144). Another example of this loss of function can be seen in the deleterious effect of knocking down or out TDP-43 (210). Giving the enormous number of targets and processes that TDP-43 is involved in, it is not realistic to try and find a single process responsible for the toxicity caused by nuclear depletion of TDP-43. However, it is important to consider the role of TDP-43 in its own regulation via a negative feedback loop (143). A loss of autoregulation leads to higher TDP-43 levels, which in turn might trigger a toxic gain of function in the cytoplasm.

Aggregation and seeding

As it has been already mentioned, TDP-43 forms oligomers (mostly dimers) in healthy neurons, as well as in muscles (114,152). The nature of the aggregates found in ALS and FTD patients,

however, is not fully understood yet. Initial reports of TDP-43 aggregates in patients did not find amyloid-specific Thioflavin-positive (ThT) inclusions (20,196) but more recent studies have suggested that TDP-43 can indeed be found in ThT reactive inclusions (211,212). The amyloid nature of TDP-43 aggregates *in vivo* is still being debated (213). On the other hand, several studies have investigated the aggregation dynamics of different TDP-43 peptides (214). While some of these studies have reported the formation of ThT-positive aggregates, it is important to consider that TDP-43 is not isolated inside the cell and that it is subjected to a plethora of interactions with the environment and within itself. All these differences could be reason why the *in vitro* and the patients' material differ.

While the amyloid behaviour of TDP-43 is still a matter for debate, several studies have stablished TDP-43's seeding capabilities in a prion-like manner. The transfection of insoluble, *in* vitro generated protein aggregates can trigger the formation of inclusions by endogenous TDP-43 (215). In addition, patients' material can also seed for further aggregation in SH-SY5Y cells that are propagated over several passages in a true prion-like behaviour (216). It was later proven that oligomeric TDP-43 can be transported across the axons and loaded into exosomes (217). Another proof of TDP-43's prion-like behaviour is the differential degradation of aggregates after exposure to trypsin, suggesting the presence of different templates or strains (218). Furthermore, TDP-43 seems to adopt different conformations *in vivo*, which can be correlated with the disease duration of patients, strongly supporting the idea that TDP-43 inclusions be formed by different strains (219).

Protein turnover

As it was mentioned before, TDP-43 has been found in association with ATG7 mRNA, and this interaction is disrupted by pathological mutations (220). In turn, the destabilization of ATG7 mRNA leads to a reduction in protein levels and an impairment of autophagy. In addition, TDP-43 can modulate TFEB localisation through its interaction with Raptor mRNA (221). The altered localisation of TFEB can have severe impacts downstream in the autophagy flux. These observations have been validated in patients' material, where an accumulation of inclusion bodies positive for LC3 and p62 can be found (222). Taking these two effects together, there seems to be a loss of TDP-43 function linking its pathology with alterations in the autophagy pathway. The upregulation of autophagy is able to reduce TDP-43 toxicity to an extent and it is at the moment an exciting treatment possibility that remains to be explored (223,224) .

Posttranslational modifications

From the moment TDP-43 was found in ALS and FTD neuronal aggregates some PTMs have been considered to go hand in hand with TDP-43 proteinopathy. Phosphorylation and ubiquitination are the most studied ones but recent studies have looked at acetylation, cysteine oxidation, SUMOylation and PARylation (214,225).

Phosphorylation

One of the first PTMs to be linked with TDP-43 pathology is phosphorylation. Serines 409 and 410 have been found to be phosphorylated in TDP-43 aggregates both in FTD and ALS cases (226). The phosphorylation at these residues is considered a golden standard for the post-mortem diagnosis of ALS and TDP-43 positive FTD cases. In addition to those residues, S375, 379, 403 and 404 have been found to be phosphorylated in patients (24,226–228). Interestingly, the species of TDP-43 that are phosphorylated are different in ALS and FTD samples. ALS spinal cord samples contain mainly phosphorylated full length TDP-43 while in FTD brain samples it is C-terminal fragments that are phosphorylated (24). While the cause of these phosphorylations is not clear, the consequences in TDP-43 pathophysiology are substantial. Phosphorylated TDP-43 becomes more insoluble and resistant to calpain cleavage, which results in TDP-43 aggregates that are more resistant to degradation (229–231). In addition, the presence of c9orf72 repeats in a mouse model has been shown to trigger TDP-43 pathological phosphorylation, linking several aspects of disease (232).

When looking at the specific enzymes involved, several kinases and phosphatases have been identified in the context of TDP-43 phosphorylation. Kinases CK1, CK2, TTBK1/2, GSK3 and HIPK2-JNK all have been found abled to phosphorylated TDP-43 in different models (233–237). On the other had S409/410 are specifically dephosphorylated by phosphatase calcineurin, which colocalises with TDP-43 aggregates (238). While the list of enzymes involved in TDP-43 phosphorylation is incomplete, it offers a suitable therapeutical target that only now is beginning to be explored (225).

Ubiquitination

Together with phosphorylation, TDP-43 first identified in ALS and FTD aggregates ubiquitinated as well (20,54). Unlike phosphorylation, the specific residues that undergo ubiquitination are not as well defined. Several studies have identified different ubiquitinated residues but none of them has a bigger impact in the total ubiquitination levels. Most of the identified lysines are

located in the N-terminal part of the protein (K79, K84, K95, K102, K114, K145, K60, K176, K181) (239–242) and only one at the C-terminal part (K263), however the C-terminal fragments found in FTD patients are profusely ubiquitinated, therefore these lysines mentioned here are far from being the only ones (20,239). The ubiquitin chains linked to TDP-43 are both K48 and K63, targeting TDP-43 both to the proteasome and to the autophagy pathway (243). This alternative in degradation seems to correspond to the soluble versus insoluble TDP-43. However, ubiquitination can also cause cytoplasmic mislocalization and shift TDP-43 to the insoluble fraction (185,244). To make it more complex, abolishing ubiquitination at K95 reduces the pathological phosphorylation at S409/410, knitting together both pathological PTMs (239).

Several enzymes have been identified as possible ubiquitin transferases of TDP-43: Parkin and UBE2E (185,244,245). The effect of all these ubiquitin transferases on TDP-43 pathology is to enhance insolubility, promote aggregation and cytoplasmic mislocalisation. In addition, UBQLN1 also has been found to alter TDP-43 solubility. Unfortunately, much less progress has been done in the identification of TDP-43 deubiquitinases. Up to the date of this study, only UBPY has been identified in a yeast two hybrid screen as a possible TDP-43 deubiquitinase that can rescue to a certain extent the insolubility, aggregation and deleterious effects on a *D. Melanogaster* model.

Acetylation

In recent years TDP-43 acetylation has been studied with remarkable advances in the understanding of its role for TDP-43 pathophysiology. TDP-43 has 20 lysines that are prone to acetylation and several of them can be ubiquitinated as well, tangling these two modifications together. Early work already suggested that acetylation might play a role in ALS/FTD, with HDAC6 mRNA stability depending on its interaction with TDP-43 (146). The reduction in functional TDP-43 levels can lead to a HDAC6-dpendent reduction in neurite growth in neuroblastoma cells (246). Another study showed that non-specific acetylation of TDP-43 via aspirin treatment can cause net charge changes that might reduce its aggregation (247). In addition, mutation in the acetyltransferase ELP3 have been linked with motor neuron degeneration in ALS (248). More specifically, K145 and K192 have been found to be acetylated in HEK293 cells. Mimicking acetylation at these residues via glutamine substitution causes a loss of RNA binding and triggers mitochondrial disfunction and pathological aggregation of TDP-43 (249). Acetylation at K145 seems to be especially relevant and it was even found in TDP-43 aggregates in ALS spinal cord samples (but not in FTD cortex samples). Interestingly, a previous study showed that binding to RNA protects lysines at the RNA recognition domain from acetic anhydride labelling, already hinting at the interaction between acetylation at the RRM1 and RNA

binding (250). More detailed examination of glutamine substitutions at these residues has shown that K145Q/K192Q TDP-43 phase-separates into intranuclear anisotropic compartments together with Hsp70 (251). Hsp70 seems to be crucial for keeping the fluidity of these membranelles organelles and a reduction in Hsp70 levels can precipitated the formation of TDP-43 aggregates.

So far, only CBP has been identified as a suitable acetyltransferase for cytoplasmic TDP-43 (249). The same group identified arsenite treatment as a trigger for K145 acetylation although the specific pathway remains elusive. In addition, HDAC1 is capable of deacetylating TDP-43 and reduce its cytotoxicity, although the specific residue or residues affected have not been identified (252). Lastly, HSF1 can reverse the acetylation-mimic driven aggregation in a cell model (253). However, given the role of HSF1 in chaperone activation, it is possible that this effect is caused by TDP-43 aggregation, regardless of the cause. Taken together, acetylation has a strong effect in the pathophysiology of TDP-43 and its regulation seems to be a promising line of research with high relevance for future therapeutics.

Cysteine oxidation

In the context of neurodegeneration, and specially in ALS, cysteine oxidation is particularly interesting because it is a PTM closely connected to the metabolic state of the rest of the cell. Cysteines can be involved in stabilising protein structure via disulphide bonds but are also involved in maintaining the redox state of the cell. Four well conserved TDP-43 cysteine residues (C173, C175, C198 and C244) have been found to be oxidated after oxidative stress, which promotes aggregation and pathological phosphorylation of TDP-43 (254). Other groups have found oxidative stress markers to be upregulated in ALS patients, supporting the idea that cysteine oxidation could indeed be behind TDP-43 aggregation (255,256). An A315T TDP-43 mouse model also recapitulates this increase in oxidative stress, which suggested a crosstalk between TDP-43 mutations, oxidative stress and cysteine oxidation (257). A recent study confirmed this showing that under chronic oxidative conditions GADD35 recruits CKI-ε to phosphorylate TDP-43 (258). An additional consideration to all this research is the possible involvement of a number of ALS mutations that introduce additional cysteines, such as G358C, S379C and G295C.

SUMOylation and PARylation

SUMOylation was originally identified found colocalising with TDP-43 aggregates in HEK293E cells, specifically SUMO2/3 (259). While intriguing it took a decade until another study looked more carefully at the functions of TDP-43 SUMOylation (260). TDP-43 overexpression related

toxicity is a well-documented phenomenon, and Maurel et al. showed that inhibition of SUMO transferases in NSC-34 cells via anacardic acid can alleviate the overexpression related toxicity. Furthermore, they identified a SUMO-binding motif in the RRM1 and K136 as a target of SUMOylation. The substitution of this lysine for arginine triggers nuclear aggregation of TDP-43, leaving an unclear picture of the effect of SUMOylation at K136.

While SUMOylation can take place only at lysines, PARylation ca occur at different amino acids, such as serine, glutamate, aspartate or lysine. Not as well characterized as other PTMs, PARylation of TDP-43 promotes phase separation and it is required for its recruitment into stress granules (180,261), both critical parts of TDP-43 physiology. PARylation is enhanced in ALS patient tissue, although this enrichment does not colocalise with TDP-43 aggregates (262). Future research will surely better determine the role and regulation of PARylation in TDP-43 proteinopathy.

C-terminal fragmentation

Together with phosphorylation and ubiquitination, C-terminal fragmentation is one of the most common PTMs found in ALS and FTD patients. 35 and 25kDa are found mainly in insoluble fractions of FTD cortex and ALS spinal cord samples (20,21,263). Most of the fragments are lacking the N-terminal part of the protein and N-terminal fragments, while also present, degrade quickly (225). Currently there are three possible origins for the C-terminal fragments: an alternative splicing event of TDP-43 (264,265), an alternative in-frame translation start site (266), or the proteolytic cleavage of full length-TDP-43. From these three hypotheses the last one, proteolytic cleavage, has been studied the most.

TDP-43 can undergo proteolytic cleavage in the context of oxidative and osmotic stress in cells (267,268). From the fragments generated, the 25kDa fragment seems to convey higher toxicity than the 35kDa one (269). Several proteases have been linked to TDP-43 cleavage, such as caspase 4 (270), asparaginyl endopeptidase (271) and calpain-I and II (193). Regarding calpain cleavage, several TDP-43 ALS mutations can influence the dynamics of the process, as discussed previously. In addition, dipeptide expansions in *c9orf72,* specifically poly-GA, can trigger TDP-43 cleavage, linking these mutations at *c9orf72* with TDP-43 proteinopathy (272). It is worth noting that generation of the fragments is not enough to trigger aggregation nor cytotoxicity. De novo-generated fragments are quickly degraded, hinting at an additional mechanism to form aggregates (273). Finally, several rat and mouse models confirm the toxicity of the C-terminal fragments, specially the 25kDa one (274,275). Other mouse models have shown that

neurodegeneration can occur in the absence of C-terminal fragments (144). While not necessary for degeneration, their toxicity has been widely confirmed.

Other TDP-43 pathology

Since TDP-43 is involved in different processes in the cell and targets thousands of RNA targets, its loss or gain of function involve several systems, some of them are just beginning to be described. One of the most recently described effects of TDP-43 proteinopathy is the impairment of endocytic processes. Overexpression of TDP-43 in cell models correlate with lower levels of endocytosis (276). In ALS patients' samples, TDP-43 has been found to colocalise with Rab5, potentially sequestering it and affecting the endocytic process. In iPSCs derived neurons a reduction in TDP-43 levels causes a reduction in the recycling of endosomes, while an overexpression has the opposite effect (277), suggesting a neuron-specific effect. Recently a detailed characterization of the MAPK/AKT/RAB11 pathway in ALS spinal cord has revealed the intricate interaction of TDP-43 with the endosomal recycling pathway (278).

Recent literature has described the interaction between TDP-43, mitochondria and cellular bioenergetics. The overexpression of TDP-43 in primary motor neurons is linked to shorter mitochondria and lower levels of mitofusin.2 (Mfn2), which could rescue the mitochondrial phenotype (155). These results were validated in a *Drosophila melanogaster* model where, upon TDP-43 overexpression, higher levels of mitochondrial fission were reported (279). Furthermore, mitochondria in ALS spinal cord samples are shorter and have an irregular inner structure (280). While all this hinted at a tight connection between TDP-43 and mitochondria, it was not until 2016 when an enrichment of TDP-43 at mitochondria in patients' samples was reported, and 3 mitochondrial targeting sequences were identified within TDP-43 sequence (108). In the mitochondria, TDP-43 binds to the mRNA and regulates the expression of the complex I members ND3 and ND6. The effect was consistent with data from overexpression mouse model. Unfortunately, several studies have tried to validate these intriguing results with little success. While the effects on mitochondrial fusion and fission are now stablished, it is unclear if TDP-43 colocalises with mitochondria (158), if cellular bioenergetic parameters are affected (165) or if indeed ND3 and 6 mRNA expression is regulated by TDP-43 (156). In conclusion, the dysregulation of mitochondrial fusion-fission events by TDP-43 has been confirmed in several studies and models, but it is still unclear if TDP-43 is indeed recruited to mitochondria and what is its function there.

Finally, there are a few indications that TDP-43 pathology might interact with metal ion homeostasis. Iron and iron-related protein levels have been found to be increased in blood sera from ALS patients (281). In a A315T mouse model, increased levels of zinc, manganese and copper were increased in spinal cord from transgenic mice (282). It is possible that aberrant levels of zinc promote TDP-43 aggregation, making a positive feedback loop resulting in more metal ion dysregulation and more TDP-43 aggregation (283). In any case, the alteration of ion homeostasis by TDP-43 is still mostly unclear and more research will surely stablish its role in TDP-43 proteinopathy.

2. 5.- Liquid-liquid phase separation in biology

The existence of membrane-less compartments in the cell was theorized over a hundred years ago (284) but it is during the last 20 years when the field has started to describe and characterize in detail this phenomenon (285). A vast number of proteins have been found to be able to phase separate (286). Received with excitement, liquid-liquid phase separation (LLPS) was used to re-examine many organelles such as stress granules (287), the different nuclear organelles and phases (288,289) and, most prominently, the nucleolus (290,291). Furthermore, misregulated phase separation has been linked to several diseases, and it is seen as a preliminary step for aggregation of certain proteins (292–294).

2. 5. 1.- Characteristics ad causes of biomolecular condensates

The current model for phase separation and the formation of biomolecular condensates is grounded on polymer chemistry and soft matter physics, and the principles were established before any biomolecular condensates were described in living cells. Biomolecular condensates are membrane-less organelles with a distinct molecular composition that display some liquid-like properties. The proteins in these organelles remain concentrated but they can go in and out, as it has been shown via fluorescence recovery after photobleaching (FRAP) experiments (295–297). In addition, they tend to adopt an spherical shape, which can be interpreted as a mechanism to optimize surface tension in a phase, and they can fuse (291,298). These characteristics allow for a dynamic system of organelles that can assemble and keep their components at a high concentration when compared to the outside environment, but at the same time be in constant exchange with the media.

The main reason molecules phase separate is their valency, or the number and type of interactions within and with other molecules. Once their solubility limit has been reached, molecules with the right valency will phase separate in the right conditions (285). Based on this, one can distinguish three different scenarios: multivalency-driven LLPS, LLPS of multimodular proteins and intrinsically disordered proteins or proteins with intrinsically disordered regions (IDRs). Multivalency, or a plethora of weak intra- and intermolecular interactions greatly increases the potential to phase separate (299,300). These interactions can reduce the solubility limit in a measurable way, causing proteins to phase separate and oligomerize (301). In this regard, disordered regions of proteins usually create multiple low affinity interactions and promote phase separation. Going up one level, valency can be measure at the scale of protein domains. Through this approach one can find structured proteins that can phase separate thanks to the interactions of their domains within and with other molecules. An example of this behaviour can be found in the in the complexes form by nephrin, Nck and n-WASP. Due to the valency of these modular proteins, they can phase separate and, thanks to nephrin interaction with bilipid layers, they can be found even in contact with membranes (300,302). In contrast to structured, modular proteins, intrinsically disordered domains can drive phase separation as well. Often these regions contain repetitive multivalent motifs (299,303,304). When characterizing these regions, it is the interactions of the single amino acids what drives the phase separation. Aromatic amino acids have high multivalency and they promote cation-pi interactions with arginine residues (299). An *in vivo* example of this can be found in the mitotic spindle protein BuGZ, which phase transition relies on aromatic and hydrophobic amino acids (305). Another example of LLPS promoting interactions can be found in glutamine, aspartate and serine residues, which can create dipolar interactions (306,307). Some prion-like domains contain residues with high valency that can indeed promote the formation of fibres. The number of β-strands interactions and their affinity will determine if the protein goes into phase separation or if it would form hydrogels and fibres (308). When trying to predict valency, it is also worth noting that the backbone of the peptide can also participate in the interactions. However, it is worth pointing out that the creation of predictive rules for biomolecular condensates has only started and will surely develop in the coming years.

2. 5. 2.- Molecular grammar and regulation

While it is an ongoing process, several control mechanisms of phase separation have been described. It is obvious that not every protein that can phase separate does so *in vivo* in a

continuous manner, and that this behaviour is tightly controlled. This can happen at least at three different levels: assembly, composition of phases and the level of the physical properties of the droplets.

The assembly of phases depends mainly in the concentration and the phase separation threshold of the members. As mentioned before, phase separation is connected to solubility and concentration of the molecules. Therefore, increasing the concentration of a protein by expression or transport to a specific location in the cell can trigger LLPS. An elegant example of this is the dissolution of nucleoli when nuclei are exposed to a hypotonic solution (309). Additionally, the size of phase separated droplets depends on concentration as well, and thus cells can modulate droplet size by changes in the concentration (310,311). A different way to regulate the assembly of LLPS entities is by directly altering their phase separation threshold. This can be done through PTMs that change the valency of their targets. An example of this is the arginine methylation of DDX4, which reduces cation-pi interactions (299), which in addition is evolutionary conserved (312). Similarly, SUMOylation of PDL is crucial for the correct segregation of PML nuclear bodies (313).

The next level at which organisms regulate phase separated entities is by modulating their composition. The members of condensates can be classified as scaffolds or clients (314). Scaffold proteins are essential for phase separation, while clients can be recruited to the phases but are not needed to keep the phase separated. The recruitment of clients depends on the valency of scaffolds that, just as we saw, can be modulated via PTMs. In addition, different stoichiometries of scaffold members will influence client recruitment. How the valency and the distribution of charges of the scaffolds influence the assembly of condensates can be described as a “spacers and stickers” model, which has developed through observations of hnRNPA1 but can be extrapolated to other phase separating proteins (315).

The last level at which cells can control phases is at the maturation or hardening process. Liquid phases can lose fluidity and harden under the right circumstances (316,317). In addition to regular, solid assemblies, certain proteins can form amyloid via β-strand interactions (318). This is accomplished by the extremely high local concentrations at separated phases (319). Through the alteration of valency and of the stoichiometry of the components it is possible to alter the association and dissociation rates of a phase, which can lead to a dissolution or to a vitrification and solidification of the condensate (320,321). In addition, there are energy-dependent processes that can modulate the physical properties of liquid phases. The most obvious of these processes is the action of chaperones, which can interact and prevent the hardening of certain

condensates (322). One example of this can be found in the disassembly of TDP-43 phase separated granules upon HSF1 chaperone program activation (253). Another regulator of RNA-binding protein phase separation is the DEAD-box ATPase, which is necessary for the turnover of P-bodies (323). Lastly, cells can regulate the localization of condensates by transporting them through the actin network. This exposes the condensates to with distinct molecular environments that can alter their function or biophysical characteristics (324,325). An example of this can be found in TDP-43 phases along the axon. As TDP-43 moves along the axon the fluidity of its phase decreases, probably due to changes in its composition and environment (150).

Through all these mechanism cells can alter and modulate in a fast and reliable the characteristics of biomolecular condensates. Unfortunately, it is not clear yet what is the use of this highly dynamic tool in cells, but there have been many advances in the last decade.

2. 5. 3.- Processes and function

While the influences of several parameters on the formation of phase separated condensates are starting to be defined, it is less clear what function do they fulfill. One of the most obvious consequences of phase separation is the increase in concentration of its components. This translates into more efficient biochemical reaction, with faster reaction kinetics. An example of this can be observed in the mRNA processing at histone locus bodies, where high local concentration of the mRNA processing machinery allows for a more efficient splicing and capping process (326). However, increasing the local concentration of a certain protein can also cause molecular crowding and therefore can have a negative impact in the efficiency of the reaction (327). Therefore, the effect of elevated local concentration is, most probably, variable depending on the process.

Another theorized function of phase separation is the sequestration of components in order to counterbalance the promiscuity of certain proteins. By concentration effectors with their targets the effectors promiscuity issue is reduced, and the reaction is more streamlined. This control of the biochemical flux would somehow parallel that of scaffold proteins in signalling pathways (328). In addition, biomolecular condensates might be able to buffer concentration of certain “clients”. Given their porous nature, they can accumulate certain molecules and buffer concentration at a local level in a highly dynamic way. So far, these two functions of phase separation have not been properly described.

LLPS in neurodegenerative disease

In recent years, phase separation has been linked to several neurodegenerative aggregation processes. Given the disordered structure of many proteins involved in neurodegeneration and the solidification process observed in some condensates, this relation was to be expected. Many intrinsically disordered proteins, or proteins with intrinsically disordered regions are found in aggregates in disease (293). Since separated phases can mature and turn into pathological aggregates, these proteins must maintain a balance between dynamic phase separation and pathological aggregation (303,310). To further support this link, mutations or PTMs can alter valency, driving LLPS maturation, or they can alter subcellular localisation, exposing the proteins to a different milieu and to a different set of chaperones that might impact in the phase separation process. Specific examples of this can be seen in the effect of different salt concentrations or pH in phase separation (329,330).

In recent years, careful re-examination of the effect of known mutations and PTMs on neurodegenerative proteinopathies in the frame of phase separation has shed light n the interaction between the two. Several pathological mutations in TDP-43, FUS, hnRNPA1 and TIA1 accelerate phase separation and further aggregation (177,331,332). A specific example is the pathological mutant G156E FUS, that forms condensates and aggregates into fibres at a faster rate than wtFUS (331,332).

PTMs by modulating valency, charge distribution and subcellular localization have the potential to disrupt LLPS balance (333). In FTLD-FUS patients, FUS is found primarily mono- or unmethylated forming aggregates (334). When polymethylated, FUS interaction with transportin is enhanced and its recruitment to SGs is reduced, modulating its phase separation behaviour (335). PARylation of FUS and TDP-43 has been reported recently to increase the recruitment of these proteins into separated phases, and its modulation has been proposed as a therapeutic approach to slow down aggregation in FTD and ALS (180,262). This raises the question about specificity of these two aggregates, why do not these proteins form a unique phase? The specific molecular grammar of each phase set these two proteins apart. TDP-43 LLPS relies heavily on the π-π intermolecular interactions of aromatic amino acids and the activity of its transient C-terminal α-helix (336,337). FUS, on the other hand, separates thanks to intermolecular hydrogen bonds, hydrophobic interactions and the glutamines from its low complexity domain (338). These differences, plus differences in the charge distribution along the protein, ensure a certain degree of specificity in the contents of a phase.

Phase separation is involved in other neurodegenerative diseases characterised by proteinopathies, such as Alzheimer's or Parkinson's disease. Alzheimer's patients' cortex is characterised by the presence aggregates containing Tau, a protein that has been found to phase separate both *in vivo* and *in vitro* (294). Detailed examination of its aggregation dynamics showed that both mutations and hyperphosphorylation can promote phase separation (339). In addition, the presence of alternative isoforms of Tau can facilitate phase separation and aggregation as well (340). Similarly, a recent study has shown that α-synuclein can phase separate, and that the phosphorylation of its acidic tail promotes further hardening and aggregation (341). The last example is another protein involved in the FTD-ALS spectrum: *c9orf72.* Instead of a point mutation, patients with alterations in this gene carry hexanucleotide expansion that can translate into dipeptide repeats at a protein level (57). This gives rise to two distinct phases, one containing RNA repeats and another amino acid foci (342,343). The repetitive nature of both and their multivalency strongly promote LLPS of both RNA and protein.

In recent years, phase separation has been established as an early event int the process of aggregation in several neurodegenerative diseases, at least in vitro. Unfortunately, the standard fixing procedures of neuropathology might interfere with the detection of LLPS events but new methods are being developed to detect them in fixed material (251). Phase separation offers a reversible process before the formation of full aggregates.

2. 6.- The acetylation system

Together with phosphorylation and ubiquitination, acetylation is one of the most common posttranslational modifications, evolutionary conserved from prokaryotes to eucaryotes (344). It was first reported at histones in the nucleus more than 50 years ago (345) but it is in the past decade when acetylation has been studied most widely. Thanks to mass-spectrometry, we now know that it is varied and ubiquitous in cells (346), and that it creates complex networks that rival those of phosphorylated residues (347,348). As an example of the intricacy of it, Lundby and colleagues reported over 15000 modifications in different rat tissues that create tissue-specific acetylation signatures (349). It is important to keep in mind that acetylation can be ε-acetylation, amino-terminal acetylation and O-linked acetylation, however in this chapter of the introduction the focus will be on ε-acetylation.

2. 6. 1.- Regulation of acetylation

In an enzymatic acetylation event, an acetyltransferase transfers an acetyl group from an acetyl CoA molecule to an ε-amino acid terminal chain of a lysine. In addition to enzymatic acetylation, there is non-enzymatic acetylation, which, under the right circumstances, can transfer an acetyl group to a lysine without an acetyltransferase. The main role of acetyl-CoA in acetylation already suggests a relation between acetylation and metabolism, which will be explored later.

The first level at which the cell can regulate acetylation is at the synthesis of Acetyl-CoA. It has been shown that, in general terms, the total acetylation level is heavily linked to the levels of Acetyl-CoA (350). While it is membrane-impermeable, nuclear and cytoplasmic pools are connected by nuclear pores. It is important notice that Acetyl-CoA is synthesized via different pathways in each compartment, therefore its pools can be differentially affected by the activity of these enzymes. As an example, in mitochondria pyruvate dehydrogenase complex and β-oxidation of fatty acids contribute the most to the acetyl-CoA pool, while in the cytoplasm it is synthesised mostly by ATP citrate synthase and acyl-CoA synthase (344). Modulation of all these processes acts as a general regulator of acetylation.

Before going in detail into enzymatic acetylation, it is important to realise that there is a non-enzymatic acetylation that acts in the background in the right conditions. It was first described in histones but recently it has been shown that it is most prevalent in the mitochondria (351,352). Its presence in mitochondria is due to the high pH and acetyl-CoA levels, the perfect conditions for non-enzymatic acetylation to happen (353,354). While the function of this type of acetylation is unclear, it seems to reduce the activity of pyruvate dehydrogenase and reduces fat metabolism during fasting in mitochondria, slowing down mitochondrial activity overall (355). Since these acetylations are quickly removed by Sirt3, it is possible to see them as either a metabolic sensor and regulator or as a form of protein damage that can accumulate over time (356). Further research on non-enzymatic protein acetylation will uncover the true function of it. Overall, the whole acetylation system is composed by acetyltransferases, deacetylases and “readers” of acetylated lysines.

Acetyltransferases and deacetylases

Taking the number of acetylation events identified, a surprisingly low number of lysine acetyltransferases (KATs) have been identified. Up until today, 13 KATs are considered canonical, and 9 more proteins have reported to have acetyltransferase activity (357). Acetyltransferases transfer the acetyl group of acetyl-CoA onto the side chain of a lysine, neutralizing its positive

charge. Most of the canonical KATs are grouped in 3 families based on their sequence similarities: GCN5, p300 and MYST. In addition, 10 other acetyltransferases do not belong to any of them (357). Compared with phosphorylation, KATs are much less specific *per se*. However, their specificity and localization are modulated by a network of interacting proteins (358). Even then, the specificity inside each family tends to be rather low, with members of the same family acetylating the same targets (359). An example of this is the overlap of p300 and CBP regarding histone 3 acetylation, both acetylate H3K18 and H3K27 (360). On the other hand, both GCN5 and pCAF can acetylate H3K9 (359). This low specificity is very important to keep in mind when dissecting acetylation pathways. The current literature contains an over representation of the most active KATs (344), which could be the product of a more hypothesis-driven approach, instead of a systematic exploration of the topic.

Table 2. 1.- Identified human acetyltransferases classification and subcellular localisation

Family	Name	Location
GNAT	HAT1	Nucleus, cytoplasm
	GCN5	Nucleus
	PCAF	Nucleus
	ELP3	Nucleus, cytoplasm
	ATAT1	Cytoplasm
p300/CBP	CBP	Nucleus, cytoplasm
	P300	Nucleus, cytoplasm
MYST	TIP60	Nucleus, cytoplasm
	MOZ	Nucleus
	MORF	Nucleus
	HBO1	Nucleus
	MOF	Nucleus
Others	TAF1	Nucleus
	TFIIIC90	Nucleus
	NCOA1	Nucleus
	NCOA2	Nucleus
	NCOA3	Nucleus, cytoplasm
	CLOCK	Nucleus, cytoplasm
	ATF2	Nucleus, cytoplasm, mitochondria
	ACAT1	Mitochondria
	NAT10	Nucleus
	GCN5L1	Mitochondria

On the other hand, lysine deacetylases (KDACs) remove acetyl groups from acetylated lysines. The 18 reported KDACs can be classified functionally in two wide groups: Zn^{2+}-dependent and NAD^{+}-dependent. Looking at the sequence similarity, they can be separated in 5 different families: I, IIa, IIb, III and V (344). This grouping is mostly consistent with the location of their

members. Family I and IV are mostly nuclear, family IIb is mostly cytoplasmic and family IIa can shift between the two compartments. In addition, family III consists of the all the NAD^+-dependent Sirtuins, which can be localized in the nucleus, cytoplasm and, interestingly in mitochondria.

Table 2. 2.- Classification and localisation of human deacetylases

Class	Name	Location
I	HDAC1	Nucleus
	HDAC2	Nucleus
	HDAC3	Nucleus
	HDAC8	Nucleus, cytoplasm
IIA	HDAC4	Nucleus, cytoplasm
	HDAC5	Nucleus, cytoplasm
	HDAC7	Nucleus, cytoplasm
	HDAC9	Nucleus, cytoplasm
IIB	HDAC6	Cytoplasm
	HDAC10	Cytoplasm
III	SIRT1	Nucleus
	SIRT2	Cytoplasm
	SIRT3	Mitochondria
	SIRT4	Mitochondria
	SIRT5	Mitochondria
	SIRT6	Nucleus
	SIRT7	Nucleolus
IV	HDAC11	Nucleus

The last member of the acetylation system is composed by proteins with acetyl-sensing domains that can “read” if a target protein is acetylated. These domains are called bromodomains and consist in ≈120 amino acids forming small helical interactions (361). There are 46 identified proteins that carry bromodomains and they are predominantly in the nucleus, mostly binding to acetylated histone tails (362).

2. 6. 2.- Functions and processes

While extremely relevant for gene regulation and epigenetic control in the nucleus, acetylation is involved with processes throughout the cell. At a basic level, acetylation and ubiquitination can compete for the same lysine residues, thus regulating protein degradation. From enzyme activity regulation to wide epigenetic changes, acetylation is present at many major cellular events.

Acetylation in the nucleus

Starting at the nucleus, acetylation at histones generally destabilises the salt bridges between histone and DNA, making the chromatin less pack and more accessible for transcription (363). Transcriptional control is also exerted via acetylation of transcription factors, such as HSF1 acetylation, which prevents its binding to Hsp70 family promoters (364). When this acetylation is removed by Sirt1, the binding is restored. A similar mechanism can be found in the transcriptional control of p53-related genes (365). Lastly, acetylation of ATM by TIP60 activates it and promotes double strand break repair (DSBR), linking acetylation to DNA repair and aging (366). Not only in DSBR, but it is also involved in single base excision repair (367).

Acetylation in the cytoplasm

In the cytoplasm acetylation regulates a plethora of processes. One of the most investigated ones is the stabilization of α-tubulin via acetylation by αTAT1, which is in turn removed by HDAC6 (368,369). K40 acetylated tubulin has been shown to be more flexible and therefore more resistant to mechanical stresses (370). In addition, axonal vesicular transport along acetylated tubulin microtubules is impaired after αTAT1 depletion and can be partially rescued by silencing HDAC6 (371). The misregulation of tubulin acetylation has been linked with several neurodegenerative diseases such as Alzheimer's and Charcot Marie Tooth diseases (372,373). Another important role of acetylation is the activation of the CCR4-CAF1-NOT complex by acetylating CAF1a K200 and K206 by CBP/p300 (374). These modifications activate the complex and trigger the poly(A) RNA degradation that eventually leads to mRNA decay. Protein folding can be impaired by acetylation of HSP90, which prevents its association with p23. This modifications, which can be removed by HDAC6, causes a decrease in chaperone activity (375,376).

The intimate relation between acetylation and metabolism has been already suggested before, looking at its role in mitochondrial non-enzymatic acetylation. In addition to that, enzymatic acetylation can impact autophagy and mitochondrial fusion dynamics. Under starvation conditions, GSK phosphorylated TIP60, which in turn acetylated ULK1. Through this pathway, starvation can promote autophagy (377). At the same time, p300 acetylation of ATG5, ATG7 and LC3 acts as an inhibitor of autophagy (378). Lastly, it has been suggested that acetylation of MFN1 regulates its stability, specially under hypoxic conditions (379). These processes contrast with the seemingly homogeneous effect of non-enzymatic acetylation in mitochondria, which overall reduces enzymatic activity. The regulation of enzymatic acetylation by KAT and KDACs

partners offer a flexibility that does not exist in the non-enzymatic modality, hinting perhaps at a later evolutionary appearance of enzymatic acetylation.

Lastly, acetylation can modulate subcellular localisation of target proteins. An example of this can be seen in the acetylation of SKP2 nuclear localisation signal by p300, which prevents its nuclear import and keep SKP2 in the cytoplasm (380). This acetylation can be removed by Sirt3 in the mitochondria, after which SKP2 is transported into the nucleus via importin. Another interesting example is the acetylation of SNC5a voltage-gated sodium channel which promotes membrane localization in cardiac tissue (381).

Acetylation and neurodegeneration

Given the wide impact of acetylation in the cell, it is not surprising that several diseases, specially cancer and metabolic disorders, have been linked to acetylation (382,383). In the past decade, a link between neurodegeneration and acetylation has been stablished, both at a general acetylation signature and also at a molecular level in ALS, FTD and Alzheimer's disease.

When looking at the brain as a whole, aged mice brain expresses more HDAC2 and shows a hypoacetylation pattern, which as seen before, can lead to more heterochromatin and less protein expression (384,385). The relation between hypoacetylation and neurodegeneration has been also observed in mice models of Alzheimer's disease (386).

By far the strongest link between neurodegeneration and acetylation is the pathological acetylation of Tau in Alzheimer's disease. Initial reports showed that acetylation of tau contributed to the proteinopathy by preventing its degradation (87). It is acetylated by CBP, p300 and deacetylate by HDAC6 (88,387) and the double acetyl-mimic K174Q/K280Q displays a slower turn over and therefore a tendency to accumulate (88). However, the role of acetylation in Tau pathophysiology is more complicated. While acetylation at K164, K175, K180 and K260 slow protein turnover (87,388), acetylation at K321 and K369 seem to have the opposite effect, leading to less phosphorylated Tau and less aggregation (388,389). In addition, the interaction between acetylation and phosphorylation is not clear. The effect of Tau acetylation seems to be very much dependent on the specific lysine residue.

As mentioned before, acetylation at K145 of TDP-43 has been found in ALS patients aggregates and it has been directly linked with loss of RNA binding, phase separation and aggregation (249,253). In addition, KDAC inhibition in an ALS mouse model of FUS aggregation has been reported to slow the disease progression (390). As with Tau, the crosstalk between acetylation

and other PTMs is not yet clear, and the effect of additional acetylation sites has not been described yet.

2. 7.- Aims of the study

TDP-43 plays a pivotal role as the main component of intracellular inclusions in both ALS and FTD-TDP-43 and in other neurodegenerative disorders as well. It is not clear however how the aggregation mechanism starts and if TDP-43 is the cause of disease or an epiphenomenon of a yet to be described process.

The effect of TDP-43 mislocalization and aggregation: the toxicity caused by these events are the product of both toxic gain- and loss-of-function. It is not clear however what are the causes of the aggregation, specifically in certain neurons and apparently mutation-independent. TDP-43 posttranslational modifications (polyubiquitinated, phosphorylated, acetylated, PARylated, SUMOylated, among others) appear to play a role but there is a lack of insight into the context and significance of these modifications for the physiology and pathology of TDP-43.

To study TDP-43 PTMs, we identified modified residues first via a mass spectrometry analysis. The analysis of wild type TDP-43 allowed us to identify residues that could be modified under physiological conditions. To gather this data, 6xHis-tagged wtTDP-43 was expressed in HEK293E cells and later purified. The analysis of the purified TDP-43 revealed several possible ubiquitination residues, investigated by Hans et al. 2018(239). The analysis also indicated four acetylated lysine residues not described previously.

The main questions in this study were at first exploratory, looking at possible functions for these acetylations. Later, the focus was placed to the relevance of acetylation for TDP-43 phase separation and pathological aggregation, as well as the manipulation of the acetylation system to modulate the acetylation-driven aggregation of TDP-43.

3.- Materials and Methods

3. 1.- Chemicals and devices

All the chemicals used in this study were analytical grade. The provider is specified in the table below (Table 3.1). The devices used to acquire data and perform the experiments described are specified in Table 3.2.

Table 3. 1.- Chemicals used in this study.

Chemical	Provider
1,4-Dithiothreitol (DTT)	Carl Roth GmbH (Karslruhe, DE)
2-propanol	Merck KGaA (Darmstadt, DE)
40% Acrylamid/Bis-Acrylamid solution 19:1	Bio-Rad
Adenine hemisulphate	Sigma
Adenosine-triphosphate (ATP)	Biomol
Agar	Becton Dickinson
Agarose	Invitrogen
Ammonium persulfate (APS)	Sigma
Ampicillin (Sodium Salt)	Sigma
Bacto peptone	Becton Dickinson
Bafilomycin A1	Sigma
BCA Protein assay kit	Pierce Protein
BigDye Terminator v.3.1 kit	Applied Biosystems
Bovine Serum Albumin (BSA)	Roth
Bradford Reagent Kit	Bio-Rad
Collagen I	Cohesion
Dimethyl sulfoxide (DMSO)	Sigma
DNA ladder mix	Fermentas
dNTPs (dATP, dCTP, dGTP, dTTP)	Fermentas
Dulbecco's modified Eagle Medium (DMEM)	Biochrom
EX 527 (CAS 49843-98-3)	Santa Cruz Biotechnology
Ex Taq DNA polymerase	Takara
Foetal bovine serum (FBS)	PAA Laboratories
Fluorescence mounting medium	Dako
FuGene 6	Roche
GoTaq Polymerase Kit	Promega
HDAC inhibitor set I and II	Sigma
Hoechst33342	Molecular Probes
Hybond-P polyvinyllidene difluoride (PVDF) membrane	Millipore
Imidazole	Merck
Immobilon Western HRP Substrate	Millipore
Magnetic RNA Pulldown kit	Thermofisher
MG-132	Sigma

Midori green	Sigma
N,N,N',N'-Tetraacetylethylenediamine (TEMED)	Merck
Ni-NTA beads	Qiagen
Nitrocellulose membrane	GE Healthcare
Non-fat dried milk powder	Sucofin
Nonident P-40 (NP-40)	United States Biological
Normal Goat Serum (NGS)	Sigma
NuPage MES/MOPS SDS Running buffer 20x	Invitrogen
Nε-Acetyl-L-lysine	Sigma
Opti-MEM	Invitrogen
Penicillin sulphate 100x	Biochrom
Poly-D-lysine (PDL)	Sigma
Polyethylene glycol (PEG)	Sigma
Ponceau S solution	Sigma
Protease inhibitor (Complete)	Roche
Protein standard (Dual colour)	Bio-Rad
Puromycin	InvivoGen
QIAfilter plasmid Maxi/MidiPrep Kit	Qiagen
QIAquick gel extraction kit	Qiagen
QIAquick PCR Purification Kit	Qiagen
RNeasy RNA extraction Kit	Qiagen
Shrimp alkaline phosphatase (SAP)	Roche
Sodium azide (NaN3)	Sigma
Sodium dodecyl sulphate (SDS)	Sigma
Sodium pyrophosphate (NaPPi)	Sigma
Staurosporine (STS)	Sigma
Streptavidin-HRP coupled	Biomol
T4 DNA ligase kit	Fermentas
Transcriptor High Fidelity cDNA Synthesis Kit	Sigma
Triton-X-100	AppliChem
Tryptone/Peptone	Roth
Tween-20	Merck
Urea	Roth
Western Blocking Reagent	Roche
Yeast extract	Sigma
β-Mercaptoethanol	Roth

Table 3. 2.- Devices used in this study.

Device	Provider
ABI PRISM 3100	Thermofisher
Agarose gel chamber	Peqlab
Bio-Dot® SF Microfiltration apparatus	Bio-Rad
Biofuge Pico Heraeus	Kendro
Centrifuge 5810 R	Eppendorf
ChemiDoc XRS+ Imaging System	Bio-Rad
Eppendorf Thermomixer	Eppendorf
Gel documentation system	Vilber Lourmat
Hera safe cell culture hood	Heraeus
iMark Microplate Absorbance Reader	Bio-Rad
Innova 4200 Incubator Shaker	New Brunswick
Micro-Pulser	Bio-Rad
Mikro 220 R	Hettichlab
Mini Trans-Blot® Cell	Bio-Rad
Multifuge 3S-R	Kendro
NanoDrop™ 2000/2000c	Thermofisher
SDS-PAGE gel chamber (PerfectBlue Twin S)	Peqlab
Sequencer (ABI 3100 Genetic Analyzer)	Applied Biosystems
Spectrophotometer (Ultrospec 2100 Pro)	Leica
TC20 Automated Cell Counter	Bio-Rad
Thermal Cycler	Applied Biosystems
Trans-Blot® Cell	Bio-Rad
Unitron Incubator Shaker	Infors
Zeiss fluorescence microscope with Apotome attachment	Zeiss

3. 2.- Buffers and solutions

All the buffers and solutions used in this study are specified in the table below. Solutions were autoclaved when the process did not compromise the buffer properties.

Table 3. 3.- Buffers used in this study.

Buffer/ solution	Chemical composition
6x Laemmli buffer	325 mM Tris 9% SDS 50% glycerol 9% ß-mercaptoethanol 0.03% bromophenol blue pH 6.8, in H_2O
8M urea buffer	10mM Tris 100mM NaH_2PO_4 8M urea 10mM Imidazole pH 8.0, in H_2O

8M urea wash buffer	10mM Tris 100mM NaH_2PO_4 8M urea 20mM Imidazole pH 6.3, in H_2O
Blocking solution (Western blot)	5% non-fat milk powder in TBST
Buffer S1	0.25M Sucrose 10mM $MgCl_2$ 1x EDTA-free Complete proteinase inhibitor, in H_2O
Buffer S3	0.88M Sucrose 10mM $MgCl_2$ 1x EDTA-free Complete proteinase inhibitor, in H_2O
Hypotonic buffer A	10mM HEPES 1.5 mM $MgCl_2$ 10 mM KCl 0.1 mM DTT 1x EDTA-free Complete proteinase inhibitor pH 7.6
LB medium	1% tryptone 0.5% yeast extract 0.5% NaCl, in H_2O
LB medium plates	LB medium 1.2% agar
LB medium plates with antibiotics	LB plates 100µg/ml ampicillin
Native Ni-NTA elution buffer	10mM Tris 100mM NaH2PO4 300mM NaCl 300mM Imidazol pH 8.0
Native Ni-NTA lysis buffer	10mM Tris 100mM NaH2PO4 300mM NaCl 10mM Imidazol pH 8.0
Native Ni-NTA wash buffer	10mM Tris 100mM NaH2PO4 300mM NaCl 20mM Imidazol pH 8.0
NP-40 buffer	50mM NaH_2PO_4 300mM NaCl 1% NP-40 pH 8.0, in H_2O
NuPAGE Transfer buffer (20x)	25 mM Bicine 25 mM Bis-Tris 1 mM EDTA pH 7.2, in H_2O
Phosphate buffered saline (PBS)	2.2mM KH_2PO_4 7.8mM Na_2HPO_4 150mM NaCl pH 7.4, in H_2O
Primary antibody solution	5% Western Blocking Reagent 0.02% NaN_3, in TBS
RIPA buffer	50mM Tris/HCl 150mM NaCl 1% NP-40 0.5% deoxycholate 0.1% SDS

	10mM NaPPi pH 8.0, in H_2O
RNA binding buffer	10mM HEPES 1 mM MgCl2 20 mM KCl 1 mM DTT 5% Glycerol pH 7.6
SDS-PAGE running buffer	25mM Tris 192mM glycine, in H_2O
SDS-PAGE separating gel buffer	1.5M Tris 0.4% SDS pH 8.8, in H_2O
SDS-PAGE stacking gel buffer	0.5M Tris 0.4% SDS pH 6.8, in H_2O
Secondary antibody solution	5% non-fat milk powder in TBST
TBST	TBS 0.1% Tween-20
Transfer buffer	25mM Tris 192mM glycine 20% Methanol, in H_2O
Tris borate buffer	9mM Tris 9mM Boric acid 2mM EDTA, in H_2O
Tris buffered saline (TBS)	50mM Tris pH 7.4 150mM NaCl, in H_2O

3. 3.- Molecular biology

3. 3. 1.- Generation of electro-competent bacteria

10ml of antibiotic-free LB medium was inoculated with DH5α and incubated at 37°C overnight with shaking. Next day, the overnight culture was added to 500ml LB medium and was incubated at 37°C with shaking until an optical density at 600nm of 0.7 was reached. Next, bacteria were pelleted at 4000g for 20 minutes at 4°C. The pellet was then washed several times with decreasing amounts ice-cold water (3x500ml, 1x250ml, 1x125ml and 1x50ml). The remaining pellet was resuspended in 10% glycerol and aliquots of 50µl were snapped frozen in liquid nitrogen.

3. 3. 2.- Molecular cloning

All the backbone plasmids used in this study plus the constructs that were used but not generated in this study are in in table 5.4. pcDNA3.1(-) wtTDP-43 was generated previously by F. Fiesel. TDP-43 was amplified by polymerase chain reaction (PCR) with ExTaq and specific

primers, which added restriction sites for the desired enzymes (shown in table 3.5). All cloning PCRs were done using a proofreading ExTaq polymerase. When the desired tag was not present in the vector, it was included in the outer primers. For point mutagenesis a two-step process was followed. The first step consisted in two separate PCRs: one from the 5' end to the mutation site, and another one from the mutation site to the end of the protein. Primers at both ends introduced restriction sites for the desired enzymes, while internal primers introduced the base substitution. In the second step, a PCR reaction was prepared with the two products obtained in the first step and the outer primers. The resulting products was a full sequence with the point mutation added. After each step products were purified from primers and enzymes via a 0.75 - 1.5% agarose gel purification. The DNA was stained using Midori green and visualized with UV illumination. The bands to be purified were excised and purified with a Gel Extraction Kit from Qiagen following the manufacturer instructions. The purified segments and the receptor plasmid were digested with restriction enzymes (Fermentas) and the backbone was dephosphorylated using a Shrimp Alkaline Phosphatase (SAP) for 10 minutes, at 37°C. The ligation was prepared by mixing both digested PCR product and dephosphorylated plasmid in a relation of 3:1 molar excess of insert to vector. The ligation reaction was incubated at overnight at 4°C.

The generation of the amber suppression plasmids E400 and E406 is described in Elsässer et al. 2016 (391), pcDNA3.1 wtTDP-43 in Fiesel (2010) and E451 in Bryson et al. (392). All Sirt1 plasmids were ordered from Addgene and were characterised in North et al. (393) (RRID: Addgene_13812, RRID: Addgene_13813, RRID: Addgene_13814, RRID: Addgene_13815, RRID: Addgene_13816, RRID: Addgene_13817, RRID: Addgene_13818). Plasmids encoding for HDAC1 and HDAC6 were characterised in Fiesel et al. (146). Plasmid encoding for HDAC2 was characterised by Reyon et al. 2012 (394). Plasmid encoding for HDAC3 was characterised by Emiliani et al. (395). Plasmids encoding for HDAC4, 5, 7 and 8 were characterised by Fischle et al. (396). Plasmids for HDAC2-5, 7 and 8 were ordered from Addgene (RRID: Addgene_36829, RRID: Addgene_13819, RRID: Addgene_13821, RRID: Addgene_13822, RRID: Addgene_13824).

Table 3. 4.- Vectors used in this study. *Vectors that were used but not generated in this thesis with their respective characterization study.*

Vector	Tag	Reference
pcDNA3.1(-)	-	Invitrogen
pcDNA3.1(-)	5'-3xFlag	Fiesel et al. 2010
pCMV-6xHis	5'-6xHis	Clontech
pcDNA3.1 (-) TDP-43	-	F. Fiesel
pCMV-Myc	5'-Myc	Clontech
pEGFP-C1	5'-EGFP	Clontech

E400	-	Elsasser et al. 2016
E406	-	Elsasser et al. 2016
E451	5'-3xFlag	Bryson et al. 2017
pCMV-Sirt1	3'-3xFlag	North et al. 2003
pCMV-Sirt2	3'-3xFlag	North et al. 2003
pCMV-Sirt3	3'-3xFlag	North et al. 2003
pCMV-Sirt4	3'-3xFlag	North et al. 2003
pCMV-Sirt5	3'-3xFlag	North et al. 2003
pCMV-Sirt6	3'-3xFlag	North et al. 2003
pCMV-Sirt7	3'-3xFlag	North et al. 2003
pCMV-HDAC1	5'-Myc	F. Fiesel
pCMV-HDAC1 H141A	5'-Myc	F. Fiesel
pCMV-HDAC2	3'-3xFlag	Reyon et al. 2012
pCMV-HDAC3	3'-3xFlag	Emiliani et al. 1998
pCMV-HDAC4	3'-3xFlag	Fischle et al. 1999
pCMV-HDAC5	3'-3xFlag	Fischle et al. 1999
pCMV-HDAC6	5'-Myc	Fiesel et al. 2010
pCMV-HDAC6 H216A	5'-Myc	S. Horn
pCMV-HDAC7	3'-3xFlag	Fischle et al. 1999
pCMV-HDAC8	3'-3xFlag	Fischle et al. 1999
pTB CFTR Exon9		Buratti et al. 2001

Table 3. 5.- Mutagenesis and cloning primers used in this study.

Primer	**Sequence** (5'-3')
TDP-43ΔGRD NotI reverse	CCCCGCGGCCGCCTAACTTCTTTCTAACTGTCTATTGCTATTG
TDP-43 6xHis BamHI reverse	CAGCGGCCGCGGATCCTTAATGGTGATGGTGATGATGCATTCCCCAGCCAGAAG
TDP-43 6xHis NheI forward	GCTAGCCATCATCACCATCACCATATGTCTGAATATATTC
TDP-43 BamHI forward	GGGGGGATCCGATGTCTGAATATATTCGGGTAACC
TDP-43 Bsp120 forward	GGGGGGGCCCACCATGTCTGAATATATTCGGGTAACCG
TDP-43 HindIII reverse	CCCCAAGCTTCTACATTCCCCAGCCAGAAG
TDP-43 NheI forward	CTACTCTAGAGCTAGCATGTCTGAATATATT
TDP-43 NotI reverse	CCCCGCGGCCGCCTACATTCCCCAGCCAGAAG
TDP-43 SalI forward	GGGGTCGACGATGTCTGAATATATTCGGGTAACCG
TDP-43 K79Q forward	GTCAACTATCCACAAGATAACAAAAGAAAAATG
TDP-43 K79Q reverse	CATTTTTCTTTTGTTATCTTGTGGATAGTTGAC
TDP-43 K79R forward	GTCAACTATCCAAGAGATAACAAAAGAAAAATG
TDP-43 K79R reverse	CATTTTTCTTTTGTTATCTCTTGGATAGTTGAC
TDP-43 K84Q forward	GATAACAAAAGACAAATGGATGAGACAG
TDP-43 K84Q reverse	CTGTCTCATCCATTTGTCTTTTGTTATC
TDP-43 K84R forward	CCAAAAGATAACAAAAGAAGAATGGATGAGACAG
TDP-43 K84R reverse	CTGTCTCATCCATTCTTCTTTTGTTATCTTTTGG
TDP-43 K121Q forward	CCGAACAGGACCTGCAAGAGTATTTTAGTAC
TDP-43 K121Q reverse	GTACTAAAATACTCTTGCAGGTCCTGTTCGG
TDP-43 K121R forward	CCGAACAGGACCTGAGAGAGTATTTTAGTAC
TDP-43 K121R reverse	GTACTAAAATACTCTCTCAGGTCCTGTTCGG

TDP-43 K136Q forward	GGTGCAGGTCCAGAAAGATCTTAAGACTGG
TDP-43 K136Q reverse	CCAGTCTTAAGATCTTTCTGGACCTGCACC
TDP-43 K136R forward	GGTGCAGGTCAGGAAAGATCTTAAGACTGG
TDP-43 K136R reverse	CCAGTCTTAAGATCTTTCCTGACCTGCACC
TDP-43 K145Q forward	GACTGGTCATTCACAGGGGTTTGGCTTTG
TDP-43 K145Q reverse	CAAAGCCAAACCCCTGTGAATGACCAGTC
TDP-43 K145R forward	GACTGGTCATTCAAGGGGGTTTGGCTTTG
TDP-43 K145R reverse	CAAAGCCAAACCCCCTTGAATGACCAGTC
TDP-43 K79TAG forward	GTTGTCAACTATCCATAGGATAACAAAAGAAAA
TDP-43 K79TAG reverse	TTTTCTTTTGTTATCCTATGGATAGTTGACAAC
TDP-43 K84TAG forward	CCAAAAGATAACAAAAGATAGATGGATGAGACAGAT
TDP-43 K84TAG reverse	ATCTGTCTCATCCATCTATCTTTTGTTATCTTTTGG
TDP-43 Q118TAG forward	CAACCGAATAGGACCTGAAAGA
TDP-43 Q118TAG reverse	TCTTTCAGGTCCTATTCGGTTG
TDP-43 K121TAG forward	GAACAGGACCTGTAGGAGTATTTTAGTA
TDP-43 K121TAG reverse	TACTAAAATACTCCTACAGGTCCTGTTC
TDP-43 K136TAG forward	CTTATGGTGCAGGTCTAGAAAGATCTTAAGACT
TDP-43 K136TAG reverse	AGTCTTAAGATCTTTCTAGACCTGCACCATAAG

3. 3. 3.- Transformation of *E. coli*

Ligation products were transformed into electrocompetent bacteria via electroporation using 0.2 mm electroporation cuvettes and a Micropulser electroporation device (Bio-Rad). The transformed bacteria were incubated for 1 hour at 37°C with antibiotic-free LB medium before plating on Ampicillin or kanamycin agar plates, depending on the selection gene encoded by the plasmid. Plates wee incubated overnight at 37°C. Next day, bacterial colonies were screened for inserts in a colony PCR using Go-Taq polymerase (Promega).

3. 3. 4.- Amplification and sequencing of plasmid DNA

The positive clones from the colony PCR were inoculated in 6ml ampicillin or kanamycin-containing LB medium and incubated overnight in a shaker at 37°C. Next day, bacteria were pelleted for 1 minute at 12000g at 4°C. Plasmid DNA isolation was performed with a Qiagen Spin Miniprep kit (Qiagen) following manufacturer's indications. DNA was resuspended in 30µl of RNAse-free water and its concentration was calculated with a Nanodrop 2000/2000c (Thermofisher), at 260nm. Constructs' sequences were analysed by using a BigDye terminator kit (Applied Biosystems) in combination with an ABI 3100 Genetic Analyser (Applied Biosystems). Sequences were analysed using Benchling web services (www.benchling.com). List of sequencing primers can be found in table 5.6.

The colonies containing validates plasmids were inoculated in 50 or 200ml, for Midi- or Maxiprep respectively, selection LB media and incubated overnight with shaking, at 37°C. Next day, bacteria were pelleted at 12000g for 10 minutes at 4°C. Plasmid DNA was then extracted using a Midi- or Maxiprep according to manufacturer's instructions. After the plasmid DNA was purified, DNA pellet was resuspended in 100 or 400µl (for Midi- or Maxiprep) of RNAse-free water and its concentration was analysed using a Nanodrop 2000/2000c.

Table 3. 6.- Sequencing and RT-PCR primers used in this study.

Primer	Sequence
Actin forward	TGACCCAGATCATGTTTGAGAC
Actin reverse	GAGGTAGTCTGTCAGGTCCC
BGH reverse	TAGAAGGCACAGTCGAGG
EGFP forward	ACGGCAACATCCTGGGG
pCMV backbone forward	GATCCGGTACTAGAGGAACTGA
pCMV backbone reverse	GCAATAGCATCACAAATTTCAC
T7 forward	TAATACGACTCACTATAGGG
TDP-43 255 forward	GGATGAGACAGATGCTTCATCAGCAG
TDP-43 390 reverse	ACGGATGTTTTCTGGACT
TDP-43 558 forward	GCCTTTGAGAAGCAGAAAAGTG
TDP-43 558 reverse	CACTTTTCTGCTTCTCAAAGGC
TDP-43 1011 forward	GGGCATGTTAGCCAGCC
pTB CFTR forward	CAACTTCAAGCTCCTAAGCCACT
pTB CFTR reverse	TAGGATTCCGGTCACCAGGAAGTTGGTTAAATCA

3. 3. 5.- RNA extraction and RT-PCR

mRNA levels were measured via reverse transcription and PCR. RNA was extracted from cells by lysing a confluent 6-well plate well in 100µl of RNeasy lysis buffer and RNA purification was performed with RNeasy spin columns according to manufacturer's instructions for cells. 600ng of RNA were used as template for the RT-PCR. The reverse transcription was done using anchored oligo-dT primers which ensured the transcription only of mRNA. The reaction was done using a Transcriptor High Fidelity cDNA Synthesis kit (Roche). The resulting DNA was diluted 1:10 and used as a template for the next PCR. The PCR was prepared with 17.9µl of diluted DNA, 5µl 5x Green GoTaq buffer, 0.1µl GoTaq polymerase and 2mM of target-specific primers, which can be found in table 5.6. The PCR product was analysed in a 2% agarose TBE gel, and the DNA was visualized with Midori green in a UV gel documentation chamber (Vilber Lourmat).

3. 4.- Cell culture

3. 4. 1.- Maintenance of cells

Human embryonic kidney HEK293E (Invitrogen) cells were grown in humidified conditions with 5% CO_2, at 37°C. Cells were maintained in Dulbecco's modified eagle medium (DMEM) supplemented with 10% foetal bovine serum (FBS). Cells were split every 3-4 days, making a 1:10 dilution. $Sh^{TDP\text{-}43}$-HEK293E and stably amber suppressed HEK293E were maintained in the same conditions. For experiments, cells were seeded at different concentrations based on the experiments and the plate surface. $Sh^{TDP\text{-}43}$-HEK293E cells were generated and characterised by F. Fiesel (146).

3. 4. 2.- Freezing and long-term storage of cells

Cells were subcultured up to 30 passages after thawing and were then discarded and replaced with newly thawed cells to prevent strong genetic alterations. For the long-term storage of cells, cells were pelleted and washed once with 37°C PBS. Then, cells were resuspended in a 10% DMSO in FBS and aliquoted in cryovials. The vials were frozen at a rate of 1°C per minute until they reached -80°C, at which point they were transferred to liquid nitrogen storage.

3. 4. 3.- DNA transient transfection of cells

HEK293E cells were transfected 24 hours after plating, at approximately 50% of confluence. The transfection was done using FuGene6 transfection reagent according to manufacturer's instructions. The desired plasmid or plasmids were mixed with the transfection reagent in a FuGene6:DNA ratio of 3:1, diluted in OptiMem and incubated for 20 minutes at room temperature. For experiments dealing with amber suppression, the ratio of FuGene:DNA was 4.5:1. After the incubation, the mixture was spread onto the cells dropwise. The expression of the transfected plasmids was analysed 48-72 hours after transfection.

3. 4. 4.- Generation of stably amber suppressed HEK293E cells

The integration of the amber suppression elements (Flag-tagged AcKRS and $4xtRNA_{AcK}^{UAG}$) was done in $sh^{TDP\text{-}43}$-HEK293E cells using the E451 plasmid (encoding, in addition to the amber suppression elements, for a puromycin resistance gene) and the PiggyBac recombinase system (Systems Biosciences). Cells were seeded in a 6-well plate and grown for 24 hours. After that, a mix of both E451 and Piggybac recombinase plasmids were transfected using FuGene6, in a 4.5:1

Fugene6:DNA ratio. 48 hours after transfection the media was changed to DMEM +10%FBS with 0.5µg/ml Puromycin. After 4 days, the media was removed, and the bottom of the plate was carefully washed with PBS at 37°C. The remaining attached cells were transferred to a T75 flask with DMEM +10% FBS with 0.5µg/ml Puromycin. After four days, cells were tested for amber suppression and AcKR expression in both Western blot and immunofluorescence. The resulting pool of cells were frozen, establishing a pool of stably amber suppressed cells.

During the generation of the original $sh^{TDP\text{-}43}$-HEK293E, an EGFP tag was introduced as means of selection. Its presence was taken advantage for the generation of clonal lines of amber suppressed cells. HEK293E from the amber suppressed pool were plated in a 10cm dish in absence of puromycin and grown until reaching confluency. Then, single cells were seeded into 96-well plates wells using a Fluorescence Assisted Cell Sorting device. After the seeding, cells were checked daily and the confluent wells were split into 48-well, 24-well and 6-well plate progressively. Single clones were tested for amber suppression and successful clones were frozen and kept in liquid nitrogen at -180°C.

3. 4. 5.- Live cell imaging

HEK293E cells were plated on glass bottom chambered slides coated with poly-D-Lysine (PDL). After 24 hours, cells were transfected with C-terminally EGFP-tagged wtTDP-43 or K136Q TDP-43. Cells were imaged 24-48 hours after transfection, while kept in a temperature-controlled chamber at 37°C and 5% CO_2. Imaging was done with an Axio observer Z1 microscope in intervals of 1 to 10 minutes during up to 6 hours.

3. 4. 6.- Fluorescence recovery after photobleaching (FRAP) measurement

Cells were plated on glass bottom chambered slides coated with PDL and like in the case of Live Cell experiments, were transfected 24 hours later with EGFP C-terminally tagged wtTDP-43 and K136Q TDP-43. Imaging and photobleaching was done with a Zeiss LSM510 Meta confocal microscope using a x63/1.4 oil objective. ROIs were determined manually and were bleached for 1s using a 405nm and a 488nm laser at variable power output. Cells were recorded for 3 minutes after bleaching. Reference ROIs were measured in non-bleached cells and were used to correct the photobleaching caused by the fluorescent imaging.

3. 5.- Protein biochemistry

3. 5. 1.- Preparation of cell lysates for Western blot

Cell media and dead cells were removed, and cells were harvested in ice-cold PBS. Then, cells were pelleted at a slow spin of 1400 rpm for 5 minutes in a prechilled centrifuge at 4°C. PBS was discarded and the pellet was washed twice more with ice-cold PBS. Washed pellets were then lysed with different volumes of urea buffer according to the size of the pellet and the DNA was sheared by passing the lysate through a 23g needle 30 times. The remaining cell debris were pelleted by spinning the samples at 18000rpm for 15 minutes at 4°C. The remaining supernatant was transfer to a new, clean vessel and protein concentration was determined with a Bradford Protein assay kit (Bio-Rad). 10µg of protein was then diluted in urea buffer and 3xLaemmli buffer to ensure the same concentration and volume across samples. Samples were boiled at 95°C for 10 minutes and analysed via Western blot.

3. 5. 2.- Solubility fractionation

Washed HEK293E cell pellets from confluent 10cm plates were lysed in RIPA buffer with proteinase inhibitor cocktail Complete for 20 minutes on ice. DNA was sheared by passing the lysate 30 times through a 23-gauge needle. The RIPA-insoluble material was then pelleted at 18000rpm for 15 minutes at 4°C, and the resulting supernatant was then transferred to a new vessel. The remaining pellet was then lysed in urea lysis buffer and the insoluble cell debris was pelleted by spinning the samples at 18000rpm for 15 minutes at 4°C. The supernatant was then transferred to a new Eppendorf tube. The protein concentration of the RIPA fraction was determined using a BCA Protein assay kit (Bio-Rad) and the urea fraction concentration using a Bradford Protein assay kit. 10µg of protein were diluted in their respective buffers and 3x Laemmli and boiled for 10 minutes at 95°C. Samples were then analysed by Western blot.

3. 5. 3.- Nuclear-cytoplasmic fractionation

Washed HEK293E cell pellets from confluent 10cm plates were resuspended in 500µl of hypotonic buffer A and incubated on ice for 5 minutes. Then cell membranes were burst with 20 strokes in an ice-cold Dounce homogenisator and the resulting samples were centrifuged at 1500rpm for 5 minutes at 4°C. 250µl of the supernatant, the cytosolic fraction, was transferred to a new vessel and the remaining supernatant was discarded. The remaining pellet contained the nuclei and residual cytoplasmic proteins. This nuclear fraction was washed twice with hypotonic buffer A and then was resuspended in 500 µl S1 buffer. It was then layered carefully

over 500µl S3 buffer and samples were then spin at 10000rpm, for 10 minutes at 4°C. The supernatant was then discarded, and the remaining pellet was then lysed with urea buffer, DNA was sheared, and insoluble material was pelleted by spinning the samples at 18000rpm for 15 minutes at 4°C. Remaining supernatant were analysed via Western blot. On the other hand, the saved cytosolic fraction was lysed by adding 62.5µl 5x RIPA buffer and incubating for 10 minutes on ice. The RIPA insoluble material was the pelleted by spinning the samples at 18000rpm for 15 minutes at 4°C. The remaining supernatant was transferred to a new Eppendorf tube and analysed via Western blot.

3. 5. 4.- Pulldown of 6xHis tagged proteins

HEK293E washed pellets from 10cm plates were lysed in 1ml Urea lysis buffer with 10mM Imidazole and the DNA was sheared by passing the lysate 30 times through a 23-gauge needle. The insoluble cell debris was pelleted by centrifugating the samples at 18000rpm for 15 minutes at 4°C. The supernatant was transferred to a clean vessel and the protein concentration was assessed with a Bradford protein assay kit. 500-1000µg of protein were incubated with 30µl of Ni-NTA agarose beads (Qiagen) in a spinning wheel overnight at 4°C. The beads were then washed 3 times with Urea washed buffer with 20mM Imidazole, spinning them for 1 minute at 10000rpm between washes. Later, the proteins were eluted by adding 50-100µl 3x Laemmli buffer and boiling them for 15 minutes at 95°C shaking at 1000rpm. The beads were then centrifuged at 10000 rpm for 1 minute and the supernatant was transferred to a new vessel. 10µg of total lysates and 10µl of eluted proteins were analysed via Western blot.

3. 5. 5.- RNA-protein pulldown

HPLC RNA oligonucleotides 5'-$(UG)_{12}$-3' and 5'-$(UC)_{12}$-3' were ordered from Sigma Aldrich. Oligomers were biotinylated using a Pierce RNA 3' End Desthiobiotinylation kit, with small variations. For each 1nmol of biotinylated cytidine bisphosphate 100pmol of RNA were added to the biotinylation reaction. The biotinylated nucleotides were purified using a chloroform:isoamyl mixture. The RNA-protein pulldown was performed using a Pierce Magnetic RNA-protein pulldown kit with small variations. Washed HEK293E cell pellets were lysed in ice-cold NP-40 buffer and insoluble material was pelleted by a centrifugation step at 18000rpm for 15 minutes at 4°C. Protein concentration was assessed using a BCA protein assay kit and 400µg of protein was used for each RNA-binding reaction. After a 1-hour incubation at room temperature, proteins were eluted in 25µl 3xLaemmli buffer. 10 µg of total lysate and 10µl of pulldown material was analysed via Western blot.

3. 5. 6.- Native protein pulldown and filter binding assay

Washed HEK293E cell pellets from 10cm plates were lysed in ice-cold Native Ni-NTA lysis buffer with 10mM Imidazole for 30 minutes on ice. Insoluble material was pelleted at 18000rpm for 15 minutes at 4°C and the remaining supernatant was transferred to a new vessel. Protein concentration was determined using a BCA protein assay kit. 500-800µg protein was incubated with 30µl Ni-NTA agarose beads overnight at 4°C. Next day, beads were washed thrice with Native Ni-NTA wash buffer with 20mM Imidazole and, after washing, proteins were eluted by incubating the beads in Binding buffer containing 300mM imidazole for 30 minutes rotating at 4°C. Beads were pelleted at 10000 rpm for 1 minute and supernatant was transferred to a new vessel. Different concentrations of purified protein were incubated with 2nM biotinylated 5'-$(UG)^{12}$-3' RNA oligomers for 30 minutes at room temperature. The resulting complexes were run through a Bio-Dot® SF Microfiltration apparatus loaded with a nitrocellulose membrane on top of a positively charged nylon membrane. After the samples run through both membranes, the membranes were crosslinked at 120J/$m^{2,}$ and biotinylated RNA was visualized using a Chemiluminescent Nucleic Acid Detection module kit according to the manufacturer's instructions.

3. 5. 7.- Western blot analysis

Samples were separated in self-casted SDS-polyacrylamide gels (7.5%, 10%, 12.5% or 15%) or 4-12% Bis-Tris NuPAGE gradient gels (Invitrogen). Gels were run at 100V in running buffer until the sample reached the bottom of the gel. Proteins were then wet-transferred to Hybond-P polyvinylidene difluoride (PVDF) membrane (Millipore) using transfer buffer, for 2:30 hours at 4°C. Membranes were then blocked with 5% Non-fat milk in TBS-T or 5%BSA in TBS-T for one hour at room temperature with gentle shaking. Next, membranes were incubated with primary antibody in primary antibody solution for 2 hours at room temperature or overnight at 4°C. Membranes were then washed 5 times with TBS-T and incubated with HRP-coupled secondary antibody in 5% Non-fat milk in TBS-T for 1 hour at room temperature. Membranes were then washed 5 times with TBS-T and proteins were visualised with the Immobilon Western chemiluminescent HRP substrate (Millipore) in a ChemiDoc XRS+ Imaging System (Bio-Rad).

Table 3. 7.- Primary antibodies used in this study.

Antibody	Company	Cat. N°	Sp	[] WB	[] IF
6xHis	Amersham	27-4710-01	Ms	1:10000	1:1000
AcetylK	Cell Signalling	9441	Rb	1:1000	
AcetylK	Cell Signalling	9814	Rb	1:1000	

Acetyl-Tubulin	Sigma	T6793	Ms	1:10000	1:5000
Actin	Sigma	A 5441	Ms	1:5000	
Coilin	BD Biosciences	612074	Ms		1:500
Dendra	Antibodies-Online	ABIN361314	Rb	1:1000	1:500
eIF3η	Santa Cruz	sc-16377	Gt		1:500
ERK	Cell Signalling	4695	Rb	1:1000	
Flag-HRP	Sigma	A8592	Ms	1:10000	
GAPDH	Biodesign International	H86504M	Ms	1:50000	
Hsp90	Cell Signalling	4874	Rb	1:1000	
myc	Sigma	11667149001	Ms	1:10000	1:500
p54nrb	BD Biosciences	611278	Ms		1:500
PARP	Cell Signalling	9542	Rb	1:2000	
phospho-p44/42 (Thr202/Tyr204)	Cell Signalling	4370	Rb	1:2000	
p-PERK (H-300)	Santa Cruz	sc-13073	Rb	1:4000	
pTDP43	M. Neumann	-	Rt	1:10	1:50
SC35	Sigma	S4045	Ms		1:5000
SMN	BD Biosciences	610646	Ms		1:5000
TDP-43	ProteinTech group	BC001487	Rb	1:8000	1:1000
TDP-43	Abnova	H00023435	Ms	1:2000	1:1000
TIAR	Cell Signalling	8509	Rb		1:500
Tubulin	Sigma	T-5168	Ms	1:10000	
Ubiquitin	Millipore	MAB1510	Ms	1:4000	
Ubiquitin	Millipore	MAB1510	Ms	1:1000	
YY1	Santa Cruz Biotechnology	sc-7341	Ms	1:2000	
β-actin	Sigma	A5441	Ms	1:50000	
hnRNPA1	Cell Signalling	5380	Rb	1:2000	

Table 3. 8.- Secondary antibodies used in this study.

Antibody	Company	Sp	[] WB	[] IF
anti-mouse-HRP	Jackson Immunoresearch	Donkey	1:10000	
anti-rabbit-HRP	Jackson Immunoresearch	Donkey	1:10000	
anti-rat-HRP	Jackson Immunoresearch	Donkey	1:10000	
anti-goat-HRP	Jackson Immunoresearch	Donkey	1:10000	
anti-rabbit-Alexa Fluor 488	Invitrogen	Goat		1:1000
anti-mouse-Alexa Fluor 488	Invitrogen	Goat		1:1000
anti-rat-Alexa Fluor 488	Invitrogen	Goat		1:1000
anti-rabbit-Alexa Fluor 568	Invitrogen	Goat		1:1000
anti-mouse-Alexa Fluor 568	Invitrogen	Goat		1:1000
anti-rat-Alexa Fluor 568	Invitrogen	Goat		1:1000
anti-rabbit-Alexa Fluor 647	Invitrogen	Goat		1:1000
anti-mouse-Alexa Fluor 647	Invitrogen	Goat		1:1000
anti-rat-Alexa Fluor 647	Invitrogen	Goat		1:1000

3. 5. 8.- Cell immunofluorescence

For immunofluorescence preparation of cells, HEK293E cells were plated in 24-well plates onto glass coverslips coated with poly-D-lysine and Collagen I. Cells were transfected 24 hours after seeding and they were fixed 72-96 hours after seeding. Cell media was removed, and cells were carefully washed with 37°C PBS. Then, cells were fixed in a 4% PFA in PBS solution for 25 minutes at room temperature, after which cells were washed thrice with PBS. After that, coverslips were incubated in 1% Triton-X-100 in PBS solution for 5 minutes at room temperature and then they were washed thrice with PBS. For the blocking, a 10% Normal Goat Serum in PBS solution was used for 1 hour at room temperature. The primary antibody incubation was done performed in 1% BSA in PBS solution for 2 hours at room temperature. Then, coverslips were washed thrice in PBS and the secondary antibody solution was added in 1% BSA in PBS solution. The secondary incubation was 2 hours long at room temperature. The nuclei were stained with Hoechst 33342 (2µg/ml/PBS) for 10min at room temperature and then coverslips were mounted on to microscope slides with Dako mounting media. Cells were analysed an ApoTome Imaging system (Axio imager z1 stand).

3. 6.- Statistical analysis

Graphical representations of TDP-43 mutants and acetylated forms was made with Pymol (version 2.4.0). Post translational modifications were modulated using the PyTMs plugin by Warnecke et al (397). Microscopy images were quantified using CellProfiler 4.1.3. Western blots and DNA gels were quantified using ImageJ 1.53. Statistical significance was calculated using Microsoft Excel 2016. P values below 0.01 were considered significant. Unpaired t-tests were performed to compare two variables and assess significance. Chi-squared test was used to assess significance in the immunofluorescence experiments.

4.- Results

4. 1.- Identification and validation of novel posttranslationally modified residues of TDP-43

At the beginning of this study, TDP-43 phosphorylation, hyper ubiquitination and proteolytic cleavage were the most studied posttranslational modifications of TDP-43. In addition, there were studies on the effect of cysteine oxidation on TDP-43 aggregation(254) and one study looking at TDP-43 acetylation (249). In order to confirm previous results and get further insight into the residues that were ubiquitinated and acetylated a mass spectrometry analysis of TDP-43 was performed in the laboratory by Dr. Hans and Dr. Gloeckner. The results of the ubiquitination analysis can be found in the literature(239). Due to the relevance of this data for this thesis, its acquisition will be described in this section.

4. 1. 1.- Mass spectrometry and *in silico* analysis of TDP-43

To achieve highly purified TDP-43, HEK293E cells were transfected with wtTDP-43 with either a C-terminal or an N-terminal 6xHis tag. To access both soluble and insoluble material, cells were lysed in urea buffer. Additionally, cells were treated with MG-132 for 6 hours prior to lysis, a proteasomal inhibitor, to increase the signal of proteasomal-targeted TDP-43. Control cells were treated with DMSO. After lysis, 6xHis tagged TDP-43 was purified via Ni-NTA chromatography and analysed in an SDS-gel stained with Coomassie Brilliant Blue. The bands corresponding to monomers of TDP-43 and the combination of all heavy weight species were analysed independently via LC-MS/MS. In total, 8 samples were analysed: 2 differently 6xHis tagged TDP-43 constructs (N- or C-terminal), each under 2 different conditions (DMSO or 6 hours of MG-132), each condition with a monomer band and the heavy weight smear.

Table 4. 1.- TDP-43 acetylated lysines found via mass spectrometry analysis. N- terminally or C-terminally tagged 6xHis TDP-43 were overexpressed in HEK293E treated with either DMSO or MG-132 for 6 hours. TDP-43 was purified via Ni-NTA and analysed in an SDS-PAGE gel. High molecular weight (HMW) smear and monomeric TDP-43 were analysed independently via LC-MS/MS. The coverage of TDP-43 amino acid sequence for the N-terminal 6xHis TDP-

43 were 45%,46%, 52% and 60%, respectively. For the C-terminal constructs the coverages were 44%, 83%, 62% and 72%.

Sample	DMSO		MG-132	
	HMW smear	Monomer	HMW smear	Monomer
6xHis-TDP-43	-	K84	K84, K121	K84, K121
TDP-43-6xHis	K84	K84, K136	K84	K79, K84, K136

Four acetylated lysines were identified confidently: K79, K84, K121 and K136 (Table 3.1). The treatment with MG-132 stabilised acetylation at K121 and at K79 but had no effect on K84 or K136 acetylation. K136 acetylation was only detected in the monomer form and not in the high molecular weight smear. It is worth noting that both K79 and K84 are located at the NLS, while K121 and K136 are located in the RRM1 (Figure 4.1). Unfortunately, the previously identified acetylation at K145 could not be confirmed. This could be due to the differences in the methodological approach, namely different cell lines (QBI-293 vs HEK293E), different TDP-43 constructs (ΔNLS TDP-43 vs wtTDP-43) and specially the presence of the acetyltransferase CBP in the paper by Cohen et al.

Figure 4. 1.- Acetylated residues identified in this study. Identified acetylated lysine residues in this study in relation to the TDP-43 domains. The black arrows represent the acetylated lysines identified in this study. The grey arrow represents the previously reported acetylated K145.

Interestingly, the analysis of the ubiquitination sites found in the same mass spectrometry data revealed that K84 was ubiquitinated after inhibiting the proteasome with MG-132 (239). The substitution of this residue to alanine caused TDP-43 to mislocalised to the cytoplasm. However, the substitution of the same residue to arginine did not have an impact in its subcellular localisation. Overall, the study by Hans et al. concludes that K84 is a crucial component of the NLS and that it might be involved in hyperubiquination events in the presence of pathogenic mutations. In addition to this interesting observation, the presence of an acetylation at the same residue makes this residue a prime target for a detailed study on the posttranslational regulation of nuclear-cytoplasmic trafficking.

The phylogenetic analysis of TDP-43 reveals that it is a well conserved protein from *C. elegans* to humans (Figure 4. 2). It is worth mentioning, however, that the nematode ortholog is not functionally conserved and that it carries an N-terminal fragment, which is not present in the

other species(398). Indeed, when the protein alignment is carefully examined, the nematode protein is the only one where residue 79 does not correspond to a lysine residue. K121 differs in both flies and nematodes from vertebrates. Overall, all four residues are well conserved in vertebrates, hinting that they might be of special functional or structural relevance.

Figure 4. 2.- Alignment of TDP-43 with its homologs in mouse, frog, zebra fish, fruit fly and worms. Amino acid sequences from *Homo sapiens* (Human), *Mus musculus* (Mouse), *Dario rerio* (Zebra fish), *Caenorhabditis elegans* (C. elegans), *Xenopus tropicalis* (Frog) and *Drosophila melanogaster* (Fruit fly). Lysine residues found to be acetylated in through LC-MS/MS have been identified with arrows. The colouring represents the degree of conservation through the 5 species.

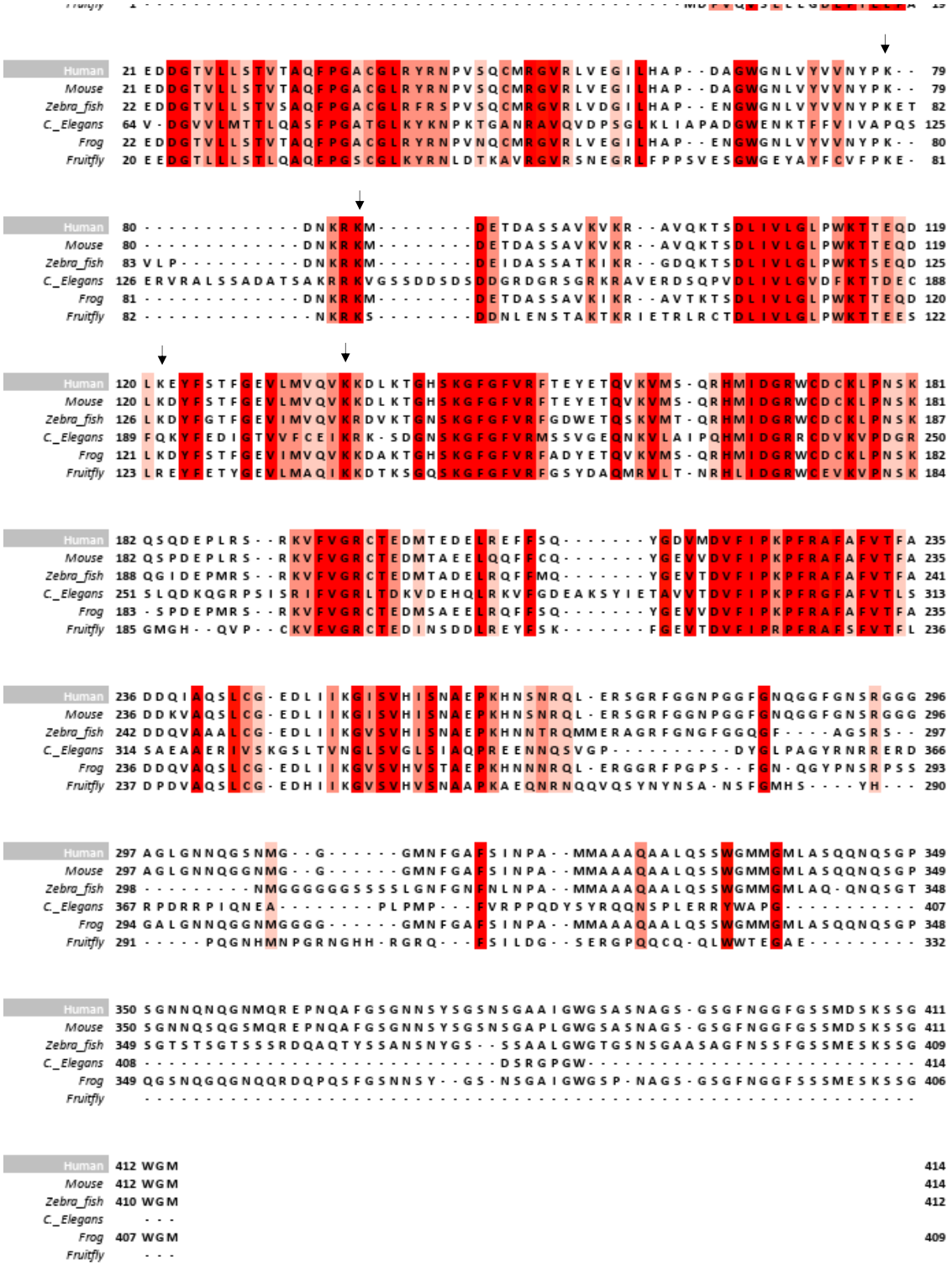

After looking at the level of conservation of the acetylated lysines, the local environment of the amino acids was examined by looking at TDP-43 resolved structure. While the whole protein structure has not been resolved, to the structure of several parts and domains have been

reported. Up to this date, the stretch between amino acids 80 and 99 have not been resolved, therefore lysines 79 and 84 had to be excluded from this analysis. The structure of both RRMs containing K121 and K136 has been published (111). K121 is located at the exterior of an α-helix with its side chain looking outwards. This makes it difficult to predict the possible impact of K121 acetylation in protein functionality, especially in RNA-protein interaction. On the other hand, K136 is situated at the core of the RNA-binding pocket of the RRM1 (Figure 4.3). It is only at 3.9 Ångstroms away from the RNA strand and a modification of this residue could interfere with either the RNA directly or, alternatively, it could interact with neighbouring amino acids and disrupt the RNA-binding pocket.

4. 1. 2.- Evaluation of impact of individual lysines in TDP-43 overall acetylation

The first step to assess the individual impact of each lysine in the total levels of acetylation of TDP-43 was to substitute each of the lysines. To model the lack of acetylation, each lysine was mutated through point-mutagenesis to arginine. While arginine has a slightly longer side chain than lysine, the structure is not too dissimilar between the two of them. More importantly, both are positively charged, and the charge distribution is very similar between both of them. Since arginine cannot be acetylated, this substitution is widely use to study acetylation (399). Similarly, to study the possible effect of specific acetylations, lysines were mutated to glutamine. Glutamine, like acetylated lysine, has a neutral charge. The side chain of glutamine is about half of the size than the one of an acetylated lysine. Both arginine and glutamine are used widely to model the effect or the lack of acetylation at lysines, but their differences should be taken in account when examining the results.

Another relevant point to take in account is the protocol to detect total acetylation. This is done by using anti-pan-acetylated lysine antibodies. There are several such antibodies available but the sensitivity to specific acetylated proteins may vary slightly among them. Therefore, it is important to find an antibody suitable to each experimental setup.

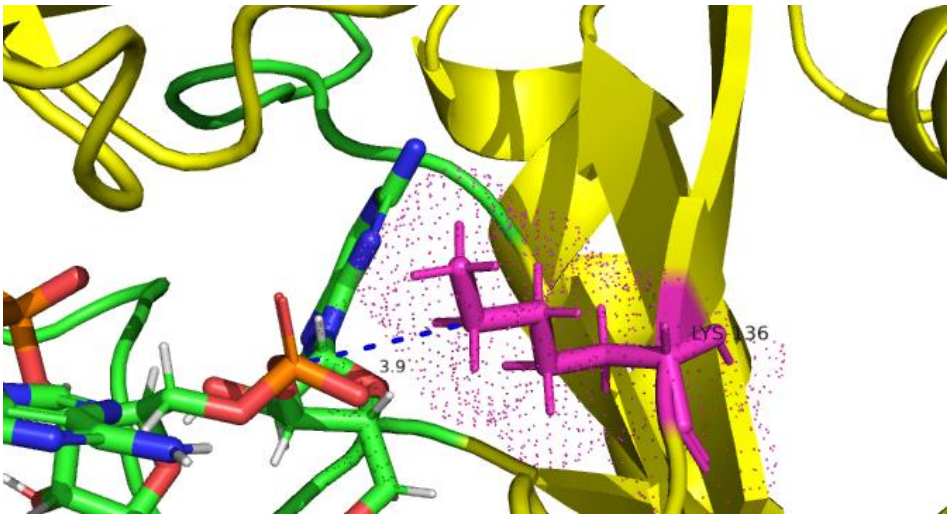

Figure 4. 3.- Structural modelling of lysine 136 in relation RNA. Higher magnification of the interaction between lysine 136 (in magenta) and RNA. The blue dotted line represents the distance between atoms (3.9 Ångstroms), The blue and green structure on the left corresponds to the RNA molecule. The cloud of dots delineates the electron densities of K136. PDB: 4BS2.

With these considerations in mind, two mutants (arginine or glutamine) per lysine were generated. Constructs were C-terminally tagged with 6xHis and cloned into a pCMV backbone. To check for protein stability and total acetylation status constructs were transfected into HEK293E cells. Proteins were extracted and 6xHis-tagged proteins were purified via Ni-NTA pulldown. Total acetylation was assessed by two different anti-pan-acetylated lysine antibodies, K-100 and K-103. K79Q, K84Q, K136R and K136Q TDP-43 mutants were expressed at higher levels than the other mutants (Figure 4.4). K121Q TDP-43 signal was barely detectable. This caused in turn a highly variable and unreliable signal in the acetylated signal from the pulldown protein. Both K-100 and K-103 antibodies detected acetylated TDP-43 at ≈45 kDa. Acetylation of the wtTDP-43 was detected. Taking in account the different protein expression level of each mutant, no single residue appears to be target for acetylation.

4. 1. 3.- Effect of HDAC6 inhibition in TDP-43 acetylation levels

As previously mentioned, HDAC6 mRNA stability is regulated by TDP-43 (146). This raised the question of the possible involvement of HDAC6 with the acetylation of TDP-43. The self-regulation of TDP-43 mRNA by itself could be consider a negative feedback loop itself so the possibility of an interaction between HDAC6 and TDP-43 at an acetylation level was raised. In addition, increasing the levels of TDP-43 acetylation would make the detection of fine differences between acetyl mutants more prominent. Tubacin is a selective inhibitor of HDAC6 (400,401) and therefore an excellent tool to assess the deacetylation potential of HDAC6 on TDP-43.

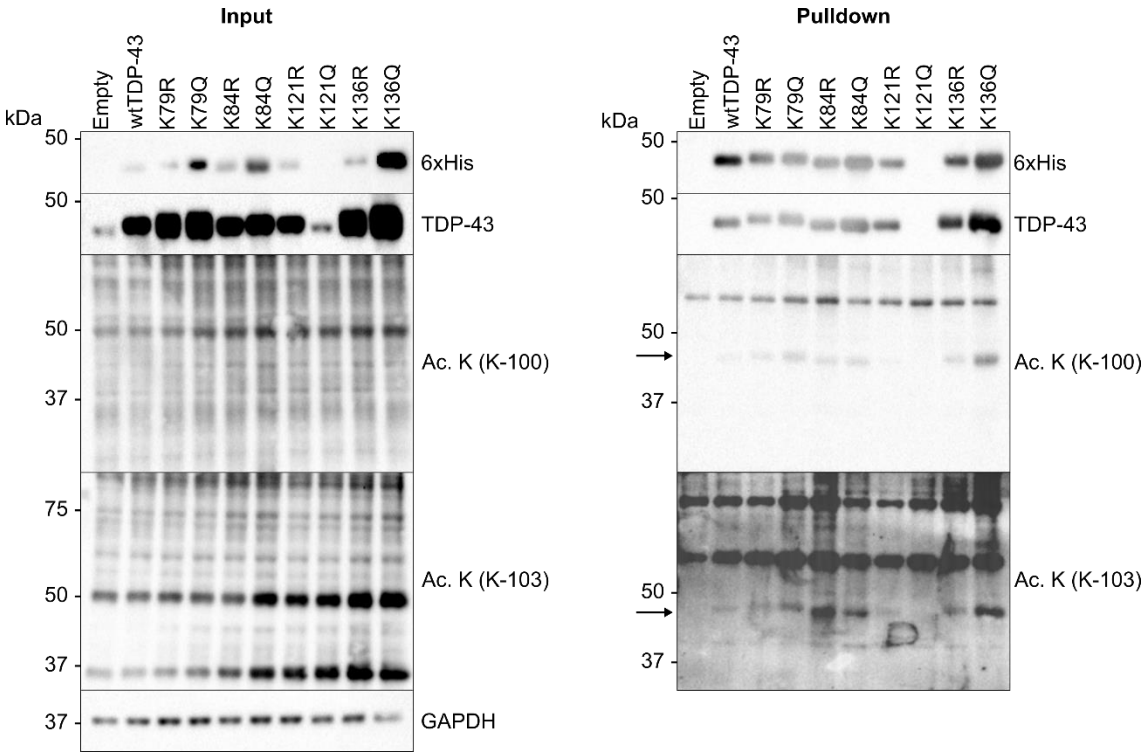

Figure 4. 4.- Pulldown of C-terminally 6xHis tag TDP-43 mutants. HEK293E cells were transfected with C-terminally 6xHis-tagged TDP-43 constructs carrying mutations at different lysine residues. Cells were lysed in urea buffer. 6xHis proteins were purified via Ni-NTA pulldown. Extracts were analysed via western blot for the expression levels of the mutants and the total acetylation status. K-100 and K-103 correspond to different pan-acetylation antibodies. GAPDH was used as a loading control. Arrow points at acetylated TDP-43. N = 2.

First, to find the appropriate concentration of tubacin, an optimization was performed. Three different timepoints (1, 6 and 24 hours) and three concentrations (2, 5 and 10µM) were used and HDAC6 inhibition was assessed by examining tubulin acetylation, a well characterised HDAC6 target (369). After looking at the data, an acute treatment of 10µM Tubacin for 2 hours was chosen (Figure 4.5).

HEK293E cells were transfected with each of the generated mutants and treated with Tubacin for 2 hours. In the case that TDP-43 is indeed deacetylated by HDAC6 under physiological conditions, the protein would become more acetylated after HDAC6 inhibition. Transfected

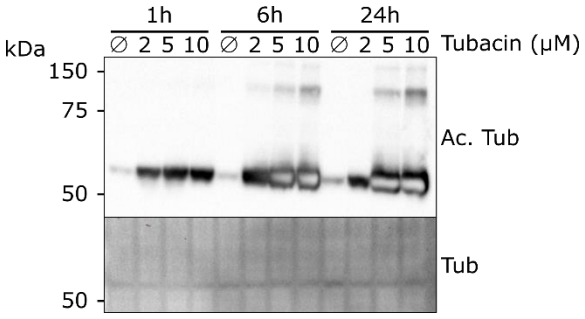

Figure 4. 5.- Optimization of time and dose of Tubacin on HEK293E cells. HEK293E cells were treated at different timepoints with increasing concentrations of Tubacin. Control cells were treated with DMSO. Protein was extracted with a urea buffer and proteins were analysed via western blot.

HEK293E cells were lysed in urea buffer and 6xHis tagged TDP-43 was analysed via western blot. wtTDP-43 acetylation did not increase upon HDAC6 inhibition (Figure 4.6). In addition, HDAC6 inhibition did not promote acetylation of any of the lysine mutants (Figure 4.6 A and B). K121Q TDP-43 showed an extremely low expression level in comparison with other constructs. In conclusion, HDAC6 does not seem to deacetylate TDP-43 under these conditions.

4. 1. 4.- Mutant specific proteasomal degradation and transcription

The strong differences in expression between mutants made any meaningful conclusion about total acetylation hard to make. At least three possible explanations could be behind this phenomenon. First, as explained before, lysine residues can be targeted both by acetylation and ubiquitination. The interaction between these two modifications in TDP-43 is not fully understood, but it could be the case that there is a competition of both E3 ligases and acetyltransferases for the same lysine residue. As found in the Mass Spectrometry analysis of TDP-43, K84 could be a target of both modifications. One of the most important roles of ubiquitination in the cell is labelling proteins for degradation via the proteasome or trigger autophagy (402). Therefore, interfering with ubiquitination by removing lysine residues or mimicking acetylation can have an impact in protein stability, which would taint the results of any subsequent analysis. The second possible explanation could be due to mRNA instability. Changes in the mRNA sequence could trigger cryptic splicing sites or accelerate the mRNA decay, leading to less translation and less protein levels. The last and hardest to examined explanation could be an interaction between the tag and specific sequence changes, leading to aberrant mRNA secondary structures that would affect translation.

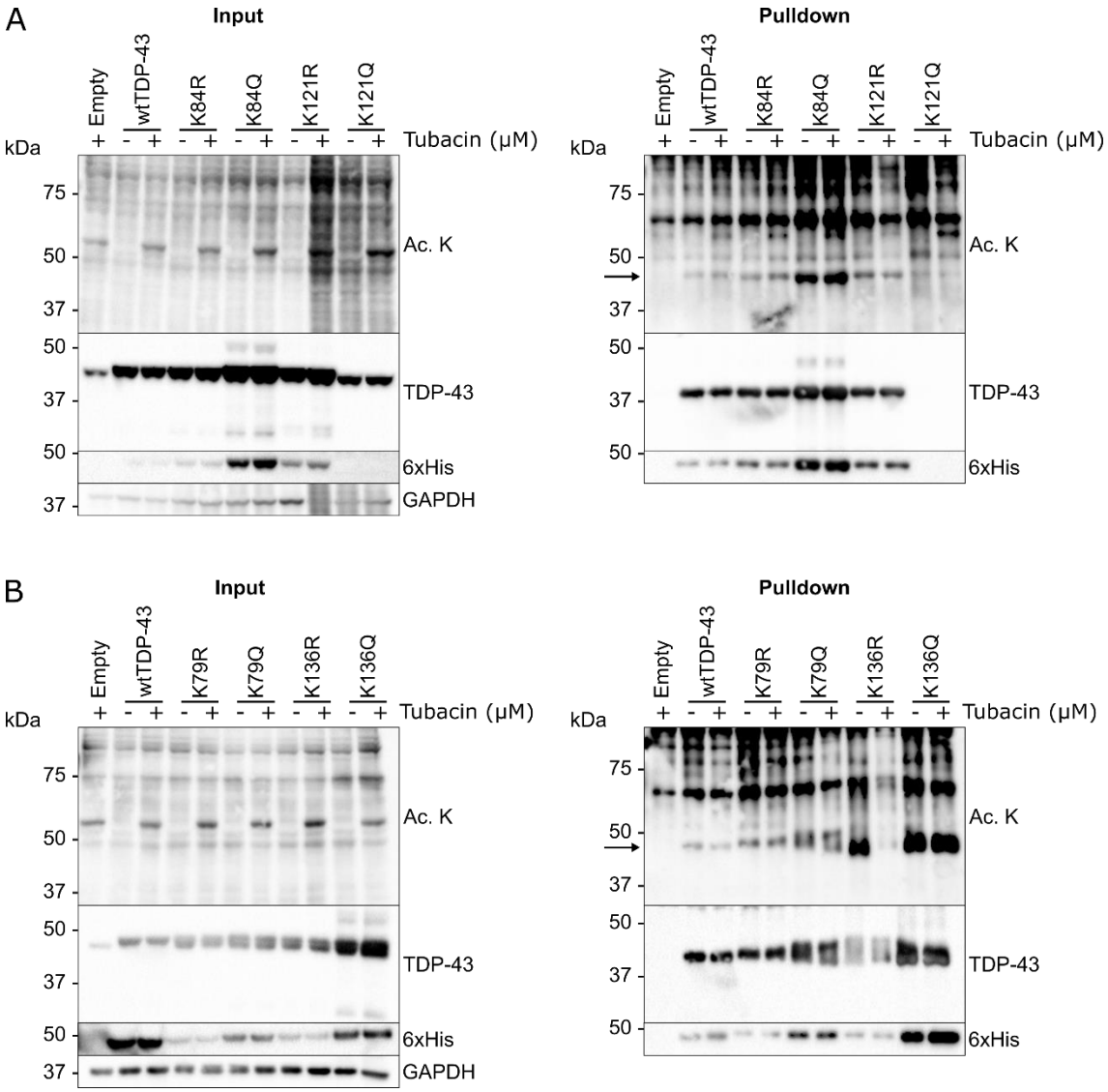

Figure 4. 6.- TDP-43 acetylation upon HDAC6 inhibition does not change. HEK293E cells were transfected with either K84 or K121 (**A**), or with K79 or K136 (**B**) TDP-43 mutants. Cells were treated with either DMSO or 10μM Tubacin for 2 hours. Afterwards cells were lysed in urea buffer and 6xHis tagged proteins were purified via Ni-NTA pulldown and analysed via western blot. GAPDH was used as a loading control. Arrow points at acetylated TDP-43. N = 3.

In order to check the first hypothesis a proteasomal inhibitor, MG-132, was used to prevent the possible fast turnover of mutant TDP-43. Transfected cells were treated with either 10 μM MG-132 or DMSO for 15 hours and then cells were lysed in urea buffer and the protein extract was analysed via western blot. Proteasomal inhibition increased the high molecular weight smear of total ubiquitinated proteins and increased the stability of all the TDP-43 mutants, except for K121Q TDP-43 (Figure 4.7 A). With this evidence we can conclude that K121Q TDP-43 is not degraded via the proteasome faster than any of the other constructs.

Next, to test the stability of the mRNA transcripts, mRNA was extracted from transfected cells 48 hours after transfection and a fragment of the TDP-43 transcript was amplified using one forward internal TDP-43 primer and a reverse primer binding to the sequence stretch between

the stop codon and the polyA signal encoded in the pCMV plasmid (Figure 4.7 B). This configuration ensures the selective amplification of the transfected TDP-43 mRNA and not of the endogenous one. The extracted mRNA was reverse transcribed, and the resulting DNA was probed with the aforementioned primers. There were no detectable differences among the different constructs (Figure 4.7C).

Since K121Q TDP-43 does not seem to have faster proteasomal turnover than the other constructs, and its mRNA levels do not differ with the other mutants used in this study so far, the 6xHis C-terminal constructs used up to this point were discarded and new N-terminal 6xHis tagged constructs were generated for all the mutations. In addition, in order to confirm the previously reported effect of acetylation at K145, both arginine and glutamine mutants were generated for that lysine as well.

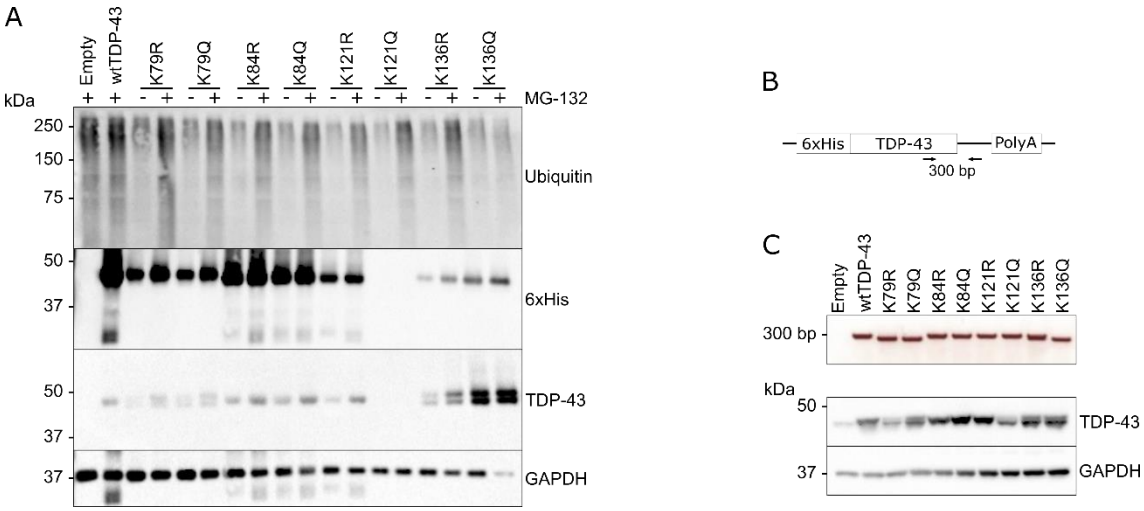

Figure 4. 7.- Effect of proteasomal inhibition on TDP-43 lysine mutants and mRNA stability assay. A) HEK293E cells were transfected with the indicated TDP-43 lysine mutants 72 hours before lysis. 15 hours before the protein extraction cells were treated with either DMSO or MG-132 (10 µM). Protein extracts were analysed via western blot. N = 2. **B)** Schematics of primer binding sites in the pCMV TDP-43 constructs for the mRNA amplification experiment. **C)** Cells were transfected 72 hours with the mentioned constructs before sample collection. Each pellet of cells was divided in two tubes, one for mRNA extraction and another one for protein extraction. mRNA was extracted using a Qiagen RNeasy kit, and after reverse transcription it was analysed via PCR. Proteins were extracted in a urea buffer and the resulting extract was analysed via Western blot.

4. 2.- Effects of TDP-43 lysine mutations on subcellular localisation and RNA interaction

After rejecting the hypothesis that the instability of K121Q TDP-43 and the variability of the other lysine mutants was caused by proteasomal degradation or mRNA decay, the C-terminal

tag was substituted by a 6xHis N-terminal tag in all the constructs. From now on, unless it is specified, N-terminally tagged constructs are used in this study.

4. 2 .1.- Impact of single lysine mutations in TDP-43 total acetylation and subcellular localisation

To determine at the stability of the N-terminally tagged TDP-43 constructs and the impact of single lysine mutants on the total level of TDP-43 acetylation, HEK293E cells were transfected with the TDP-43 constructs and lysed in urea buffer. 6xHis tagged proteins were purified from the total extract via an Ni-NTA purification and the samples were analysed via Western blot. In comparison to the previous experiments with C-terminal 6xHis tag, the new constructs have a more consistent level of expression (Figure 4.8A). N-terminal tagged K121Q TDP-43 had similar levels of expression to the other mutants and only K84Q and K136Q showed expression levels slightly above other constructs. The similar level of expression made the examination of the impact of each lysine in TDP-43 total acetylation level possible. When looking at the purified protein acetylation levels, considering the slight differences in the level of 6xHis TDP-43, no single lysine substitution had a consistent impact in the total level of acetylation of TDP-43 (Figure 4.8A, right panel, black arrow). If only the lysines examined were acetylated, there would be reduction of total acetylation of around a fifth of the total acetylation level after mutagenizing one of them to arginine or glutamine. Since this is not the case, it is possible that TDP-43 is acetylated in residues that escaped our analysis. Two examples of undetected acetylation sites are the residues K145 and K192 (249) previously reported as acetylated. Nevertheless, even if the identified residues are not the only acetylated residues, they could play a role in TDP-43 biology.

A first approach to test the impact of acetylation at these residues is to check if the lysine substitution had an influence ion TDP-43 subcellular distribution. In order to check if this is the case, HEK293E cells were transfected with the different lysine mutant constructs of TDP-43 and the cells were immunostained for 6xHis (Figure 4.8B). wtTDP-43 showed the expected nuclear distribution reported for endogenous TDP-43 (104). Similarly, both acetyl-mimic and acetyl-dead mutations at K79 and K121 residues showed the same nuclear localisation as wtTDP-43 (Figure 4.8B and C). In addition, mimicking acetylation at K145 via glutamine substitution evoked a dotted nuclear distribution, similar to the previous report on K145Q mimic mutant (249,253). The results of this experiment so far confirm observations in the literature about K145 and uncovers 4 new lysine substitutions. It also shows that under unstressed conditions acetylation at K79 and K121 do not play a role in the subcellular localisation of TDP-43.

In contrast, lysine substitutions at K84 and K136 had marked effects on TDP-43 distribution. While K84R, acetyl-dead mutant is mostly located in the nucleus, most cells expressing K84Q acetyl-mimic TDP-43 showed a cytoplasmic mislocalisation of the protein (Figure 4.8B and C). On the other hand, both acetyl-dead and acetyl-mimic mutants at K136 showed a nuclear but granular distribution very different from the diffuse staining of wtTDP-43. The distribution of K136 mutants was strikingly similar to the one of K145Q (249) and the RNA-deficient binding mutant FFLL (246). In the case of FFLL TDP-43, two phenylalanines at the RRM1 (F147 and F149) are mutated to leucines. This change causes a complete loss of RNA-binding capabilities of TDP-43 (135).

Taken together, these results suggest that K79 and K121 acetylation play no role in the distribution of TDP-43 under physiological conditions. K84, however, seem to regulate to a certain extent the nuclear-cytoplasmic trafficking of TDP-43. This residue is particularly interesting due to its location directly at the NLS bipartite sequence and its involvement with both acetylation and ubiquitination (239). Since the acetyl-dead did not show any changes in subcellular localisation, but the acetyl-mimic did, it is likely that acetylation plays a role in the nuclear-cytoplasmic shuttling of TDP-43. In contrast, the possible role of acetylation at K136 is less clear since both acetyl-mimic and -dead mutants show the same effect. At a minimum, the drastic changes in subcellular distribution after a conservative mutation such as lysine-to-arginine hints at a critical role of this residue in TDP-43 physiology. The position of this lysine in the RRM1 and the similar distribution to FFLL TDP-43 suggest that K136 is an important residue for RNA-protein interactions.

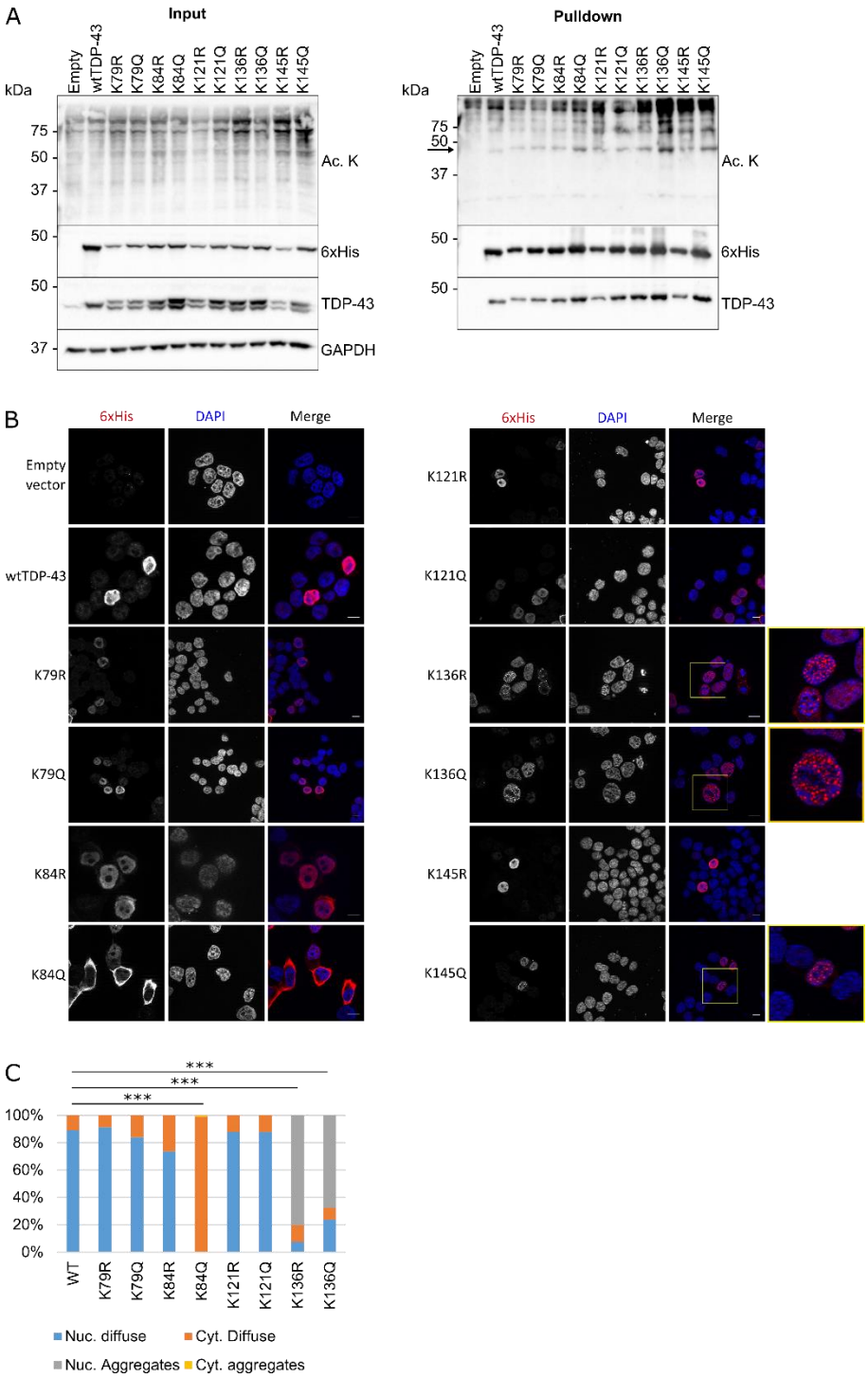

Figure 4. 8.- Single lysine impact in TDP-43 total acetylation and subcellular localisation. A) HEK293E cells were transfected with N-terminally 6xHis tagged TDP-43 72 hours before lysis. After that time, cells were lysed in urea buffer, 6xHis tagged proteins were purified via Ni-NTA pulldown and both input and pulldown sample sets were analysed via western blot. Black arrow marks TDP-43 expected band. N = 2. **B)** Cells were fixed and immunostained 72 hours after transfection with different TDP-43 constructs. Scale bar represents 10 µm. N = 3. **C)** Classification of subcellular distribution of mutant TDP-43 observed in **B)**. 300 cells per group examined. Comparison made through a Chi square test. *** = $p < 0.001$.

With these results in mind, it is possible that after a lysine substitution there is an acetylation of other lysines as a compensatory mechanism. This would mask the loss of the one mutagenized lysine in TDP-43 total acetylation. To explore the interaction between the identified residues

and the proportion of total acetylation detected, a series of mutants with only one lysine available were generated (K79, K84, K121 and K136). These constructs were cloned with an N-terminal 6xHis tag and were transfected to HEK293E cells. The total acetylation was monitored after TDP-43 Ni-NTA purification using a pan-acetyl antibody. The introduction of several mutations led to increased protein levels of K84R/K121R/K136R (marked as K79) and K79R/K84R/K121R (marked as K136) constructs (Figure 4.9A, left panel). This could be due to the removal of multiple possible ubiquitination sites. Taking these expression differences in account, the elimination of several acetylation targets does not diminish the total acetylation of TDP-43 (Figure 4.9A, right panel, black arrow). The impact of several lysine on subcellular localisation was examined by staining the same transfected cells for TDP-43. Similarly, to the single mutants observed in Figure 4.8B, whenever K136 was mutated to arginine, TDP-43 adopted a dotted nuclear pattern (Figure 4.9B).

Since there are no detectable changes in the total level of acetylation after multiple lysine substitutions, we can conclude that TDP-43 acetylation goes beyond the results of the mass spectrometry analysis (Table 4.1). In addition to the results of the multiple lysine substitution acetylation assessment, the lack of residue K145 in the mass spectrometry analysis further supports this idea. Nevertheless, from the pool of acetylated lysines that was detected, experiments with both single and multiple mutant constructs hint that K84 has a significant role in nuclear-cytoplasmic shuttling and K136 substitutions can trigger a droplet-like nuclear distribution of TDP-43.

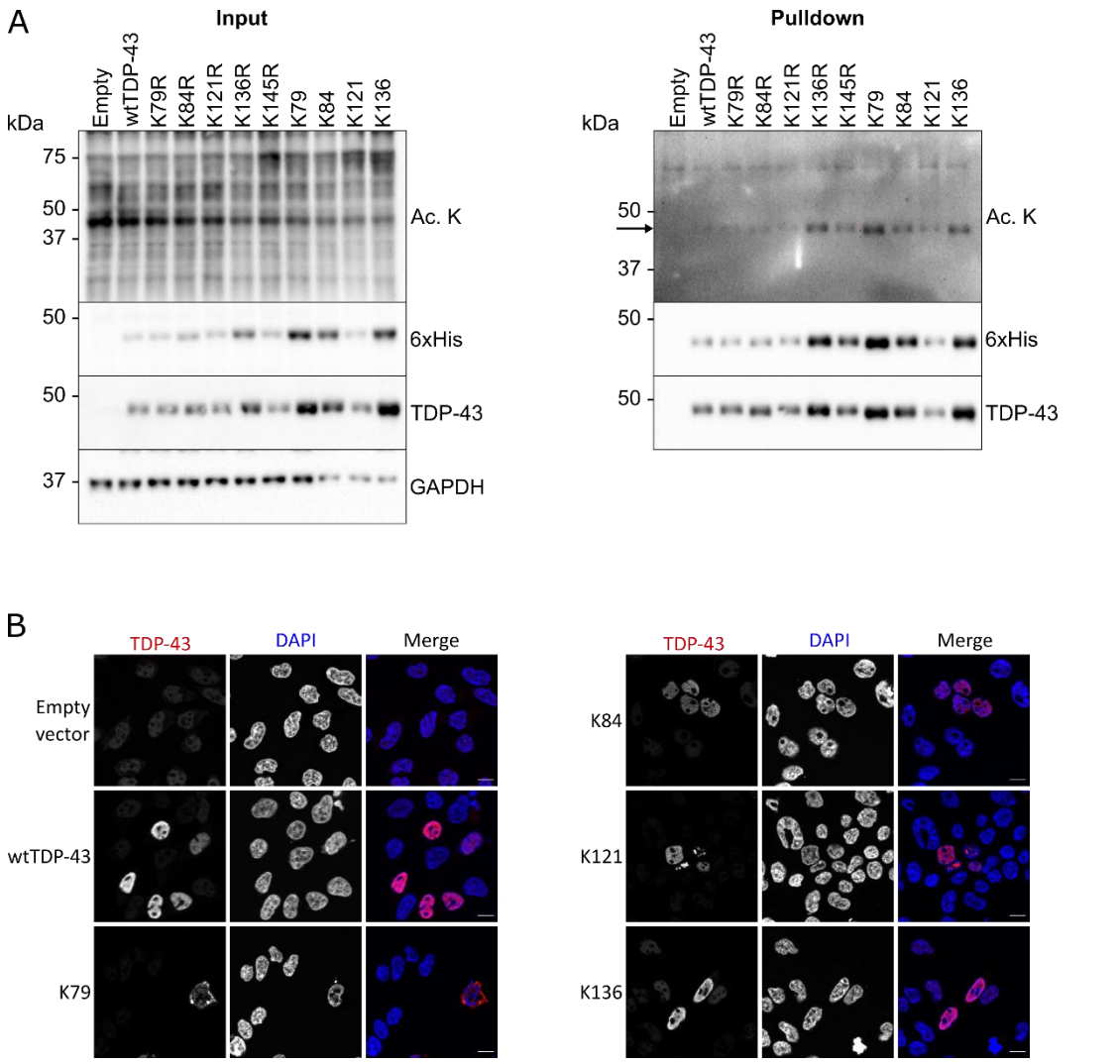

Figure 4. 9.- Multiple lysine mutants support critical relevance of K84 and K136. A) Cells were transfected with 6xHis tagged single or multiple lysine mutants. The constructs used for the multiple mutants are K84R/K121R/K136R, K79R/K121R/K136R, K79R/K84R/K136R and K79R/K84R/K121R, marked as K79, K84, K121 and K136, respectively. Proteins were extracted with a urea buffer and 6xHis tagged proteins were purified via Ni-NTA pulldown. Samples were analysed via western blot and total acetylation was assessed with an anti-pancetylation antibody. **B)** Cells were transfected with multiple lysine mutants and prepared for immunofluorescence.

4. 2. 2.- Mimicking acetylation at K84 triggers cytoplasmic mislocalization of TDP-43

After observing the cytoplasmic mislocalisation caused by K84Q substitution in immunofluorescence, two different cytoplasmic-nuclear fractionation was performed to validate and quantify this result. As a control, a $_{mut}$NLS TDP-43 construct was added to the analysis. This construct has a series of amino acid substitutions at the NLS that prevent its import into the nucleus (403). This construct was used as a control for cytoplasmic mislocalisation of TDP-43.

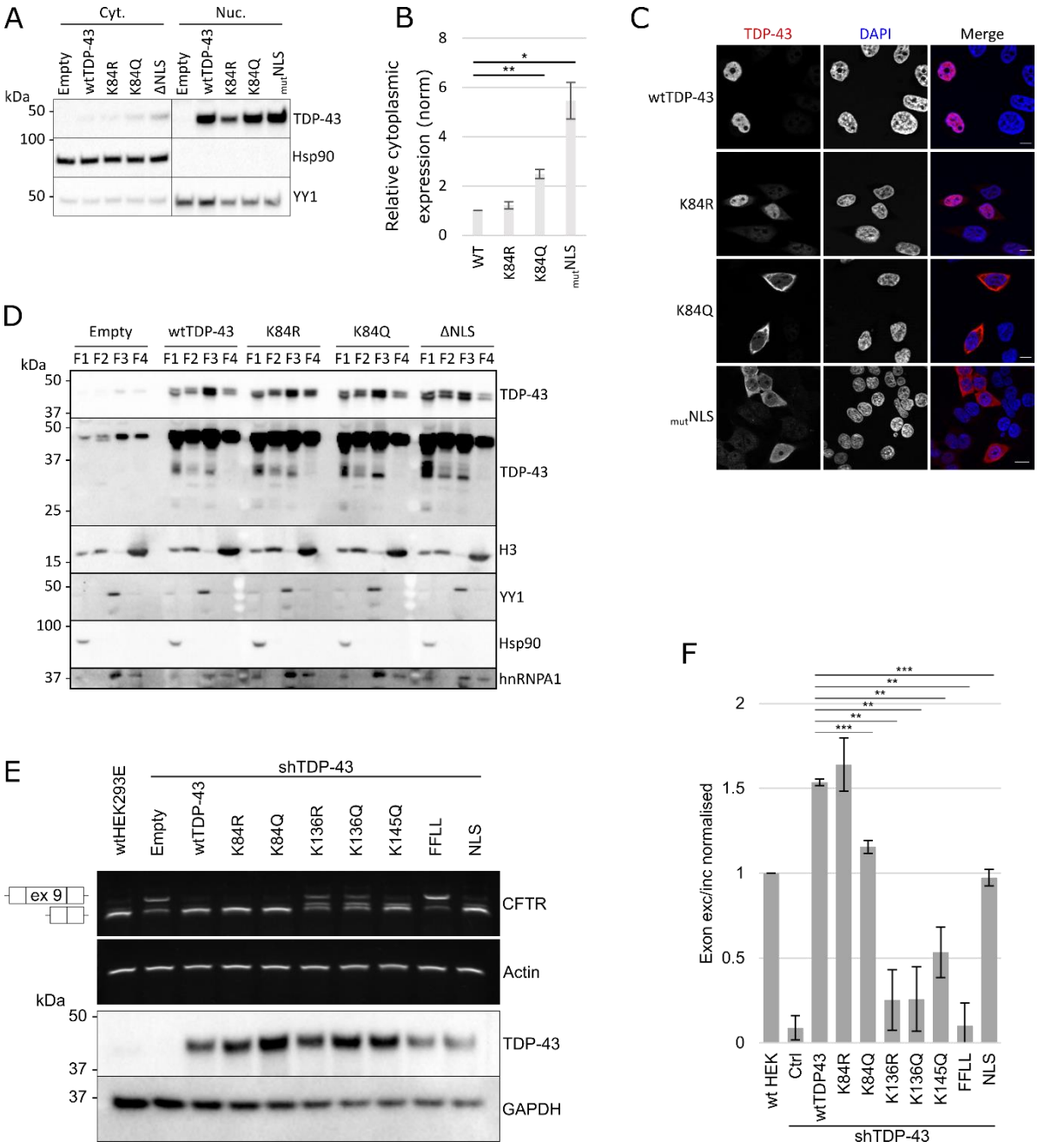

Figure 4. 10.- K84Q triggers cytoplasmic mislocalization of TDP-43 and substitutions at K136 reduce TDP-43 RNA binding capabilities. A) HEK293E cells were transfected with different 6xHis tagged constructs either empty or with TDP-43 mutants. Cytoplasmic and nuclear fractions were separated and later analysed by western blot. N = 2. * = $p < 0.05$, ** = $p < 0.01$. B) Quantification of changes in cytoplasmic fraction of TDP-43 normalized to wtTDP-43, shown in A). * = $p < 0.05$, ** = $p < 0.01$. C) Cells transfected with different 6xHis tagged TDP-43 constructs were fixed for immunofluorescence and stained with α-TDP-43 antibody. D) TDP-43 transfected sh^{TDP-43}-HEK293E and proteins were fractionated in four fractions using a subcellular protein fractionation kit for cultured cells (Thermo Fisher) according to manufacturer's instructions: F1 (cytoplasmic soluble), F2 (membrane bound), F3 (nuclear soluble) and F4 (histone bound). Hsp90, YY1 and H3 were used as markers for the cytoplasmic, nuclear soluble and histone bound fractions, respectively. N = 2. E) wtHEK293E and sh^{TDP-43}-HEK293E cells were cotransfected with a *CFTR* minigene construct and different TDP-43 constructs. Cells were lysed, mRNA was extracted, and targets were analysed via rtPCR. Upper panels show PCR product, lower panels show protein levels. N = 3. F) Quantification of splicing assay in D. ** = $p < 0.01$

Matching the results of the immunofluorescence (Fig 4.8B, Fig 4.10C), the cytoplasmic fractionation showed a significant increase of K84Q TDP-43 in the cytoplasm (Fig 4.10A, B, D).

The increase was not as pronounced as the one of $_{mut}$NLS TDP-43, which has three mutations at the NLS (K82A/K83A/K84A), in comparison to the single substitution of K84Q TDP-43. It is worth mentioning that there in the fractionation there is a sizable amount of nuclear TDP-43 in both K84Q and $_{mut}$NLS TDP-43 constructs. This nuclear TDP-43 seems to be sufficient for the splicing of mRNA targets (vide infra). In immunofluorescence, there is a noticeable signal from the nuclear TDP-43 (Fig. 4.10C) which seems to be much lower than the cytoplasmic one. The apparent contradiction between the fractionation and the immunofluorescence has been observed in the literature as well (239). Nevertheless, the nuclear-cytoplasmic fractionation showed a significant increase in cytoplasmic K84Q when compared to wtTDP-43 and no changes in distribution of K84R TDP-43, validating the observations in immunofluorescence and the idea that K84 is a key residue of TDP-43 NLS.

4. 2. 3.- K136 mutants display less splicing activity of *CFTR* exon 9

The similarities between K136 mutants and FFLL TDP-43 suggested that K136R and K136Q mutations could impair the RNA-related functions of TDP-43. In addition to the dotted pattern, as previously mentioned K136 is located in the RRM1, which hints at a possible role for K136 in protein-RNA interaction.

To test the involvement of K136 in the RNA splicing functions of TDP-43, first a suitable experimental setup had to be chosen. HEK293E cells have endogenous levels of wtTDP-43 that can interfere with RNA splicing assays. For this reason, sh^{TDP-43}-HEK293E cells expressing a shRNA against endogenous TDP-43 were used. The cells were already described by Fiesel et al. (146). TDP-43 has been reported to processed *CFTR* transcript and mediate the exclusion of exon 9 (135). For this experiment wtHEK293E and sh^{TDP-43}-HEK293E cells were cotransfected with a *CFTR* minigene construct containing exons 9-11 and different TDP-43 mutants. When endogenous TDP-43 is present, exon 9 from the *CFTR* transcript is spliced giving rise to a smaller transcript (Fig. 4.10E, first lane). Overexpression of wtTDP-43 can rescue exon 9 exclusion in a TDP-43 KD context. K84R TDP-43, which remained nuclear, shows similar splicing activity to wtTDP-43 (Fig 4.10E and F), however K84Q displayed reduced splicing capabilities, comparable to $_{mut}$NLS TDP-43. The partial rescue matches the residual nuclear distribution of both K84Q and $_{mut}$NLS TDP-43 observed before (Fig 4.10A-D). On the other hand, both K136R and K136Q showed a strong decrease in exon 9 exclusion. This decrease was more pronounced than the K145Q loss of function but not as marked as the RNA-binding deficient FFLL TDP-43. In addition to *CFTR*, a set of other known RNA targets of TDP-43 (Sort1, MADD, SKAR and HDAC6) were tested. Unfortunately, a rescue of these targets' processing could not be achieved in the sh^{TDP-43}-

HEK293E context even after transfecting wtTDP-43 (data not shown). Therefore, the analysis of K136 role in the processing of these targets was not possible.

Together, these results support the impact of K84 in nuclear-cytoplasmic shuttling and strengthen the link between K136, RNA binding and the droplet-like nuclear distribution

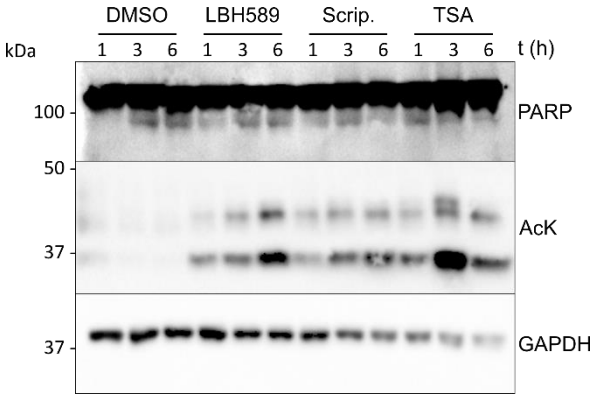

Figure 4. 11.- Time optimisation of different KDAC inhibitors in sh^{TDP-43}-HEK293E cells. Untransfected sh^{TDP-43}-HEK293E cells were treated with either DMSO (0.1%), LBH589 (2µM), Scriptaid (6µM) or TSA (1µM) for different time lengths. Cells treated for 1, 3 or 6 hours with the indicated inhibitor before lysis in urea buffer. Cell death and acetylation changes were assessed via Western blot.

observed previously.

4. 3.- Modulation of TDP-43 acetylation via inhibition of endogenous KDACs

The previous results hinted at a possible role of TDP-43 acetylation in both subcellular localisation and RNA processing. These are two aspects of TDP-43 biology critical for its physiology and proteinopathy. This prompted the search for endogenous deacetylases acting upon it. Previous reports have found that HDAC1 and HDAC6 can potentially deacetylate TDP-43 (249,252). HDAC1 has been proposed to deacetylate TDP-43 and to promote TDP-43 toxicity in an overexpression model by acting downstream of it. In contrast, TDP-43 interaction with HDAC6 has been already described in this thesis (see introduction). To study the potential modulation of TDP-43 acetylation by these or other KDACs, a small library of 11 KDAC's inhibitors was used. The full list and the KDACs inhibited by each component are listed in Table 4.2. There is a very limited number of KDACs in mammalian cells, which makes the systematic inhibition of almost every one of them a feasible enterprise. The use of both broad-spectrum and specific inhibitors allows the identification of the KDAC or KDACs involved in TDP-43 deacetylation.

Table 4. 2.- KDAC inhibitors used in this study. List of KDAC inhibitors used and their respective targets. Concentration and treatment length are specified in the respective experiments. Some compounds had a broad-spectrum effect on whole groups of deacetylases while others were selective for specific KDACs.

Chemical	Targets
CI994	HDAC1
	HDAC3
	HDAC6
	HDAC8
LBH589	HDAC1
	HDAC6
	HDAC8
SAHA	HDAC1
	HDAC2
	HDAC3
	HDAC6
	HDAC8
	HDAC10
SBHA	HDAC1
	HDAC3
Scriptaid	HDAC I group
TSA	HDAC1
	HDAC2
	HDAC3
	HDAC6
	HDAC8
	HDAC10
Apidicin	HDAC1
	HDAC3
M344	HDAC1
	HDAC6
Na-4-PB	HDAC Class I
Splitomycin	HDAC Class III
Valproic acid	HDAC Class I

The first step was to stablish timepoints for the treatments long enough to cause a change in acetylation but avoiding at the same time treatment-related toxicity. Based on previous experience in the research group, the 3 most toxic compounds (LBH589, Scriptaid and Trichostatin A (TSA)) were tested for 3 different timepoints: 1, 3 and 6 hours. Untransfected $sh^{TDP\text{-}43}$-HEK293E cells were treated 1, 3 or 6 hours before lysis with either DMSO, LBH589, Scriptaid and TSA at 0.1%, 2µM, 6µM and 1µM, respectively. Apoptosis was assessed by PARP cleavage and KDAC inhibition with a pan-acetyl antibody. $sh^{TDP\text{-}43}$-HEK293E proved to be sensitive to all treatments even after one hour, however total acetylation in response to the

treatments reached a plateau at different timepoints depending on the inhibitor (Fig 4.11). For Scriptaid and TSA, a timepoint of 3 hours was chosen. For LBH589 and all the other KDAC inhibitors not shown in this experiment 6 hours was chosen as the treatment length.

4. 3. 1.- KDAC inhibition increases TDP-43 total acetylation

Once the treatment times were selected, the next step was to look at the effect of KDAC inhibition on the total level of acetylation of TDP-43. As before, this was done by transfection and purification of 6xHis tagged wtTDP-43 in sh^{TDP-43}-HEK293E. Purified samples were analysed via western blot with a pan-acetyl antibody.

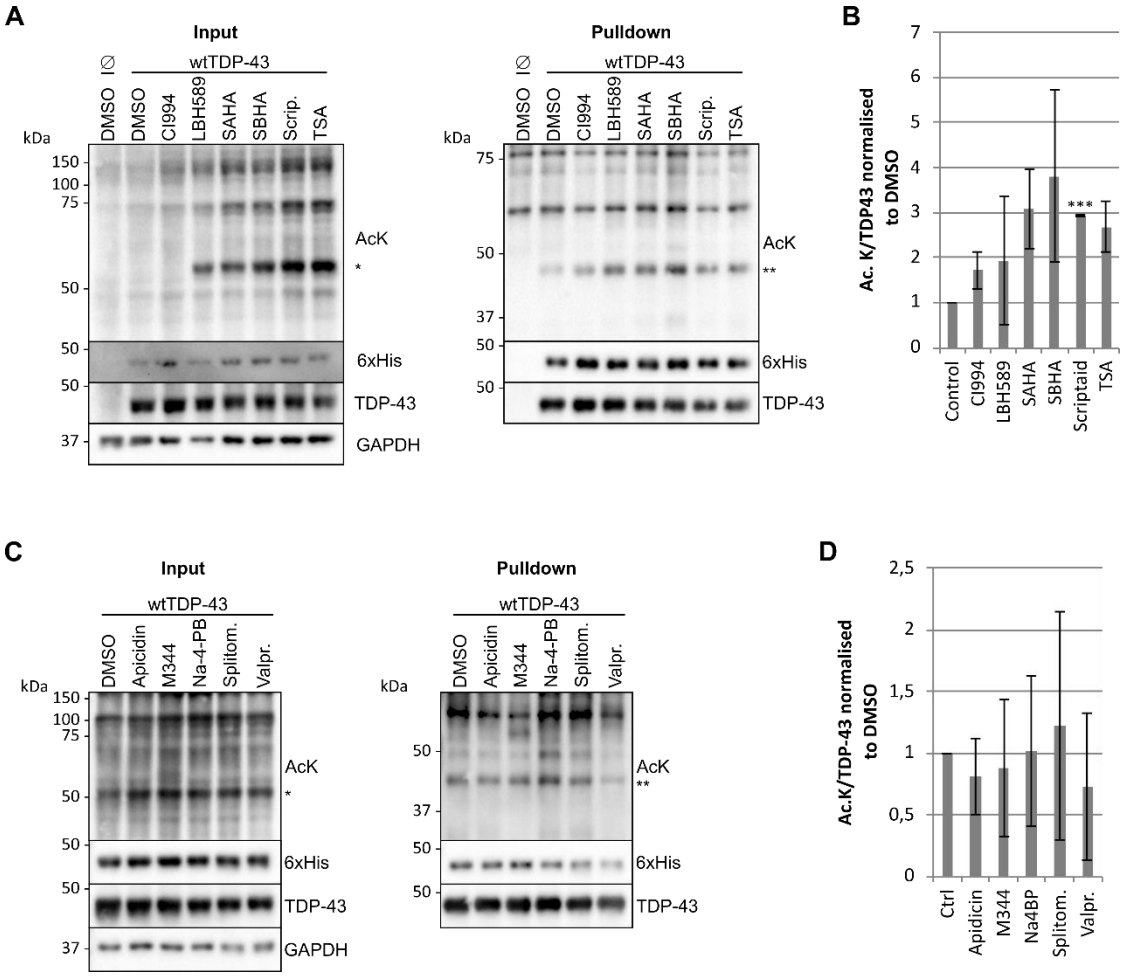

Figure 4. 12.- KDAC inhibition alter total acetylation of TDP-43. A) sh^{TDP-43}-HEK293E cells were transfected with 6xHis-tagged wtTDP-43 or an empty plasmid 72 hours before lysis. Additionally, they were treated with Scriptaid (6µm) and TSA (1µm) for 3 hours and with DMSO (0.1%), CI994 (50µm), LBH589 (2µm), SAHA (2µm) and SBHA (30µm) for 6 hours before lysis in urea buffer. 6xHis tagged proteins were purified via Ni-NTA purification and samples were analysed via western blot. N = 3. B) Quantification of total acetylation in relation to TDP-43 levels after pulldown from A). N = 3 and comparison via t-test. *** = $p < 0.001$. Mind the different scale in the Y-axis compared to D). C) Cells were transfected as in A) and were treated with M344 for 3 hours and with DMSO (0.01%), Apicidin, Na-4-PB, Splitomicin and Valproic acid for 6 hours before lysis in urea buffer. N = 2. D) Quantification of C) and comparison via t-test.

As it was mentioned before, altering the acetylation system might have an indirect impact in protein ubiquitination and stability. However, none of the tested compounds had a strong effect on overexpressed wtTDP-43 stability. From the 11 different KDAC inhibitors used only Scriptaid caused a consistent increase of TDP-43 total acetylation (Fig. 4.12A-D, band marked with **). SAHA, SBHA and TSA seem to promote TDP-43 total acetylation as well, however the high variability prevented these treatments from reaching any significance. These four compounds are inhibiting KDAC class I, as seen in Table 4. 2. In a similar way, the effect of Splitomycin appeared to be able to enhance TDP-43 acetylation but the high variability did not allow it to reach significance when compared to DMSO treated cells. All other compounds did not have a significant effect on TDP-43 total acetylation. In addition, there are additional bands detected by the pan-acetyl antibody. The band around 55kDa (marked with and asterisk) that is present after KDACi treatment may correspond to acetylated tubulin, while there are bands at 75 and 130kDa in the input that could correspond to other acetylated proteins, already present without any KDACi treatment. In addition, the bands observed in the purified fraction at 75 and 55-60 kDa seem to be proteins that unspecifically bind to the Ni-NTA beads.

Overall, these results suggest that modulation of TDP-43 total levels of acetylation through KDAC inhibition is possible. However, by only being able to look at the total level of acetylation, it is unclear if there is a selectivity of certain KDACs towards specific lysines. At this point of the study, it is not possible to discern if Scriptaid, SAHA, SBHA or TSA have any impact on K84 and K136 acetylation.

4. 3. 2.- KDAC inhibition does not impact TDP-43 subcellular distribution or RNA splicing activity

The characterization of the TDP-43 glutamine substitutions suggested that acetylation at K84 can shift TDP-43 into the cytoplasm. The impact of the glutamine substitution at K84 was detectable in both immunofluorescence and nuclear-cytoplasmic fractionation. Additionally, K136Q TDP-43 displayed a dotted nuclear pattern and a loss of RNA splicing activity. If these changes are indeed caused by acetylation at these residues and if the increase of acetylation seem after KDAC inhibition is affecting K84 and K136, cells treated with KDAC inhibitors will display those changes in TDP-43 physiology. To test this hypothesis, HEK293E cells with endogenous levels of TDP-43 were treated with the set of inhibitors that had a higher impact in total TDP-43 acetylation (LBH589, SAHA, SBHA, Scriptaid and TSA). After the treatment, the distribution of TDP-43 was assessed via immunofluorescence and nuclear-cytoplasmic fractionation.

The use of KDAC inhibitors did not result in a significant shift of endogenous TDP-43 to the cytoplasm (Fig 4.13A-C). Costaining of TDP-43 and panacetylated lysine did not reveal an increase of acetylation at TDP-43 granules, nor an increase in the number or granules (Fig 4.13A). However, it is worth mentioning that inhibition of KDACs, especially class I, increases the acetylation of several histones, making any reliable assessment of other nuclear proteins acetylation status via immunofluorescence almost impossible. The dotted-pattern distribution of K136R and K136Q TDP-43 was not recapitulated after KDAC inhibition (Figure 4.13A). DMSO treated cells show only the RNA-processing bodies where TDP-43 is enriched under physiological conditions. These do not increase in number nor colocalise with the panacetylated lysine signal after any of the treatment.

To test the effect of acetylation via KDAC inhibition in TDP-43 RNA processing, HEK293E cells were transfected with the CFTR minigene construct and treated with SBHA, SAHA or TSA. In addition, $sh^{TDP\text{-}43}$-HEK293E were cotransfected with both wtTDP-43 and the CFTR minigene and were treated with the same inhibitors. Neither endogenous nor overexpressed TDP-43 CFTR splicing activity was affected by any of the selected treatments (Fig 4.13C).

Together with the results from section 3. 3. 1, the data suggests that while it is possible to modulate the acetylation status of TDP-43 via KDAC inhibition to a certain extent, the increase in total acetylation is not specifically affecting K84 and K136. Even if a fraction of the observed increase in acetylation corresponds to K84 or K136, it does trigger a detectable change in nuclear-cytoplasmic shuttling nor RNA splicing activity. The lack of antibodies about single acetylated lysines at this point does not allow for more detailed investigation into the impact of KDAC inhibition in TDP-43 acetylation status.

4. 4.- Amino acid substitutions at K136 trigger pathological phosphorylation, loss of solubility and RNA-binding deficiencies

Recent research has proposed loss of RNA-binding to prompt pathological characteristic of TDP-43 such as loss of solubility and aggregation (404). This hypothesis suggests that RNA-binding counteracts the aggregation potential of free-roaming TDP-43 and sets the loss of RNA-binding at the beginning of TDP-43 proteinopathy pathway. As it has been showed before, glutamine substitution at K136 causes a nuclear distribution that resembles the one from the RNA-binding deficient FFLL (246) (Fig 4.8). Therefore, it is possible the acetylation-driven loss of TDP-43 RNA-binding contributes to its proteinopathy. To test this idea, K136R and K136Q RNA binding

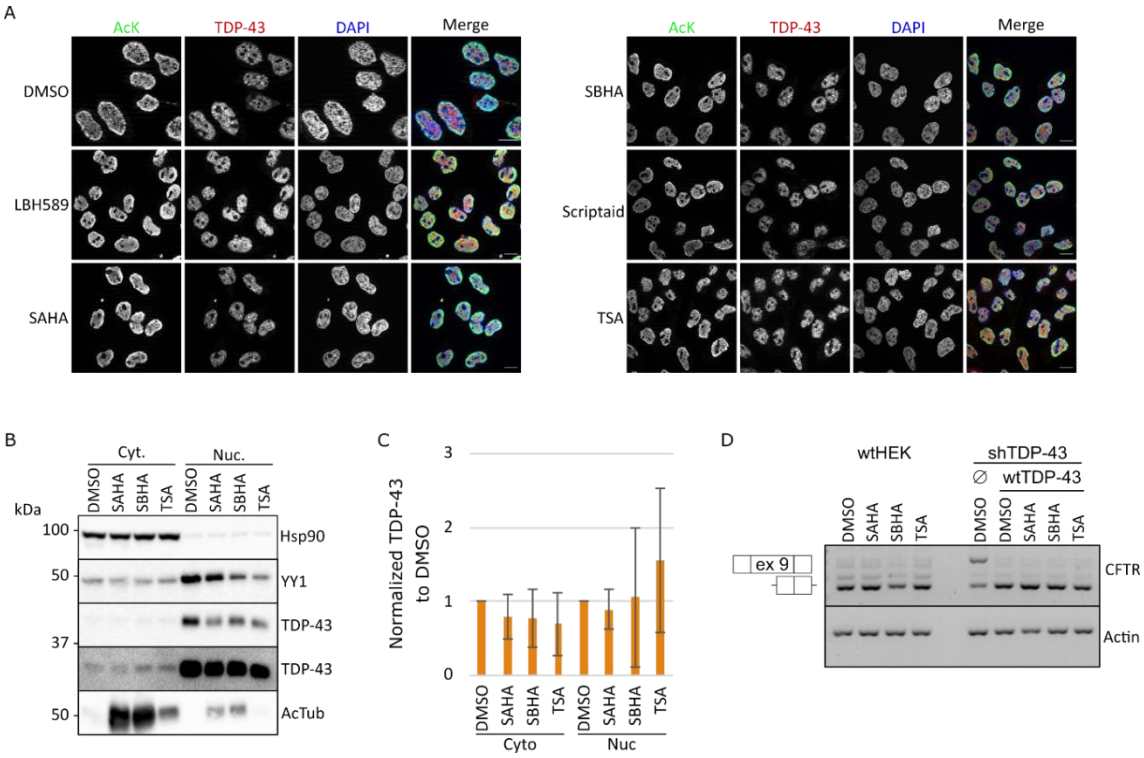

Figure 4. 13.- KDAC inhibition does not impact TDP-43 distribution or splicing capabilities. A) wtHEK293E cells were treated for 6 hours with either 0.01% DMSO, 2µM LBH589, 2µM SAHA or 30µM SBHA, or for 3 hours with 6µM Scriptaid or 1µM TSA. Cells were then fixed and costained with anti-TDP-43 and anti-panacetyl-lysine antibody. Scale bar represents 10µm. B) wtHEK293E cells were treated with either DMSO, SAHA, SBHA or TSA at the same concentrations and times than in A. Cytoplasmic and nuclear fractions were separated and analysed via western blot. C) Quantification of B. N = 3. No significant differences were detected. D). wtHEK293E were transfected with a CFTR minigene construct and treated with DMSO, SAHA, SBHA and TSA at the same concentrations and times than in A and B. In parallel, sh^{TDP-43}-HEK293E cells were cotransfected 48 hours before RNA extraction with the CFTR minigene construct and either 6xHis empty plasmid or 6xHis-tagged wtTDP-43. Before the extraction cells were treated with either DMSO, SAHA, SBHA or TSA under the same conditions than in A. THE extracted RNA was retrotranscribed and Actin and CFTR transcripts were analysed via PCR. N = 2.

capabilities and pathological characteristics were characterized in detail.

4. 4. 1.- K136R and K136Q TDP-43 have reduced solubility, enhanced ubiquitination and are pathologically phosphorylated

One of the main markers for aggregation potential and disease is the loss of TDP-43 solubility (20,24,405). To test if K136/Q substitution shifted TDP-43 into the insoluble fraction, HEK293E cells were transiently transfected with different 6xHis-tagged TDP-43 constructs. To avoid any interference from endogenous TDP-43 $sh^{TDP\text{-}43}$-HEK293 were used. To assess the solubility, a RIPA-Urea fractionation assay was performed. As a control for pure RNA-binding loss, 3xFlag tagged FFLL TDP-43 was used. The fractions were then analysed via western blot. Both K136R and K136Q TDP-43 display a strong loss of solubility indicated by the shift to the urea fraction (Fig 4.14A). In contrast, it is worth noting that FFLL TDP-43 does not display the same shift into the insoluble fraction, suggesting that K136R and K136Q mutations impact TDP-43 solubility not only via RNA-binding reduction.

Next, the posttranslational modifications of K136 mutants were assessed. It has been reported that TDP-43 is phosphorylated at serines 409/410 and ubiquitinated (23,54,226). To test is this was the case for the K136 TDP-43 mutants, cells were transiently transfected with 6xHis tagged TDP-43, lysed in urea buffer and tagged proteins were purified via Ni-NTA beads. As a positive control for ubiquitination MG-132, a proteasomal inhibitor, was used. Both K136R and K136Q TDP-43 showed a ubiquitinated smear indicative of polyubiquitin chains (Figure 4.14B). In addition, pS409/410 specific antibodies showed that both mutants are phosphorylated at these residues.

Lastly, to validate the phosphorylation at S409/410 observed in Western blot, cells were transfected with the same wtTDP43 and K136R/Q mutants, fixed and costained for TDP-43 and pS409/410 TDP-43. When observed, only K136R/Q aggregates showed pS409/410 TDP-43, while the smaller aggregates and more diffuse TDP-43 did not colocalise with p409/410 (Fig 4.14C).

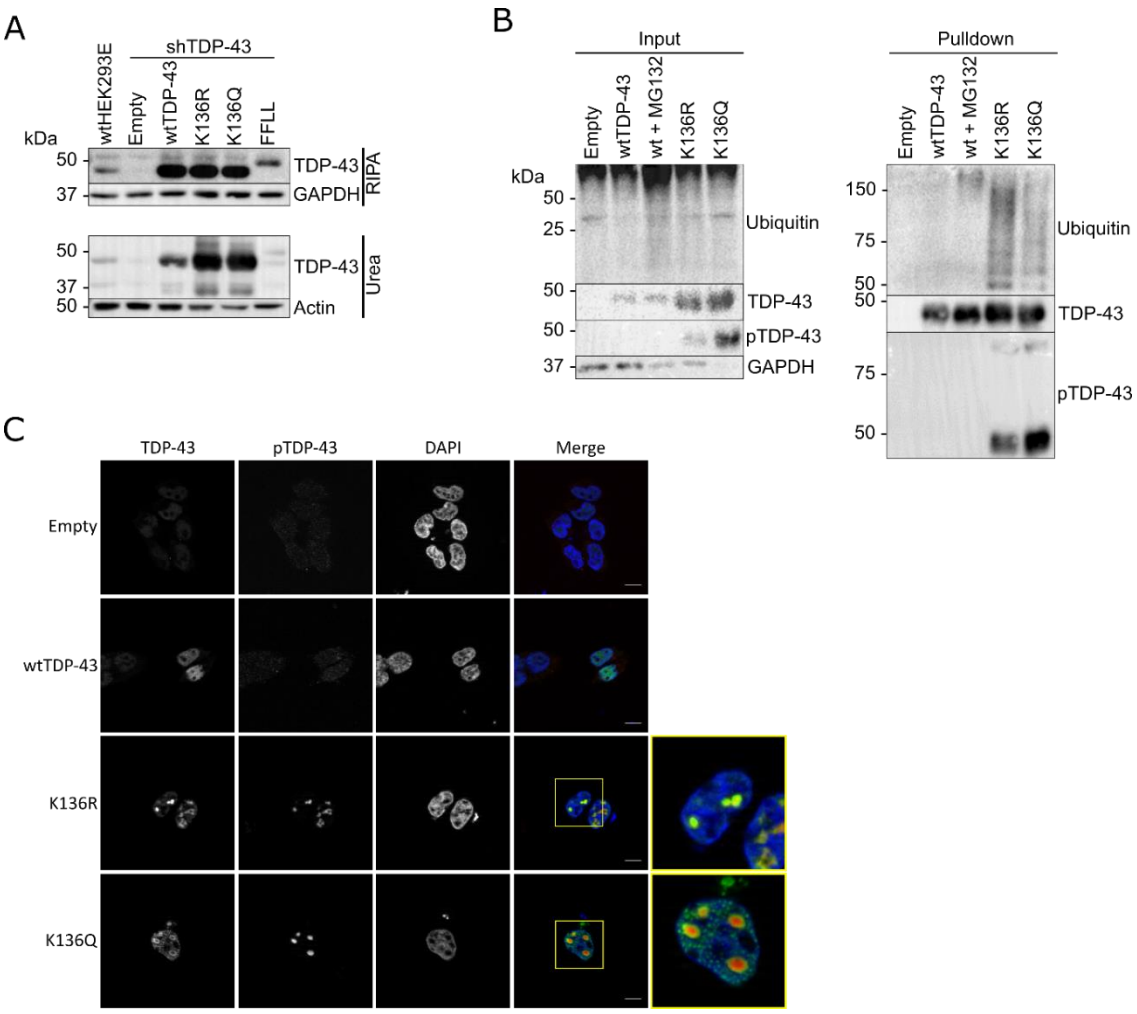

Figure 4. 14.- Biochemical characterization of K136R and K136Q TDP-43. A) Both transiently transfected sh^{TDP-43}-HEK293 and wtHEK293E cells were lysed and RIPA- and Urea-soluble fractions were separated. Fractions were analysed via western blot. N = 2. B) sh^{TDP-43}-HEK293 were transfected with different 6xHis TDP-43 constructs. As a ubiquitination control, one of the samples was treated with MG132 20µM for 6 hours before lysis. Cells were lysed in urea buffer and 6xHis tagged proteins were isolated via Ni-NTA purification. Samples were analysed via western blot. N = 3. C) Transfected sh^{TDP-43}-HEK293 cells were transfected with 6xHis TDP-43 constructs for 72 hours and then were fixed and costained for immunofluorescence. Scale bar represents 10µm.

While KDAC inhibition did not result in a loss of RNA splicing capabilities, the loss of solubility in the presence of KDAC inhibitors was not measure. To test if any of the previously used KDAC inhibitors influenced wtTDP-43 solubility, wtTDP-43 or K136R TDP-43 were transfected and cells were treated with either DMSO, SAHA, SBHA or TSA. Since KDAC inhibition did not have any detectable effect on endogenous TDP-43 subcellular localisation or function, the overexpression of TDP-43 would allow to detect smaller changes in solubility due to the wider range of expression. After analysing the soluble and insoluble fractions, treatment with SAHA increased the insolubility of wtTDP-43, although not to the levels of K136R TDP-43 (Fig 4.15). In addition, all treatments increased the insolubility of K136R TDP-43.

Even though the KDAC inhibitor treatment did not cause a complete shift into the insoluble fraction, this biochemical characterization of K136R/Q mutants shows at a minimum that substitutions at this position can trigger a loss of solubility, hyperubiquitination and pathological phosphorylation, that cannot be matched by KDACi treatment and that matches the main characteristics of TDP-43 aggregates found in FTD and ALS patients with TDP-43 proteinopathy.

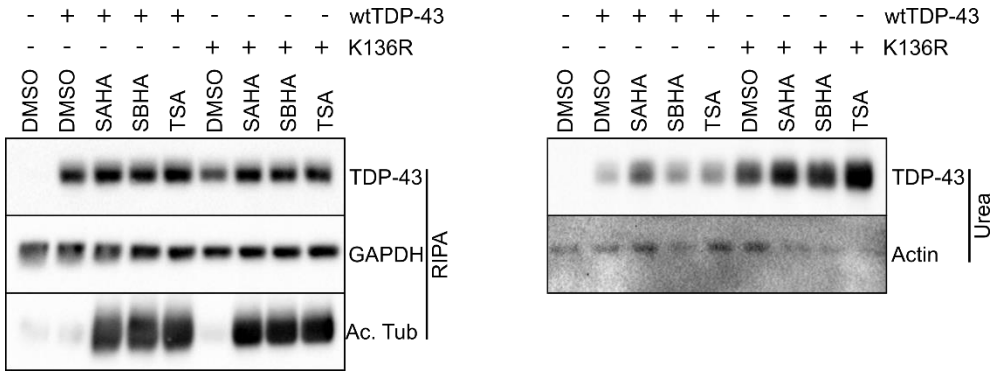

Figure 4. 15.- Effects of KDAC inhibition on wild-type and mutant TDP-43. sh^{TDP-43}-HEK293 were transfected with either an empty plasmid, 6xHis tagged wtTDP-43 or K136 TDP-43. Cells were treated with different KDAC inhibitors under the conditions already mentioned. Cells were lysed and RIPA- and Urea-soluble fractions were separated and analysed via western blot. N = 2.

4. 4. 2.- K136Q acetyl-mimic mutation prevents binding of TDP-43 to its RNA targets

While both acetyl-mimic and acetyl-dead substitutions at K136 cause a loss of RNA splicing of CFTR exon 9 (Fig 4.10E), it is unclear if these mutations interfere with the splicing activity of TDP-43 or with the binding of TDP-43 to mRNA. Since TDP-43 is involved in several stages of the protein production pathway (described in the introduction), fine tuning of its interaction with RNA might cause CFTR splicing deficiencies through different mechanisms.

To test the effect of mimicking acetylation at K136 in TDP-43 binding to RNA, an RNA-protein pulldown was performed. As a bait the $(UG)_{12}$ sequence was used (135,246) and as a negative RNA-binding control $(UC)_{12}$ sequence was added to the assay. wtTDP-43 could bind specifically to the $(UG)_{12}$ but not to the $(UC)_{12}$ control bait (Fig 4.15A). On the other hand, K136Q TDP-43 displayed a reduced, but not completely lost, binding affinity to the preferred $(UG)_{12}$ sequence. None of the mutants showed any binding to the naked beads.

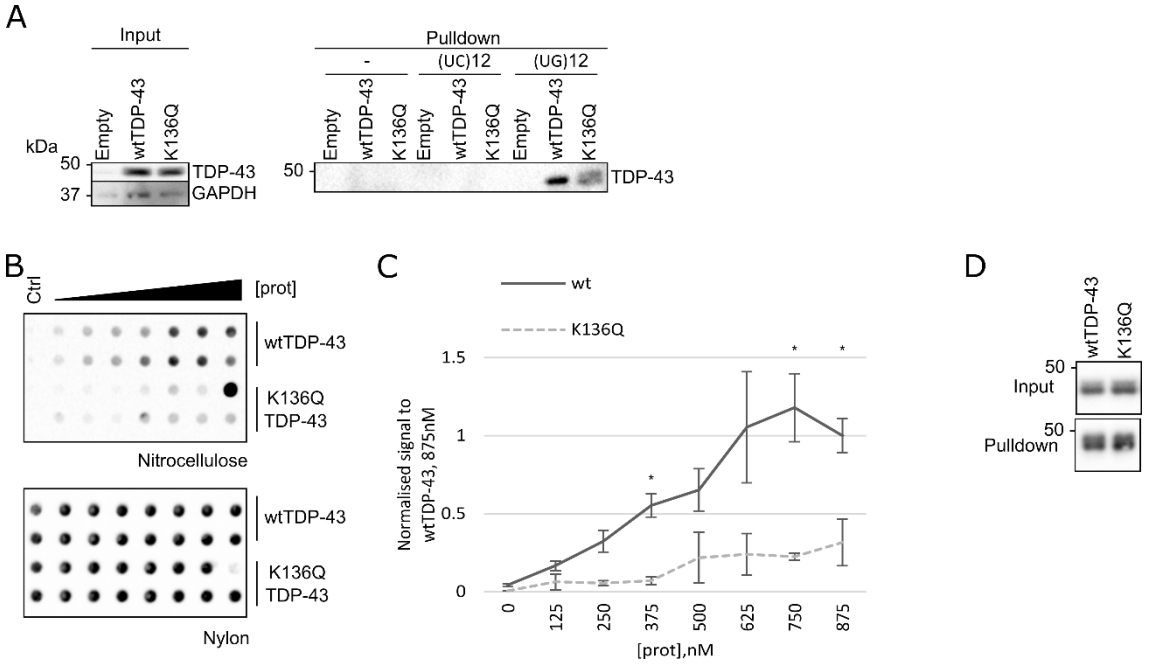

Figure 4. 16.- Acetyl mimic K136Q reduces RNA-binding capabilities of TDP-43. A) RNA-protein pulldown of wt and K136Q TDP-43. HEK293E cells were transfected with 6xHis-tagged TDP-43 constructs. After lysis, protein extracts were incubated with biotinylated $(UC)_{12}$ or $(UG)_{12}$ oligomers. Protein-RNA complexes were later purified via magnetic streptavidin beads. Proteins were eluted and analysed via Western blotting. B) RNA-filter binding assay of wt and K136Q TDP-43. Increasing concentrations of 6xHis tagged TDP-43 was incubated with biotinylated $(UG)_{12}$ oligomers. RNA-protein complexes were analysed via an RNA-filter binding assay containing nitrocellulose and nylon membranes. Membranes were incubated with HRP-coupled streptavidin. C) Quantification 3 replicates of the filter binding assay shown in A. N = 2. * = $p > 0.05$. D) Representative protein levels of TDP-43 before and after the native purification for the filter biding assay.

To confirm the apparent effect of K136Q substitution on TDP-43 binding, a filter-trap binding assay was performed. Increasing concentrations of purified 6xHis-tagged TDP-43 was incubated with biotinylated $(UG)_{12}$ oligomers. The complexes were incubated and washed through a nitrocellulose membrane on top of a positively charged nylon membrane. RNA bound to TDP-43 remains on the nitrocellulose membrane, while free RNA flows to the nylon membrane. The assay showed that in the presence of an excess of RNA, increasing concentrations of wtTDP-43 can bind a higher proportion of RNA than K136Q TDP-43 (Fig 4.16B-D).

Altogether, K136Q TDP-43 displayed a reduced RNA binding affinity both in the RNA-protein pulldown and in the filter binding assay. The apparent partial loss of binding is supported as well by the partial loss of CFTR splicing activity (Fig 4.10E-F).

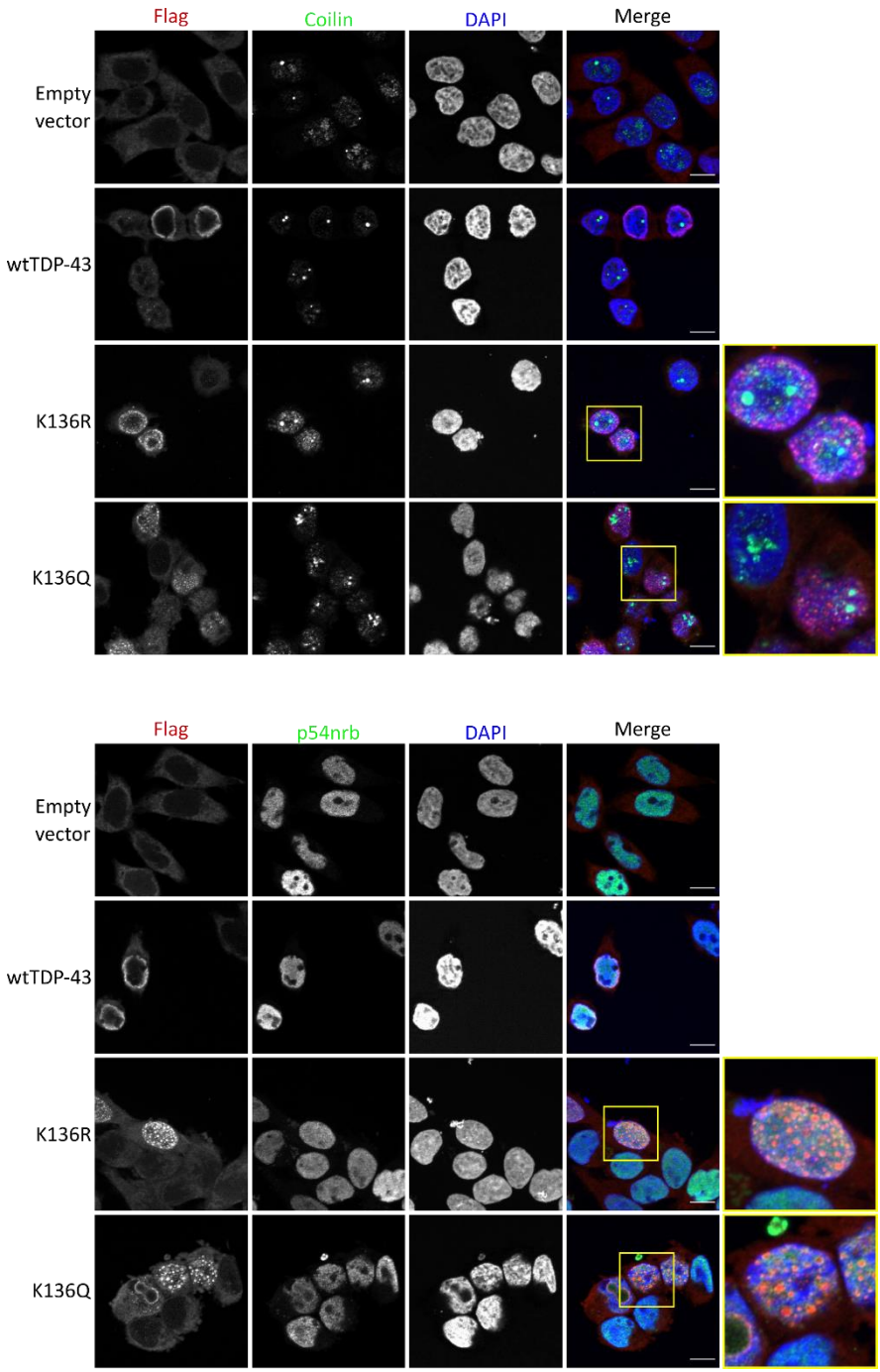

Figure 4. 17.- K136Q TDP-43 does not colocalise with Cajal bodies nor paraspeckles. Cells were transfected with different Flag-tagged TDP-43 constructs, fixed and costained with α-Flag and with either α-coilin or α-p54nrb. N = 2. Scale bar represents 10µm.

4. 4. 3.- K136Q aggregates do not colocalise with any of the major nuclear compartments

After observing the segregation of K136Q TDP-43 into individual nuclear entities, the first question that came up was the composition of these aggregates or if the amino acid substitution triggers an enrichment of TDP-43 in specific subnuclear compartments. To check if this was the case, transfected cells were costained with Flag (against Flag-tagged TDP-43) and antibodies

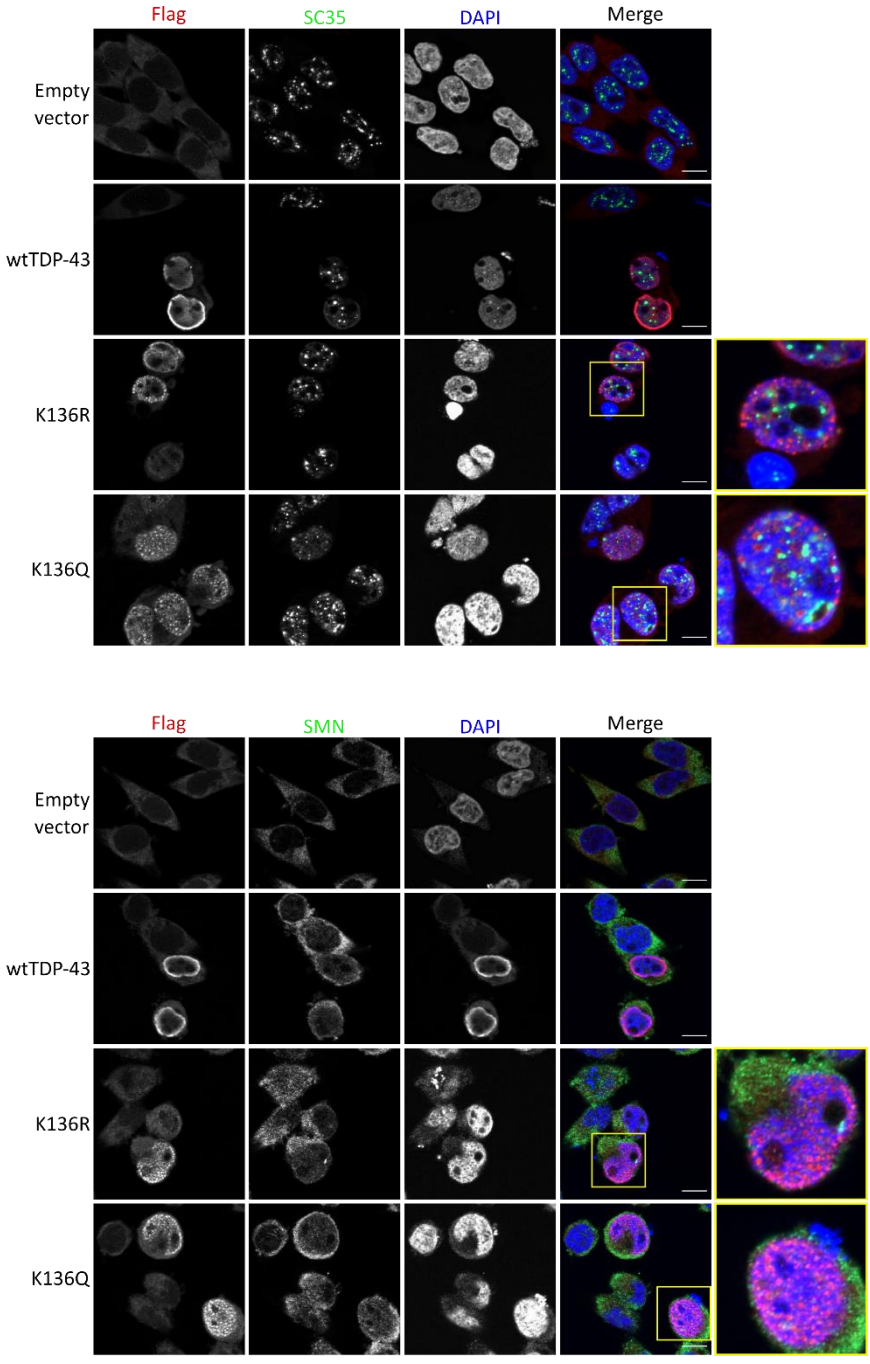

Figure 4. 18.- K136Q is not enriched in nuclear speckles nor SMN granules. Cells were transfected with Flag-tagged TDP-43 constructs and after 72 hours were costained with α-Flag and with either α-SC35 or α-SMN. N = 2. Scale bar represents 10µm.

against SC35 (SRSF2), Coilin, SMN and p54, each of them a marker of a subnuclear compartment. SC35 is a component of nuclear speckles, Coilin and SMN are markers of Cajal bodies and p54 is a core element of paraspeckles(288,406). None of the markers colocalised with neither wild type

nor mutant TDP-43 (Fig 4.17 and 4.18). SMN antibody only showed exclusively cytoplasmic signal and little to no staining of Cajal bodies, raising concerns about its specificity. However, for the purpose of this experiment coilin identified Cajal bodies unequivocally.

Since the analysis of nuclear bodies' markers colocalising with TDP-43 returned no results, it suggests that K136 amino acid substitutions induce the formation of a new, distinct nuclear phase. These inclusions could be formed by stable interactions between TDP-43 molecules alone or with another partner or could be formed by liquid-liquid phase separation mechanisms. To distinguish between the two of them, a more detailed study of TDP-43 behaviour is needed at this point.

4. 4. 4.- K136Q TDP-43 forms liquid droplets that coalescence over time

While the trigger and aggregation process of TDP-43 are not fully described, in recent years RNA-binding has been proposed as a counterbalance to the aggregation propensity of free TDP-43 (251,404). The observed reduction in RNA-splicing capabilities found in K136R and K136Q is similar to K145Q TDP-43 (Fig 4.10E), which was reported to form aggregates (249,253). These results, together with the subcellular distribution observed in immunofluorescence and the apparent loss of solubility, suggested that the amino acid substitutions at K136 could trigger the formation of aggregates as well.

To check if the K136R/Q dots observed in immunofluorescence were indeed phase separated droplets, a fluorescence recovery after photobleaching (FRAP) assay was performed. For live cell imaging C-terminally EGFP tagged TDP-43 constructs were generated. wtTDP-43 transfected cells showed a diffuse, nuclear distribution of TDP-43 that recovered quickly, reaching 50% of the normalised fluorescence 25 seconds after bleaching (Fig 4.19A-B). When K136Q TDP-43 was analysed, the fluorescence recovery was slower, taking up to 100 seconds to recover half of the fluorescence in the smaller aggregates and barely recovering at all in bigger aggregates. Due to this considerable difference, an arbitrary distinction between smaller than 0.5µm and bigger than 1µm was used to analyse the results (Fig 4.19B). The percentage of immobile, non-recoverable fraction are significantly different between the 3 types of distribution (diffuse, small and big aggregates) (Fig 4.19C).

The progressive loss of fluorescence recovery is one but not the only characteristic of LLPS (407). Another characteristic of phase separated droplets is the ability to fuse among them and coalescence into bigger entities. To test if this was the case for K136Q TDP-43, EGFP-tagged TDP-43 was transfected and the cells were imaged for up to 3 hours in a live cell imaging set up, allowing a close-up look into the dynamics of the phase separated granules (Sup. Video 1-3). In the videos some K136Q TDP-43 droplets fuse into bigger bodies (Fig 4.19D) and when comparing the beginning and the end of the recordings there seems to be a trend for bigger aggregates over time. To quantitatively analyse if this was indeed the case, cells were transfected and fixed

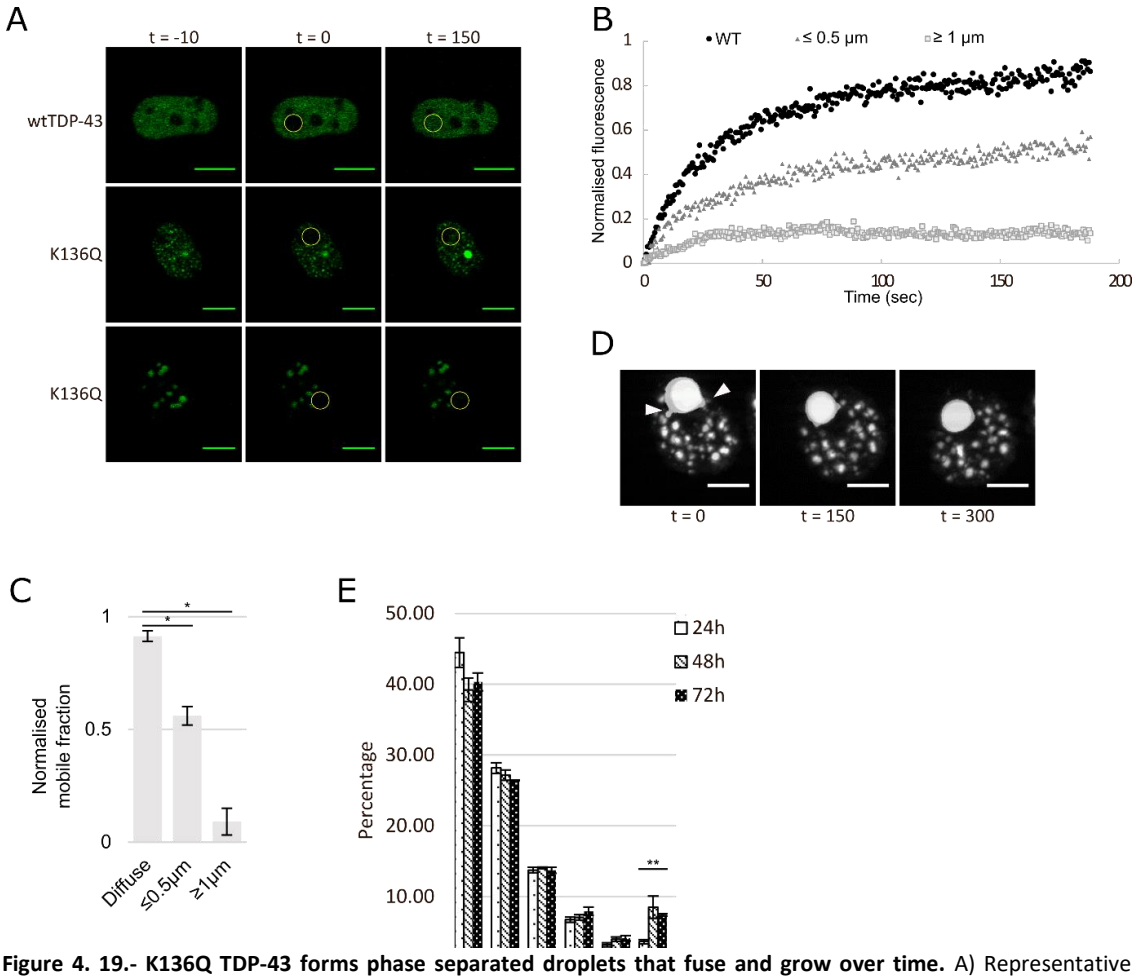

Figure 4. 19.- K136Q TDP-43 forms phase separated droplets that fuse and grow over time. A) Representative images of FRAP analysis of different TDP-43 aggregates. HEK293E cells were transfected with different C-terminally EGFP-tagged TDP-43 constructs. Bleached area marked in yellow. Cells were recorded for up to 150 seconds after bleaching. Time in seconds. Scale bar represents 5µm. B) Quantification of normalised fluorescence of bleached spots in the FRAP analysis. Aggregates were split in two categories depending on the size. 3 cells quantified per group. C) Quantification of the normalised mobile fraction of the FRAP analysis. 3 cells analysed per group. * = p <0.05. D) Representative frames of live cell recordings. Cells were transfected with EGFP-tagged K136Q TDP-43 and recorded for up to 3 hours. White arrows mark fusing droplets. Time in seconds. E) Histogram of K136Q TDP-43 aggregate size at 24, 48 and 72 hours after transfection. Cells were transfected and fixed and prepared for immunofluorescence at different timepoints after transfection. 100 transfected cells were analysed for each time point. ** = p < 0.01.

24, 48 or 72 hours after transfection and the resulting images were analysed then in a semi-automatic manner. 24 hours after transfection the percentage of K136Q TDP-43 droplets bigger

than 10µm is slightly below 5%, and this percentage increases after 48 hours to around 8% (Fig 4.19E). The increase of aggregates bigger than 10µm is significant and, while not significant, there is a decreasing trend in the smallest size of aggregates quantified.

These results show that K136Q TDP-43 can form phase separated droplets that fuse and increase in size over time and, additionally, lose fluidity during this process. This supports the idea of a progressive loss of fluidity in LLPS bodies that eventually turn into solid aggregates. This process could be triggered by the loss of RNA-binding caused by acetylation at K136. However, the nature of the mutagenesis approach is limited and therefore a more precise method to study acetylation is needed to prove its involvement in the process.

4. 5.- Site-specific acetylation of TDP-43 via amber suppression in HEK293E cells

Up until this point, acetyl-mimic K136Q TDP-43 recapitulates the hyperubiquitination, C-terminal phosphorylation and aggregation potential that characterises pathological TDP-43 inclusions. However, K136R TDP-43 acetyl-dead carries the same posttranslational modifications and apparent loss of RNA splicing activity. Therefore, it is not possible to elucidate if these effects are due to the mimicking of acetylation of the glutamine substitution or an artifact affecting the protein backbone.

To examine the possible artifacts introduced by point mutagenesis a clash analysis of the mutants was performed on PyMOL with the NMR structure of TDP-43 bound to RNA (PBD: 4BS2). K136 is located in the RNA binding pocket of the RRM1 in close proximity to F147 and F149 (Fig. 4.20). When the molecular clashes are analysed, K136R seem to clash not with the RNA but with residues in the amino acid chain (represented with the red circles in Fig 4.20, central right panel). This could disrupt the local structure of the RNA binding pocket and prevent binding to the nucleotide chain in an artificial way. On the other hand, AcK136 only shows clashes with the RNA chain, suggesting that the modification can truly have a modulatory effect on TDP-43's binding to RNA. This case shows the limitations of point-mutagenesis to study posttranslational modifications at structural sensitive residues and highlights the need for a better model system.

After these limitations became apparent, the point mutagenesis approach was replaced with site-specific incorporation of unnatural amino acids via amber suppression. While not completely devoid of limitations, amber suppression can introduce truly acetylated lysine at specific sites. In addition to prevent structural artifacts, the introduction of truly acetylated lysine allows the examination of the *in vivo* deacetylation dynamics.

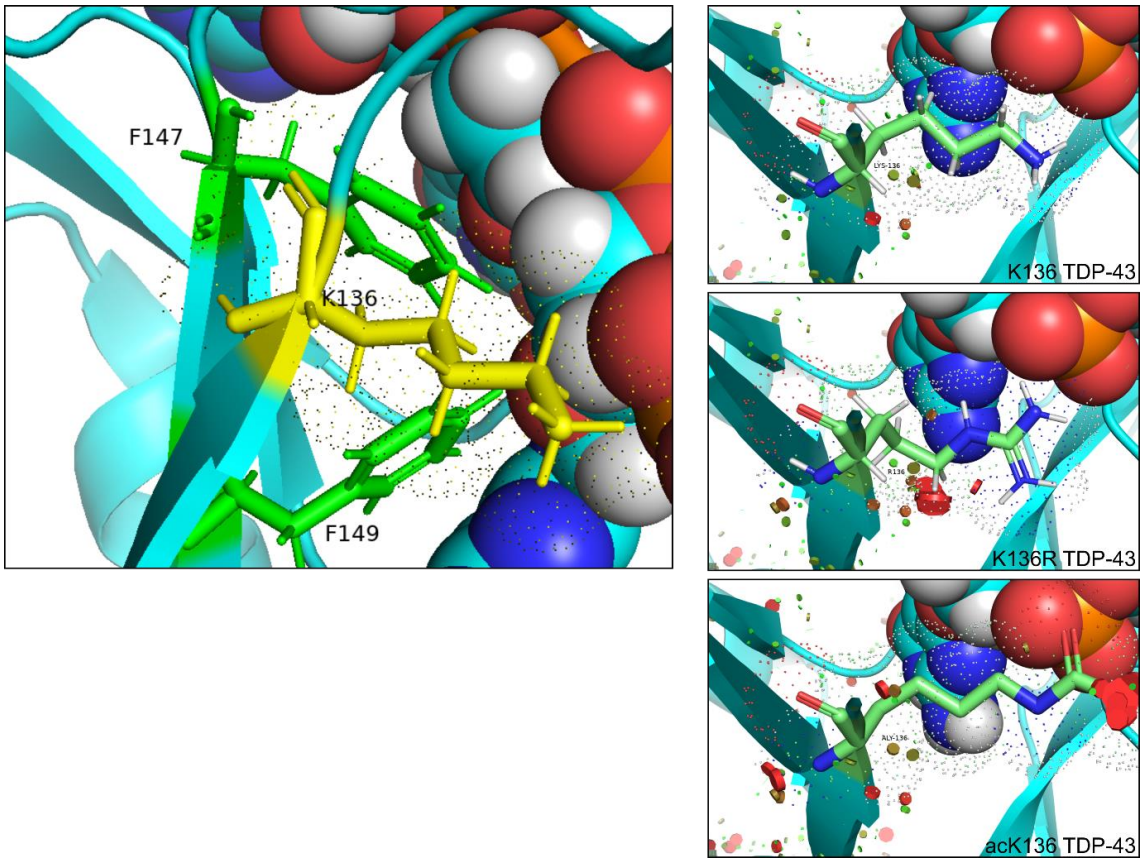

Figure 4. 20.- Close up of molecular environment of K136. Left panel shows the position of K136 sidechain in respect to F147, F149 (green) and RNA (represented by the globular structure on the right). The dotted cloud represents the true size of the molecule. Right panels show the points of contact of K136, K136R and acetylated K136. Points of contact are represented by green circles; clashes are represented by red circles. The size of the circle corresponds to the magnitude of the clash. PBD: 4BS2.

4. 5. 1.- Amber suppression optimization in HEK293E cells

The first step to implement amber suppression in live HEK cells was to stablish an experimental set up to introduce acetylated lysine at a desired amino acid position. As described in the introduction, the amber system consists of 3 components: several copies of the $tRNA^{AcK}_{UAG}$, the acetyllysine-tRNA synthethase (AcKRS) and supply of acetylated lysine in the cell media. To stablish the method, two plasmids were generously provided by Dr. Simon J Elsässer (Karolinska Institute, Sweden): plasmid E451 encoding for 4 copies of $tRNA^{AcK}_{UAG}$ and one of AcKRS and plasmid E406 encoding for 4 copies of $tRNA^{AcK}_{UAG}$ and one of AcKRS C-terminally tagged with a Dendra fluorescent protein, with an amber stop codon between the AcKRS sequence and the Dendra tag (Fig 4.21A). The purpose of this second construct (E406) was to optimize the amber suppression system with a simple, fluorescent readout: The Dendra tag can only be transcribed if there is successful incorporation of acetyllysine at the amber stop codon of AcKRS.

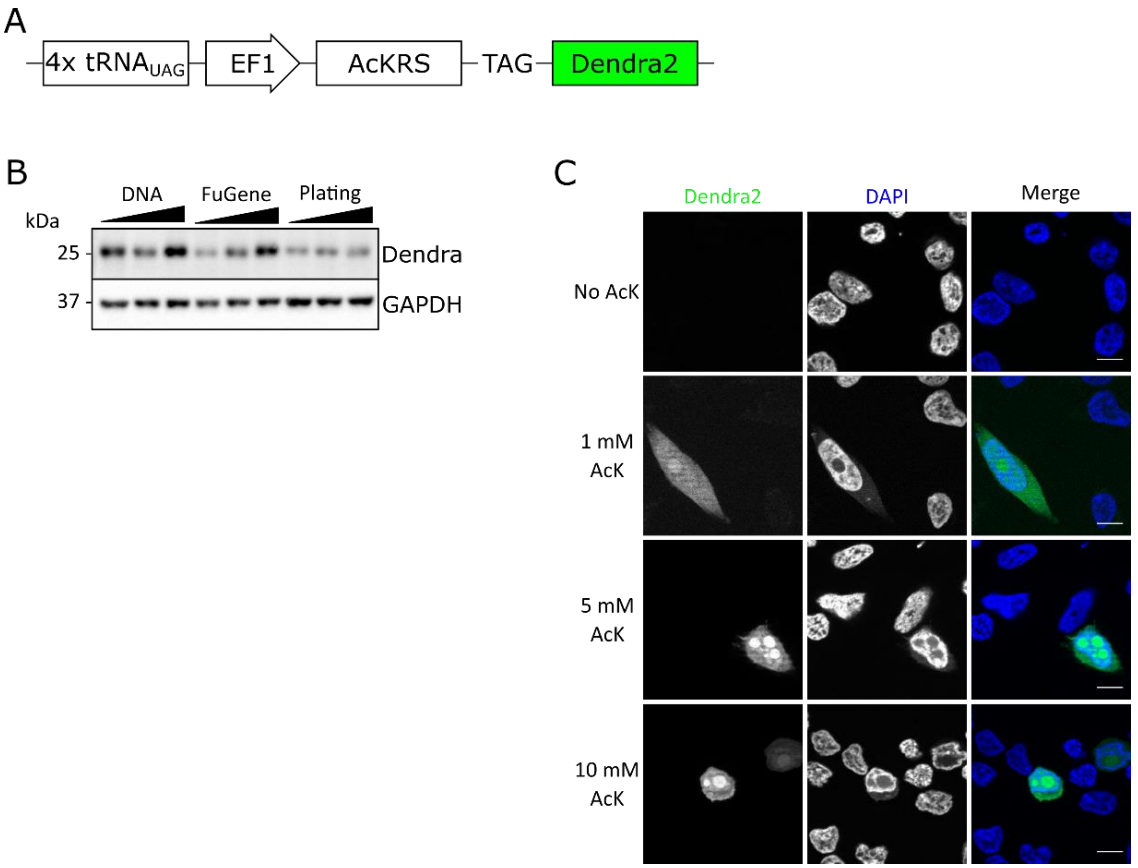

Figure 4. 21.- Optimization of amber suppression in HEK293E cells. A) Schematic of E406 plasmid, used to calibrate the amber suppression system. AcKRS is under the control of the EF1 promotor. The amber stop codon of AcKRS was followed by a Dendra2 coding sequence. B) Different parameters were tested to optimise the transfection of the amber suppression components and the successful incorporation of acetyllysine. HEK293E cells were transfected with the usual 1µg of AcKRS-Dendra2 plasmid, 2µg or 5µg. Different amounts of FuGene were tested (3:1, 4.5:1 and 6:1 µl per µg of DNA) and different concentrations of ($0.5x10^5$, $0.75x10^5$ and $1x10^5$ cells/mL). Cells were lysed in urea buffer and protein extracts were analysed via western blot. N = 1. C) Cells were transfected with the AcKRS-Dendra2 plasmid and were treated with different concentrations of acetyllysine for 24 hours before fixing and staining the nuclei with Hoechst. Scale bar represents 10 µm.

To find the best conditions for amber suppression *in vivo*, different transfection conditions and acetyllysine concentrations were tested. An increase in either DNA or transfection reagent (FuGene) increased the efficiency of the acetllysine incorporation (Fig 4.21B). Based on the indications of the manufacturer, the transfection reagent FuGene can be toxic at high concentrations, therefore increasing both the amount of DNA and FuGene was not a feasible option. For all following experiments, an increased amount of DNA was used in the transfection protocols (details can be found in the Materials and Methods section). After selecting the transfection conditions, different concentrations of acetyllysine were tested in immunofluorescence. Interestingly, the Dendra2-tagged AcKRS was located in the nucleolus of the cells, and every concentration achieved a robust incorporation of acetyllysine and subsequent translation of Dendra2 (Fig 4.21C). While immunofluorescence is an inherently qualitative method, there seems to be a plateau in Dendra2 signal in cells treated with 5mM and 10mM acetyllysine (Fig 4.21C). For this reason, a concentration of 5mM acetyllysine was used in subsequent experiments.

4. 5. 2.- Site-specific incorporation of acetylated lysine triggers cytoplasmic mislocalisation and phase separation in TDP-43

After selecting the optimal conditions for amber suppression in HEK293E cells, a new set of TDP-43 constructs for amber suppression were generated. Amber stop codons were introduced at either K84 or K136, the amber stop codon at the end of the DNA sequence was substituted by an ochre codon (TAA) and a 6xHis tag was transferred from the N-terminal end to a C-terminal position (Fig 4.22A). By doing so, the 6xHis tag can only be translated after successful incorporation of acetyllysine, allowing a reliable readout for amber suppressed TDP-43 in immunofluorescence. Instead of the self-containing Dendra2 plasmid used for the optimization (Fig. 4.21A), an optimised version of the AcKRS was used for all subsequent experiments (Fig 4.22A, E451). This construct was provided by Dr. Simon Elsässer and generated by continuous directed evolution by Bryson et al. (392).

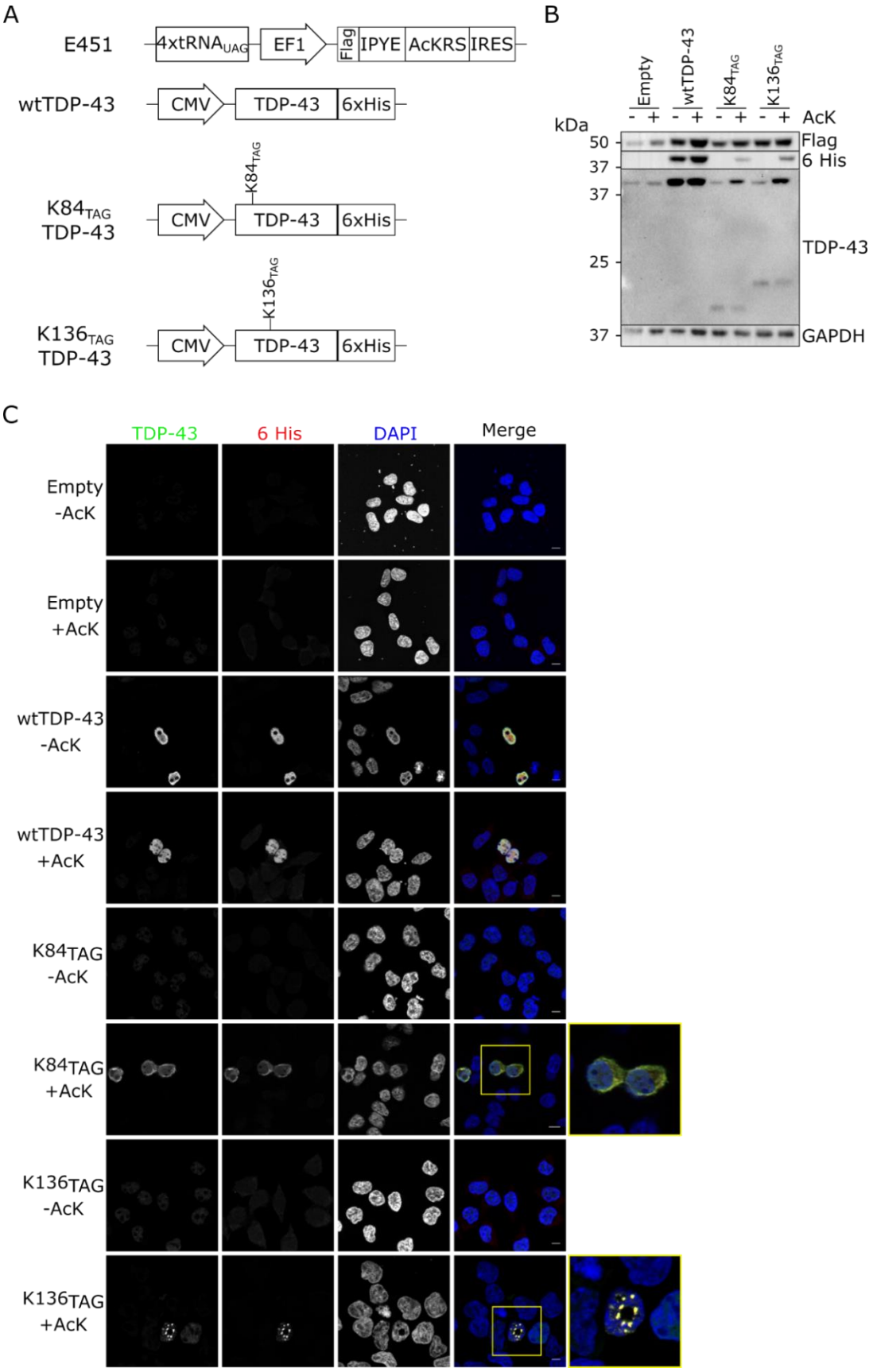
A
E451
4xtRNA$_{UAG}$
EF1
Flag
IPYE
AcKRS
IRES
wtTDP-43
CMV
TDP-43
6xHis
K84$_{TAG}$ TDP-43
K84$_{TAG}$
K136$_{TAG}$ TDP-43
K136$_{TAG}$
B
Empty
wtTDP-43
K84$_{TAG}$
K136$_{TAG}$
AcK
kDa
50
37
37
25
37
Flag
6 His
TDP-43
GAPDH
C
TDP-43
6 His
DAPI
Merge
Empty -AcK
Empty +AcK
wtTDP-43 -AcK
wtTDP-43 +AcK
K84$_{TAG}$ -AcK
K84$_{TAG}$ +AcK
K136$_{TAG}$ -AcK
K136$_{TAG}$ +AcK

Figure 4. 22.- Site-specific introduction of acetyllysine can trigger cytoplasmic mislocalisation and phase separation of TDP-43. A) Plasmids used to amber suppress TDP-43. E451 was generously provided Dr. Elsässer and characterised by Dr. Bryson. B) sh^{TDP-43}-HEK293 cells were cotransfected with E451 and either an empty or a TDP-43 construct. The cells were treated with 5mM acetyllysine for 24 hours before lysis in urea buffer. Samples were analysed via western blot. N = 2. C) Cells were cotransfected with E451 and a specific TDP-43 construct. Cells were treated with 5mM acetyllysine for 24 hours before fixation.

With these tools ready, sh^{TDP-43}-HEK293 cells were cotransfected with the E451 plasmid (containing 4 copies of $tRNA^{AcK}_{UAG}$ and the AcKRS) and different TDP-43 constructs carrying stop codons at either K84 or K136. Cells were treated for 24 hours with acetyllysine before fixation or lysis in urea buffer. The optimized Flag-tagged AcKRS was successfully expressed, and the protein levels were unperturbed by the acetyllysine treatment. While wtTDP-43 expression was not altered by the acetyllysine treatment, the 6xHis C-terminal tag of $K84_{TAG}$ and $K136_{TAG}$ TDP-43 was only detected in the presence of acetyllysine, showing successful acetyllysine incorporation of at those lysines (Fig 4.22B). In addition, truncated fragments can be observed for both mutants. These bands match the predicted size of the truncated forms that do not incorporate acetyllysine successfully (10 and 15kDa respectively). In addition, these truncated forms decrease as acetyllysine is added and full length TDP-43 is transcribed. The immunofluorescence analysis of amber suppressed TDP-43 showed that introduction of acetyllysine at K84 can induce cytoplasmic mislocalisation and that, at K136, it can trigger phase separation (Fig 4.22C). With these results it is possible to confirm the previous experiments using K84Q and K136Q TDP-43 constructs. On one hand, acetylation at K84 can modulate nuclear shuttling to a certain extent and on the other, acetylation at K136 causes TDP-43 to phase separate and form nuclear droplets.

After establishing an efficient amber suppression experimental setup, the validity of the point mutagenesis approach to study K79 and K121 was in question. For that reason, a set of constructs were generated carrying amber stop codons at those positions. In addition, as an extra control, an amber stop codon was introduced at Q118. The residue was chosen because of its location at the RRM1 and the similarities between glutamine and acetyllysine structures. Amber suppression could be performed successfully at these residues, but no changes were detected in TDP-43 cellular distribution (Fig 4.23A and B). These results act as a control for the specific effects observed in acK84 and acK136 TDP-43. These effects are not caused by an amber suppression artifact, they are the true effect of acetylation at K84 and K136.

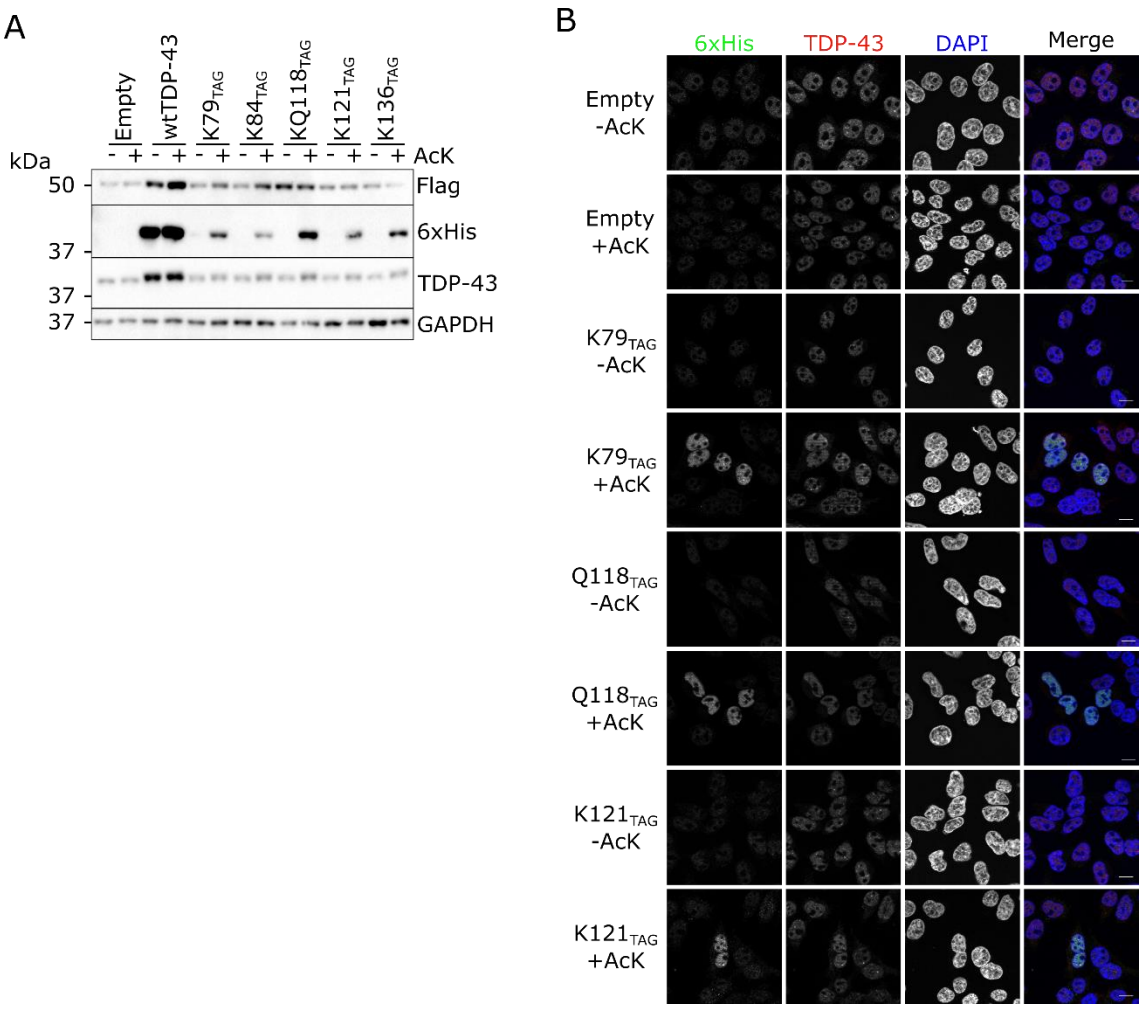

Figure 4. 23.- Acetylation at K79 and K121 does not impact TDP-43 subcellular localisation. A) HEK293E cells were cotransfected with E451 and TDP-43 constructs carrying amber stop codons at different positions. Cells were treated with 5mM acetyllysine for 24 hours before lysis in urea buffer. Samples were analysed via western blot. N = 1. B) The same cells from A) were prepared for immunofluorescence and costained for TDP-43 and 6xHis. Scale bar represents 10µm.

4. 5. 3.- Generation of stably amber suppressed sh^{TDP-43}-HEK293E cells

The previous results showed that it is possible to introduce acetyllysine into TDP-43 via amber suppression to study the effect of site-specific acetylations. Amber suppression has limited efficiency, manifested in the truncated TDP-43 band still present after amber suppression (Fig 4.22B) and it relies on protein overexpression. One of the concerns of transient transfection is the high protein expression, which is concentrated in those few transfected cells. To overcome this limitation, a stably amber suppressed cell line was generated. This was accomplished by using the PiggyBac recombinase system in sh^{TDP-43}-HEK293E cells. The plasmid E451 previously used to transfect the amber suppression components (Fig 4.22A) contains two inverted terminal repeat (ITRs) flanking the amber suppression components and a puromycin resistance gene. To integrate these elements into the cell genome, sh^{TDP-43}-HEK293E cells were cotransfected with

plasmid E451 and a plasmid containing the PiggyBac transposase. Cells that had successfully integrated the amber suppression components together with the puromycin resistance gene were selected with puromycin treatment.

To further optimise the system, a series of constructs were generated with TDP-43 under and EF1 promoter and that carried 4 additional copies of the $tRNA_{UAG}^{AcK}$ sequence (Fig 4.24A). These plasmids were transiently transfected, and their expression was compared to the previous pCMV TDP-43 plasmids (Fig 4.22A) The resulting pool of stably transfected cells showed a lower expression of the Flag-AcKRS and slightly lower amber suppression efficiency, observed by the intensity of the $K136_{TAG}$ TDP-43 band (Fig 4.24B). It is important to mention that for this experiment a monoclonal α-TDP-43 antibody generated against positions 205-222, therefore recognising only amber suppressed TDP-43 and none of the N-terminal truncated forms. In addition, when compared to the pCMV plasmids, the new EF1 TDP-43 constructs did not improve the amber suppression efficiency. The immunofluorescence analysis showed that AcKRS is located in the nucleoli, but it leaves it when acetyllysine is provided and there is an amber stop codon to suppress (Fig 4.24C). While the new EF1 plasmid did not improve the amber suppression efficiency, the integration of the AcKRS provided a more homogeneous expression throughout the cell population.

To improve the amount of AcKRS translated by the stably amber suppressed cells, individual clonal lines were generated. When the sh^{TDP-43}-HEK293E used in this study was generated, the sh^{TDP-43} sequence was tagged with EGFP to select the silenced cells (146). This tag was used in this study to segregate via fluorescence assisted cell sorting (FACS) the pool of stably amber suppressed cells and grow monoclonal lines. The clonal lines did show differences in Flag-AcKRS between lines and homogeneous expression within the lines as expected (Fig 4.25A and B). However, after several passages all clones lost the amber suppression capabilities (Fig 4.25C). Since the AcKRS was still detectable, it is possible that the $tRNA_{UAG}^{AcK}$ sequences were removed from the genome.

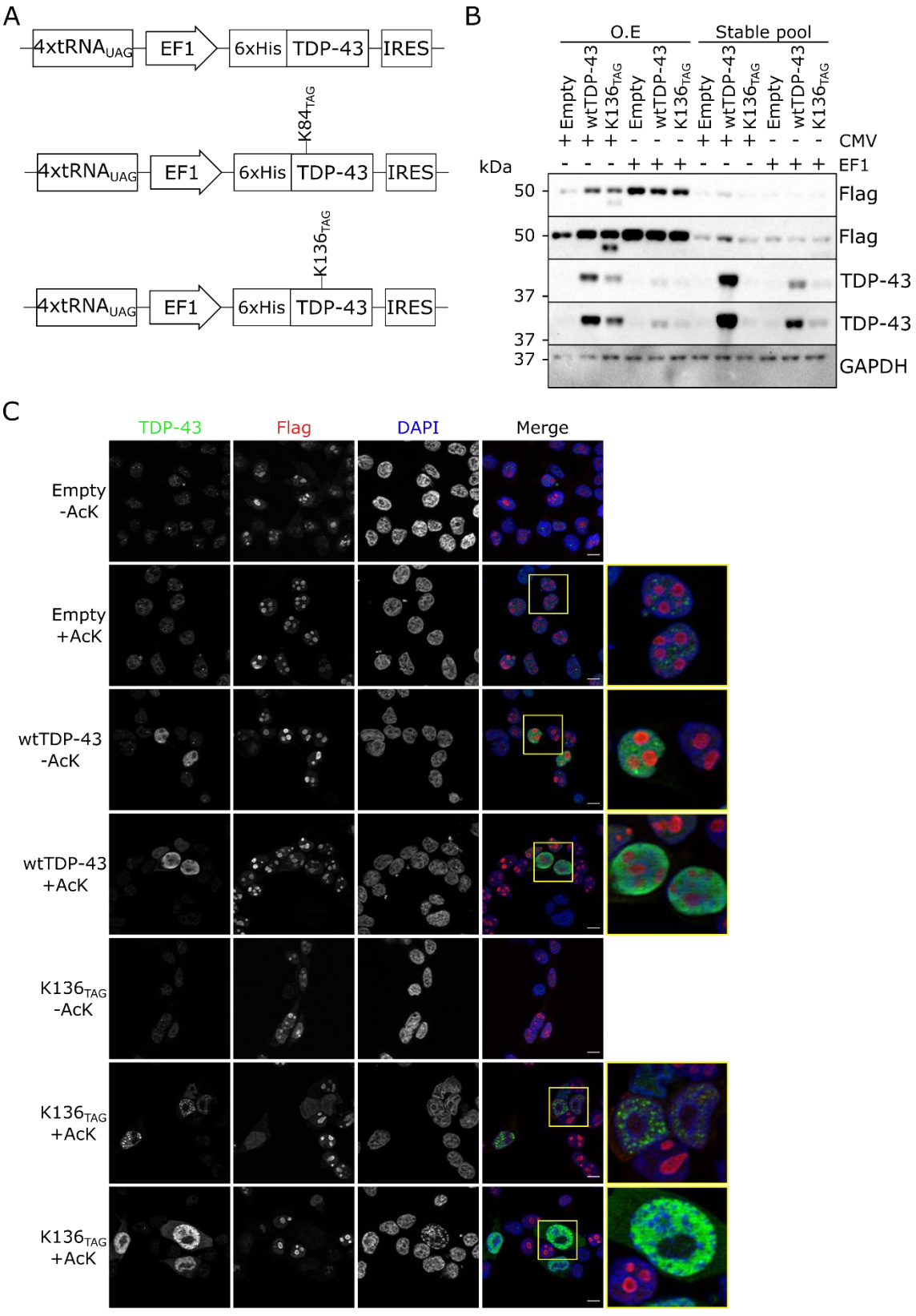

Figure 4. 24.- Generation of a stably amber suppressed pool of sh^{TDP-43}-HEK293E. A) pEF1 plasmids used to increase the number of tRNA$_{UAG}^{AcK}$ copies. B) Comparison of transiently transfected cells and stably amber suppressed cells and promoter efficiency. Cells were either cotransfected with E451 and different TDP-43 constructs, or in the case of the pool of amber suppressed cells only with TDP-43 constructs. All cells were treated with 5mM acetyllysine for 24

hours before lysis in urea buffer. Protein samples were analysed via western blot N = 1. C) Stably amber suppressed cells were transfected with different pEF1 TDP-43 constructs. Cells were treated with 5mM acetyllysine for 24 hours before fixation and costaining for TDP-43 and Flag. Scale bar represents 10µm.

Stably amber suppression is a very artificial system involving very basic cellular mechanisms; therefore, it is possible that alien tRNA sequences are specifically targeted for degradation. In addition, HEK293E cells are cancer cell lines with poor genetic stability. The low integration capabilities of HEK293E cells in the context of amber suppression was confirmed by Dr. Elssäser (personal communication). With this information and the generated data in mind, the generation of a stably amber supressed cell line was rejected, and transient transfection was selected as the method of choice for future experiments.

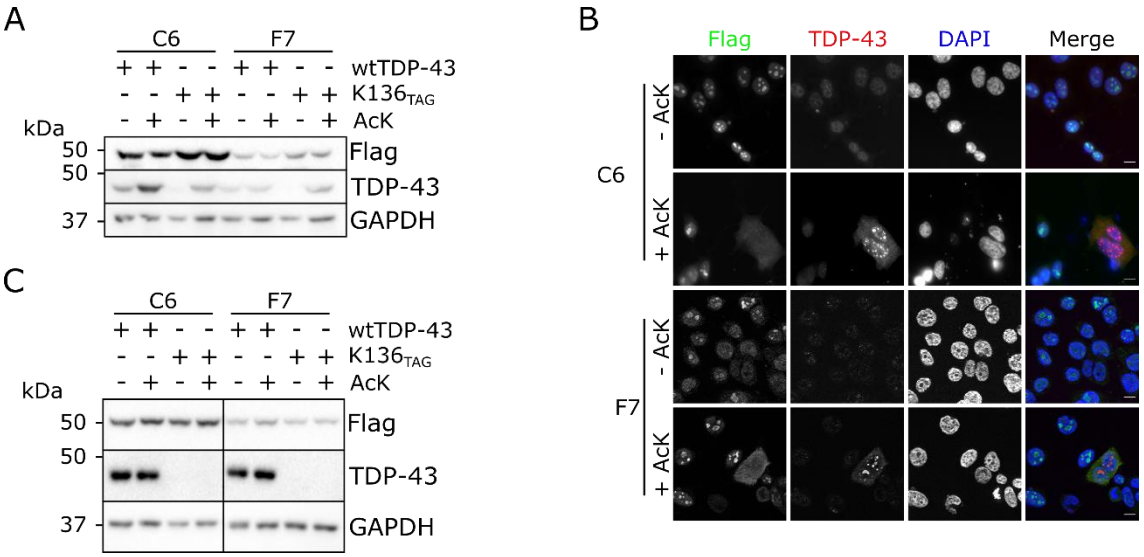

Figure 4. 25.- HEK293E stably amber suppressed monoclonal lines are not stable. A) Single clone colonies were grown from pool of $sh^{TDP\text{-}43}$-HEK293E selected after E451 integration. Cells were transfected with pCMV TDP-43 constructs and treated with 5mM acetyllysine for 24 hours before lysis in urea buffer. N = 1. B) Same cells from A) were fixed 25 hours after acetyllysine treatment and costained with α-Flag and α-TDP-43 (aa205-222). Scale bar represents 10 µm. C) Same clones from A), analysed after 10 passages (5 weeks). Cells had the same transfection and treatment than A), with the same lysis in Urea buffer. N = 2.

4. 6.- Characterization of amber suppressed TDP-43

After testing and optimizing the amber suppression system, the next step in the study was to characterize the truly acetylated TDP-43 to discern between point mutagenesis artefacts and the true acetylation effect. To do this, amber suppressed TDP-43 was analysed functionally and biochemically.

4. 6. 1.- Acetylated TDP-43 droplets are not detectably phosphorylated but have reduced splicing capabilities

To test if amber suppressed TDP-43 retained the pathological phosphorylation observed in the point mutant K136Q construct, amber suppressed cells were lysed or fixed for immunofluorescence and the levels of S409/410 phosphorylation were assessed in both western blot and immunofluorescence. Amber suppressed TDP-43 did not show any pathological phosphorylation in neither western blot nor immunofluorescence (Fig 4.26A and B). To see if they previously observed loss of CFTR splicing capabilities could be recapitulated by K136 acetylation, RNA was purified from amber suppressed cells and CFTR splicing status was analysed via PCR. While acetylation at K136 did not trigger any detectable C-terminal phosphorylation, it did cause an increase in CFTR exon 9 inclusion (Fig 4.26C).

These results suggest that while K136 acetylation impairs RNA splicing and triggers phase separation, the modification does not cause phosphorylation at the C-terminal domain of TDP-43. One of the reasons for this could be the difference in expression levels between K136Q and $K136_{TAG}$ TDP-43 (Fig 4.26A). Another reason could be the nature of the K136Q amino acid substitution. Glutamine and arginine contain delocalised electrons that can influence phase separation (408), accelerating the separation and triggering event further down the line of pathological aggregation. Together, these results support the previous assumption that acetylation at K136 is linked to a reduction in TDP-43 splicing capabilities, which eventually leads to phase separation. The determinants of this LLPS, however, remained to be determined.

4. 6. 2.- C-terminal domain is necessary for TDP-43 phase separation

Several parts of TDP-43 have been linked with its homodimerization and aggregation (409). From those, the unstructured C-terminal domain is widely considered to be crucial in homodimerization and protein-protein interaction. To test if the domain was involved in acetylation-driven LLPS, a new C-terminally tagged construct carrying an amber stop codon at position 136 and a deletion of the C-terminal domain (274-414). In addition, to check if the phase separation observed depended on the nuclear ecosystem, a mutNLS/$K136_{TAG}$ construct was generated.

The new plasmids and E451 were cotransfected into sh^{TDP-43}-HEK293E cells and the location and distribution of the 6xHis-tagged TDP-43 was analysed via western blot and immunofluorescence. Every construct was successfully translated to a similar level of K136$_{TAG}$ TDP-43 (Fig 4.27C). While 60% of the cells expressing K136$_{TAG}$ TDP-43 displayed some sort of nuclear aggregate, deleting the C-terminal domain reduce the percentage of cells with nuclear aggregates to <5% (Fig 4.27A

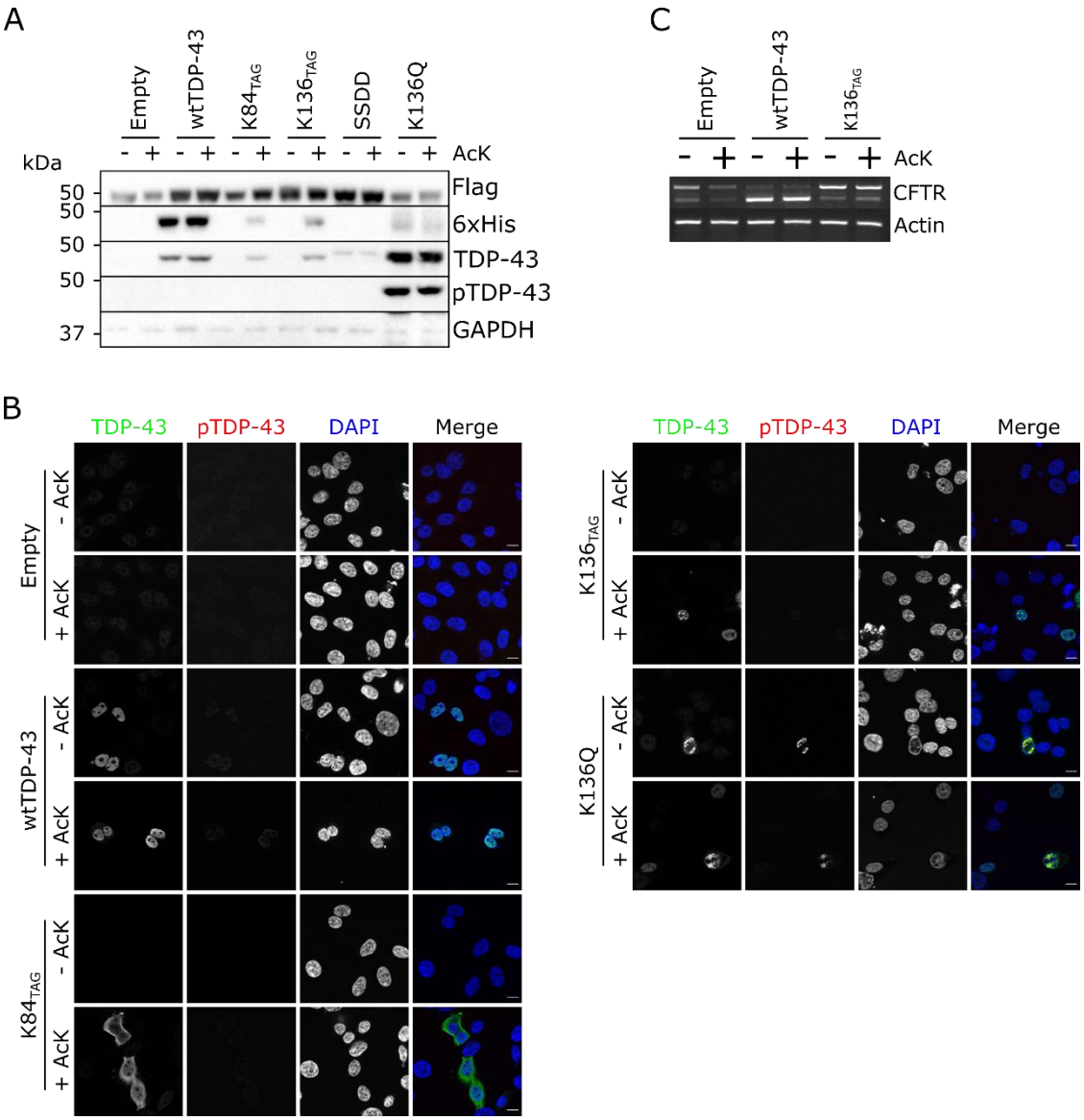

Figure 4. 26.- Phosphorylation state and splicing capabilities characterization of amber suppressed TDP-43. A) Transiently amber suppressed sh^{TDP-43}-HEK293E cells were transfected with different TDP-43 constructs and treated with 5mM acetyllysine for 24 hours before lysis in urea buffer. Protein lysates were analysed via western blot. N = 4. B) Amber suppressed sh^{TDP-43}-HEK293E cells were transfected with the mentioned TDP-43 constructs, treated for 24 hours with 5mM acetyllysine and fixed for immunofluorescence analysis. Scale bar represents 10 µm C) Transiently amber suppressed cells were cotransfected with different TDP-43 constructs and a CFTR minigene. RNA was isolated and targets were amplified after rtPCR. N = 2.

and B). The introduction of mutations at the NLS caused acetylated TDP-43 to form droplets in the cytoplasm, albeit to a lesser extent than in the nucleus (Fig 4.27A and B).

These results suggest that the C-terminal domain of TDP-43 is not only involved in classical protein-protein interactions but also in liquid-liquid phase separation. In addition, under the right circumstances acetylated TDP-43 can phase separate in the cytoplasm as well, giving rise to cytoplasmic aggregates. These would be even closer to the pathological aggregates found in patients, which could be the result of a two-step aggregation process.

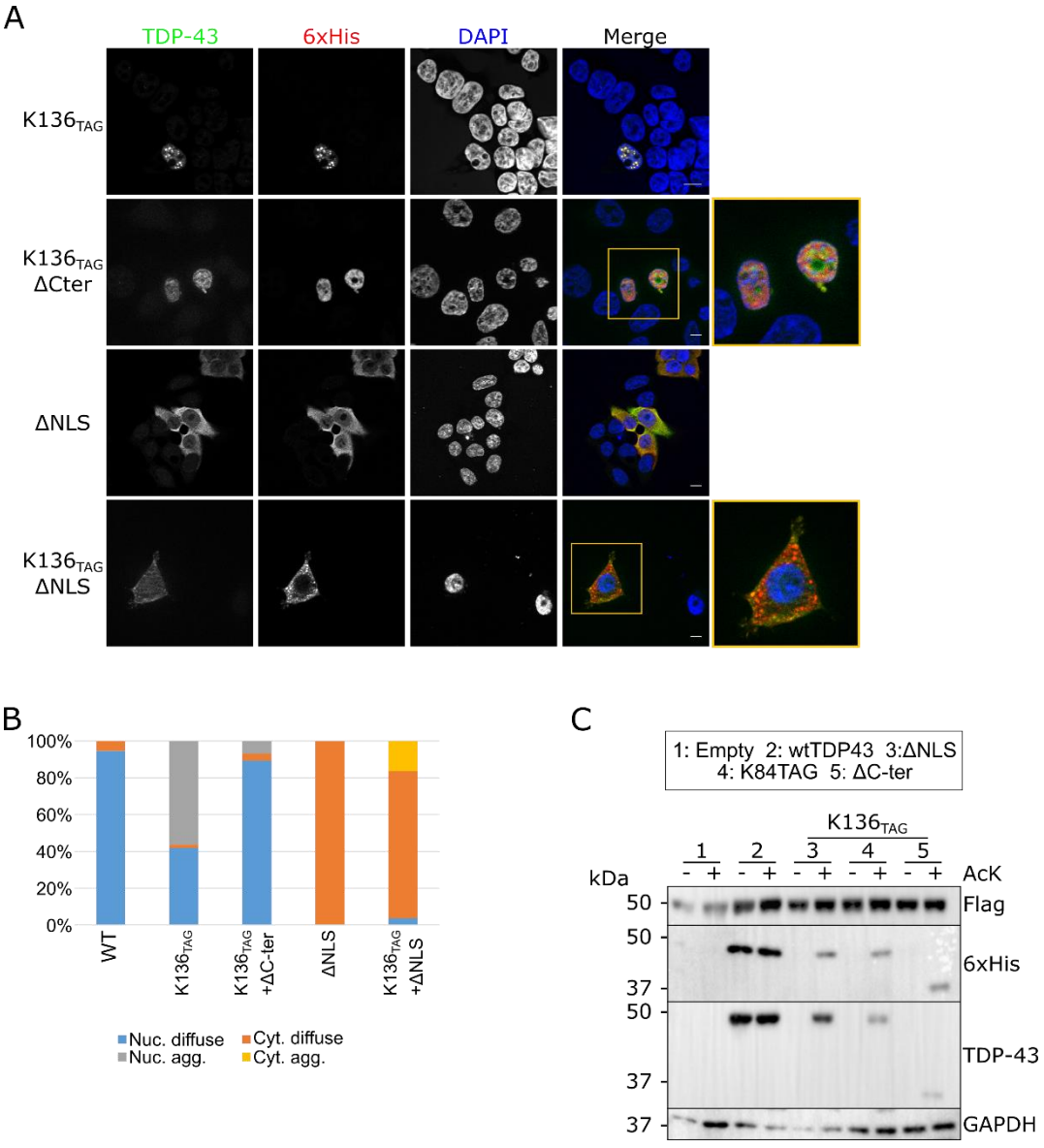

Figure 4. 27.- TDP-43 LLPS is dependent on C-terminal domain and can form in the cytoplasm. A) sh^{TDP-43}-HEK293E were cotransfected with different C-terminally 6xHis tagged TDP-43 constructs and plasmid E451. They were treated for 24 hours with 5mM acetyllysine before fixation. Scale bar represents 10 µm. B) Quantification of cells in A) based in the compartment were TDP-43 was found predominantly. 250 cells were analysed per group. C) sh^{TDP-43}-HEK293E were cotransfected with E451 plasmid and different C-terminally tagged TDP-43 constructs. Lanes 3-5 have $K136_{TAG}$ in addition to the mutation indicated in the upper panel. Cells were treated for 24 hours with 5mM acetyllysine before lysis in urea buffer.

4. 6. 3.- Diffuse acetylated TDP-43 is degraded in the absence of acetyllysine

The previous results suggest that the LLPS observed is an initial step for TDP-43 aggregation, an idea supported by Mann et al. and Cohen et al., among others. This would mean that is the process is stopped at an early step, i.e., the phase separation or the initiation of the aggregate formation, there would be no bigger aggregates, with all the pathological insight that this conveys.

To test if the acetylated TDP-43 droplets and aggregates observed can dissolve, a series of acetyllysine washout experiments were performed. By limiting the supply of acetylated lysine to amber suppressed cells once the LLPS has taken place, the further translation of acetylated TDP-43 would be stopped, and the cell would be allowed to deal with the current aggregates and droplets. This could happen via protein degradation or via deacetylation of TDP-43. Amber suppressed cells were incubated for 24 hours with acetyllysine and then the media was exchanged to an acetyllysine-free media for either 8 or 24 hours before analysis. The protein levels of C-terminally 6xhis-tagged TDP-43 were reduced after 8 and 24 hours of acetyllysine deprivation (Fig 4.28A and B). Interestingly, this reduction was not observed in the wtTDP-43, hinting at a targeted degradation of the aggregation-prone acetylated TDP-43. In addition, TDP-43 droplets persisted after 8 hours of acetyllysine washout but disappeared when the cells grew for 24 hours without amber suppression (Fig 4.28C). These results suggest that phase separated TDP-43 can dissolve when the concentration of RNA-binding deficient species is low enough, however it is unclear if acetylation-driven solid aggregates can disengage as well.

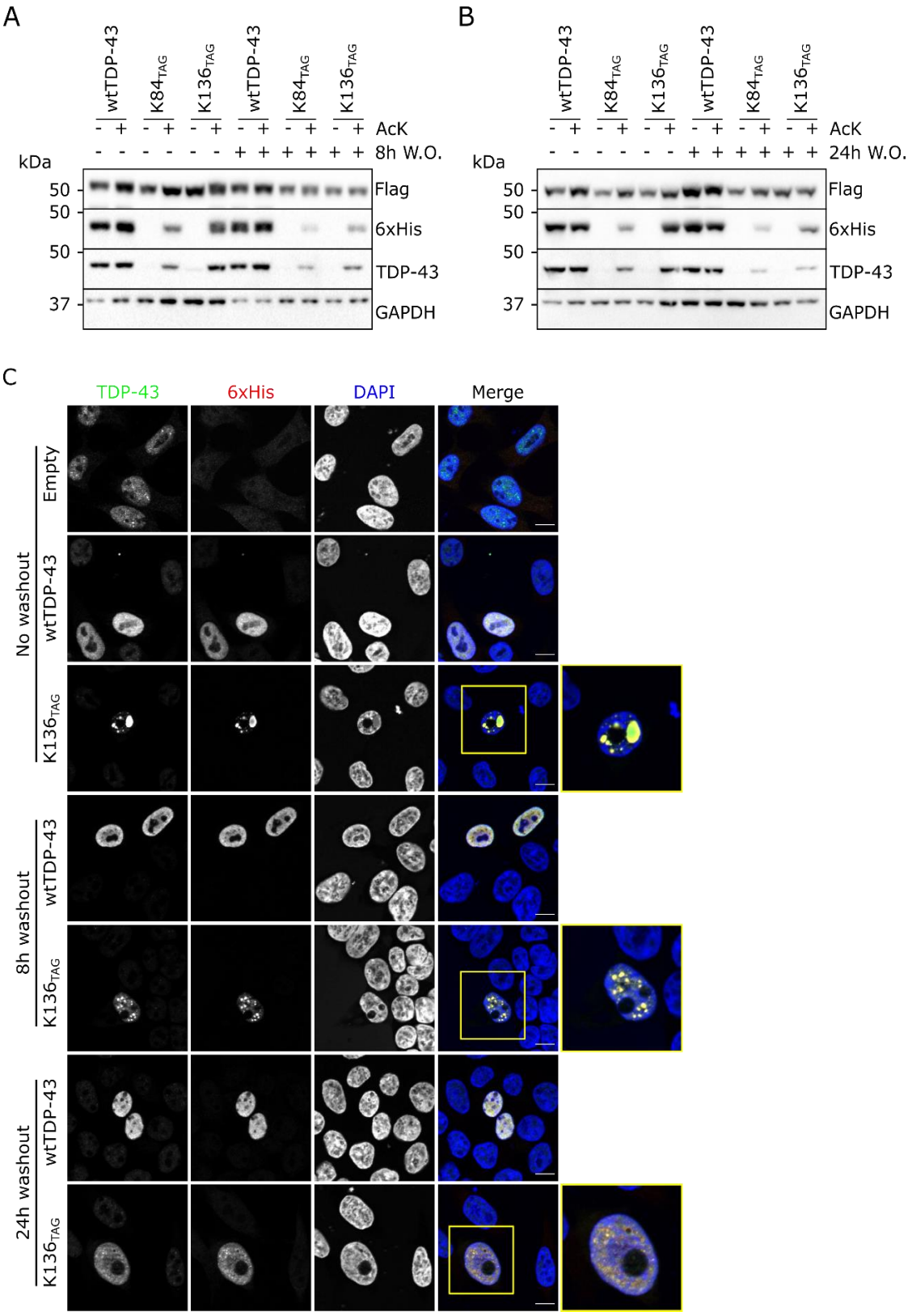

Figure 4. 28.- Removing acetyllysine from the media eventually reduces amber suppression and droplet formation. A) and B) sh^{TDP-43}-HEK293E were cotrasfected with plasmid E451 and different TDP-43 constructs. Cells were treated with 5mM acetyllysine for 24 hours and afterwards the media was exchanged to an acetyllysine free media for 8 hours

(A) or for 24 hours (B) in the labelled lanes. Cells were lysed in urea buffer and protein lysates were analysed via western blot. N = 2. C) Cells were transfected and treated under the same conditions than in A) and B) and were later fixed and prepared for immunofluorescence. They were then costained with α-6xHis and α-TDP-43 antibodies. Scale bar represents 10 µm.

While it was not possible at this point to evaluate the acetylation status of K136, these results suggest that the overexpressed acetylated TDP-43 is degraded by the cell. After 24 hours there is a remarkable reduction of amber suppressed TDP-43, but no aggregates nor droplets are detected in immunofluorescence, which suggest a concentration dependent formation of droplets, a well reported characteristic of phase separated molecules, supporting even more the liquid nature of the acetylated TDP-43 entities.

4. 7.- Generation of site-specific acetylated TDP-43 antibodies

One of the limitations of this study was the inability to detect the specific acetylation at K84 and K136 of TDP-43. The use of pan-acetyllysine antibodies can only detect changes in total acetylation levels, which in the case of proteins acetylated at several residues is only partially informative and cannot detect fine differences. To overcome this issue and to expand the scope of the study, antibodies targeting specifically acetylated forms of TDP-43 were generated.

The generation of the antibodies was done in collaboration by Dr. Regina Feederle and Andrew Flatley from the Monoclonal antibody core facility at the Helmholtz Centre in Munich. The synthetic peptides used for immunization were the (KDNKR(Ac)KMDETD) for acetylated K84 and the LMVQV(Ac)KKDLKT for K136. Rats were immunized with a mix of both peptides in a Freund's incomplete adjuvant, with a booster injection 6-8 weeks after. 3 days after the booster injection animals were sacrificed and splenocytes were isolated and fused with mouse myeloma cells (P3X63-Ag8.653). An initial screening of each hybridoma supernatant was performed against the synthetic peptides and the successful ones were tested against the full amber suppressed protein in western blot and immunofluorescence. After identifying the suitable candidates, the most sensitive and specific hybridoma lines were expanded and subcloned.

Modelling the immunogenicity of K84 and K136 showed that K84 is more immunogenic and therefore easier targeted by antibodies than K136 (Dr. Feederle, personal communication). This had an impact in the length of the process and the number of antibodies that had to be tested.

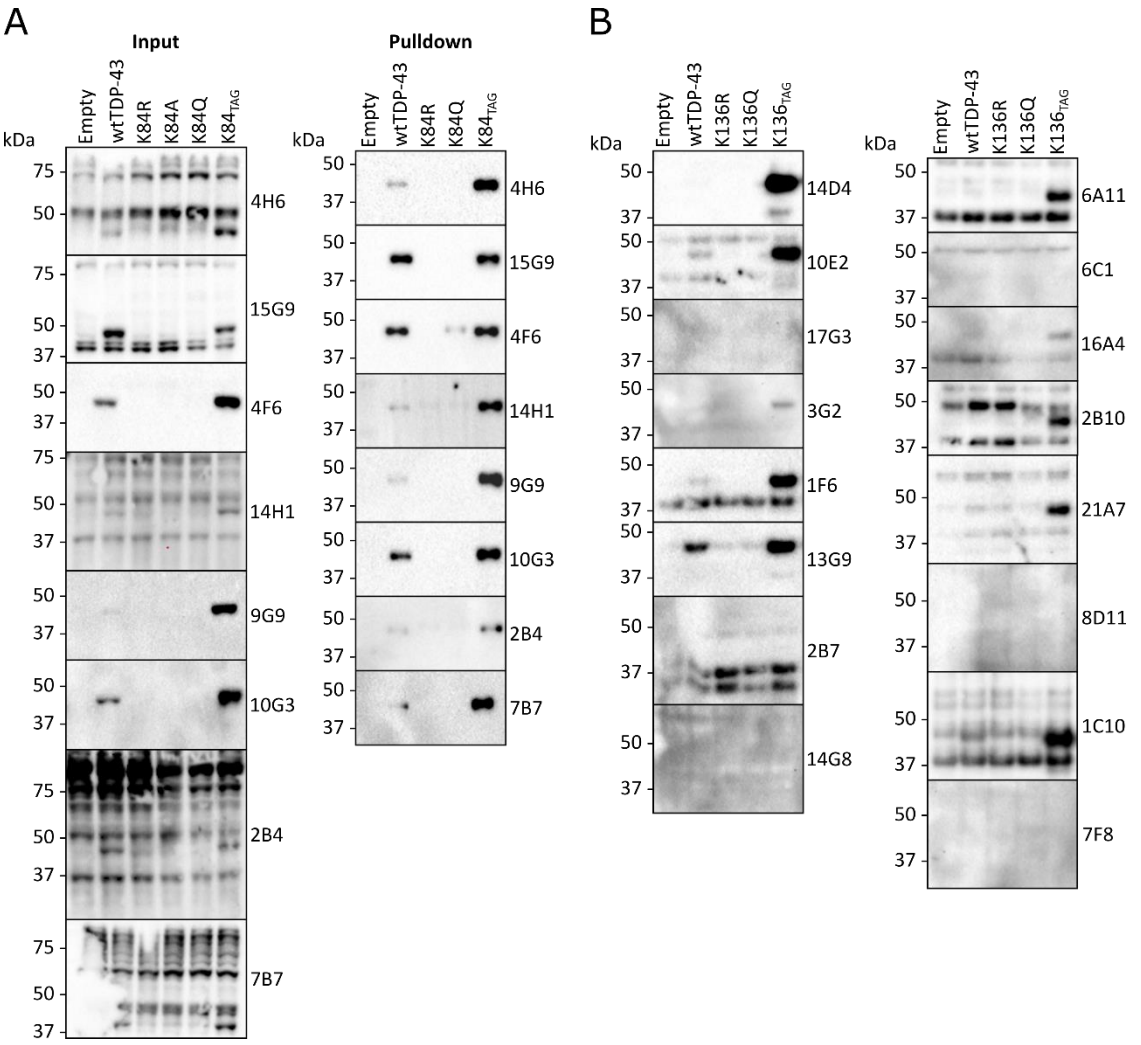

Figure 4. 29.- Hybridoma primary supernatant test. A) sh^{TDP-43}-HEK293E cells were transfected with different TDP-43 constructs and E451 plasmid. All but K84A TDP-43 containing an N-terminal 6xHis tag. Cells were treated with 5mM acetylated lysine for 24 hours before lysis. Lysis was done in urea buffer and 6xHis tagged proteins were purified via Ni-NTA purification. Both total lysate and purified fractions were analysed via Western blot. B) Like in A), cells were transfected with different TDP-43 constructs and E451 plasmid and treated with acetylated lysine before lysis. Lysates were analysed via Western blot.

To test the hybridoma primary supernatant cells were transfected with different TDP-43 constructs, lysed in urea buffer and the lysates were tested in Western blot. In the case of the α-K84, 6xHis tagged TDP-43 (all constructs but K84A) was purified via Ni-NTA pulldown. Given the large number of antibodies tested for acK136, only total lysates were tested. To test for unspecific binding of the antibody to other parts of TDP-43 sequence, K/R and K/A constructs were used. The positive control was amber suppressed TDP-43. α-acK84 primary supernatant antibodies performed in general better than their K136 counterparts (Fig 4.29A). While some of them bound to proteins other than TDP-43, most of them showed a strong sensitivity towards

acetylated K84. α-acK136 antibodies were in general more prone to detect additional bands or to be unsuccessful altogether in Western blot (Fig. 4.29B). From this screening, clones 9G9 for acK84 and 14D4 for K136 were selected. It is interesting to notice the 35kDa band detected by the 14D4 antibody.

The supernatant produced by the subcloned, stable lines was tested both in western blot and immunofluorescence against amber suppressed TDP-43. Both α-AcK136 TDP-43 and α-AcK84 TDP-43 specifically recognise acetylated TDP-43 both in western blot and immunofluorescence with high specificity (Fig 4.30 A-D). It is worth noting that despite the low expression levels of amber suppressed TDP-43 the α -acetylated TDP-43 antibodies do not cross-react with wtTDP-43. In addition to the full-length band, the α-AcK136 TDP-43 detects the same faint ~35 kDa band (Fig 4.30A). The significance of this band remains to be determined.

The generation of these new antibodies against acetylated TDP-43 provides a new and powerful tool to further study the dynamics of acetylation at these sites and the potential conditions or KDAC/KATs involved in TDP-43 acetylation.

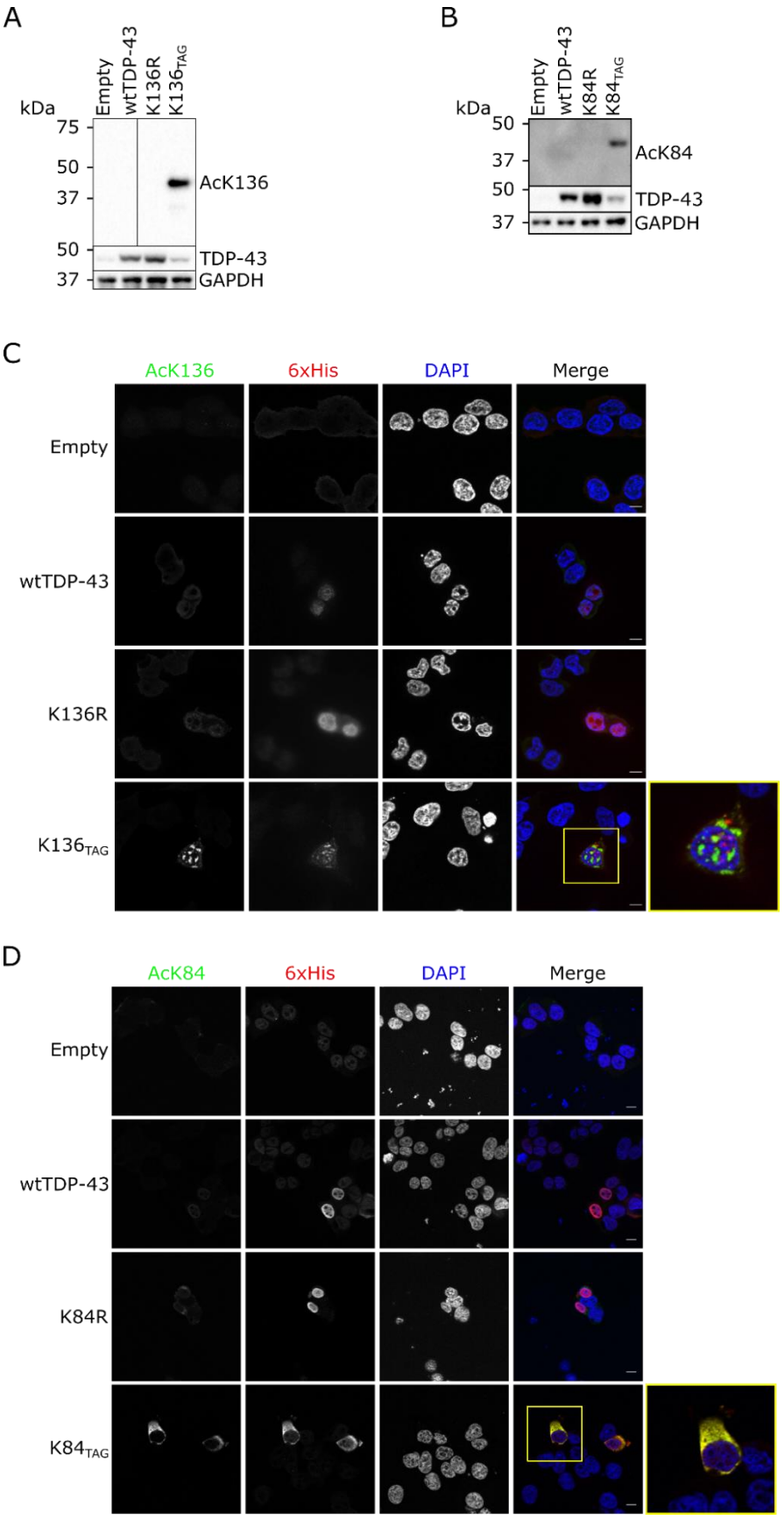
A
Empty
wtTDP-43
K136R
K136TAG
kDa
75
50
37
50
37
AcK136
TDP-43
GAPDH
B
Empty
wtTDP-43
K84R
K84TAG
kDa
50
37
50
37
AcK84
TDP-43
GAPDH
C
AcK136
6xHis
DAPI
Merge
Empty
wtTDP-43
K136R
K136TAG
D
AcK84
6xHis
DAPI
Merge
Empty
wtTDP-43
K84R
K84TAG

Figure 4. 30.- Anti acetylated TDP-43 antibodies specifically recognise amber suppressed TDP-43. A) and B) sh^{TDP-43}-HEK293E cells were transfected with plasmid E451 and different C-terminally 6xHis-tagged TDP-43 constructs. Cells were treated with 5mM acetyllysine for 24 hours before lysis in urea buffer. Lysates were analysed via western blot. N = 3. C) and D) Cells with the same transfection and treatment paradigm than in A and B were fixed and costained with α-6xHis and α-acetylated TDP-43 antibodies. Scale bar represents 10μm.

4. 8.- Modulators of K136 TDP-43 acetylation

With the newly developed anti acetylated TDP-43 antibodies, the next step in the study was to find modulators of TDP-43 acetylation at specific residues. Due to the more noticeable impact of K136 acetylation in the pathophysiology of TDP-43, the study focused more on this residue.

4. 8. 1.- No cellular stressor influences decisively K136 acetylation

K136 acetylation was initially found in a mass spectrometry analysis which has an extremely high sensibility. However, even the highly sensitive antibodies developed could not detect acetylation of wtTDP-43 under normal conditions (Fig 4.30). Taking in account the deleterious effect of K136 acetylation, it is unlikely that K136 is acetylated by default. Most probably, acetylation at K136 only happens in response to a specific stimulus or stress.

To identify these stimuli, HEK293E cells were treated with a series of stressors in order to identify those acetylating the endogenous TDP-43. Sorbitol and sodium arsenite has been reported to trigger the localization of TDP-43 to stress granules (410,411), therefore TDP-43 acetylation levels were tested in the presence of these stressors. In addition, the Sirtuin inhibitor Ex527 was used to examine if inhibition of endogenous sirtuins can result in an increase of acetylation. Among these treatments only sorbitol triggered the appearance of cytoplasmic acetylated aggregates that colocalized with TDP-43 (Fig 4.31A and B). To validate these results, a western blot of treated wtHEK293E cells and a pulldown of transiently expressed 6xHis tagged TDP-43 was performed. Unfortunately, while there was a detectable phosphorylation of ERK triggered by arsenite and sorbitol, there was no detectable signal of endogenous acetylated K136 TDP-43 in western blot (Fig 4.32A). It is possible that the localized high TDP-43 concentration at the cytoplasmic aggregated observed in Figure 4.30A was above detection limit, unlike the analysis in western blot. To try to solve this issue, HEK293E cells were transfected with 6xHis tagged TDP-43, which was later purified and analysed via Western blot.

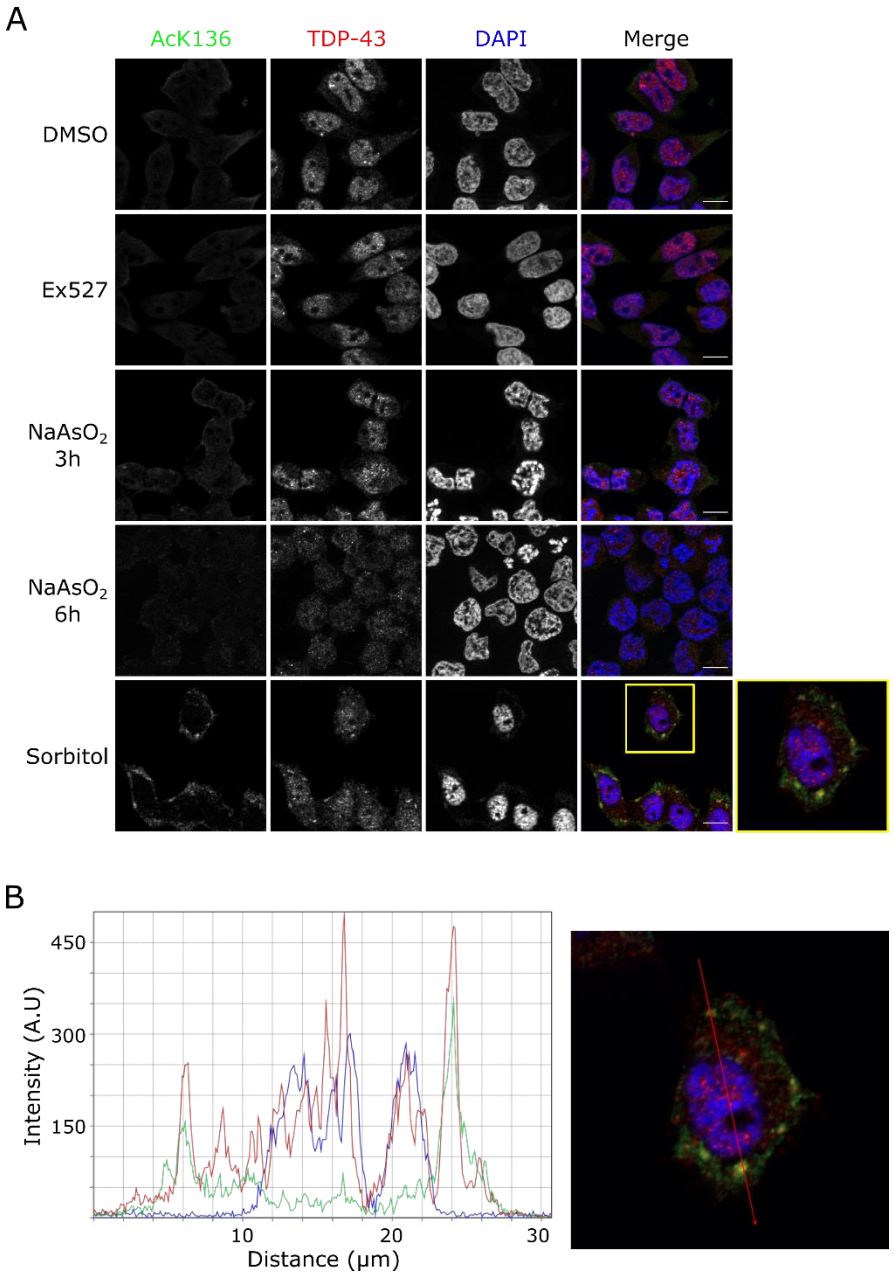

Figure 4. 31.- acK136 antibody detects cytoplasmic acetylated TDP-43 after sorbitol treatment. A) HEK293E cells were treated with either 0.1% DMSO, 10µM Ex527 or 100µM NaArs for 6 hours; or 250µM NaArs or 0.4M Sorbitol for 3 and 1 hours, respectively. Cells were then fixed and costained with α-acK136 and α-TDP-43 antibodies. Scale bar represents 10µm. B) Representative intensity profile of a cell treated with Sorbitol and costained with α-acK136 TDP-43 (green) and α-TDP-43 (red).

This would increase the amount of TDP-43 in the total lysate and allowed for a detail examination of TDP-43 in the purified fraction. Both arsenite and sorbitol elicited a phosphorylation of ERK and a polyubiquitination of TDP-43 (Fig 4.32B). Sorbitol treated cells displayed the most noticeable hyperubiquitination of TDP-43, which is represented by a high molecular smear in the pulldown fraction (Fig 4.32B, right panel). This was already shown by

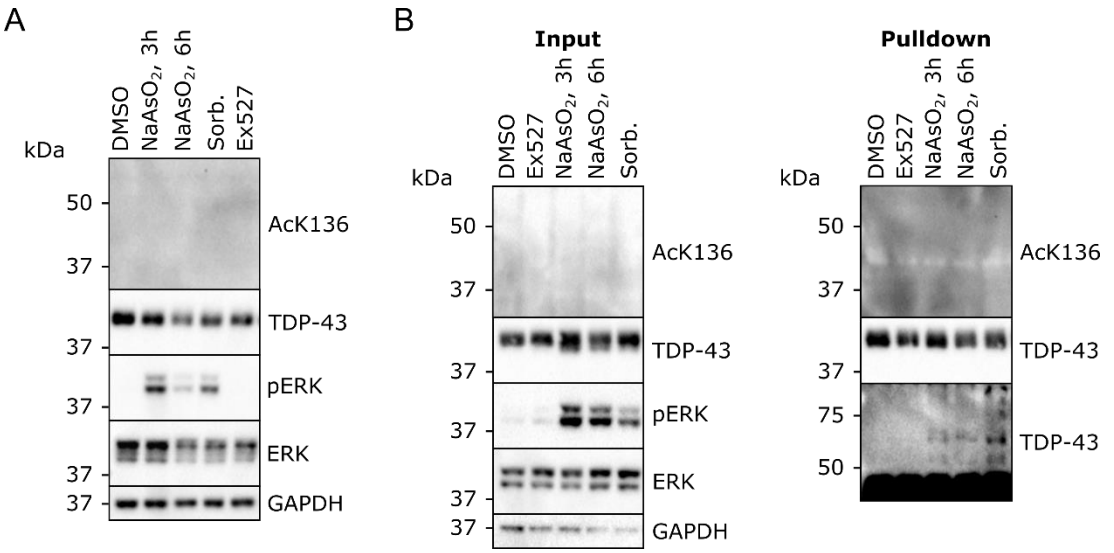

Figure 4. 32.- Effect of sodium arsenite and sorbitol in K136 acetylation. A) HEK293E were treated with either 0.1% DMSO for 6 hours, either 250µM or 100µM sodium arsenite for 3 hours and 6 hours respectively, 0.4M sorbitol for 1 hour, or 10µM Ex527 for 6 hours. Cells were then lysed in urea buffer and lysates were analysed via western blot. N = 2. B) HEK293E cells were transfected with C-terminally 6xHis-tagged wtTDP-43 and were treated with the same compounds used in A). Cells were lysed in urea buffer and 6xHis tagged proteins were purified via Ni-NTA purification. Total lysates and purified fractions were analysed via western blot. N = 2.

Hans et al. (410). While the different treatments did elicit the expected response, there was no detectable acetylation at K136 in the total lysate nor in the purified fraction.

Due to the inconsistencies of these results, a series of control experiments were done. To assess if the cytoplasmic acetylated aggregates observed after sorbitol treatment were truly TDP-43, the same treatment was done in $sh^{TDP\text{-}43}$-HEK293E. In addition, the TDP-43 silenced cells were transfected with different C-terminally 6xHis-tagged TDP-43 constructs, including amber suppressed $K136_{TAG}$ TDP-43. If the observed aggregates were indeed acetylated TDP-43, one would expect a reduction of signal in the $sh^{TDP\text{-}43}$-HEK293E cells and an increase of signal after transfection with wtTDP-43. In addition, K136R TDP-43 should not increase the signal from the α-acK136 TDP-43 antibody, allowing for a negative control of the acetylation at K136. To image stress granules α-eIF3η and α-TIAR antibodies were used. After treating the cells with

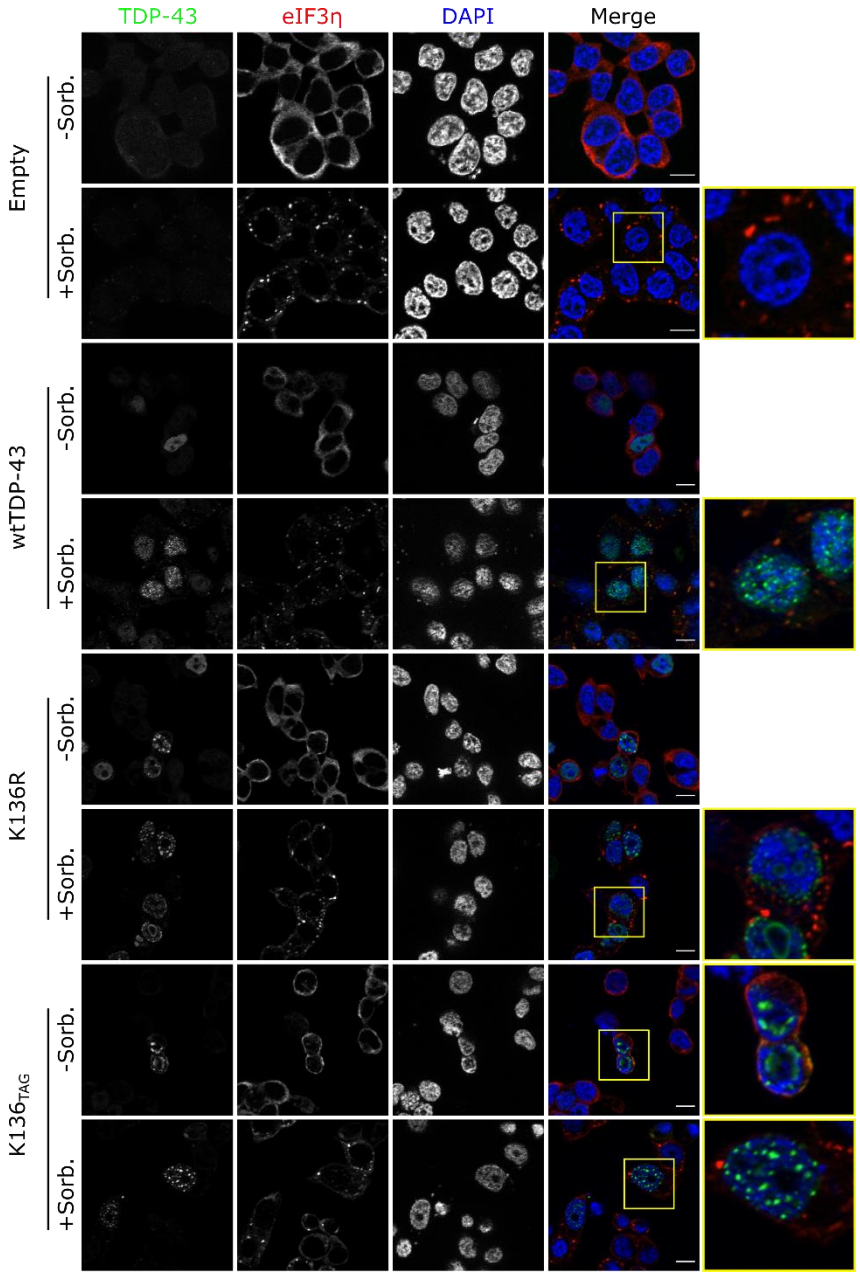

Figure 4. 33.- Sorbitol treatment triggers the formation of stress granules, but TDP-43 is not recruited to them. shTDP-43-HEK293E cells were cotransfected with plasmid E451 and different TDP-43 constructs. Cells were treated with 5mM acetylated lysine for 24 hours and with 0.4M sorbitol for 1 hour before fixation. Scale bar represents 10µm.

acetyllysine and sorbitol, the transfected TDP-43 did not localize to stress granules, however wtTDP-43 displayed a nuclear granular distribution not observed in the endogenous TDP-43 (Fig 4.33). Neither the mutant K136R nor the amber suppressed TDP-43 colocalised with the eIF3η-rich stress granules. In addition, the acetylated antibody stained a portion of the stress granules caused by sorbitol even in the absence of TDP-43 (Fig 4. 34). The transfection of any TDP-43 constructs did not alter the behaviour of the α-acetylated K136 antibody.

Taken together, these results suggest that the recognition of stress granules by the α-acK136 TDP-43 antibody is caused by cross reactivity of the antibody with a stress granule component.

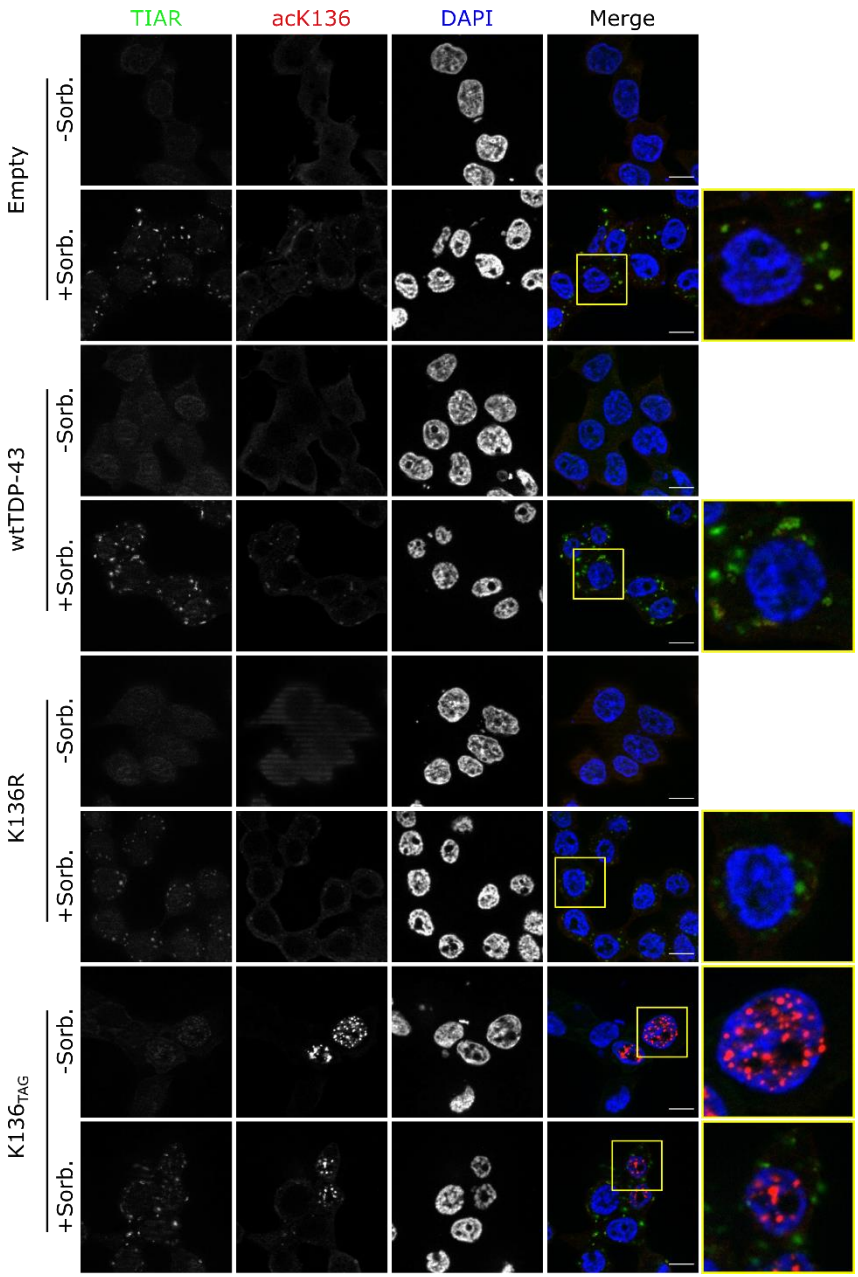

Figure 4. 34.- Acetylated cytoplasmic aggregates are present in the absence of TDP-43. shTDP-43-HEK293E cells were cotransfected with plasmid E451 and different TDP-43 constructs. Cells were treated with 5mM acetylated lysine for 24 hours and with 0.4M sorbitol for 1 hour before fixation. Scale bar represents 10µm.

Unfortunately, a blast alignment of the immunization peptide did not return any known member of stress granules. Since the treatment did not trigger a mislocalisation of TDP-43 into stress granules the effect of acetylation at K136 in TDP-43 stress granule-related functions could not be studied. The current data does not support the hypothesis that sorbitol triggers localization of acetylated TDP-43 at the stress granules.

4. 8. 2.- Modulation of K136 acetylation by cellular deacetylases

The previous study of cellular conditions that could acetylate K136 was limited by the library of drugs available. While the cellular conditions greatly vary, the acetylation system is comprised

by a reduced numbers of acetyltransferases and deacetylases (344). The amber suppression method in combination with specific acetyl-TDP-43 antibodies provide a clear readout for the activity of deacetylases.

To identify the deacetylase responsible for K136 TDP-43 deacetylation, HDAC1-8 and sirtuins 1-7 were subcloned and cotransfected into HEK293E cells together with plasmid E451 and $K136_{TAG}$ TDP-43. From the 8 HDACs studied, HDAC1 and HDAC6 greatly reduced the acetylation levels of TDP-43 (Fig 4.35A). However, careful examination of the results showed that amber suppressed TDP-43 levels were reduced. To stablish if this reduction was due to the deacetylase activity of HDAC1 and 6, inactive mutants were subcloned and their effect on amber suppressed TDP-43 was evaluated. Both active and inactive mutants of HDAC1 and 6 severely decreased the amount of amber suppressed TDP-43 (Fig. 4.35B). Since the inactive HDAC1 and 6 mutants do not seem to be compatible with amber suppression, the effect of these deacetylases on K136 acetylation status could not be assessed. While the precise involvement of these two deacetylases with the amber suppression method deserves a deeper study, it is unfortunately out of the scope of this thesis.

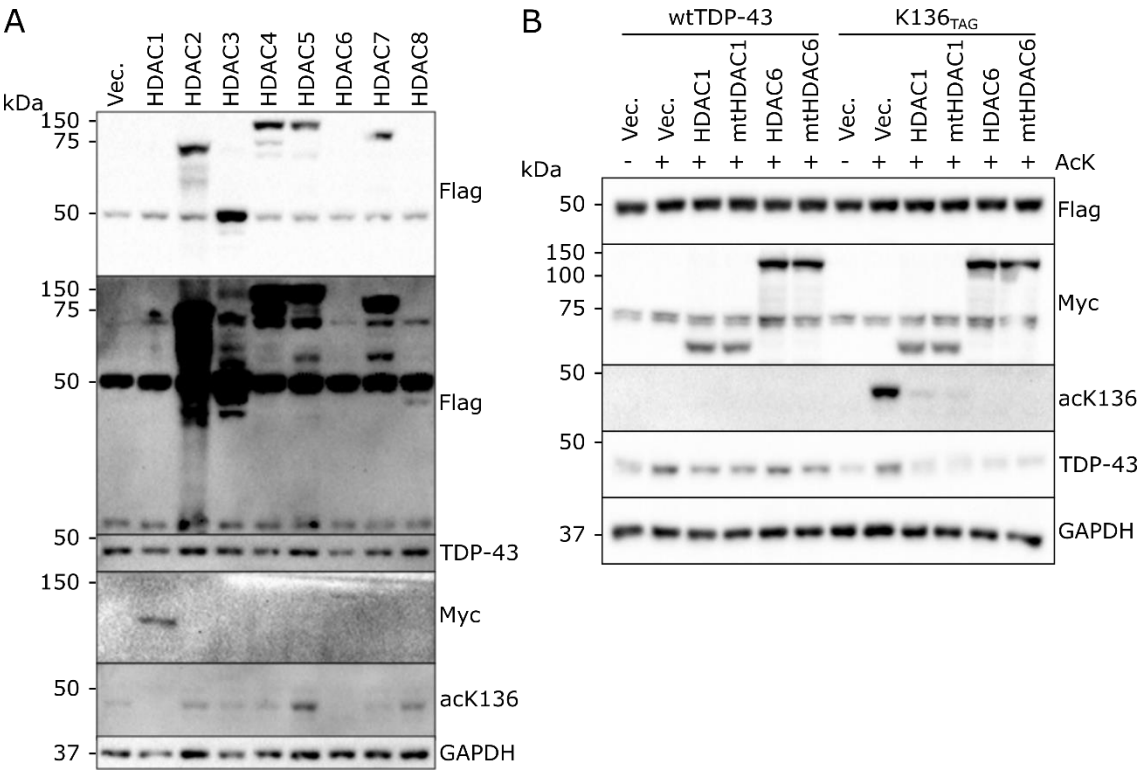

Figure 4. 35.- HDAC1-8 do not deacetylate K136, but HDAC1 and 6 prevent amber suppression. A) sh^{TDP-43}-HEK293E cells were cotransfected with plasmid E451, $K136_{TAG}$ TDP-43 and different HDAC constructs. HDAC1 and 6 were N-terminally myc-tagged, while all the other HDACs were N-terminally Flag-tagged. Cells were treated with 5mM acetyllysine for 24 hours before lysis in urea buffer. Lysates were analysed via western blot. N = 3. B) Cells were cotransfected with plasmid E451, $K136_{TAG}$ TDP-43 and different HDAC1 and HDAC6 constructs. mtHDAC1 corresponds to H141A HDAC1 and mtHDAC6 corresponds to H216Y HDAC6. After 24 hours in the presence of 5mM acetyllysine cells were lysed in urea buffer and protein extracts were analysed via western blot. N = 3.

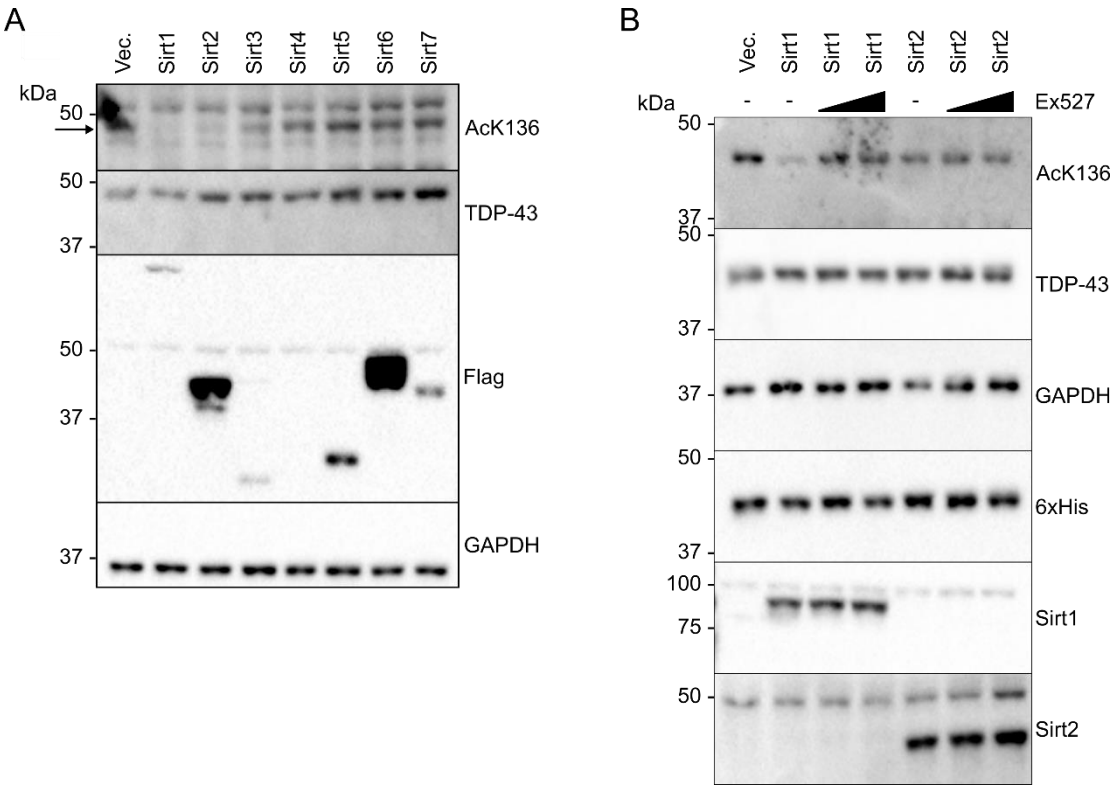

Figure 4. 36.- Sirtuin 1 deacetylates TDP-43 K136 and this deacetylation can be prevented using Sirt1 inhibitors. A) shTDP-43-HEK293E cells were cotransfected with E451, $K136_{TAG}$ TDP-43 and different C-terminally Flag-tagged Sirtuin constructs. Cells were treated for 24 hours with acetyllysine before lysis in urea buffer. Lysates were analysed via western blot. Acetylated TDP-43 marked with a black arrow. N = 2. B) Transiently amber suppressed cells were cotransfected with $K136_{TAG}$ TDP-43 and either an empty vector, Sirt1 or Sirt2 constructs. Cells were treated with 5mM acetyllysine and, in addition, with either 0.1% DMSO, 1 or 10µM Ex527 for 24 hours before lysis in urea buffer. Samples analysed via western blot. N = 3.

After testing HDAC1-8 effect on K136 acetylation, the same procedure was used to test the effect of Sirtuins1-7. Transiently amber suppressed cells were cotransfected with $K136_{TAG}$ TDP-43 and different sirtuin constructs. The sirtuin screen showed that acetylation at K136 was greatly reduced, but did not disappear, when Sirtuin 1 was overexpressed (Fig 4.35A), and to a lesser extent when Sirtuin 2 was present. To confirm that these results are caused by the deacetylase activity of Sirtuin 1, the highly specific Sirtuin 1 inhibitor Ex527 was used to inhibit the deacetylase activity of the overexpressed Sirtuin 1. Inhibition of Sirtuin 1 for 24 hours

rescued the acetylation levels without Sirtuin 1 overexpression (Fig. 4.36B). Together, these data demonstrate that Sirtuin 1 is responsible for K136 deacetylation, and that this reaction can be inhibited by the use at low concentrations of Ex527.

Next, to test if the reduction in acetylation was matched by a change in the phase separation

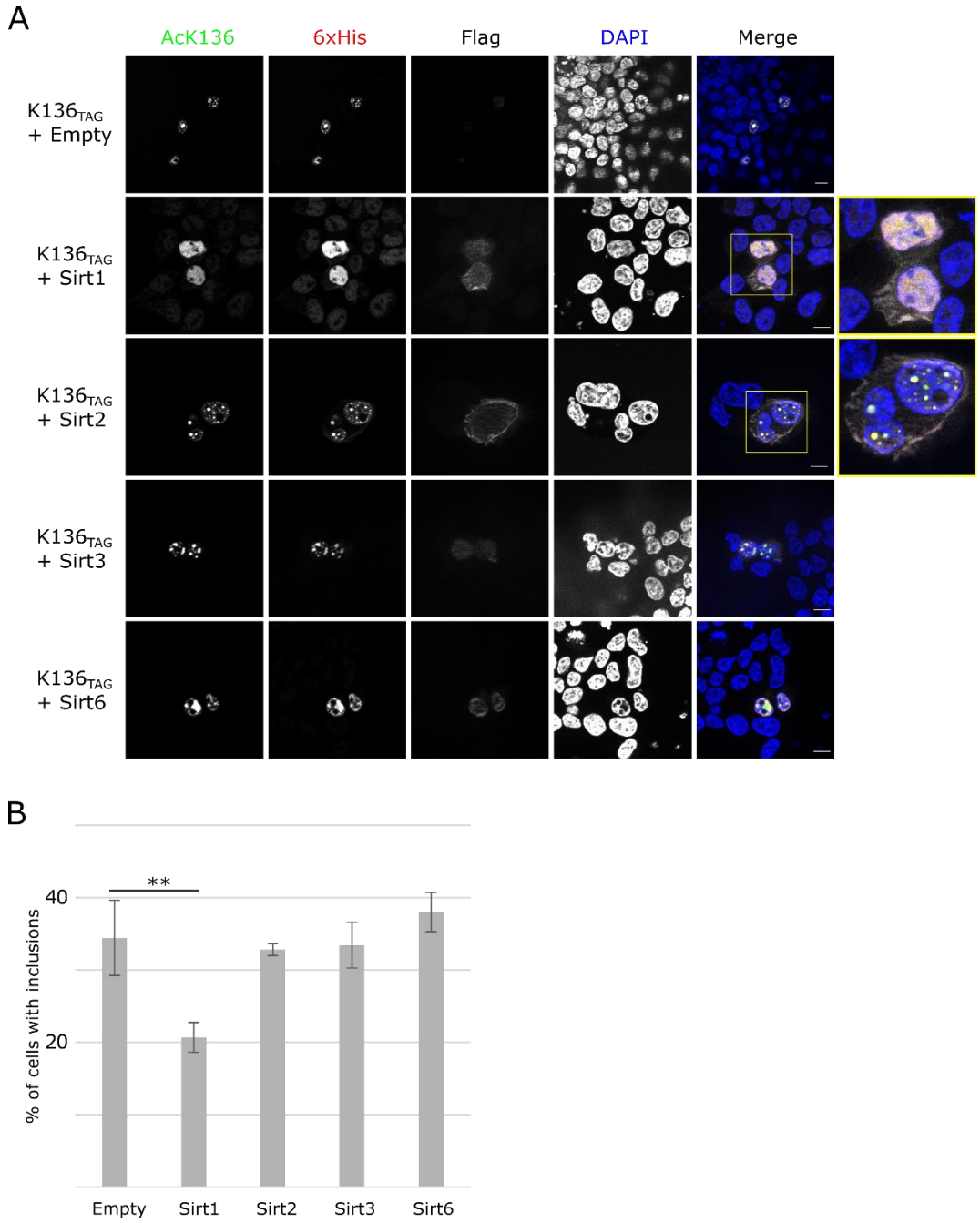

Figure 4. 37.- Sirtuin 1 overexpression abolishes TDP-43 acetylation-induced phase separation. A) sh^{TDP-43}-HEK293E cells were cotransfected with plasmid E451, $K136_{TAG}$ TDP-43 and different Flag-tagged sirtuin constructs. Cells were treated for 24 hours with acetylated lysine before fixation and staining. Scale bar represents 10µm. B) Quantification of the number of cells with 6xHis positive inclusion. 200 cells counted per condition.

behaviour of acetylated TDP-43, amber suppressed cells were transiently transfected with different sirtuin constructs with similar levels of expression to Sirtuin 1 and 2. Cells transfected

with Sirtuin 1 decreased the percentage of cells with nuclear inclusions from around 40% to 20% (Fig 4.37A and B). While Sirtuin 1 reduced the percentage of cells with inclusions, it did not remove completely the acetylation, observed both in western blot and immunofluorescence (Fig 4.36B and Fig 4.37A), it did reduce the number of cells with aggregates. This suggest that there is a concentration dependent mechanism triggering the formation of inclusions, a hallmark of phase separation.

5.- Discussion

ALS was first described almost 200 years ago but it was not until 2006 when the scientific community started to unveil the link between Frontotemporal Dementia and ALS and the mechanisms that caused neuronal death (20,21). While several TDP-43 mutations have been linked with ALS, the vast majority of ALS patients and ~50% of FTD cases (FTLD-TDP) develop cytoplasmic TDP-43 aggregates in absence of mutations in the *TARDBP* gene (44). In addition to this, extensive research of TDP-43 PTMs has proved that some of them are clearly linked with loss of function and toxicity (225). However, the specific pathway leading to protein inclusions and the aggregation process itself is still not clear and in need of further research.

In this study, we identified four novel acetylation targets in TDP-43 nuclear localisation signal and RNA-recognition domain 1. To study the effect of these acetylation sites, both point mutants and amber suppression were used. From these 4 residues, acetylation at K84 and K136 had a detectable impact in TDP-43 physiology. While acetylation at K84 promoted cytoplasmic mislocalization of TDP-43, acetylation at K136 reduced TDP-43's RNA binding capability, which in turn caused it to phase separate and eventually for aggregates. These results confirm and expand the recent interest on TDP-43 acetylation (249,251), and they help solidify the relation between TDP-43, phase separation and aggregation.

5. 1.- Novel acetylation sites in the context of TDP-43 function and structure

Before this study extensive work had been done regarding TDP-43 phosphorylation (227,230,231,412) and ubiquitination (242,244,245). This is not surprising given the strong link between these two modifications and TDP-43 proteinopathy (20). While the interest for other posttranslational modifications is growing, at the start of this project only Cohen et al. had characterise in detail the effect of glutamine substitutions at acetylation sites and had stablish a link between acetylation and pathology (249). As it was mentioned in the introduction, acetylation is involved in a plethora of processes, and it is closely related with metabolism and energy regulation. Since ALS has a robust metabolic component, and PTMs have a strong influence in aggregation and toxicity, a more detailed examination of TDP-43 acetylation pattern was done.

For comparison, in their study Cohen et al. performed a mass spectrometry analysis of TDP-43 to characterize its acetylation sites and found only 2 acetylation targets, K145 and K192, none of which could be validated in our study. In this analysis, Dr. Hans used a wtTDP-43 overexpression system, whereas Cohen et al. used a coexpression set up of ΔNLS TDP-43 and CBP. As it was mentioned before, given promiscuity of KATs and the specific subcellular location of many of them, the use of nuclear export deficient construct and the overexpression of a highly active KAT can have an impact in the resulting data. Another TDP-43 mass spectrometry dataset was published the same year, done with insoluble material extracted from ALS spinal cord (240). In this case, neither of the acetylation sites in ours or in Cohen et al. studies were identified, only acetylation at K82. However due to the small sample size, lack comparison with healthy controls and failure to detect phosphorylation at S409/410 reliably make this study difficult to interpret. To the present day these are the only two mass spectrometry datasets looking at TDP-43 acetylation.

The mass spectrometry provided a qualitative measurement of TDP-43 PTMs in the presence of a proteasomal inhibitor, both at the monomer and at the high molecular smear level. While acetylation at K84 and K136 was present in most of the conditions, K79 and K121 seems to be prevalent only after proteasomal inhibition with MG-132 (Table 3.1). The coverage of the amino acid sequence varied between 44% and 82%, thus it is best to approach this data as a qualitative measurement of PTMs ad not as a quantitative record of all possible PTMs, as shown by the multiple mutant analysis of total acetylation (Figure 4.9). The acetylation at K84 was particularly interesting because the residue can also be ubiquitinated (239), which could lead to an acetylation-ubiquitination competition for the same lysine at a functionally important region such as the NLS. Acetylation at both K79 and K121 did not trigger any differences in localisation of splicing capabilities. Since both acetylation sites were only found after proteasomal inhibition the role of them could depend on proteasomal activity, acting as small modifiers of TDP-43 activity.

Acetylation at K136 takes place at a very conserved region in the core of the RNA-binding pocket of TDP-43. K136 is located in an antiparallel β-sheet in the RRM1, presumably forming hydrogen bonds with G134, K137, K145, F147 and K149 (413). Therefore, K136 is not only in close contact with RNA itself (111), but it is a core structural element of the RRM1 that interacts with K145, F147 and K149, all key residues for TDP-43 RNA-binding (246,249,251). There is some evidence of posttranslational modifications at this site, specifically SUMOylation of K136 was shown to promote aggregation and impair neurite growth in an overexpression model (260) and recently another study came out identifying SENP1 as a deSUMOylation enzyme of TDP-43 (414). These

studies support the hypothesis that this is a crucial residue in the regulation of TDP-43 RNA-binding and, together with our results portrait a complex PTM interaction network regulating TDP-43 RNA-binding dynamics.

5. 2.- Multiple lysines are acetylated in TDP-43

Mass spectrometry analysis of TDP-43 returned four novel acetylated residues but did not convey any quantitative information. In order to examine if one of the lysines was contributing to the total level of acetylation more than the others, and to investigate the role of each of the acetylation sites, a series of mutants were generated. Each lysine was mutated either to arginine or to glutamine, to mimic the lack or the presence of acetylation, respectively. Initially, the constructs were carrying a 6xHis C-terminal tag that was eventually substitute by an N-terminal tag. These constructs were transfected into HEK293E cells that were later lysed and the 6xHis tagged proteins in the lysates were purified via Western blot.

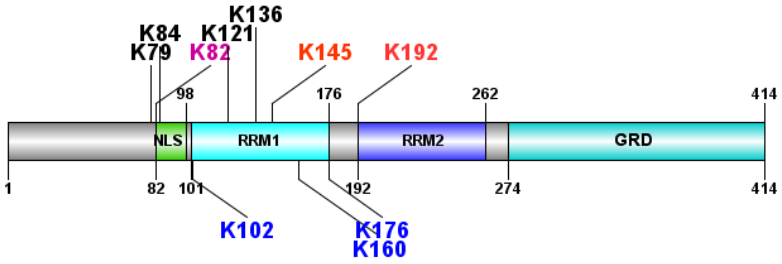

Figure 5. 1.- Identified TDP-43 acetylation sites. Identified acetylation sites of TDP-43 in relation to its domain structure. Residues in pink were identified by Kametani et al., residues in red were identified by Cohen et al., residues in blue were identified in high throughput analysis and residues in black were identified in this study.

The first issue we encountered was the high variability in expression and the complete failure to translate of C-terminally tagged K121Q TDP-43. To test if this was due to RNA instability of enhanced proteasomal degradation RNA levels and MG132 treatments were used. Analysis of reverse transcribed RNA from transfected cells revealed no differences between any of the mutant TDP-43 RNAs (Fig 4. 7C) and MG132 treatment failed to rescue K121Q TDP-43 levels. Since the change of the tag from being C-terminal to N-terminal rescued completely the expression of K121Q (Fig 4. 8A), the tag could have had a rare interaction with the transcript, preventing its translation, although further experiments should be done to clarify this point.

The examination of TDP-43 total acetylation using panacetyl antibodies did not show any difference among the mutants (Fig 4.8A). There were also no differences when only one of the

4 lysines was available (Fig 4.9A). The different expression levels of the TDP-43 mutants made this analysis challenging and underlines the need for stable and reproducible systems to study PTMs. As mentioned before, other groups have identified lysines that were not present in our Mass spectrometry data (K82, K145, K192). In addition to these, 2 high throughput studies looking at the total acetylome have identified K102, K160 and K176 as acetylated residues of TDP-43 (Fig. 5.1) (415,416). The function of these 3 acetylation sites has not been characterised yet but they might be contributing to the total acetylation seem in this study. In addition, acetylation prediction tool GPS-PAIL 2.0 (417) predict acetylation sites at K95, K114, K181, K263 and K408. While not confirmed experimentally, there is a possibility that they are acetylated to a certain extent, making more difficult to assess the individual impact of lysines in the total level of acetylation of TDP-43. Cohen et al. have shown how the double mutant K145R/K192R TDP-43 have reduced total acetylation when combined with a mutated NLS, CBP over expression and TSA treatment to boost acetylation (249). While it is possible that these two residues are predominantly acetylated under these extreme conditions, it is unclear if this is the case in more physiological setting. Taking in consideration the number of TDP-43 RNA targets, the proportion of acetylation sites at RRM1 and RRM2 could be a hint of TDP-43 RNA-binding regulation mechanisms and target selectivity.

Interestingly, several of the aforementioned residues have been found to be ubiquitinated (239,240,242). This suggests exciting scenarios where acetylation prevents ubiquitination and vice versa, opening the door to precise modulation of ubiquitination via KAT/KDAC inhibition and activation. One of the reasons of the expression differences between mutants could be the interaction between acetylation, ubiquitination, and protein stability. Another reason could simply be an artefactual effect of amino acid substitution in TDP-43 protein structure and stability. While there have been no studies looking at the interaction between these two modifications at a single lysine, hopefully further research will uncover the crosstalk of lysine modifications in TDP-43 pathophysiology.

5. 3.- KDACi treatment did not have a significant impact on TDP-43 total acetylation

Next, we wanted to modulate the total levels of TDP-43 acetylation in a significant way by inhibiting endogenous deacetylases. The first approach was the inhibition of HDAC6 via the highly specific inhibitor Tubacin. The reason why HDAC6 was first chosen was due to the intimate

relation between the two of them (see introduction for details). To recapitulate, HDAC6 mRNA stability is regulated via direct TDP-43 binding, affecting HDAC6 protein levels (146). HDAC6-related TDP-43 toxicity can therefore be rescued via HDAC6 overexpression, such as neurite growth, and potentially can reduce TDP-43 protein levels and aggregation (418). Lastly and most importantly, HDAC6 overexpression has been reported to reduce TDP-43 level of acetylation (249). To examine if this was the case in our study too, cells were transfected with the different TDP-43 constructs and were treated with Tubacin before lysis in urea buffer and 6xHis proteins were purified. The Western blot analysis of the lysates with α-panacetyl antibody did not show any differences in total TDP-43 acetylation.

There are two significant changes in the experiment set up that could explain the differences between Cohen et al. study and this work. The first one is the use of a different cell line (QBI-293 vs HEK293E), which could express HDAC6 partners differently and therefore slightly change its selectivity. As explained in the introduction, KAT and KDACs have in general very low selectivity and depend on complexes to tune their activity (344,357). The second and more relevant difference is the usage of a ΔNLS TDP-43 constructs which expresses predominantly in the cytoplasm (249). This is particularly relevant because HDAC6 is a cytoplasmic deacetylase, and it would not have access to nuclear TDP-43. In order to be able to deacetylase TDP-43 a first insult is needed, that would trigger cytoplasmic mislocalisation, or it would have access only to the small pool of cytoplasmic TDP-43.

Perhaps a more concerning point is the lack of consensus about the role of TDP-43 acetylation in its proteinopathy. Research first describing the relation between TDP-43 and HDAC6 found that a TDP-43 loss of function resulted in HDAC6 mRNA instability, which lead to neurite outgrowth deficiency (146,419), which has been confirmed by later studies where HDAC6 overexpression alleviates TDP-43 aggregation and neurotoxicity via upregulation of the UPS (418). On the other hand, recent work by Fazal et al. portraits a different picture, where HDAC6 inhibition via Tubastatin A treatment can reduce mutant TDP-43 insolubility in iPSCs derived motor neurons (420). It is therefore not clear if HDAC6 can be protective or a promotor of TDP-43 toxicity. One of the differences of this study and Fazal et al. article is the use of Tubastatin A instead of Tubacin. Both are highly selective HDAC6 inhibitors but it is worth noting that HDAC6 contains two separate deacetylase domains, which could be affected differently by different inhibitors (421). In addition to them, HDAC6 also contain a ubiquitin-binding domain (422). The differences between the aforementioned papers could be due to alterations in the balance of these 3 enzymatic domains, and the different approaches to modulate their activity. In our hands, inhibition of HDAC6 via Tubacin did not increase the total levels of TDP-43.

From all the other KDAC inhibitors used in this study, only Scriptaid treatment showed a consistent increase in TDP-43 total acetylation, and only SAHA treatment caused a decrease in solubility in wtTDP-43. The influence on scriptaid on TDP-43 has not been described before and further research into it must be done. In the context of this research, Scriptaid treatment was abandoned due to the lack of subcellular localisation and distribution alterations. The other KDAC inhibitor mentioned, SAHA, was already reported to interact with TDP-43, specially in the context of proteasomal impairment via bortuzemid treatment (251). While not looking directly at acetylation, Yu et al. showed that inhibition of KDACs with SAHA in addition to proteasomal inhibition can trigger the formation of phase separated TDP-43 droplets. These droplets can be caused by acetylation-mimic K145Q mutations (249) or, as seen in this work, by true acetylation at K136. However, while SAHA did increase wtTDP-43 insolubility, it did not cause it t form aggregates nor lose its RNA-splicing capabilities. This suggest that the mechanisms through which SAHA increases TDP-43 insolubility are not linked to K136 or K145 acetylation.

From the other KDAC inhibitor treatment (CI994, LBH589, SBHA, TSA, Apicidin, M344, Na-4-PB, Splitomycin and valproic acid) no significant acetylation nor changes in TDP-43 behaviour was detected. For the first 4, a consistent increase in ether acetylated tubulin and/or other non-specified acetylated proteins (detected with panacetyl antibody) could be detected. For Apicidin, M344, Na-4-PB, Splitomycin and Valproic acid no increase of acetylation of specific proteins was detected. Therefore, it is possible that higher concentrations or longer treatment with these inhibitors would be necessary to see changes in TDP-43 acetylation. However, the concentrations and times were assigned after a titration to avoid cell death, assessed via PARP cleavage (data not shown). Any increase of concentration or time might result in cellular death and toxicity artifacts.

The lack of any detectable changes after different KDAC inhibitors is unfortunate, especially when several of them are being used or propose as treatments for several diseases, mainly cancer and neurodegeneration (423–428). Nevertheless, the few existing proteins with deacetylating activity makes them a tricky target for the development of drugs since the inhibition of a specific KDAC can have a broad impact in the cell acetylome.

5. 4.- Use of amber suppression in eukaryotic cells to study acetylation

Thanks to recent advances in amber suppression methods, the range of models and noncanonical amino acids that can be used to study fine dynamics is rapidly increasing, also in the field of neuroscience (429). A seminal study used amber suppression to examine the role of different amino acids in the potassium channel Kv1.4, being able to modulate its activity through the introduction of non-canonical amino acids (430). One of the innovative approaches of this study is the use of amber suppression to study the effect of TDP-43 acetylation. The most extended method to study acetylation at specific residues is to introduce a point mutation either to arginine or to glutamine, in order to mimic the absence of the presence of acetylation at the specific residue (87,249,346,431). The selection of these residues is based on the similar size to non-acetylated and acetylated lysine respectively, and the charge. When an acetyl group is transferred to a lysine, its positive charge is neutralized. Arginine has a positive charge, resembling unacetylated lysine, while glutamine has none. While this is a widely used technique to study acetylation, it is important to bear in mind that even with the charge similarities, there are structural differences between glutamine and acetylated lysine, and between arginine and lysine that can interfere with normal protein function at structurally delicate sites, creating artefactual results (Fig 5.2). One example of this can be seen in the granular distribution of both K136R and K136Q TDP-43 in this work, but also in other studies (346).

To circumvent this issue, we collaborated with Dr. Elsässer who had developed an amber suppressed-based site-directed acetylation set up, allowing for precise introduction of acetylated lysine in an amino acid chain (432). This method was already proven useful in the examination of histone modifications, opening the door to precise study of epigenetic markers

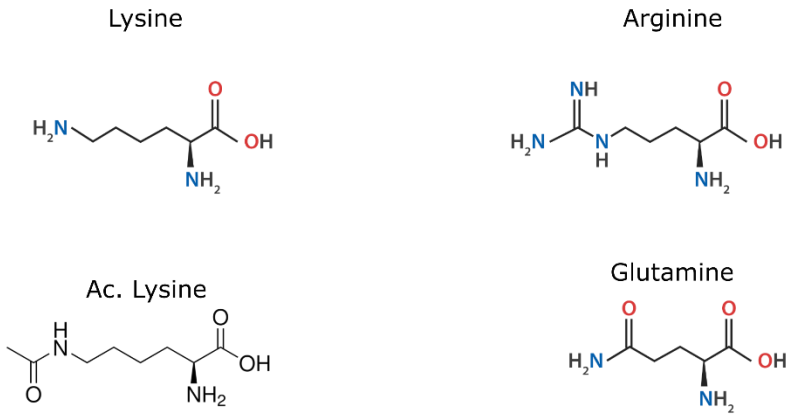

Figure 5. 2.- Structural comparisons between lysine, acetylated lysine, arginine, and glutamine.

(391). In addition, the AcK-RNA synthetase used in this study was generated by Bryson et al. via directed evolution, achieving a high efficiency in the incorporation of acetylated lysine to the amber $tRNA^{AcK}_{UAG}$ (392) . This system allows not only for a more precise way to examine the role of acetylation, but also to study deacetylation events that would be impossible to deal with using glutamine substitutions. However, one of the limitations of this approach is that even after optimizing the activity of the tRNA synthetase, the expression level achieved is usually lower than that of non-amber suppressed proteins. This is a point worth taking in account but in his case, the overexpression of wtTDP-43 can be toxic at high levels, as it has been reported. Thus, a reduction in TDP-43 levels bring it closer to endogenous levels and prevent toxic TDP-43 overexpression.

After identifying the optimal conditions for amber suppression in HEK293E cells, we attempted to generate a stable amber suppressed cell line, with a similar protocol to the one described by Dr. Elsässer (432). Unfortunately, in our hands the generated cells lost their ability to perform amber suppression and we were not able to use them for further experiments. Since the signal from the AcK RNA synthetase tag was still detectable, it is possible that the sequences corresponding to the 4 $tRNA^{AcK}_{UAG}$ copies were excised and removed. However, without a proper examination through sequencing of the cells it is only a hypothesis. The reason of this elimination could be the intrinsic genomic instability of immortalized cell lines (433,434), which may trigger genomic deletions, even leading to different karyotypes. In addition to the reported genomic variability, HEK293E cells are particularly difficult to stably amber suppressed (Dr. Simon Elsässer, personal communication). For this reasons, transient transfection of the amber suppression machinery was used.

A point of concern for stable or transient amber suppression is its effect on the total protein expression pattern and the possibility of a chaperone stress response to unexpected proteins

with an overrun stop codon. However, the total proteome of stably amber suppressed cells was examined and there was no evidence of an increase in unfolded protein response proteins (432). Further research and development of more efficient RNA synthetases and tRNA configurations can make in the future amber suppression the method of choice to study PTMs.

5. 5.- K84 acetylation modulates subcellular localisation

By using both point mutagenesis and amber suppression we managed to identify two lysine residues which through acetylation regulate two major functions of TDP-43: nuclear-cytoplasmic trafficking and RNA-binding activity. Regarding nuclear-cytoplasmic trafficking, both acetylation-mimic K84Q and acK84 TDP-43 displayed a reduction in nuclear localisation.

TDP-43 contains a bipartite nuclear localisation signal (NLS) spanning amino acids 82-98 that regulates its subcellular localisation (104,403). Through this NLS, TDP-43 interacts with importin β (or karyopherin-β1) and the complex is imported into the nucleus (105). The mass spectrometry analysis of wtTDP-43 uncovered two acetylation sites at or around the NLS: K79 and K84. Neither acetylation-mimic nor incorporation of acetylated lysine at K79 resulted in detectable changes in TDP-43 distribution (Fig. 4.8B and C, Fig. 4.23B). It might be important to notice that acetylation at this residue was detected only after MG132, therefore its effect might be noticeable only after proteasomal inhibition. However, proteasomal inhibition of both K79R and K79Q did not alter TDP-43 protein levels significantly (Fig. 4.7A). While acetylation at K79 had not been previously described, it has been found to be SUMOylated in high throughput studies (435) and ubiquitinated in spinal cord from one ALS patient. The significance of these modifications is unclear.

On the other hand, K84 is directly in the bipartite NLS of TDP-43 at the core of one of the NLS1 (K82-R83-K84). The mislocalization observed in the K84Q mutant is more pronounced that the one observed in amber suppressed acK84 TDP-43 when analysed via immunofluorescence, potentially establishing K84 as a modulator of nuclear import. This difference could be due to the structural differences of the substitution or due to *in vivo* deacetylation events. As it was mentioned before, while glutamine substitutions mimic the charge of the acetylated lysine they are mimicking, structurally there are important differences between the two residues (Fig. 5.2). The shorter side chain of the glutamine might have a bigger impact than the acetylated lysine. In addition to size differences, acetylated lysines can be targeted by endogenous KDACs and

therefore there could be deacetylation events tampering the effect of the acetylation introduced.

The more concerning difference of this analysis is the difference between the immunofluorescence data and the nuclear-cytoplasmic fractionation of K84Q. While virtually every cell expressing K84Q TDP-43 displays cytoplasmic mislocalisation (Fig. 4.8B and C), there is a sizeable amount of TDP-43 still detectable in the cytoplasmic fraction (Fig. 4.10A). This is consistent with the ability of K84Q TDP-43 to participate in the splicing of the CFTR minigene (Fig. 4.10E). In our hands, mutNLS behaves in a similar way: it is present mostly in the cytoplasm of cells when analysed via immunofluorescence, but it can be detected in the nuclear fraction, and it can still perform CFTR splicing. Careful examination of K84Q TDP-43 cells showed that, while almost all of them had a predominantly cytoplasmic expression of K84Q TDP-43, there was not a complete loss of nuclear localisation (addressed in (436)). It is possible that the cytoplasmic fraction is more accessible than the nuclear one, tainting the results of the immunofluorescence. This behaviour of mutNLS in immunofluorescence and Western blot can be observed as well in the seminal works of Winton et al. and Nishimura et al. (105,403) and, to a lesser extent in Ayala et al. (104). The concern about antibody accessibility and nuclear permeability was already raised by Winton et al. and could be a determining factor when assessing TDP-43 subcellular localisation.

Acetylation at K84 is a novel finding of this study, however other posttranslational modifications were found at this position. In the same data set that was used in this study, generated by Dr. Friederike Hans and Dr. Johannes Gloeckner, K84 was found to be ubiquitinated with an without proteasomal inhibition, as it was in the case of acetylation, suggesting that this is a modification that can be found under normal physiological conditions (239). In that study, a systematic characterization of all lysine residues in the C-terminal region plus 4 ubiquitinated lysines in the N-terminal region (K84, K95, K176, K181). K84A TDP-43 was expressed predominantly in the cytoplasm, while K84R TDP-43 remain mostly nuclear, confirming the behaviour of K84R TDP-43 observed in this thesis and highlighting the relevance of K84 as a modulator of TDP-43 subcellular localisation. In addition, both K84A and K84R TDP-43 mutants become more ubiquitinated after MG-132 treatment, perhaps for the presence of additional ubiquitin ligases in the cell cytoplasm. K84 also has been found to be SUMOylated in several other studies (435,437–439), however there is a lack of detailed analysis looking at the effect of this SUMOylation, however it is most probable linked to a loss of importin binding and an increase in cytoplasmic TDP-43. Further research is needed to confirm if this is the case.

The consequences of a cytoplasmic mislocalisation of TDP-43 are manifold. While in ALS and FTD material there is a loss of nuclear TDP-43, with its corresponding nuclear loss of function, acK84 TDP-43 retains some nuclear localization, and K84Q TDP-43 is even capable of performing CFTR splicing properly. Therefore, acetylation at K84 alone would not trigger a loss of TDP-43 nuclear activity. However, several studies have looked at the effect of pure cytoplasmic mislocalization by using ΔNLS TDP-43 in different models. In the context of pathological mutations and TDP-43 silencing, several studies have found links between TDP-43 and dendritic spine and neurite maintenance (419,440,441), however it seems that cytoplasmic mislocalisation of ΔNLS TDP-43 is enough to impact dendritic spines in a ΔNLS TDP-43 mouse model (442). In addition to dendritic growth, cytoplasmic TDP-43 can sequester part of the nuclear import machinery, such as importin-α and Nup62, which can have an impact in the global nuclear import in the cell, with proteins such as hnRNPA1 or FUS (411). Another reported effect of TDP-43 cytoplasmic mislocalisation is the reduction in total translation through its interaction and sequestration of RACK1 (443,444). While the studies mentioned look at specific pathways affected by the purely cytoplasmic ΔNLS TDP-43, there is a consensus in the literature regarding the toxicity caused by cytoplasmic mislocalization of TDP-43 (445). Interestingly, this toxicity is independent of the formation of aggregates (202,446). However, the shift to the cytoplasm puts TDP-43 in a different milieu, where it can b exposed to KATs, kinases, and other proteins that might push it into the phosphorylated aggregates that can be observed in ALS and FTD patients. If the toxicity does not depend on the presence of aggregates, they might be an epiphenomenon of the disorder. Further research uncovering the specific mechanism causing TDP-43 mislocalisation, and not so much the aggregation, might help slowing or preventing neuronal death.

5. 6.- K136 acetylation reduces RNA-binding and can trigger phase separation

The mass spectrometry analysis of wtTDP-43 revealed a putative acetylation site at K136. As with K84 acetylation, two different approaches were taken to explore the effect of this acetylation. The first was the substitution of K136 for an acetyl-mimic or an acetyl-dead amino acid (glutamine or arginine, respectively) and examined the subcellular localisation and function of TDP-43. Both K136R and K136Q mutants displayed the same dotted nuclear pattern, quite similar from wtTDP-43 (Fig 3.8B and C). In addition, proteasomal inhibition via MG132 increased protein levels slightly but not more than wtTDP-43 or any of the other TDP-43 mutants (Fig.

4.7A). The remarkable similarity of the nuclear droplets of K136R and K136Q TDP43 to the distribution of the RNA-binding deficient F147L/F149L TDP-43 mutant prompt the examination of the RNA-splicing and binding capabilities of these mutants. The results found will be discuss in this section.

5. 6. 1.- Acetylation at K136 reduces TDP-43 RNA-binding capabilities

To examine if K136 substitutions resulted in a loss of RNA-binding capabilities, the splicing activity of the TDP-43 humans was assessed using a number of known targets in sh^{TDP-43}-HEK293E cells. Both K136R and K136Q TDP-43 showed a loss of CFTR splicing capabilities but did not show any detectable reduction in splicing capabilities of other targets. In addition to this, K136R showed a reduction in binding to polyUG oligomers both in an RNA-protein pulldown and in a filter binding assay (Fig 4.16). These results are similar to those found by Cohen et al. regarding K145Q/K192Q TDP-43 (249), however in our hands K136R/Q showed a stronger reduction in RNA binding and CFTR splicing.

The similarities between both acetyl-mimic and acetyl-dead substitutes suggested a possible artifact due to the differences between the amino acid substitutions and the truly acetylated lysine (Fig. 4.2). These differences are also addressed in the section 3. 5 of this work, where a detailed examination of the possible artifacts caused by arginine and glutamine substitutions can be found (Fig 4.20). With this concerns in mind, an amber suppression system was used to examine the effect of the truly acetylated K136. The successfully amber suppressed TDP-43 displayed the same granular pattern and the same reduction in CFTR splicing capabilities, supporting the idea that K136Q TDP-43 is indeed an appropriate model of K136 acetylation. Nevertheless, the similarities between K136R and acK136 should be seen as a cautionary tale against lysine substitutions to study acetylation. While in most cases it is a good model, sensitive positions might require other methods to study acetylation.

The first detected link between K136 and RNA processing was found by Izumikawa et al. when looking at the role of TDP-43 in the processing of mitochondrial tRNA (156). K136A TDP-43 expression in T-Rex 203 cells resulted in mitochondrial expression of TDP-43 and reduced levels of mt-$tRNA^{Asn}$ and mt-$tRNA^{Gln}$, however the reduction was not as pronounced as with FFLL TDP-43. Nevertheless, this reduction did not translate in a proliferation deficit after 48 hours of induction of expression via doxycycline. Next, two studies looked at the role of SUMOylation at

K136. Maurel et al. identified K136 as a SUMOylation motif and established it as a key residue for TDP-43 overexpression-related toxicity (260). While the nuclear, granular distribution of K136R is confirmed in this study, the focus is put on the ameliorating effect of this substitution in TDP-43 cytotoxicity. The last study looking at K136 SUMOylation focus on its impact on RNA processing of a number of TDP-43 targets (414). In this study, the validate the SUMOylation site prediction and confirm the loss of RNA splicing activity of K136R TDP-43. In contrast to this thesis, Maraschi et al. confirm that K136R substitution reduces TDP-43 splicing of several targets, plus the binding to their respective mRNAs. However, the effect is not seen in the endogenous transcript, but in a transfected minigene. Since the reduction in K136R RNA binding is only partial, the overexpression of TDP-43 targets might be the only way to make the subtle differences detectable. While the aforementioned studies have looked at the SUMOylation of TDP-43, it is worth noting that K136 has not been found to be SUMOylated in any Mass Spectrometry analysis up to this date. The hypothesis that TDP-43 can be SUMOylated at K136 is based on the presence of a SUMOylation motif, but it is still unclear if SUMOylation does take place at this specific lysine.

As it was mentioned before K136 is at the core of the RNA binding pocket of the RRM1. When TDP-43 is bound to RNA, the residue is hidden by the RNA molecule, making it inaccessible to both KATs and KDACs. That being the case, K136 can only be posttranslationally modified when there is no RNA bound, and it could be a way to prevent RNA rebinding when TDP-43 is disengaging from stress granules or from local translation events. Alternatively, given the different effects of K136 acetylation on different TDP-43 targets, it could serve as a mechanism to modulate RNA activity. Given the amount of RNA targets that TDP-43 reduction affects (141), posttranslational modifications of the RNA binding site could offer certain degree of control in which RNA sequences TDP-43 binds predominantly. The subcellular localisation where all these mechanisms come together is the mitochondria. In the past years the research body looking at the role of TDP-43 in mitochondria has grown considerably, showing that TDP-43 can localise to mitochondria and that it can regulate the stability of mitochondrial mRNA ND3 and ND6 (108,160). As it was mentioned in the introduction, the mitochondria offers the most suitable environment in the cell to trigger non-enzymatic acetylation thanks to its high acetyl-CoA concentration and high pH. This would circumvent at least partially the accessibility issue of K136, since no bulky KATs would be needed to acetylate K136. In addition, both acetyl-CoA concentration and pH are tightly linked to metabolism, and one could imagine a negative feedback system where high amounts of acetyl-CoA modulate mitochondrial function by triggering non-enzymatic acetylation of TDP-43 RRM1, which would in turn release its inhibition

of ND3 and ND6 mRNAs. The further oxidative phosphorylation could increase ROS levels, which is a marker of ALS ad FTD and can promote the pathological phosphorylation of TDP-43 (258,447). Another interesting mitochondrial effect of TDP-43 non-enzymatic acetylation could be the aggregation of unbound TDP-43 into solid aggregates, which have been found both in cells and in patients material (160). In conclusion, acetylation of TDP-43 RRM1 could be a promoter of TDP-43 pathology in mitochondria by reducing its RNA binding and promoting aggregation.

However, from the different Sirtuins tested in this study, only Sirt1 had any detectable effect on K136 acetylation, suggesting that the deacetylation of this residue takes place in the nucleus and not in the mitochondria. Artificially enhancing mitochondrial localisation could promote interactions with mitochondrial sirtuins, but the high degree of artificiality would put that system into question. While a mitochondrial acetylation-mediated control of TDP-43 function could fit some of the current TDP-43 research, a more detailed examination of it is necessary to establish its validity. The current study only supports the acetylation-meditated inhibition of TDP-43 RNA binding, and its subsequent phase separation and aggregation, which would be discuss in the following section.

5. 6. 2.- Acetylated TDP-43 phase separates and aggregates

While studying the impact of K136 acetylation, we observed that both K136R/Q and acK136 TDP-43 formed a nuclear, droplet like distribution. Examination of the consistency of these inclusions using FRAP showed that the smaller the inclusions the faster the fluorescence recovery rate, however as the inclusions were getting bigger the recovery rate got slower and for big, irregular inclusions there was no recovery of fluorescence (Fig. 4.19). The fast and medium fluorescence recovery is a characteristic of phase separated organelles that are permeable or semipermeable to the outside environment (407). To further examine the nature of these inclusions, an EGFP-tagged K136Q TDP-43 was expressed in cells and its behaviour was recorded in a live imaging set up for up to 6 hours (Sup. Video 1 and 2). In these videos, TDP-43 droplets become bigger over time and fusion events can be seen, although the contribution of free-roaming TDP-43 seems to be bigger. Indeed, when the size of droplets is analysed 24 and 48 hours after transfection, there is a significant increase in the percentage of bigger aggregates and a trend for a reduction in the number of small aggregates (Fig 4.19). All this data combined supports the

conclusion that both acetyl mimic and amber suppressed TDP-43 form phase separated droplets that can fuse and grow overtime, becoming solid aggregates.

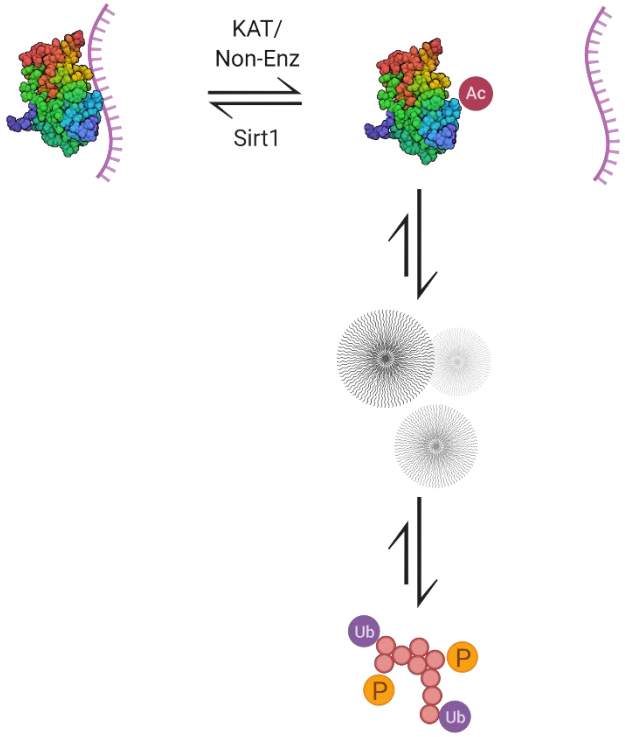

As with K84 before, the comparison of K136Q and acK136 TDP-43 shows some differences between the behaviour of the two proteins. While both form phase separated droplets, K136Q aggregates eventually are ubiquitinated and phosphorylated at serines 409/410, acK136 TDP-43 is not phosphorylated or hyperubiquitinated at detectable levels. There are three reasons for this difference in behaviour: differences in protein expression levels, changes in valency and

Figure 5. 3.- Model of TDP-43 acetylation-driven aggregation. Acetylation at K136 prevents RNA-binding and free roaming TDP-43 forms separated phases. These phases can, with time, lose fluidity and become solid aggregates.

deacetylation events. One of the possible disadvantages of amber suppression which was already discussed in this section is the low efficiency of the system which results in less protein expression than non-amber suppressed. The higher expression level of wtTDP-43 could increase its concentration and speed up the aggregation process. The second reason could be due to the changes in TDP-43 valency introduced with the glutamine substitution. In general terms, glutamines can promote phase separation through the introduction of dipolar interactions (306,307). Specifically, glutamine residues drive phase separation of FUS (338), therefore the glutamine introduced in the K136Q TDP-43 could be not only preventing RNA binding, but also increasing the solidity of TDP-43 phases and promoting the formation of hydrogels and solid aggregates that would, eventually get hyperubiquitinated and phosphorylated. The last possible

reason for the differences between K136Q and acK136 TDP-43 could be the presence of deacetylation event removing the acetyl group from amber suppressed TDP-43 and therefore rescuing its RNA-binding capabilities. A combination of these three mechanisms probably is responsible for the differences in behaviour and aggregation observed in the study.

The propensity of acK136 to phase separate, get phosphorylated and ubiquitinated is similar to the behaviour of K145Q/K192Q (249,251). This double mutant has shown to recapitulate the hyperubiquitination and pathological phosphorylation found in patient material, as well as being able to phase separate, an aspect which has been deeply studied in the recent article by Yu et al. Together, these studies and the present thesis paint a picture where RNA-binding loss caused by RRM1 acetylation at several residues drives TDP-43 into separated phases which can turn into pathological aggregates.

Another novel finding of this study was the essential role of the C-terminal low complexity domain in phase separation. The deletion of the C-terminal domain reverted the phase separated acK136 TDP-43 to a homogeneous nuclear distribution (Fig 4.27). As previously mentioned in the introduction, this part of TDP-43 has been linked to protein-protein interaction, aggregation and most of the mutations that have been linked to ALS are located in it (118,119,247,448). This domain could not only promote aggregation directly, but also mediate TDP-43 phase separation which in turn originates pathological aggregates (336,337). Indeed, experiments with synthetic phase separating proteins found that both RNA-binding domains and low complexity domains are needed to optimally form separated phases (310).

The disengagement of RNA is a critical step in the phase separation process of TDP-43. While they not characterised as phase-separated organelles, the FFLL TDP-43 inclusions observed by Voigt et al. would be investigated as such nowadays (246). Another RNA-binding deficient construct, K145Q TDP-43 also presented what would be later consider LLPS, which in retrospective suggests that loss of RNA-binding promotes LLPS (249,253). Indeed, experiments examining the total proteome solubility found that enzymatic degradation of RNA causes a massive loss in solubility in 1300 proteins, including non-RNA binding proteins that most probably are part of separated phases, such as tau or huntingtin (449). An specific demonstration of this was achieved through an optogenetic system where the pathological aggregation of TDP-43 could be prevented by using bait oligonucleotides to change the equilibrium between free TDP-43 and RNA-bound TDP-43 (404). This elegant experiment established the idea that RNA binding can keep the aggregation-prone TDP-43 in check. The binding of TDP-43 to RNA can fundamentally change its valency, preventing it from forming

phase separated condensates. Careful examination of LLPS kinetics showed that there a low [RNA]:[RNA-binding protein] index is optimal for phase separation, while an increase in RNA concentration or the addition of a molecular crowder to an *in vitro* experiment can prevent phase separation of RNA-binding proteins (450).

Perhaps the question one should ask now is the role, if any, these phase-separated inclusions play in TDP-43 physiology. As it was mentioned in the introduction, phase separation can add a level of control in terms of concentration and interactors to protein behaviour. First, the increase in concentration can impact the reaction kinetics and create highly efficient membranelles organelles which might be involved in mRNA processing (326,450,451). Indeed, RNA binding proteins are prone to phase separated, which can both inhibit or enhance their activity (452). In addition, the vast number of TDP-43 targets suggest the presence of a regulatory mechanisms, which was suggested before to be acetylation, but phase separation can be a control mechanism as well, sequestering and promoting certain interactions over others, like scaffold proteins in a signalling pathway (328,450). A recent study looked into the protein complexes formed in TDP-43 RNA-binding deficient droplets and found that the chaperone Hsp70 was present at the core of the droplet and that it was essential for the regulation of the fluidity of TDP-43 (251). However, it is important to realise that these functions are only hypothetical and that phase separation of hnRNPs could be a by-product of evolution of unstructured domains. Further research will uncover the true function, if any, of phase separation.

5. 7.- Antibody generation against acetylated TDP-43

At the beginning of this study a combination of panacetyl antibodies and point mutants was used to examine the impact of single acetylation sites. Through this approach, we concluded that the acetylated residues found in this study were not the only ones in TDP-43, but also none of them was a more prominent acetylation site than any of the other ones.

Pan-acetyl antibodies are great tools to examine the total level of acetylation of proteins or to examine major acetylation sites, however there are two main issues with this approach. The first one is the variability in sensitivity to specific residues from these antibodies. This issue was briefly examined in this paper when two different pan-acetyl antibodies were used to examine the acetylation of the same lysates, showing two similar but not identical patterns (Fig 4.4). Therefore, it is important to choose a panacetyl antibody at the beginning of a study, since changing it can give controversial results. The other obvious limitation is the poor resolution

when working with multiple acetylation sites. Detailed examination of acetylation kinetics and the influence of KATs and KDACs at specific residues is not possible most of the times. For these reasons we generated two antibodies that specifically detected acK84 and acK136 TDP-43, respectively.

The initial assessment of immunogenicity for these two residues showed that K84 was highly immunogenic, while K136 had much lower immunogenicity (Dr. Regina Feederle, personal communication). Because of this, a much higher number of antibodies had to be tested for K136 than for K84. In addition, different subclones for K136 were tested to find the most suitable one (data not shown). After testing several batches of primary supernatants, we found adequate antibodies for both acK84 and acK136. Interestingly, the antibody against acK136 also detected a 35kDa band only in the amber suppression lane (Fig. 4.29B). The significance of this band is unknow but if it is a cleavage product caused by K136 acetylation it would be another difference between the point mutants and the truly acetylated TDP-43, further reinforcing the adequacy of the model used.

A last reason to generate antibodies against acK84 and acK136 TDP-43 specifically was the goal to use them to test if these modifications were present in disease, in a similar manner to Cohen et al. (249). Both antibodies were tested in spinal cord and cortex samples from ALS and FTD patients respectively but unfortunately the results were inconclusive (data not shown). Further refinement of the antibodies and the staining protocols might give more definite results about the contribution of these modifications to TDP-43 proteinopathy.

5. 8.- Regulation of K136 TDP-43 acetylation

One of the benefits of a specific α-acK136 TDP-43 antibody is the possibility to study which cellular conditions or enzymes promote acetylation at this specific site. First, we looked for conditions that would promote TDP-43 K136 acetylation but using a series of different stressors and examining the levels of acK136 acetylation. From all the stressors tested, sorbitol elicited what at first looked like weak acetylation of TDP-43 cytoplasmic granules (Fig. 4.31). Unfortunately, this acetylation was not detected in western blot (Fig. 4.32A), which could speak in favour of high local concentrations of acK136 TDP-43 in granules, with signal to diluted and low to be detected in Western blot. To confirm if this was the case, sh^{TDP-43}-HEK293E cells were transfected with a series of TDP-43 constructs and treated with sorbitol. However, there was no detectable acetylation in Western blot of the total nor the purified TDP-43 fractions and, in addition, there was cytoplasmic acetylation of K136R TDP-43, which suggests that the signal

detected was the unspecific detection of another stress granule protein, rather than TDP-43. Together, these experiments returned inconclusive results about the acetylation state of K136 under the set of stressors tested.

Several studies looking at RRM modifications have tried to establish the conditions where TDP-43 RRM1 is modified without much success. When TDP-43 is mislocalized to the cytoplasm and in the presence of overexpressed CBP, K145 can be acetylated (249), however as it was mentioned in the introduction the use of highly promiscuous and active KATs might results in false positive results. Up to this date, no other study has established a condition where endogenous TDP-43 is acetylated or loses its RNA binding capabilities, which could be an indicator of RRM acetylation.

5. 8. 1.- KATs and KDACs interacting with TDP-43

After the no acetylating condition was found, we looked for the enzymes that could directly modulate TDP-43 acetylation, the responsible KATs and KDACs. Miriam Schmidt examined the effect of several KATs on TDP-43 acetylation (as a part of her BSc Thesis, data not shown), with the conclusion that p300 had a modest effect on K136 acetylation but not strong enough to elicit a subcellular localization change. In this regard, it is important to notice that KATs do not work in isolation but in complexes that regulate their activity and interaction partners. Therefore, it is possible that different KATs could influence TDP-43 in the right protein complex. Unfortunately, the regulation of acetylation in non-histone proteins is not fully understood and the effects of KAT overexpression are difficult to predict. The results from Miriam Schmidt suggest that p300 could acetylate K136, however more research is needed to unveil the precise regulation.

While the search for KATs was done by a bachelor student as a part of her thesis, we perform a systematic analysis of the effect of different KDACs on TDP-43 acetylation. To do this, we took advantage of both the specific α-acK136 antibody developed and the amber suppression system that was established in this thesis. Amber suppressed HEK293E cells were transfected with HDAC1-8 and Sirt1-7 and K136 acetylation levels were analysed. From the 8 HDACs tested, HDAC1 and HDAC6 showed an apparent significant reduction in K136 acetylation, not surprisingly since both have been linked to TDP-43 acetylation (249,252,453). However, the overexpression of HDAC1 and 6 caused a reduction in total TDP-43 levels and, furthermore, the introduction of mutations at their respective catalytic sites did not revert this effect. This suggests that the effect that HDAC1 and HDAC6 has on amber suppression is not due to their

deacetylation activity, but through another, uncovered mechanism. One of the possible explanations can be found in the interaction of HDAC6 and GlyRS (454). In this study, Mo et al. show how HDAC6 can interact with GlyRS, which causes an HDAC6 toxic gain of function leading to tubulin deacetylation an axonal transport deficit. While this can contribute to ALS and FTD as well, the important message from this study is the interaction potential of HDAC6 with RNA synthetases. Unfortunately, the synthetic nature of the AcKRS used in this study makes it hard to predict possible interactions between the two of them, but it is a possibility to keep in mind.

While the analysis of HDAC1-8 activity on K136 acetylation did not show any conclusive results, the analysis of the activity of Sirtuins on K136 showed how Sirt1 can deacetylate K136 and revert TDP-43 phase separation (Fig 4.35 and 4.36). To confirm the effect of Sirt1 on TDP-43 a selective Sirt1 inhibitor, Ex527, was used to inhibit the activity of the overexpressed Sirt1, resulting in a rescue of K136 acetylation levels (Fig 4.35). It is important to notice that Sirt1 reduces K136 acetylation but does not remove it completely, which could be seen both in Western blot and immunofluorescence. The reduction in acetylation, however, is enough to reduce the number of cells showing TDP-43 inclusions, which suggests that there is a critical amount of acetylated TDP-43 needed to trigger mass phase separation in the cell. This is yet another proof that the TDP-43 inclusions that form in the amber suppressed construct are indeed phase separated molecules, since their separation depend on the concentration of their components.

An interaction at mRNA regulation level between Sirt1 and TDP-43 has been already characterised (455). In their study, Yu et al. describe an interaction between TDP-43 and Sirt1 mRNA, where a downregulation of TDP-43 or his partners FMRP and STAU1 results in a reduction of Sirt1 mRNA levels and subsequent reduction in Sirt1 protein levels. Sirt1 protein levels can be rescued by TDP-43, which binds to the 3'UTR region of its mRNA through both RRMs. Putting these findings in the context of TDP-43 acetylation, a positive feedback loop emerges, where a deacetylation of TDP-43 promotes its binding to Sirt1 mRNA, increasing its stability and protein expression which in turn would keep TDP-43 RRM deacetylated and able to regulate Sirt1 expression. An imbalance at both TDP-43 RNA-binding capabilities or Sirt1 activity would cause a cascade of increasing TDP-43 and lower levels of Sirt1 expression. Giving the involvement of Sirt1 in reducing inflammation and suppressing neurotoxicity in Alzheimer's disease and traumatic brain injury models (456), the destabilisation of this relation can have a noticeable impact in neurotoxicity not only limited to ALS and FTD. For the moment, no significant relation between Sirt1 and ALS and FTD specifically has been described but this study and the already reported role of Sirt1 in neuroprotection hints at a role of the deacetylase also in TDP-43 proteinopathies.

5. 9.- Outlook

The regulation and consequences of TDP-43 aggregates in ALS and FTD has been one of the most pressing questions in the study of the ALS-FTD spectrum since the discovery of TDP-43 in pathological aggregates. While we still do not know their origin and their toxicity mechanisms, there has been a steady progress looking at how posttranslational modifications alter TDP-43 physiology and how the aggregation process takes place. One of the most recent advances has been a theoretical one, more than a practical one: the understanding of TDP-43 aggregation in the frame of phase separation. In this study, we characterise the function of four novel acetylation sites and established a link between acetylation, RNA binding, phase separation and aggregation. These results leave unanswered questions and create new ones that need to be resolved to prove an acetylation-driven aggregation model of TDP-43.

One of the main criticisms of the study is the lack of neuronal background in the HEK293E cells used. Transcriptional and translational regulation depend heavily on cell type and external conditions, therefore HEK293E cells offer a limited model of the situation in an aged brain or spinal cord. Therefore, a confirmation of the results of this project in a neuronal-like context would strengthen its conclusions. The most accessible and fast way to improve the model would be to confirm these results in amber suppressed SH-SY5Y cells, a neuronal-like model derived from neuroblastoma. While not completely neuronal, these cells retain many characteristics of neuronal cells, and their transcriptome is closer to cortical or spinal neurons than HEK293E cells. Another model closer to motor neurons would be the murine motor neuron-derived NSC34 cells. These cells are a fusion product of murine motor neurons from mouse spinal cord with mouse glioblastoma cells (457), which bring them even closer to motor neurons than SH-SY5Y cells. The obvious disadvantage of using NSC34 cells is its murine nature and the possibility that mRNA targets of protein partners of TDP-43 differ from the situation in humans. This brings us to what could be the most reliable cell model of disease, which is iPSCs-derived neurons from ALS-FTD patients. Several protocols have been establish to derive motor neurons from human iPSCs (458,459). This approach has been already taken, specially to create high-throughput drug testing platforms (460–462), but the combination of amber suppression methods and specific acetylated TDP-43 antibodies offer new possibilities to study TDP-43 aggregation in depth. Interestingly, a study using iPSCs-derived motor neurons from ALS patients found that anacardic acid, and TSA can modulate arsenite-related toxicity (463). A more in-depth analysis of the effect

of these drugs in TDP-43 PTMs would help with the understanding of TDP-43 PTM's related toxicity.

iPSCs-derived neurons are perhaps the state-of-the-art technology to model human disease. However, there is a unique aspect of motor neurons that it is not recapitulated in this model and that allegedly has an impact of ALS pathology: the extremely long axonal tracts of motor neurons in the human body. The energy required to maintain these structures has been hypothesized to be one of the causes of ALS motor neuron selectivity but unfortunately cannot be modelled in *in vitro* conditions. Since *in vivo* motor neurons are significantly longer, animal models offer a possible solution to this issue. There are several ALS mouse, zebrafish and fly models which offer a portrait of motor neuron local environment which cannot be recapitulated *in vitro*. Therefore, it would be of interest to generate an amber suppressed fly model that allows to examine TDP-43 acetylation-driven phase separation in live cells and, more importantly, that allows to test compounds that trigger or prevent TDP-43 K136 acetylation. To generate this model the same PiggyBac system that as tried in HEK293E cells in this study could be used, allowing for a quick repurpose of the system.

Another interesting point that could not be fully studied in this project is the interaction between acetylation and other posttranslational modifications. The characterisation of K136R/Q TDP-43 showed an increase in general ubiquitination and S409/410 phosphorylation, which are pathological PTMs found in patients. However, the specific ubiquitination targets and the quality of the ubiquitinations were not characterised. In addition, phosphorylation at other serine residues have been linked to TDP-43 pathology (S375, S379, S403 and S404) (227,228) and the relationship between those and acetylation has not been uncovered yet. In addition, an N-terminal serine phosphorylation at S48, has been linked to a disruption in phase separation and oligomerization via the N-terminal domain. It would be interesting to examine the relation between S48 and K136 PTMs with both specific antibodies, and the synergy that can emerge in relation to phase separation.

An aspect that was only partially resolved in this study was the regulation of K136 acetylation via endogenous KATs and KDACs, specifically its deacetylation via Sirt1. Since the set of stressors tested did not show a robust increase of K136 acetylation, a different set or a combination of them could help in the establishment of TDP-43 acetylation conditions. As an example of this, Yu et al. used a combination of KDAC inhibitors and proteasome inhibitors to promote TDP-43 phase separation (251). Another example of a combination of hits would be the use of ΔNLS TDP-43 constructs to promote mislocalization to the cytoplasm in combination with KDAC

inhibitors. However, to prevent artifacts as much as possible, a combination of stressors would be the method of choice. An additional condition to test could be the conditioned media from TDP-43-aggregating cells or iPSCs-derived motor neurons from patients.

In relation to the enzymes responsible of K84 and K136 acetylation, the work of Miriam Schmidt showed the nuances of the overexpression of acetyl transferases alone. As it was mentioned before, there is a lack of knowledge regarding the method of action of KATs. A deeper understanding in the complexes and regulation of localisation of each KAT would greatly improve the planning and interpretation of these experiments. Alternatively, once the cellular conditions responsible for TDP-43 acetylation have been found, one could identify TDP-43 interacting proteins through a comparison of mass spectrometry interactomes and build up the acetylation system "bottom up". This method, while more laborious, ensures a model closer to reality and avoids the oversimplification that comes with overexpression experiments.

The identification of phase separated TDP-43 that was mentioned in the previous paragraph is a critical point for the understanding of TDP-43 biomolecular condensates. The most straightforward way to tackle it would be to use a proximity labelling approach, by tagging K136Q TDP-43 with a TurboID biotin ligase and provide biotin to the cells. The choice of K136Q over amber suppression would ensure a higher signal-to-noise ratio because of its higher expression, however amber suppression could be an alternative with a C-terminal tag that could only express in successfully suppressed cells. The biotinylated proteins could be easily purified and analysed via Mass spectrometry, providing a comprehensive picture of the components of TDP-43 phase separation. This could help identify KDACs and their complex members or even scaffold and client elements from these phases that modulate its action. While the role of them is still unknown, the members of the phases would give a clearer idea of the possible functions TDP-43 might play *in vivo*.

The generation of K136Q TDP-43 TurboID constructs would allow to label and analyse RNA molecules as well. As it was discussed in the section before, the acetylation of the RRM1 does not cause a complete lack of RNA binding, but a reduction of it regarding specific targets. Therefore, the identification of RNA targets that are affected specifically by K136 or K145 acetylation could be key to understand TDP-43 physiology and to identify the pathways that are aberrantly altered in the context of phase separated TDP-43, which might differ from Knock out models. This could represent a therapeutical target, aiming not at aggregating TDP-43 itself, but at the consequences of its aggregation.

Perhaps the most important unanswered question of this study is the relevance of TDP-43 acetylation at K84 and K136 for ALS and FTD. While the point mutants and the amber suppressed recapitulate some of the characteristics of pathological TDP-43, no acetylated TDP-43 has been found in patients' material. The predicted low immunogenicity of K136 foreshadowed the difficulty of finding the modification in pathological material. The lack of success in this regard could mean that TDP-43 is not acetylated at K136, however phases are not well kept after fixation and acetylated TDP-43 may be seeding bigger aggregates. Therefore, a more sensitive method is needed to decisively identify acetylated TDP-43 in patients' material, or to confirm that it plays no role or an insignificant one in TDP-43 aggregation. A method that would increase the sensitivity of Western blot would be the use of Simoa® Technology (464), a ultrasensitive method that is already in use to detect markers of other neurodegenerative diseases such neurofilaments, amyloid or tau in CSF and blood (465–467). The development of this method would require an optimization process with the purified protein, cell lysates and eventually pathological material and would allow to either detect acetylated TDP-43 in patients' material or to confirm that acK136 TDP-43 does not play a role in disease or, if there is any acetylated protein, it is under detection level.

Even though the questions described were out of the scope of this thesis, the development of amber suppression to study neurodegenerative disease and the characterization of four new acetylation sites will certainly improve the insight about TDP-43 pathophysiology. The understanding and regulation of these will surely help in the future to diagnose, treat and follow the course of these devastating diseases that will become, at some point, a problem from the past.

6.- Bibliography

1. Rowland LP. How amyotrophic lateral sclerosis got its name: the clinical-pathologic genius of Jean-Martin Charcot. Arch Neurol. 2001 Mar;58(3):512–515.

2. Tubbs RS, Riech S, Verma K, Mortazavi MM, Loukas M, Benninger B, et al. Sir Charles Bell (1774-1842) and his contributions to early neurosurgery. Childs Nerv Syst. 2012 Mar;28(3):331–335.

3. van den Bos MAJ, Geevasinga N, Higashihara M, Menon P, Vucic S. Pathophysiology and Diagnosis of ALS: Insights from Advances in Neurophysiological Techniques. Int J Mol Sci. 2019 Jun 10;20(11).

4. Olney NT, Spina S, Miller BL. Frontotemporal Dementia. Neurol Clin. 2017 May;35(2):339–374.

5. Alzheimer A. Über eigenartige Krankheitsfälle des späteren Alters. Zeitschrift für die gesamte Neurologie und Psychiatrie. 1911;4(1):356–385.

6. Constantinidis J Fau - Richard J, Richard J Fau - Tissot R, Tissot R. Pick's disease. Histological and clinical correlations. (0014-3022 (Print)).

7. Román G. Vascular dementia: a historical background. Int Psychogeriatr. 2003;15 Suppl 1:11–13.

8. Grad LI, Rouleau GA, Ravits J, Cashman NR. Clinical spectrum of amyotrophic lateral sclerosis (ALS). Cold Spring Harb Perspect Med. 2017 Aug 1;7(8).

9. Ragagnin AMG, Shadfar S, Vidal M, Jamali MS, Atkin JD. Motor neuron susceptibility in ALS/FTD. Front Neurosci. 2019 Jun 27;13:532.

10. Kiernan MC, Vucic S, Cheah BC, Turner MR, Eisen A, Hardiman O, et al. Amyotrophic lateral sclerosis. Lancet. 2011 Mar 12;377(9769):942–955.

11. Hardiman O, Al-Chalabi A, Chio A, Corr EM, Logroscino G, Robberecht W, et al. Amyotrophic lateral sclerosis. Nat Rev Dis Primers. 2017 Oct 5;3:17071.

12. Logroscino G, Traynor BJ, Hardiman O, Chiò A, Mitchell D, Swingler RJ, et al. Incidence of amyotrophic lateral sclerosis in Europe. J Neurol Neurosurg Psychiatry. 2010 Apr;81(4):385–390.

13. Elamin M, Bede P, Byrne S, Jordan N, Gallagher L, Wynne B, et al. Cognitive changes predict functional decline in ALS: a population-based longitudinal study. Neurology. 2013 Apr 23;80(17):1590–1597.

14. Chiò A, Logroscino G, Traynor BJ, Collins J, Simeone JC, Goldstein LA, et al. Global epidemiology of amyotrophic lateral sclerosis: a systematic review of the published literature. Neuroepidemiology. 2013 Jul 11;41(2):118–130.

15. Zaldivar T, Gutierrez J, Lara G, Carbonara M, Logroscino G, Hardiman O. Reduced frequency of ALS in an ethnically mixed population: a population-based mortality study. Neurology. 2009 May 12;72(19):1640–1645.

16. Al-Chalabi A, Hardiman O, Kiernan MC, Chiò A, Rix-Brooks B, van den Berg LH. Amyotrophic lateral sclerosis: moving towards a new classification system. Lancet Neurol. 2016 Oct;15(11):1182–1194.

17. Chiò A, Calvo A, Moglia C, Mazzini L, Mora G, PARALS study group. Phenotypic heterogeneity of amyotrophic lateral sclerosis: a population based study. J Neurol Neurosurg Psychiatry. 2011 Jul;82(7):740–746.

18. Pehar M, Harlan BA, Killoy KM, Vargas MR. Role and therapeutic potential of astrocytes in amyotrophic lateral sclerosis. Curr Pharm Des. 2017;23(33):5010–5021.

19. Okamoto K, Mizuno Y, Fujita Y. Bunina bodies in amyotrophic lateral sclerosis. Neuropathology. 2008 Apr;28(2):109–115.

20. Neumann M, Sampathu DM, Kwong LK, Truax AC, Micsenyi MC, Chou TT, et al. Ubiquitinated TDP-43 in frontotemporal lobar degeneration and amyotrophic lateral sclerosis. Science. 2006 Oct 6;314(5796):130–133.

21. Arai T, Hasegawa M, Akiyama H, Ikeda K, Nonaka T, Mori H, et al. TDP-43 is a component of ubiquitin-positive tau-negative inclusions in frontotemporal lobar degeneration and amyotrophic lateral sclerosis. Biochem Biophys Res Commun. 2006 Dec 22;351(3):602–611.

22. Bede P, Iyer PM, Schuster C, Elamin M, Mclaughlin RL, Kenna K, et al. The selective anatomical vulnerability of ALS: “disease-defining” and “disease-defying” brain regions. Amyotroph Lateral Scler Frontotemporal Degener. 2016 Apr 18;17(7-8):561–570.

23. Kwong LK, Neumann M, Sampathu DM, Lee VM-Y, Trojanowski JQ. TDP-43 proteinopathy: the neuropathology underlying major forms of sporadic and familial

frontotemporal lobar degeneration and motor neuron disease. Acta Neuropathol. 2007 Jul;114(1):63–70.

24. Neumann M. Molecular neuropathology of TDP-43 proteinopathies. Int J Mol Sci. 2009 Jan 9;10(1):232–246.

25. Saberi S, Stauffer JE, Schulte DJ, Ravits J. Neuropathology of amyotrophic lateral sclerosis and its variants. Neurol Clin. 2015 Nov;33(4):855–876.

26. Onyike CU, Diehl-Schmid J. The epidemiology of frontotemporal dementia. Int Rev Psychiatry. 2013 Apr;25(2):130–137.

27. Petrides M. Lateral prefrontal cortex: architectonic and functional organization. Philos Trans R Soc Lond B, Biol Sci. 2005 Apr 29;360(1456):781–795.

28. Rascovsky K, Hodges JR, Knopman D, Mendez MF, Kramer JH, Neuhaus J, et al. Sensitivity of revised diagnostic criteria for the behavioural variant of frontotemporal dementia. Brain. 2011 Sep;134(Pt 9):2456–2477.

29. Vinceti G, Olney N, Mandelli ML, Spina S, Hubbard HI, Santos-Santos MA, et al. Primary progressive aphasia and the FTD-MND spectrum disorders: clinical, pathological, and neuroimaging correlates. Amyotroph Lateral Scler Frontotemporal Degener. 2019 May;20(3-4):146–158.

30. Gorno-Tempini ML, Hillis AE, Weintraub S, Kertesz A, Mendez M, Cappa SF, et al. Classification of primary progressive aphasia and its variants. Neurology. 2011 Mar 15;76(11):1006–1014.

31. Herrmann N, Black SE, Chow T, Cappell J, Tang-Wai DF, Lanctôt KL. Serotonergic function and treatment of behavioral and psychological symptoms of frontotemporal dementia. Am J Geriatr Psychiatry. 2012 Sep;20(9):789–797.

32. Pijnenburg YAL, Sampson EL, Harvey RJ, Fox NC, Rossor MN. Vulnerability to neuroleptic side effects in frontotemporal lobar degeneration. Int J Geriatr Psychiatry. 2003 Jan;18(1):67–72.

33. Kortte KB, Rogalski EJ. Behavioural interventions for enhancing life participation in behavioural variant frontotemporal dementia and primary progressive aphasia. Int Rev Psychiatry. 2013 Apr;25(2):237–245.

34. Mackenzie IRA, Neumann M, Bigio EH, Cairns NJ, Alafuzoff I, Kril J, et al. Nomenclature for neuropathologic subtypes of frontotemporal lobar degeneration: consensus recommendations. Acta Neuropathol. 2009 Jan;117(1):15–18.

35. Mackenzie IRA, Neumann M, Bigio EH, Cairns NJ, Alafuzoff I, Kril J, et al. Nomenclature and nosology for neuropathologic subtypes of frontotemporal lobar degeneration: an update. Acta Neuropathol. 2010 Jan;119(1):1–4.

36. Mandelkow E-M, Mandelkow E. Biochemistry and cell biology of tau protein in neurofibrillary degeneration. Cold Spring Harb Perspect Med. 2012 Jul;2(7):a006247.

37. Dickson DW, Kouri N, Murray ME, Josephs KA. Neuropathology of frontotemporal lobar degeneration-tau (FTLD-tau). J Mol Neurosci. 2011 Nov;45(3):384–389.

38. Mackenzie IRA, Neumann M, Baborie A, Sampathu DM, Du Plessis D, Jaros E, et al. A harmonized classification system for FTLD-TDP pathology. Acta Neuropathol. 2011 Jul;122(1):111–113.

39. Mackenzie IRA, Baborie A, Pickering-Brown S, Du Plessis D, Jaros E, Perry RH, et al. Heterogeneity of ubiquitin pathology in frontotemporal lobar degeneration: classification and relation to clinical phenotype. Acta Neuropathol. 2006 Nov;112(5):539–549.

40. Neumann M, Mackenzie IRA. Review: Neuropathology of non-tau frontotemporal lobar degeneration. Neuropathol Appl Neurobiol. 2019 Feb;45(1):19–40.

41. Mackenzie IRA, Neumann M. FET proteins in frontotemporal dementia and amyotrophic lateral sclerosis. Brain Res. 2012 Jun 26;1462:40–43.

42. Svetoni F, Frisone P, Paronetto MP. Role of FET proteins in neurodegenerative disorders. RNA Biol. 2016 Nov;13(11):1089–1102.

43. Holm IE, Isaacs AM, Mackenzie IRA. Absence of FUS-immunoreactive pathology in frontotemporal dementia linked to chromosome 3 (FTD-3) caused by mutation in the CHMP2B gene. Acta Neuropathol. 2009 Nov;118(5):719–720.

44. Abramzon YA, Fratta P, Traynor BJ, Chia R. The overlapping genetics of amyotrophic lateral sclerosis and frontotemporal dementia. Front Neurosci. 2020 Feb 5;14:42.

45. Ling S-C, Polymenidou M, Cleveland DW. Converging mechanisms in ALS and FTD: disrupted RNA and protein homeostasis. Neuron. 2013 Aug 7;79(3):416–438.

46. Nguyen HP, Van Broeckhoven C, van der Zee J. ALS Genes in the Genomic Era and their Implications for FTD. Trends Genet. 2018 Mar 28;34(6):404–423.

47. Brown CA, Lally C, Kupelian V, Flanders WD. Estimated prevalence and incidence of amyotrophic lateral sclerosis and SOD1 and c9orf72 genetic variants. Neuroepidemiology. 2021 Jul 9;1–12.

48. Greaves CV, Rohrer JD. An update on genetic frontotemporal dementia. J Neurol. 2019 Aug;266(8):2075–2086.

49. Renton AE, Majounie E, Waite A, Simón-Sánchez J, Rollinson S, Gibbs JR, et al. A hexanucleotide repeat expansion in C9ORF72 is the cause of chromosome 9p21-linked ALS-FTD. Neuron. 2011 Oct 20;72(2):257–268.

50. Renton AE, Chiò A, Traynor BJ. State of play in amyotrophic lateral sclerosis genetics. Nat Neurosci. 2014 Jan;17(1):17–23.

51. Van Langenhove T, van der Zee J, Sleegers K, Engelborghs S, Vandenberghe R, Gijselinck I, et al. Genetic contribution of FUS to frontotemporal lobar degeneration. Neurology. 2010 Feb 2;74(5):366–371.

52. van Swieten JC, Heutink P. Mutations in progranulin (GRN) within the spectrum of clinical and pathological phenotypes of frontotemporal dementia. Lancet Neurol. 2008 Oct;7(10):965–974.

53. Moore KM, Nicholas J, Grossman M, McMillan CT, Irwin DJ, Massimo L, et al. Age at symptom onset and death and disease duration in genetic frontotemporal dementia: an international retrospective cohort study. Lancet Neurol. 2020 Feb;19(2):145–156.

54. Neumann M, Kwong LK, Truax AC, Vanmassenhove B, Kretzschmar HA, Van Deerlin VM, et al. TDP-43-positive white matter pathology in frontotemporal lobar degeneration with ubiquitin-positive inclusions. J Neuropathol Exp Neurol. 2007 Mar;66(3):177–183.

55. Ranganathan R, Haque S, Coley K, Shepheard S, Cooper-Knock J, Kirby J. Multifaceted Genes in Amyotrophic Lateral Sclerosis-Frontotemporal Dementia. Front Neurosci. 2020 Jul 7;14:684.

56. Laaksovirta H, Peuralinna T, Schymick JC, Scholz SW, Lai S-L, Myllykangas L, et al. Chromosome 9p21 in amyotrophic lateral sclerosis in Finland: a genome-wide association study. Lancet Neurol. 2010 Oct;9(10):978–985.

57. DeJesus-Hernandez M, Mackenzie IR, Boeve BF, Boxer AL, Baker M, Rutherford NJ, et al. Expanded GGGGCC hexanucleotide repeat in noncoding region of C9ORF72 causes chromosome 9p-linked FTD and ALS. Neuron. 2011 Oct 20;72(2):245–256.

58. Majounie E, Renton AE, Mok K, Dopper EGP, Waite A, Rollinson S, et al. Frequency of the C9orf72 hexanucleotide repeat expansion in patients with amyotrophic lateral sclerosis and frontotemporal dementia: a cross-sectional study. Lancet Neurol. 2012 Apr;11(4):323–330.

59. Rutherford NJ, Heckman MG, Dejesus-Hernandez M, Baker MC, Soto-Ortolaza AI, Rayaprolu S, et al. Length of normal alleles of C9ORF72 GGGGCC repeat do not influence disease phenotype. Neurobiol Aging. 2012 Dec;33(12):2950.e5–7.

60. Nordin A, Akimoto C, Wuolikainen A, Alstermark H, Jonsson P, Birve A, et al. Extensive size variability of the GGGGCC expansion in C9orf72 in both neuronal and non-neuronal tissues in 18 patients with ALS or FTD. Hum Mol Genet. 2015 Jun 1;24(11):3133–3142.

61. Solomon DA, Stepto A, Au WH, Adachi Y, Diaper DC, Hall R, et al. A feedback loop between dipeptide-repeat protein, TDP-43 and karyopherin-α mediates C9orf72-related neurodegeneration. Brain. 2018 Oct 1;141(10):2908–2924.

62. Pang W, Hu F. Cellular and physiological functions of C9ORF72 and implications for ALS/FTD. J Neurochem. 2021 May;157(3):334–350.

63. Reddy K, Zamiri B, Stanley SYR, Macgregor RB, Pearson CE. The disease-associated r(GGGGCC)n repeat from the C9orf72 gene forms tract length-dependent uni- and multimolecular RNA G-quadruplex structures. J Biol Chem. 2013 Apr 5;288(14):9860–9866.

64. Mann DMA, Rollinson S, Robinson A, Bennion Callister J, Thompson JC, Snowden JS, et al. Dipeptide repeat proteins are present in the p62 positive inclusions in patients with frontotemporal lobar degeneration and motor neurone disease associated with expansions in C9ORF72. Acta Neuropathol Commun. 2013 Oct 14;1:68.

65. Gendron TF, Bieniek KF, Zhang Y-J, Jansen-West K, Ash PEA, Caulfield T, et al. Antisense transcripts of the expanded C9ORF72 hexanucleotide repeat form nuclear RNA foci and undergo repeat-associated non-ATG translation in c9FTD/ALS. Acta Neuropathol. 2013 Dec;126(6):829–844.

66. Waite AJ, Bäumer D, East S, Neal J, Morris HR, Ansorge O, et al. Reduced C9orf72 protein levels in frontal cortex of amyotrophic lateral sclerosis and frontotemporal degeneration brain with the C9ORF72 hexanucleotide repeat expansion. Neurobiol Aging. 2014 Jul;35(7):1779.e5–1779.e13.

67. Levine TP, Daniels RD, Gatta AT, Wong LH, Hayes MJ. The product of C9orf72, a gene strongly implicated in neurodegeneration, is structurally related to DENN Rab-GEFs. Bioinformatics. 2013 Feb 15;29(4):499–503.

68. Aoki Y, Manzano R, Lee Y, Dafinca R, Aoki M, Douglas AGL, et al. C9orf72 and RAB7L1 regulate vesicle trafficking in amyotrophic lateral sclerosis and frontotemporal dementia. Brain. 2017 Apr 1;140(4):887–897.

69. Xiao S, McKeever PM, Lau A, Robertson J. Synaptic localization of C9orf72 regulates post-synaptic glutamate receptor 1 levels. Acta Neuropathol Commun. 2019 Oct 24;7(1):161.

70. Ho WY, Tai YK, Chang J-C, Liang J, Tyan S-H, Chen S, et al. The ALS-FTD-linked gene product, C9orf72, regulates neuronal morphogenesis via autophagy. Autophagy. 2019 May;15(5):827–842.

71. Abo-Rady M, Kalmbach N, Pal A, Schludi C, Janosch A, Richter T, et al. Knocking out C9ORF72 Exacerbates Axonal Trafficking Defects Associated with Hexanucleotide Repeat Expansion and Reduces Levels of Heat Shock Proteins. Stem Cell Rep. 2020 Mar 10;14(3):390–405.

72. Kim ES, Chung CG, Park JH, Ko BS, Park SS, Kim YH, et al. C9orf72-associated arginine-rich dipeptide repeats induce RNA-dependent nuclear accumulation of Staufen in neurons. Hum Mol Genet. 2021 Jun 9;30(12):1084–1100.

73. Stepto A, Gallo J-M, Shaw CE, Hirth F. Modelling C9ORF72 hexanucleotide repeat expansion in amyotrophic lateral sclerosis and frontotemporal dementia. Acta Neuropathol. 2014 Mar;127(3):377–389.

74. Rosen DR, Siddique T, Patterson D, Figlewicz DA, Sapp P, Hentati A, et al. Mutations in Cu/Zn superoxide dismutase gene are associated with familial amyotrophic lateral sclerosis. Nature. 1993 Mar 4;362(6415):59–62.

75. Eleutherio ECA, Silva Magalhães RS, de Araújo Brasil A, Monteiro Neto JR, de Holanda Paranhos L. SOD1, more than just an antioxidant. Arch Biochem Biophys. 2021 Jan 15;697:108701.

76. Kaur SJ, McKeown SR, Rashid S. Mutant SOD1 mediated pathogenesis of Amyotrophic Lateral Sclerosis. Gene. 2016 Feb 15;577(2):109–118.

77. Mackenzie IRA, Bigio EH, Ince PG, Geser F, Neumann M, Cairns NJ, et al. Pathological TDP-43 distinguishes sporadic amyotrophic lateral sclerosis from amyotrophic lateral sclerosis with SOD1 mutations. Ann Neurol. 2007 May;61(5):427–434.

78. Cenik B, Sephton CF, Kutluk Cenik B, Herz J, Yu G. Progranulin: a proteolytically processed protein at the crossroads of inflammation and neurodegeneration. J Biol Chem. 2012 Sep 21;287(39):32298–32306.

79. Petkau TL, Leavitt BR. Progranulin in neurodegenerative disease. Trends Neurosci. 2014 Jul;37(7):388–398.

80. Baker M, Mackenzie IR, Pickering-Brown SM, Gass J, Rademakers R, Lindholm C, et al. Mutations in progranulin cause tau-negative frontotemporal dementia linked to chromosome 17. Nature. 2006 Aug 24;442(7105):916–919.

81. Cruts M, Gijselinck I, van der Zee J, Engelborghs S, Wils H, Pirici D, et al. Null mutations in progranulin cause ubiquitin-positive frontotemporal dementia linked to chromosome 17q21. Nature. 2006 Aug 24;442(7105):920–924.

82. Yin F, Dumont M, Banerjee R, Ma Y, Li H, Lin MT, et al. Behavioral deficits and progressive neuropathology in progranulin-deficient mice: a mouse model of frontotemporal dementia. FASEB J. 2010 Dec;24(12):4639–4647.

83. Beel S, Herdewyn S, Fazal R, De Decker M, Moisse M, Robberecht W, et al. Progranulin reduces insoluble TDP-43 levels, slows down axonal degeneration and prolongs survival in mutant TDP-43 mice. Mol Neurodegener. 2018 Oct 16;13(1):55.

84. Chornenkyy Y, Fardo DW, Nelson PT. Tau and TDP-43 proteinopathies: kindred pathologic cascades and genetic pleiotropy. Lab Invest. 2019 Jul;99(7):993–1007.

85. Kadavath H, Hofele RV, Biernat J, Kumar S, Tepper K, Urlaub H, et al. Tau stabilizes microtubules by binding at the interface between tubulin heterodimers. Proc Natl Acad Sci USA. 2015 Jun 16;112(24):7501–7506.

86. Sato C, Barthélemy NR, Mawuenyega KG, Patterson BW, Gordon BA, Jockel-Balsarotti J, et al. Tau kinetics in neurons and the human central nervous system. Neuron. 2018 Mar 21;97(6):1284–1298.e7.

87. Min S-W, Cho S-H, Zhou Y, Schroeder S, Haroutunian V, Seeley WW, et al. Acetylation of tau inhibits its degradation and contributes to tauopathy. Neuron. 2010 Sep 23;67(6):953–966.

88. Min S-W, Chen X, Tracy TE, Li Y, Zhou Y, Wang C, et al. Critical role of acetylation in tau-mediated neurodegeneration and cognitive deficits. Nat Med. 2015 Oct;21(10):1154–1162.

89. Hintermayer MA, Volkening K, Moszczynski AJ, Donison N, Strong MJ. Tau protein phosphorylation at Thr175 initiates fibril formation via accessibility of the N-terminal phosphatase-activating domain. J Neurochem. 2020 Nov;155(3):313–326.

90. Hernández F, García-García E, Avila J. Microtubule depolymerization and tau phosphorylation. J Alzheimers Dis. 2013;37(3):507–513.

91. Schwalbe M, Biernat J, Bibow S, Ozenne V, Jensen MR, Kadavath H, et al. Phosphorylation of human Tau protein by microtubule affinity-regulating kinase 2. Biochemistry. 2013 Dec 17;52(50):9068–9079.

92. de Calignon A, Fox LM, Pitstick R, Carlson GA, Bacskai BJ, Spires-Jones TL, et al. Caspase activation precedes and leads to tangles. Nature. 2010 Apr 22;464(7292):1201–1204.

93. Cirulli ET, Lasseigne BN, Petrovski S, Sapp PC, Dion PA, Leblond CS, et al. Exome sequencing in amyotrophic lateral sclerosis identifies risk genes and pathways. Science. 2015 Mar 27;347(6229):1436–1441.

94. Masuda A, Takeda J-I, Ohno K. FUS-mediated regulation of alternative RNA processing in neurons: insights from global transcriptome analysis. Wiley Interdiscip Rev RNA. 2016 May;7(3):330–340.

95. Mackenzie IR, Rademakers R, Neumann M. TDP-43 and FUS in amyotrophic lateral sclerosis and frontotemporal dementia. Lancet Neurol. 2010 Oct 1;9(10):995–1007.

96. Humphrey J, Birsa N, Milioto C, McLaughlin M, Ule AM, Robaldo D, et al. FUS ALS-causative mutations impair FUS autoregulation and splicing factor networks through intron retention. Nucleic Acids Res. 2020 Jul 9;48(12):6889–6905.

97. Wang X, Arai S, Song X, Reichart D, Du K, Pascual G, et al. Induced ncRNAs allosterically modify RNA-binding proteins in cis to inhibit transcription. Nature. 2008 Jul 3;454(7200):126–130.

98. Wang W-Y, Pan L, Su SC, Quinn EJ, Sasaki M, Jimenez JC, et al. Interaction of FUS and HDAC1 regulates DNA damage response and repair in neurons. Nat Neurosci. 2013 Oct;16(10):1383–1391.

99. Arenas A, Chen J, Kuang L, Barnett KR, Kasarskis EJ, Gal J, et al. Lysine acetylation regulates the RNA binding, subcellular localization and inclusion formation of FUS. Hum Mol Genet. 2020 Sep 29;29(16):2684–2697.

100. Vance C, Rogelj B, Hortobágyi T, De Vos KJ, Nishimura AL, Sreedharan J, et al. Mutations in FUS, an RNA processing protein, cause familial amyotrophic lateral sclerosis type 6. Science. 2009 Feb 27;323(5918):1208–1211.

101. Kino Y, Washizu C, Aquilanti E, Okuno M, Kurosawa M, Yamada M, et al. Intracellular localization and splicing regulation of FUS/TLS are variably affected by amyotrophic lateral sclerosis-linked mutations. Nucleic Acids Res. 2011 Apr;39(7):2781–2798.

102. Ishigaki S, Fujioka Y, Okada Y, Riku Y, Udagawa T, Honda D, et al. Altered Tau Isoform Ratio Caused by Loss of FUS and SFPQ Function Leads to FTLD-like Phenotypes. Cell Rep. 2017 Jan 31;18(5):1118–1131.

103. Buratti E. Functional Significance of TDP-43 Mutations in Disease. Adv Genet. 2015 Aug 7;91:1–53.

104. Ayala YM, Zago P, D'Ambrogio A, Xu Y-F, Petrucelli L, Buratti E, et al. Structural determinants of the cellular localization and shuttling of TDP-43. J Cell Sci. 2008 Nov 15;121(Pt 22):3778–3785.

105. Nishimura AL, Zupunski V, Troakes C, Kathe C, Fratta P, Howell M, et al. Nuclear import impairment causes cytoplasmic trans-activation response DNA-binding protein accumulation and is associated with frontotemporal lobar degeneration. Brain. 2010 Jun;133(Pt 6):1763–1771.

106. Pinarbasi ES, Cağatay T, Fung HYJ, Li YC, Chook YM, Thomas PJ. Active nuclear import and passive nuclear export are the primary determinants of TDP-43 localization. Sci Rep. 2018 May 4;8(1):7083.

107. Ederle H, Funk C, Abou-Ajram C, Hutten S, Funk EBE, Kehlenbach RH, et al. Nuclear egress of TDP-43 and FUS occurs independently of Exportin-1/CRM1. Sci Rep. 2018 May 4;8(1):7084.

108. Wang W, Wang L, Lu J, Siedlak SL, Fujioka H, Liang J, et al. The inhibition of TDP-43 mitochondrial localization blocks its neuronal toxicity. Nat Med. 2016 Aug;22(8):869–878.

109. Kuo P-H, Doudeva LG, Wang Y-T, Shen C-KJ, Yuan HS. Structural insights into TDP-43 in nucleic-acid binding and domain interactions. Nucleic Acids Res. 2009 Apr;37(6):1799–1808.

110. Flores BN, Li X, Malik AM, Martinez J, Beg AA, Barmada SJ. An Intramolecular Salt Bridge Linking TDP43 RNA Binding, Protein Stability, and TDP43-Dependent Neurodegeneration. Cell Rep. 2019 Apr 23;27(4):1133–1150.e8.

111. Lukavsky PJ, Daujotyte D, Tollervey JR, Ule J, Stuani C, Buratti E, et al. Molecular basis of UG-rich RNA recognition by the human splicing factor TDP-43. Nat Struct Mol Biol. 2013 Dec;20(12):1443–1449.

112. Mompeán M, Romano V, Pantoja-Uceda D, Stuani C, Baralle FE, Buratti E, et al. The TDP-43 N-terminal domain structure at high resolution. FEBS J. 2016 Apr;283(7):1242–1260.

113. Chang C, Wu T-H, Wu C-Y, Chiang M, Toh EK-W, Hsu Y-C, et al. The N-terminus of TDP-43 promotes its oligomerization and enhances DNA binding affinity. Biochem Biophys Res Commun. 2012 Aug 24;425(2):219–224.

114. Afroz T, Hock E-M, Ernst P, Foglieni C, Jambeau M, Gilhespy LAB, et al. Functional and dynamic polymerization of the ALS-linked protein TDP-43 antagonizes its pathologic aggregation. Nat Commun. 2017 Jun 29;8(1):45.

115. Shiina Y, Arima K, Tabunoki H, Satoh J. TDP-43 dimerizes in human cells in culture. Cell Mol Neurobiol. 2010 May;30(4):641–652.

116. Hornbeck PV, Zhang B, Murray B, Kornhauser JM, Latham V, Skrzypek E. PhosphoSitePlus, 2014: mutations, PTMs and recalibrations. Nucleic Acids Res. 2015 Jan;43(Database issue):D512–20.

117. Wang A, Conicella AE, Schmidt HB, Martin EW, Rhoads SN, Reeb AN, et al. A single N-terminal phosphomimic disrupts TDP-43 polymerization, phase separation, and RNA splicing. EMBO J. 2018 Mar 1;37(5).

118. Cassel JA, Reitz AB. Ubiquilin-2 (UBQLN2) binds with high affinity to the C-terminal region of TDP-43 and modulates TDP-43 levels in H4 cells: characterization of inhibition by nucleic acids and 4-aminoquinolines. Biochim Biophys Acta. 2013 Jun;1834(6):964–971.

119. Majumder P, Chu J-F, Chatterjee B, Swamy KBS, Shen C-KJ. Co-regulation of mRNA translation by TDP-43 and Fragile X Syndrome protein FMRP. Acta Neuropathol. 2016 Aug 12;132(5):721–738.

120. D'Ambrogio A, Buratti E, Stuani C, Guarnaccia C, Romano M, Ayala YM, et al. Functional mapping of the interaction between TDP-43 and hnRNP A2 in vivo. Nucleic Acids Res. 2009 Jul;37(12):4116–4126.

121. Kato M, Han TW, Xie S, Shi K, Du X, Wu LC, et al. Cell-free formation of RNA granules: low complexity sequence domains form dynamic fibers within hydrogels. Cell. 2012 May 11;149(4):753–767.

122. Guenther EL, Cao Q, Trinh H, Lu J, Sawaya MR, Cascio D, et al. Atomic structures of TDP-43 LCD segments and insights into reversible or pathogenic aggregation. Nat Struct Mol Biol. 2018 Jun;25(6):463–471.

123. Casafont I, Bengoechea R, Tapia O, Berciano MT, Lafarga M. TDP-43 localizes in mRNA transcription and processing sites in mammalian neurons. J Struct Biol. 2009 Sep;167(3):235–241.

124. Wang I-F, Reddy NM, Shen C-KJ. Higher order arrangement of the eukaryotic nuclear bodies. Proc Natl Acad Sci USA. 2002 Oct 15;99(21):13583–13588.

125. Kawahara Y, Mieda-Sato A. TDP-43 promotes microRNA biogenesis as a component of the Drosha and Dicer complexes. Proc Natl Acad Sci USA. 2012 Feb 28;109(9):3347–3352.

126. Di Carlo V, Grossi E, Laneve P, Morlando M, Dini Modigliani S, Ballarino M, et al. TDP-43 regulates the microprocessor complex activity during in vitro neuronal differentiation. Mol Neurobiol. 2013 Dec;48(3):952–963.

127. King IN, Yartseva V, Salas D, Kumar A, Heidersbach A, Ando DM, et al. The RNA-binding protein TDP-43 selectively disrupts microRNA-1/206 incorporation into the RNA-induced silencing complex. J Biol Chem. 2014 May 16;289(20):14263–14271.

128. Buratti E, De Conti L, Stuani C, Romano M, Baralle M, Baralle F. Nuclear factor TDP-43 can affect selected microRNA levels. FEBS J. 2010 May;277(10):2268–2281.

129. Hawley ZCE, Campos-Melo D, Strong MJ. Evidence of A Negative Feedback Network Between TDP-43 and miRNAs Dependent on TDP-43 Nuclear Localization. J Mol Biol. 2020 Dec 4;432(24):166695.

130. Matamala JM, Arias-Carrasco R, Sanchez C, Uhrig M, Bargsted L, Matus S, et al. Genome-wide circulating microRNA expression profiling reveals potential biomarkers for amyotrophic lateral sclerosis. Neurobiol Aging. 2018;64:123–138.

131. Campos-Melo D, Droppelmann CA, He Z, Volkening K, Strong MJ. Altered microRNA expression profile in Amyotrophic Lateral Sclerosis: a role in the regulation of NFL mRNA levels. Mol Brain. 2013 May 24;6:26.

132. De Conti L, Akinyi MV, Mendoza-Maldonado R, Romano M, Baralle M, Buratti E. TDP-43 affects splicing profiles and isoform production of genes involved in the apoptotic and mitotic cellular pathways. Nucleic Acids Res. 2015 Oct 15;43(18):8990–9005.

133. Polymenidou M, Lagier-Tourenne C, Hutt KR, Huelga SC, Moran J, Liang TY, et al. Long pre-mRNA depletion and RNA missplicing contribute to neuronal vulnerability from loss of TDP-43. Nat Neurosci. 2011 Apr;14(4):459–468.

134. Ling JP, Pletnikova O, Troncoso JC, Wong PC. TDP-43 repression of nonconserved cryptic exons is compromised in ALS-FTD. Science. 2015 Aug 7;349(6248):650–655.

135. Buratti E, Baralle FE. Characterization and functional implications of the RNA binding properties of nuclear factor TDP-43, a novel splicing regulator of CFTR exon 9. J Biol Chem. 2001 Sep 28;276(39):36337–36343.

136. Mohagheghi F, Prudencio M, Stuani C, Cook C, Jansen-West K, Dickson DW, et al. TDP-43 functions within a network of hnRNP proteins to inhibit the production of a truncated human SORT1 receptor. Hum Mol Genet. 2016 Feb 1;25(3):534–545.

137. Fiesel FC, Weber SS, Supper J, Zell A, Kahle PJ. TDP-43 regulates global translational yield by splicing of exon junction complex component SKAR. Nucleic Acids Res. 2012 Mar;40(6):2668–2682.

138. Mercado PA, Ayala YM, Romano M, Buratti E, Baralle FE. Depletion of TDP 43 overrides the need for exonic and intronic splicing enhancers in the human apoA-II gene. Nucleic Acids Res. 2005 Oct 27;33(18):6000–6010.

139. Bose JK, Wang I-F, Hung L, Tarn W-Y, Shen C-KJ. TDP-43 overexpression enhances exon 7 inclusion during the survival of motor neuron pre-mRNA splicing. J Biol Chem. 2008 Oct 24;283(43):28852–28859.

140. Sephton CF, Cenik C, Kucukural A, Dammer EB, Cenik B, Han Y, et al. Identification of neuronal RNA targets of TDP-43-containing ribonucleoprotein complexes. J Biol Chem. 2011 Jan 14;286(2):1204–1215.

141. Tollervey JR, Curk T, Rogelj B, Briese M, Cereda M, Kayikci M, et al. Characterizing the RNA targets and position-dependent splicing regulation by TDP-43. Nat Neurosci. 2011 Apr;14(4):452–458.

142. Gu J, Wu F, Xu W, Shi J, Hu W, Jin N, et al. TDP-43 suppresses tau expression via promoting its mRNA instability. Nucleic Acids Res. 2017 Jun 2;45(10):6177–6193.

143. Ayala YM, De Conti L, Avendaño-Vázquez SE, Dhir A, Romano M, D'Ambrogio A, et al. TDP-43 regulates its mRNA levels through a negative feedback loop. EMBO J. 2011 Jan 19;30(2):277–288.

144. Igaz LM, Kwong LK, Lee EB, Chen-Plotkin A, Swanson E, Unger T, et al. Dysregulation of the ALS-associated gene TDP-43 leads to neuronal death and degeneration in mice. J Clin Invest. 2011 Feb;121(2):726–738.

145. Strong MJ. The evidence for altered RNA metabolism in amyotrophic lateral sclerosis (ALS). J Neurol Sci. 2010 Jan 15;288(1-2):1–12.

146. Fiesel FC, Voigt A, Weber SS, Van den Haute C, Waldenmaier A, Görner K, et al. Knockdown of transactive response DNA-binding protein (TDP-43) downregulates histone deacetylase 6. EMBO J. 2010 Jan 6;29(1):209–221.

147. Colombrita C, Onesto E, Megiorni F, Pizzuti A, Baralle FE, Buratti E, et al. TDP-43 and FUS RNA-binding proteins bind distinct sets of cytoplasmic messenger RNAs and differently regulate their post-transcriptional fate in motoneuron-like cells. J Biol Chem. 2012 May 4;287(19):15635–15647.

148. Freibaum BD, Chitta RK, High AA, Taylor JP. Global analysis of TDP-43 interacting proteins reveals strong association with RNA splicing and translation machinery. J Proteome Res. 2010 Feb 5;9(2):1104–1120.

149. Alami NH, Smith RB, Carrasco MA, Williams LA, Winborn CS, Han SSW, et al. Axonal transport of TDP-43 mRNA granules is impaired by ALS-causing mutations. Neuron. 2014 Feb 5;81(3):536–543.

150. Gopal PP, Nirschl JJ, Klinman E, Holzbaur ELF. Amyotrophic lateral sclerosis-linked mutations increase the viscosity of liquid-like TDP-43 RNP granules in neurons. Proc Natl Acad Sci USA. 2017 Mar 21;114(12):E2466–E2475.

151. Nagano S, Jinno J, Abdelhamid RF, Jin Y, Shibata M, Watanabe S, et al. TDP-43 transports ribosomal protein mRNA to regulate axonal local translation in neuronal axons. Acta Neuropathol. 2020 Aug 16;140(5):695–713.

152. Vogler TO, Wheeler JR, Nguyen ED, Hughes MP, Britson KA, Lester E, et al. TDP-43 and RNA form amyloid-like myo-granules in regenerating muscle. Nature. 2018 Oct 31;563(7732):508–513.

153. Majumder P, Chen Y-T, Bose JK, Wu C-C, Cheng W-C, Cheng S-J, et al. TDP-43 regulates the mammalian spinogenesis through translational repression of Rac1. Acta Neuropathol. 2012 Aug;124(2):231–245.

154. Hong K, Li Y, Duan W, Guo Y, Jiang H, Li W, et al. Full-length TDP-43 and its C-terminal fragments activate mitophagy in NSC34 cell line. Neurosci Lett. 2012 Nov 21;530(2):144–149.

155. Wang W, Li L, Lin W-L, Dickson DW, Petrucelli L, Zhang T, et al. The ALS disease-associated mutant TDP-43 impairs mitochondrial dynamics and function in motor neurons. Hum Mol Genet. 2013 Dec 1;22(23):4706–4719.

156. Izumikawa K, Nobe Y, Yoshikawa H, Ishikawa H, Miura Y, Nakayama H, et al. TDP-43 stabilises the processing intermediates of mitochondrial transcripts. Sci Rep. 2017 Aug 9;7(1):7709.

157. Salvatori I, Ferri A, Scaricamazza S, Giovannelli I, Serrano A, Rossi S, et al. Differential toxicity of TAR DNA-binding protein 43 isoforms depends on their submitochondrial localization in neuronal cells. J Neurochem. 2018 Aug 1;146(5):585–597.

158. Onesto E, Colombrita C, Gumina V, Borghi MO, Dusi S, Doretti A, et al. Gene-specific mitochondria dysfunctions in human TARDBP and C9ORF72 fibroblasts. Acta Neuropathol Commun. 2016 May 5;4(1):47.

159. Xu Y-F, Gendron TF, Zhang Y-J, Lin W-L, D'Alton S, Sheng H, et al. Wild-type human TDP-43 expression causes TDP-43 phosphorylation, mitochondrial aggregation, motor deficits, and early mortality in transgenic mice. J Neurosci. 2010 Aug 11;30(32):10851–10859.

160. Wang P, Deng J, Dong J, Liu J, Bigio EH, Mesulam M, et al. TDP-43 induces mitochondrial damage and activates the mitochondrial unfolded protein response. PLoS Genet. 2019 May 17;15(5):e1007947.

161. Lu J, Duan W, Guo Y, Jiang H, Li Z, Huang J, et al. Mitochondrial dysfunction in human TDP-43 transfected NSC34 cell lines and the protective effect of dimethoxy curcumin. Brain Res Bull. 2012 Dec 1;89(5-6):185–190.

162. Briese M, Saal-Bauernschubert L, Lüningschrör P, Moradi M, Dombert B, Surrey V, et al. Loss of Tdp-43 disrupts the axonal transcriptome of motoneurons accompanied by impaired axonal translation and mitochondria function. Acta Neuropathol Commun. 2020 Jul 24;8(1):116.

163. Stoica R, De Vos KJ, Paillusson S, Mueller S, Sancho RM, Lau K-F, et al. ER-mitochondria associations are regulated by the VAPB-PTPIP51 interaction and are disrupted by ALS/FTD-associated TDP-43. Nat Commun. 2014 Jun 3;5:3996.

164. Davis SA, Itaman S, Khalid-Janney CM, Sherard JA, Dowell JA, Cairns NJ, et al. TDP-43 interacts with mitochondrial proteins critical for mitophagy and mitochondrial dynamics. Neurosci Lett. 2018 Jun 21;678:8–15.

165. Kawamata H, Peixoto P, Konrad C, Palomo G, Bredvik K, Gerges M, et al. Mutant TDP-43 does not impair mitochondrial bioenergetics in vitro and in vivo. Mol Neurodegener. 2017 May 8;12(1):37.

166. Ou SH, Wu F, Harrich D, García-Martínez LF, Gaynor RB. Cloning and characterization of a novel cellular protein, TDP-43, that binds to human immunodeficiency virus type 1 TAR DNA sequence motifs. J Virol. 1995 Jun;69(6):3584–3596.

167. Abhyankar MM, Urekar C, Reddi PP. A novel CpG-free vertebrate insulator silences the testis-specific SP-10 gene in somatic tissues: role for TDP-43 in insulator function. J Biol Chem. 2007 Dec 14;282(50):36143–36154.

168. ENCODE Project Consortium. An integrated encyclopedia of DNA elements in the human genome. Nature. 2012 Sep 6;489(7414):57–74.

169. Morera AA, Ahmed NS, Schwartz JC. TDP-43 regulates transcription at protein-coding genes and Alu retrotransposons. Biochim Biophys Acta Gene Regul Mech. 2019 Oct 23;1862(10):194434.

170. Kedersha N, Anderson P. Mammalian Stress Granules and Processing Bodies. Translation Initiation: Cell Biology, High-Throughput Methods, and Chemical-Based Approaches. Elsevier; 2007. p. 61–81.

171. Zhang K, Daigle JG, Cunningham KM, Coyne AN, Ruan K, Grima JC, et al. Stress granule assembly disrupts nucleocytoplasmic transport. Cell. 2018 May 3;173(4):958–971.e17.

172. Loganathan S, Lehmkuhl EM, Eck RJ, Zarnescu DC. To Be or Not To Be…Toxic-Is RNA Association With TDP-43 Complexes Deleterious or Protective in Neurodegeneration? Front Mol Biosci. 2019;6:154.

173. Advani VM, Ivanov P. Stress granule subtypes: an emerging link to neurodegeneration. Cell Mol Life Sci. 2020 Dec;77(23):4827–4845.

174. Wheeler JR, Matheny T, Jain S, Abrisch R, Parker R. Distinct stages in stress granule assembly and disassembly. Elife. 2016 Sep 7;5.

175. Aulas A, Stabile S, Vande Velde C. Endogenous TDP-43, but not FUS, contributes to stress granule assembly via G3BP. Mol Neurodegener. 2012 Oct 24;7:54.

176. McDonald KK, Aulas A, Destroismaisons L, Pickles S, Beleac E, Camu W, et al. TAR DNA-binding protein 43 (TDP-43) regulates stress granule dynamics via differential regulation of G3BP and TIA-1. Hum Mol Genet. 2011 Apr 1;20(7):1400–1410.

177. Dewey CM, Cenik B, Sephton CF, Dries DR, Mayer P, Good SK, et al. TDP-43 is directed to stress granules by sorbitol, a novel physiological osmotic and oxidative stressor. Mol Cell Biol. 2011 Mar;31(5):1098–1108.

178. Aulas A, Caron G, Gkogkas CG, Mohamed N-V, Destroismaisons L, Sonenberg N, et al. G3BP1 promotes stress-induced RNA granule interactions to preserve polyadenylated mRNA. J Cell Biol. 2015 Apr 13;209(1):73–84.

179. Colombrita C, Zennaro E, Fallini C, Weber M, Sommacal A, Buratti E, et al. TDP-43 is recruited to stress granules in conditions of oxidative insult. J Neurochem. 2009 Nov;111(4):1051–1061.

180. McGurk L, Gomes E, Guo L, Mojsilovic-Petrovic J, Tran V, Kalb RG, et al. Poly(ADP-Ribose) Prevents Pathological Phase Separation of TDP-43 by Promoting Liquid Demixing and Stress Granule Localization. Mol Cell. 2018 Sep 6;71(5):703–717.e9.

181. Zhang P, Fan B, Yang P, Temirov J, Messing J, Kim HJ, et al. Chronic optogenetic induction of stress granules is cytotoxic and reveals the evolution of ALS-FTD pathology. Elife. 2019 Mar 20;8.

182. Parker SJ, Meyerowitz J, James JL, Liddell JR, Crouch PJ, Kanninen KM, et al. Endogenous TDP-43 localized to stress granules can subsequently form protein aggregates. Neurochem Int. 2012 Mar;60(4):415–424.

183. Winton MJ, Van Deerlin VM, Kwong LK, Yuan W, Wood EM, Yu C-E, et al. A90V TDP-43 variant results in the aberrant localization of TDP-43 in vitro. FEBS Lett. 2008 Jun 25;582(15):2252–2256.

184. Van Deerlin VM, Leverenz JB, Bekris LM, Bird TD, Yuan W, Elman LB, et al. TARDBP mutations in amyotrophic lateral sclerosis with TDP-43 neuropathology: a genetic and histopathological analysis. Lancet Neurol. 2008 May;7(5):409–416.

185. Kim SH, Shi Y, Hanson KA, Williams LM, Sakasai R, Bowler MJ, et al. Potentiation of amyotrophic lateral sclerosis (ALS)-associated TDP-43 aggregation by the proteasome-targeting factor, ubiquilin 1. J Biol Chem. 2009 Mar 20;284(12):8083–8092.

186. Finelli MJ, Liu KX, Wu Y, Oliver PL, Davies KE. Oxr1 improves pathogenic cellular features of ALS-associated FUS and TDP-43 mutations. Hum Mol Genet. 2015 Jun 15;24(12):3529–3544.

187. Chiang C-H, Grauffel C, Wu L-S, Kuo P-H, Doudeva LG, Lim C, et al. Structural analysis of disease-related TDP-43 D169G mutation: linking enhanced stability and caspase cleavage efficiency to protein accumulation. Sci Rep. 2016 Feb 17;6:21581.

188. Nonaka T, Arai T, Buratti E, Baralle FE, Akiyama H, Hasegawa M. Phosphorylated and ubiquitinated TDP-43 pathological inclusions in ALS and FTLD-U are recapitulated in SH-SY5Y cells. FEBS Lett. 2009 Jan 22;583(2):394–400.

189. Watanabe S, Kaneko K, Yamanaka K. Accelerated disease onset with stabilized familial amyotrophic lateral sclerosis (ALS)-linked mutant TDP-43 proteins. J Biol Chem. 2013 Feb 1;288(5):3641–3654.

190. Ling S-C, Albuquerque CP, Han JS, Lagier-Tourenne C, Tokunaga S, Zhou H, et al. ALS-associated mutations in TDP-43 increase its stability and promote TDP-43 complexes with FUS/TLS. Proc Natl Acad Sci USA. 2010 Jul 27;107(30):13318–13323.

191. Ihara R, Matsukawa K, Nagata Y, Kunugi H, Tsuji S, Chihara T, et al. RNA binding mediates neurotoxicity in the transgenic Drosophila model of TDP-43 proteinopathy. Hum Mol Genet. 2013 Nov 15;22(22):4474–4484.

192. Guo W, Chen Y, Zhou X, Kar A, Ray P, Chen X, et al. An ALS-associated mutation affecting TDP-43 enhances protein aggregation, fibril formation and neurotoxicity. Nat Struct Mol Biol. 2011 Jun 12;18(7):822–830.

193. Yamashita T, Hideyama T, Hachiga K, Teramoto S, Takano J, Iwata N, et al. A role for calpain-dependent cleavage of TDP-43 in amyotrophic lateral sclerosis pathology. Nat Commun. 2012;3:1307.

194. Guo Y, Wang Q, Zhang K, An T, Shi P, Li Z, et al. HO-1 induction in motor cortex and intestinal dysfunction in TDP-43 A315T transgenic mice. Brain Res. 2012 Jun 15;1460:88–95.

195. Weerasekera A, Crabbé M, Tomé SO, Gsell W, Sima D, Casteels C, et al. Non-invasive characterization of amyotrophic lateral sclerosis in a hTDP-43A315T mouse model: A PET-MR study. Neuroimage Clin. 2020 Jun 25;27:102327.

196. Johnson BS, Snead D, Lee JJ, McCaffery JM, Shorter J, Gitler AD. TDP-43 is intrinsically aggregation-prone, and amyotrophic lateral sclerosis-linked mutations accelerate aggregation and increase toxicity. J Biol Chem. 2009 Jul 24;284(30):20329–20339.

197. Arnold ES, Ling S-C, Huelga SC, Lagier-Tourenne C, Polymenidou M, Ditsworth D, et al. ALS-linked TDP-43 mutations produce aberrant RNA splicing and adult-onset motor neuron disease without aggregation or loss of nuclear TDP-43. Proc Natl Acad Sci USA. 2013 Feb 19;110(8):E736–45.

198. Chen Q, Zhou J, Huang C, Huang B, Bi F, Zhou H, et al. Temporal Expression of Mutant TDP-43 Correlates with Early Amyotrophic Lateral Sclerosis Phenotype and Motor Weakness. Curr Neurovasc Res. 2018;15(1):3–9.

199. Zhou H, Huang C, Chen H, Wang D, Landel CP, Xia PY, et al. Transgenic rat model of neurodegeneration caused by mutation in the TDP gene. PLoS Genet. 2010 Mar 26;6(3):e1000887.

200. Tong J, Huang C, Bi F, Wu Q, Huang B, Zhou H. XBP1 depletion precedes ubiquitin aggregation and Golgi fragmentation in TDP-43 transgenic rats. J Neurochem. 2012 Nov;123(3):406–416.

201. Tong J, Huang C, Bi F, Wu Q, Huang B, Liu X, et al. Expression of ALS-linked TDP-43 mutant in astrocytes causes non-cell-autonomous motor neuron death in rats. EMBO J. 2013 Jul 3;32(13):1917–1926.

202. Barmada SJ, Skibinski G, Korb E, Rao EJ, Wu JY. Cytoplasmic mislocalization of TDP-43 is toxic to neurons and enhanced by a mutation associated with familial ALS. 2010;30(2).

203. Serio A, Bilican B, Barmada SJ, Ando DM, Zhao C, Siller R, et al. Astrocyte pathology and the absence of non-cell autonomy in an induced pluripotent stem cell model of TDP-43 proteinopathy. Proc Natl Acad Sci USA. 2013 Mar 19;110(12):4697–4702.

204. Araki W, Minegishi S, Motoki K, Kume H, Hohjoh H, Araki YM, et al. Disease-associated mutations of TDP-43 promote turnover of the protein through the proteasomal pathway. Mol Neurobiol. 2014 Dec;50(3):1049–1058.

205. Mutihac R, Alegre-Abarrategui J, Gordon D, Farrimond L, Yamasaki-Mann M, Talbot K, et al. TARDBP pathogenic mutations increase cytoplasmic translocation of TDP-43 and cause reduction of endoplasmic reticulum Ca^{2+} signaling in motor neurons. Neurobiol Dis. 2015 Mar;75:64–77.

206. Orrù S, Coni P, Floris A, Littera R, Carcassi C, Sogos V, et al. Reduced stress granule formation and cell death in fibroblasts with the A382T mutation of TARDBP gene: evidence for loss of TDP-43 nuclear function. Hum Mol Genet. 2016 Oct 15;25(20):4473–4483.

207. Hasegawa M, Hara-Miyauchi C, Ohta H, Sakimura K, Okano H, Okano HJ. Analysis of RNA metabolism in peripheral WBCs of TDP-43 KI mice identifies novel biomarkers of ALS. Neurosci Res. 2016 May;106:12–22.

208. Giannini M, Bayona-Feliu A, Sproviero D, Barroso SI, Cereda C, Aguilera A. TDP-43 mutations link Amyotrophic Lateral Sclerosis with R-loop homeostasis and R loop-mediated DNA damage. PLoS Genet. 2020 Dec 10;16(12):e1009260.

209. Giordana MT, Piccinini M, Grifoni S, De Marco G, Vercellino M, Magistrello M, et al. TDP-43 redistribution is an early event in sporadic amyotrophic lateral sclerosis. Brain Pathol. 2010 Mar;20(2):351–360.

210. Lee EB, Lee VM-Y, Trojanowski JQ. Gains or losses: molecular mechanisms of TDP43-mediated neurodegeneration. Nat Rev Neurosci. 2012 Jan;13(1):38–50.

211. Bigio EH, Wu JY, Deng H-X, Bit-Ivan EN, Mao Q, Ganti R, et al. Inclusions in frontotemporal lobar degeneration with TDP-43 proteinopathy (FTLD-TDP) and amyotrophic lateral sclerosis (ALS), but not FTLD with FUS proteinopathy (FTLD-FUS), have properties of amyloid. Acta Neuropathol. 2013 Mar;125(3):463–465.

212. Robinson JL, Geser F, Stieber A, Umoh M, Kwong LK, Van Deerlin VM, et al. TDP-43 skeins show properties of amyloid in a subset of ALS cases. Acta Neuropathol. 2013 Jan;125(1):121–131.

213. Capitini C, Fani G, Vivoli Vega M, Penco A, Canale C, Cabrita LD, et al. Full-length TDP-43 and its C-terminal domain form filaments in vitro having non-amyloid properties. Amyloid. 2021 Mar;28(1):56–65.

214. Prasad A, Bharathi V, Sivalingam V, Girdhar A, Patel BK. Molecular Mechanisms of TDP-43 Misfolding and Pathology in Amyotrophic Lateral Sclerosis. Front Mol Neurosci. 2019 Feb 14;12:25.

215. Furukawa Y, Kaneko K, Watanabe S, Yamanaka K, Nukina N. A seeding reaction recapitulates intracellular formation of Sarkosyl-insoluble transactivation response element (TAR) DNA-binding protein-43 inclusions. J Biol Chem. 2011 May 27;286(21):18664–18672.

216. Nonaka T, Masuda-Suzukake M, Arai T, Hasegawa Y, Akatsu H, Obi T, et al. Prion-like properties of pathological TDP-43 aggregates from diseased brains. Cell Rep. 2013 Jul 11;4(1):124–134.

217. Feiler MS, Strobel B, Freischmidt A, Helferich AM, Kappel J, Brewer BM, et al. TDP-43 is intercellularly transmitted across axon terminals. J Cell Biol. 2015 Nov 23;211(4):897–911.

218. Shimonaka S, Nonaka T, Suzuki G, Hisanaga S-I, Hasegawa M. Templated Aggregation of TAR DNA-binding Protein of 43 kDa (TDP-43) by Seeding with TDP-43 Peptide Fibrils. J Biol Chem. 2016 Apr 22;291(17):8896–8907.

219. Laferrière F, Maniecka Z, Pérez-Berlanga M, Hruska-Plochan M, Gilhespy L, Hock E-M, et al. TDP-43 extracted from frontotemporal lobar degeneration subject brains displays distinct aggregate assemblies and neurotoxic effects reflecting disease progression rates. Nat Neurosci. 2019 Jan;22(1):65–77.

220. Bose JK, Huang C-C, Shen C-KJ. Regulation of autophagy by neuropathological protein TDP-43. J Biol Chem. 2011 Dec 30;286(52):44441–44448.

221. Xia Q, Wang H, Hao Z, Fu C, Hu Q, Gao F, et al. TDP-43 loss of function increases TFEB activity and blocks autophagosome-lysosome fusion. EMBO J. 2016 Jan 18;35(2):121–142.

222. King A, Maekawa S, Bodi I, Troakes C, Al-Sarraj S. Ubiquitinated, p62 immunopositive cerebellar cortical neuronal inclusions are evident across the spectrum of TDP-43 proteinopathies but are only rarely additionally immunopositive for phosphorylation-dependent TDP-43. Neuropathology. 2011 Jun;31(3):239–249.

223. Barmada SJ, Serio A, Arjun A, Bilican B, Daub A, Ando DM, et al. Autophagy induction enhances TDP43 turnover and survival in neuronal ALS models. Nat Chem Biol. 2014 Aug;10(8):677–685.

224. Huang C, Yan S, Zhang Z. Maintaining the balance of TDP-43, mitochondria, and autophagy: a promising therapeutic strategy for neurodegenerative diseases. Transl Neurodegener. 2020 Oct 30;9(1):40.

225. Buratti E. TDP-43 post-translational modifications in health and disease. Expert Opin Ther Targets. 2018 Mar;22(3):279–293.

226. Neumann M, Kwong LK, Lee EB, Kremmer E, Flatley A, Xu Y, et al. Phosphorylation of S409/410 of TDP-43 is a consistent feature in all sporadic and familial forms of TDP-43 proteinopathies. Acta Neuropathol. 2009 Feb;117(2):137–149.

227. Hasegawa M, Arai T, Nonaka T, Kametani F, Yoshida M, Hashizume Y, et al. Phosphorylated TDP-43 in frontotemporal lobar degeneration and amyotrophic lateral sclerosis. Ann Neurol. 2008 Jul;64(1):60–70.

228. Neumann M, Frick P, Paron F, Kosten J, Buratti E, Mackenzie IR. Antibody against TDP-43 phosphorylated at serine 375 suggests conformational differences of TDP-43 aggregates among FTLD-TDP subtypes. Acta Neuropathol. 2020 Nov;140(5):645–658.

229. Igaz LM, Kwong LK, Chen-Plotkin A, Winton MJ, Unger TL, Xu Y, et al. Expression of TDP-43 C-terminal Fragments in Vitro Recapitulates Pathological Features of TDP-43 Proteinopathies. J Biol Chem. 2009 Mar 27;284(13):8516–8524.

230. Zhang Y-J, Gendron TF, Xu Y-F, Ko L-W, Yen S-H, Petrucelli L. Phosphorylation regulates proteasomal-mediated degradation and solubility of TAR DNA binding protein-43 C-terminal fragments. Mol Neurodegener. 2010 Aug 30;5:33.

231. Yamashita T, Teramoto S, Kwak S. Phosphorylated TDP-43 becomes resistant to cleavage by calpain: A regulatory role for phosphorylation in TDP-43 pathology of ALS/FTLD. Neurosci Res. 2016 Jun;107:63–69.

232. Schludi MH, Becker L, Garrett L, Gendron TF, Zhou Q, Schreiber F, et al. Spinal poly-GA inclusions in a C9orf72 mouse model trigger motor deficits and inflammation without neuron loss. Acta Neuropathol. 2017 Aug;134(2):241–254.

233. Sreedharan J, Neukomm LJ, Brown RH, Freeman MR. Age-Dependent TDP-43-Mediated Motor Neuron Degeneration Requires GSK3, hat-trick, and xmas-2. Curr Biol. 2015 Aug 17;25(16):2130–2136.

234. Kametani F, Nonaka T, Suzuki T, Arai T, Dohmae N, Akiyama H, et al. Identification of casein kinase-1 phosphorylation sites on TDP-43. Biochem Biophys Res Commun. 2009 May 1;382(2):405–409.

235. Carlomagno Y, Zhang Y, Davis M, Lin W-L, Cook C, Dunmore J, et al. Casein kinase II induced polymerization of soluble TDP-43 into filaments is inhibited by heat shock proteins. PLoS One. 2014 Mar 4;9(3):e90452.

236. Liachko NF, McMillan PJ, Strovas TJ, Loomis E, Greenup L, Murrell JR, et al. The tau tubulin kinases TTBK1/2 promote accumulation of pathological TDP-43. PLoS Genet. 2014 Dec 4;10(12):e1004803.

237. Meyerowitz J, Parker SJ, Vella LJ, Ng DC, Price KA, Liddell JR, et al. C-Jun N-terminal kinase controls TDP-43 accumulation in stress granules induced by oxidative stress. Mol Neurodegener. 2011 Aug 8;6:57.

238. Liachko NF, Saxton AD, McMillan PJ, Strovas TJ, Currey HN, Taylor LM, et al. The phosphatase calcineurin regulates pathological TDP-43 phosphorylation. Acta Neuropathol. 2016 Oct;132(4):545–561.

239. Hans F, Eckert M, von Zweydorf F, Gloeckner CJ, Kahle PJ. Identification and characterization of ubiquitinylation sites in TAR DNA-binding protein of 43 kDa (TDP-43). J Biol Chem. 2018 Oct 12;293(41):16083–16099.

240. Kametani F, Obi T, Shishido T, Akatsu H, Murayama S, Saito Y, et al. Mass spectrometric analysis of accumulated TDP-43 in amyotrophic lateral sclerosis brains. Sci Rep. 2016 Mar 16;6:23281.

241. Kim W, Bennett EJ, Huttlin EL, Guo A, Li J, Possemato A, et al. Systematic and quantitative assessment of the ubiquitin-modified proteome. Mol Cell. 2011 Oct 21;44(2):325–340.

242. Dammer EB, Fallini C, Gozal YM, Duong DM, Rossoll W, Xu P, et al. Coaggregation of RNA-binding proteins in a model of TDP-43 proteinopathy with selective RGG motif methylation and a role for RRM1 ubiquitination. PLoS One. 2012 Jun 21;7(6):e38658.

243. Scotter EL, Vance C, Nishimura AL, Lee Y-B, Chen H-J, Urwin H, et al. Differential roles of the ubiquitin proteasome system and autophagy in the clearance of soluble and aggregated TDP-43 species. J Cell Sci. 2014 Mar 15;127(Pt 6):1263–1278.

244. Hans F, Fiesel FC, Strong JC, Jäckel S, Rasse TM, Geisler S, et al. UBE2E ubiquitin-conjugating enzymes and ubiquitin isopeptidase Y regulate TDP-43 protein ubiquitination. J Biol Chem. 2014 Jul 4;289(27):19164–19179.

245. Hebron ML, Lonskaya I, Sharpe K, Weerasinghe PPK, Algarzae NK, Shekoyan AR, et al. Parkin ubiquitinates Tar-DNA binding protein-43 (TDP-43) and promotes its cytosolic accumulation via interaction with histone deacetylase 6 (HDAC6). J Biol Chem. 2013 Feb 8;288(6):4103–4115.

246. Voigt A, Herholz D, Fiesel FC, Kaur K, Müller D, Karsten P, et al. TDP-43-mediated neuron loss in vivo requires RNA-binding activity. PLoS One. 2010 Aug 18;5(8):e12247.

247. Prasad A, Sivalingam V, Bharathi V, Girdhar A, Patel BK. The amyloidogenicity of a C-terminal region of TDP-43 implicated in Amyotrophic Lateral Sclerosis can be affected by anions, acetylation and homodimerization. Biochimie. 2018 Jul;150:76–87.

248. Simpson CL, Lemmens R, Miskiewicz K, Broom WJ, Hansen VK, van Vught PWJ, et al. Variants of the elongator protein 3 (ELP3) gene are associated with motor neuron degeneration. Hum Mol Genet. 2009 Feb 1;18(3):472–481.

249. Cohen TJ, Hwang AW, Restrepo CR, Yuan C-X, Trojanowski JQ, Lee VMY. An acetylation switch controls TDP-43 function and aggregation propensity. Nat Commun. 2015 Jan 5;6:5845.

250. Bhardwaj A, Myers MP, Buratti E, Baralle FE. Characterizing TDP-43 interaction with its RNA targets. Nucleic Acids Res. 2013 May;41(9):5062–5074.

251. Yu H, Lu S, Gasior K, Singh D, Vazquez-Sanchez S, Tapia O, et al. HSP70 chaperones RNA-free TDP-43 into anisotropic intranuclear liquid spherical shells. Science. 2021 Feb 5;371(6529).

252. Sanna S, Esposito S, Masala A, Sini P, Nieddu G, Galioto M, et al. HDAC1 inhibition ameliorates TDP-43-induced cell death in vitro and in vivo. Cell Death Dis. 2020 May 14;11(5):369.

253. Wang P, Wander CM, Yuan C-X, Bereman MS, Cohen TJ. Acetylation-induced TDP-43 pathology is suppressed by an HSF1-dependent chaperone program. Nat Commun. 2017 Jul 19;8(1):82.

254. Cohen TJ, Hwang AW, Unger T, Trojanowski JQ, Lee VMY. Redox signalling directly regulates TDP-43 via cysteine oxidation and disulphide cross-linking. EMBO J. 2012 Mar 7;31(5):1241–1252.

255. Pedersen WA, Fu W, Keller JN, Markesbery WR, Appel S, Smith RG, et al. Protein modification by the lipid peroxidation product 4-hydroxynonenal in the spinal cords of amyotrophic lateral sclerosis patients. Ann Neurol. 1998 Nov;44(5):819–824.

256. Kabuta C, Kono K, Wada K, Kabuta T. 4-Hydroxynonenal induces persistent insolubilization of TDP-43 and alters its intracellular localization. Biochem Biophys Res Commun. 2015 Jul 24;463(1-2):82–87.

257. Bargsted L, Medinas DB, Martínez Traub F, Rozas P, Muñoz N, Nassif M, et al. Disulfide cross-linked multimers of TDP-43 and spinal motoneuron loss in a TDP-43A315T ALS/FTD mouse model. Sci Rep. 2017 Oct 27;7(1):14266.

258. Goh CW, Lee IC, Sundaram JR, George SE, Yusoff P, Brush MH, et al. Chronic oxidative stress promotes GADD34-mediated phosphorylation of the TAR DNA-binding protein TDP-43, a modification linked to neurodegeneration. J Biol Chem. 2018 Jan 5;293(1):163–176.

259. Seyfried NT, Gozal YM, Dammer EB, Xia Q, Duong DM, Cheng D, et al. Multiplex SILAC analysis of a cellular TDP-43 proteinopathy model reveals protein inclusions associated with SUMOylation and diverse polyubiquitin chains. Mol Cell Proteomics. 2010 Apr;9(4):705–718.

260. Maurel C, Chami AA, Thépault R-A, Marouillat S, Blasco H, Corcia P, et al. A role for SUMOylation in the Formation and Cellular Localization of TDP-43 Aggregates in Amyotrophic Lateral Sclerosis. Mol Neurobiol. 2020 Mar;57(3):1361–1373.

261. Duan Y, Du A, Gu J, Duan G, Wang C, Gui X, et al. PARylation regulates stress granule dynamics, phase separation, and neurotoxicity of disease-related RNA-binding proteins. Cell Res. 2019 Feb 6;29(3):233–247.

262. McGurk L, Mojsilovic-Petrovic J, Van Deerlin VM, Shorter J, Kalb RG, Lee VM, et al. Nuclear poly(ADP-ribose) activity is a therapeutic target in amyotrophic lateral sclerosis. Acta Neuropathol Commun. 2018 Aug 29;6(1):84.

263. Igaz LM, Kwong LK, Xu Y, Truax AC, Uryu K, Neumann M, et al. Enrichment of C-terminal fragments in TAR DNA-binding protein-43 cytoplasmic inclusions in brain but not in spinal cord of frontotemporal lobar degeneration and amyotrophic lateral sclerosis. Am J Pathol. 2008 Jul;173(1):182–194.

264. D'Alton S, Altshuler M, Lewis J. Studies of alternative isoforms provide insight into TDP-43 autoregulation and pathogenesis. RNA. 2015 Aug;21(8):1419–1432.

265. Xiao S, Sanelli T, Chiang H, Sun Y, Chakrabartty A, Keith J, et al. Low molecular weight species of TDP-43 generated by abnormal splicing form inclusions in amyotrophic lateral sclerosis and result in motor neuron death. Acta Neuropathol. 2015 Jul;130(1):49–61.

266. Nishimoto Y, Ito D, Yagi T, Nihei Y, Tsunoda Y, Suzuki N. Characterization of alternative isoforms and inclusion body of the TAR DNA-binding protein-43. J Biol Chem. 2010 Jan 1;285(1):608–619.

267. Dormann D, Capell A, Carlson AM, Shankaran SS, Rodde R, Neumann M, et al. Proteolytic processing of TAR DNA binding protein-43 by caspases produces C-terminal fragments with disease defining properties independent of progranulin. J Neurochem. 2009 Aug;110(3):1082–1094.

268. Wobst HJ, Delsing L, Brandon NJ, Moss SJ. Truncation of the TAR DNA-binding protein 43 is not a prerequisite for cytoplasmic relocalization, and is suppressed by caspase inhibition and by introduction of the A90V sequence variant. PLoS One. 2017 May 16;12(5):e0177181.

269. Kitamura A, Nakayama Y, Shibasaki A, Taki A, Yuno S, Takeda K, et al. Interaction of RNA with a C-terminal fragment of the amyotrophic lateral sclerosis-associated TDP43 reduces cytotoxicity. Sci Rep. 2016 Jan 13;6:19230.

270. Li Q, Yokoshi M, Okada H, Kawahara Y. The cleavage pattern of TDP-43 determines its rate of clearance and cytotoxicity. Nat Commun. 2015 Jan 29;6:6183.

271. Herskowitz JH, Gozal YM, Duong DM, Dammer EB, Gearing M, Ye K, et al. Asparaginyl endopeptidase cleaves TDP-43 in brain. Proteomics. 2012 Aug;12(15-16):2455–2463.

272. Lee Y-B, Baskaran P, Gomez-Deza J, Chen H-J, Nishimura AL, Smith BN, et al. C9orf72 poly GA RAN-translated protein plays a key role in amyotrophic lateral sclerosis via aggregation and toxicity. Hum Mol Genet. 2017 Dec 15;26(24):4765–4777.

273. Pesiridis GS, Tripathy K, Tanik S, Trojanowski JQ, Lee VM-Y. A “two-hit” hypothesis for inclusion formation by carboxyl-terminal fragments of TDP-43 protein linked to RNA depletion and impaired microtubule-dependent transport. J Biol Chem. 2011 May 27;286(21):18845–18855.

274. Dayton RD, Gitcho MA, Orchard EA, Wilson JD, Wang DB, Cain CD, et al. Selective Forelimb Impairment in Rats Expressing a Pathological TDP-43 25 kDa C-terminal Fragment to Mimic Amyotrophic Lateral Sclerosis. Mol Ther. 2013 May 21;

275. Caccamo A, Majumder S, Oddo S. Cognitive decline typical of frontotemporal lobar degeneration in transgenic mice expressing the 25-kDa C-terminal fragment of TDP-43. Am J Pathol. 2012 Jan;180(1):293–302.

276. Liu G, Coyne AN, Pei F, Vaughan S, Chaung M, Zarnescu DC, et al. Endocytosis regulates TDP-43 toxicity and turnover. Nat Commun. 2017 Dec 12;8(1):2092.

277. Schwenk BM, Hartmann H, Serdaroglu A, Schludi MH, Hornburg D, Meissner F, et al. TDP-43 loss of function inhibits endosomal trafficking and alters trophic signaling in neurons. EMBO J. 2016 Nov 2;35(21):2350–2370.

278. Mitra J, Hegde PM, Hegde ML. Loss of endosomal recycling factor RAB11 coupled with complex regulation of MAPK/ERK/AKT signaling in postmortem spinal cord specimens of sporadic amyotrophic lateral sclerosis patients. Mol Brain. 2019 Jun 13;12(1):55.

279. Altanbyek V, Cha S-J, Kang G-U, Im DS, Lee S, Kim H-J, et al. Imbalance of mitochondrial dynamics in Drosophila models of amyotrophic lateral sclerosis. Biochem Biophys Res Commun. 2016 Dec 9;481(3-4):259–264.

280. Mori F, Tanji K, Zhang H-X, Nishihira Y, Tan C-F, Takahashi H, et al. Maturation process of TDP-43-positive neuronal cytoplasmic inclusions in amyotrophic lateral sclerosis with and without dementia. Acta Neuropathol. 2008 Aug;116(2):193–203.

281. Veyrat-Durebex C, Corcia P, Mucha A, Benzimra S, Mallet C, Gendrot C, et al. Iron metabolism disturbance in a French cohort of ALS patients. Biomed Res Int. 2014 Jul 2;2014:485723.

282. Dang TNT, Lim NKH, Grubman A, Li Q-X, Volitakis I, White AR, et al. Increased metal content in the TDP-43(A315T) transgenic mouse model of frontotemporal lobar degeneration and amyotrophic lateral sclerosis. Front Aging Neurosci. 2014 Feb 11;6:15.

283. Caragounis A, Price KA, Soon CPW, Filiz G, Masters CL, Li Q-X, et al. Zinc induces depletion and aggregation of endogenous TDP-43. Free Radic Biol Med. 2010 May 1;48(9):1152–1161.

284. Montgomery TSH. Comparative cytological studies, with especial regard to the morphology of the nucleolus. J Morphol. 1898 Nov;15(2):265–582.

285. Banani SF, Lee HO, Hyman AA, Rosen MK. Biomolecular condensates: organizers of cellular biochemistry. Nat Rev Mol Cell Biol. 2017 May;18(5):285–298.

286. McSwiggen DT, Mir M, Darzacq X, Tjian R. Evaluating phase separation in live cells: diagnosis, caveats, and functional consequences. Genes Dev. 2019 Dec 1;33(23-24):1619–1634.

287. Decker CJ, Parker R. P-bodies and stress granules: possible roles in the control of translation and mRNA degradation. Cold Spring Harb Perspect Biol. 2012 Sep 1;4(9):a012286.

288. Mao YS, Zhang B, Spector DL. Biogenesis and function of nuclear bodies. Trends Genet. 2011 Aug;27(8):295–306.

289. Mir M, Bickmore W, Furlong EEM, Narlikar G. Chromatin topology, condensates and gene regulation: shifting paradigms or just a phase? Development. 2019 Sep 25;146(19).

290. Weber SC, Brangwynne CP. Inverse size scaling of the nucleolus by a concentration-dependent phase transition. Curr Biol. 2015 Mar 2;25(5):641–646.

291. Brangwynne CP, Mitchison TJ, Hyman AA. Active liquid-like behavior of nucleoli determines their size and shape in Xenopus laevis oocytes. Proc Natl Acad Sci USA. 2011 Mar 15;108(11):4334–4339.

292. Alberti S, Dormann D. Liquid-Liquid Phase Separation in Disease. Annu Rev Genet. 2019 Dec 3;53:171–194.

293. Aguzzi A, Altmeyer M. Phase separation: linking cellular compartmentalization to disease. Trends Cell Biol. 2016 Jul;26(7):547–558.

294. Zbinden A, Pérez-Berlanga M, De Rossi P, Polymenidou M. Phase separation and neurodegenerative diseases: A disturbance in the force. Dev Cell. 2020 Oct 12;55(1):45–68.

295. Dundr M, Hebert MD, Karpova TS, Stanek D, Xu H, Shpargel KB, et al. In vivo kinetics of Cajal body components. J Cell Biol. 2004 Mar 15;164(6):831–842.

296. Phair RD, Misteli T. High mobility of proteins in the mammalian cell nucleus. Nature. 2000 Apr 6;404(6778):604–609.

297. Taylor NO, Wei M-T, Stone HA, Brangwynne CP. Quantifying Dynamics in Phase-Separated Condensates Using Fluorescence Recovery after Photobleaching. Biophys J. 2019 Oct 1;117(7):1285–1300.

298. Platani M, Goldberg I, Swedlow JR, Lamond AI. In vivo analysis of Cajal body movement, separation, and joining in live human cells. J Cell Biol. 2000 Dec 25;151(7):1561–1574.

299. Nott TJ, Petsalaki E, Farber P, Jervis D, Fussner E, Plochowietz A, et al. Phase transition of a disordered nuage protein generates environmentally responsive membraneless organelles. Mol Cell. 2015 Mar 5;57(5):936–947.

300. Li P, Banjade S, Cheng H-C, Kim S, Chen B, Guo L, et al. Phase transitions in the assembly of multivalent signalling proteins. Nature. 2012 Mar 7;483(7389):336–340.

301. Flory PJ. Principles of polymer chemistry. books.google.com; 1953.

302. Banjade S, Rosen MK. Phase transitions of multivalent proteins can promote clustering of membrane receptors. Elife. 2014 Oct 16;3.

303. Molliex A, Temirov J, Lee J, Coughlin M, Kanagaraj AP, Kim HJ, et al. Phase separation by low complexity domains promotes stress granule assembly and drives pathological fibrillization. Cell. 2015 Sep 24;163(1):123–133.

304. Burke KA, Janke AM, Rhine CL, Fawzi NL. Residue-by-Residue View of In Vitro FUS Granules that Bind the C-Terminal Domain of RNA Polymerase II. Mol Cell. 2015 Oct 15;60(2):231–241.

305. Jiang H, Wang S, Huang Y, He X, Cui H, Zhu X, et al. Phase transition of spindle-associated protein regulate spindle apparatus assembly. Cell. 2015 Sep 24;163(1):108–122.

306. Crick SL, Jayaraman M, Frieden C, Wetzel R, Pappu RV. Fluorescence correlation spectroscopy shows that monomeric polyglutamine molecules form collapsed structures in aqueous solutions. Proc Natl Acad Sci USA. 2006 Nov 7;103(45):16764–16769.

307. Crick SL, Ruff KM, Garai K, Frieden C, Pappu RV. Unmasking the roles of N- and C-terminal flanking sequences from exon 1 of huntingtin as modulators of polyglutamine aggregation. Proc Natl Acad Sci USA. 2013 Dec 10;110(50):20075–20080.

308. Kwon I, Kato M, Xiang S, Wu L, Theodoropoulos P, Mirzaei H, et al. Phosphorylation-regulated binding of RNA polymerase II to fibrous polymers of low-complexity domains. Cell. 2013 Nov 21;155(5):1049–1060.

309. Berry J, Weber SC, Vaidya N, Haataja M, Brangwynne CP. RNA transcription modulates phase transition-driven nuclear body assembly. Proc Natl Acad Sci USA. 2015 Sep 22;112(38):E5237–45.

310. Lin Y, Protter DSW, Rosen MK, Parker R. Formation and Maturation of Phase-Separated Liquid Droplets by RNA-Binding Proteins. Mol Cell. 2015 Oct 15;60(2):208–219.

311. Han TW, Kato M, Xie S, Wu LC, Mirzaei H, Pei J, et al. Cell-free formation of RNA granules: bound RNAs identify features and components of cellular assemblies. Cell. 2012 May 11;149(4):768–779.

312. Kirino Y, Vourekas A, Kim N, de Lima Alves F, Rappsilber J, Klein PS, et al. Arginine methylation of vasa protein is conserved across phyla. J Biol Chem. 2010 Mar 12;285(11):8148–8154.

313. Dellaire G, Ching RW, Dehghani H, Ren Y, Bazett-Jones DP. The number of PML nuclear bodies increases in early S phase by a fission mechanism. J Cell Sci. 2006 Mar 15;119(Pt 6):1026–1033.

314. Banani SF, Rice AM, Peeples WB, Lin Y, Jain S, Parker R, et al. Compositional Control of Phase-Separated Cellular Bodies. Cell. 2016 Jul 28;166(3):651–663.

315. Martin EW, Holehouse AS, Peran I, Farag M, Incicco JJ, Bremer A, et al. Valence and patterning of aromatic residues determine the phase behavior of prion-like domains. Science. 2020 Feb 7;367(6478):694–699.

316. Feric M, Vaidya N, Harmon TS, Mitrea DM, Zhu L, Richardson TM, et al. Coexisting liquid phases underlie nucleolar subcompartments. Cell. 2016 Jun 16;165(7):1686–1697.

317. Boke E, Ruer M, Wühr M, Coughlin M, Lemaitre R, Gygi SP, et al. Amyloid-like Self-Assembly of a Cellular Compartment. Cell. 2016 Jul 28;166(3):637–650.

318. Fändrich M, Fletcher MA, Dobson CM. Amyloid fibrils from muscle myoglobin. Nature. 2001 Mar 8;410(6825):165–166.

319. Xiang S, Kato M, Wu LC, Lin Y, Ding M, Zhang Y, et al. The LC Domain of hnRNPA2 Adopts Similar Conformations in Hydrogel Polymers, Liquid-like Droplets, and Nuclei. Cell. 2015 Nov 5;163(4):829–839.

320. Halfmann R. A glass menagerie of low complexity sequences. Curr Opin Struct Biol. 2016 Jun;38:18–25.

321. Khan T, Kandola TS, Wu J, Venkatesan S, Ketter E, Lange JJ, et al. Quantifying nucleation in vivo reveals the physical basis of prion-like phase behavior. Mol Cell. 2018 Jul 5;71(1):155–168.e7.

322. Kroschwald S, Maharana S, Mateju D, Malinovska L, Nüske E, Poser I, et al. Promiscuous interactions and protein disaggregases determine the material state of stress-inducible RNP granules. Elife. 2015 Aug 4;4:e06807.

323. Hondele M, Sachdev R, Heinrich S, Wang J, Vallotton P, Fontoura BMA, et al. DEAD-box ATPases are global regulators of phase-separated organelles. Nature. 2019 Sep;573(7772):144–148.

324. Feric M, Brangwynne CP. A nuclear F-actin scaffold stabilizes ribonucleoprotein droplets against gravity in large cells. Nat Cell Biol. 2013 Oct;15(10):1253–1259.

325. Kaizuka Y, Douglass AD, Varma R, Dustin ML, Vale RD. Mechanisms for segregating T cell receptor and adhesion molecules during immunological synapse formation in Jurkat T cells. Proc Natl Acad Sci USA. 2007 Dec 18;104(51):20296–20301.

326. Tatomer DC, Terzo E, Curry KP, Salzler H, Sabath I, Zapotoczny G, et al. Concentrating pre-mRNA processing factors in the histone locus body facilitates efficient histone mRNA biogenesis. J Cell Biol. 2016 Jun 6;213(5):557–570.

327. Kuznetsova IM, Zaslavsky BY, Breydo L, Turoverov KK, Uversky VN. Beyond the excluded volume effects: mechanistic complexity of the crowded milieu. Molecules. 2015 Jan 14;20(1):1377–1409.

328. Good MC, Zalatan JG, Lim WA. Scaffold proteins: hubs for controlling the flow of cellular information. Science. 2011 May 6;332(6030):680–686.

329. Franzmann TM, Alberti S. Protein phase separation as a stress survival strategy. Cold Spring Harb Perspect Biol. 2019 Jun 3;11(6).

330. Rabouille C, Alberti S. Cell adaptation upon stress: the emerging role of membrane-less compartments. Curr Opin Cell Biol. 2017 Aug;47:34–42.

331. Patel A, Lee HO, Jawerth L, Maharana S, Jahnel M, Hein MY, et al. A Liquid-to-Solid Phase Transition of the ALS Protein FUS Accelerated by Disease Mutation. Cell. 2015 Aug 27;162(5):1066–1077.

332. Murakami T, Qamar S, Lin JQ, Schierle GSK, Rees E, Miyashita A, et al. ALS/FTD Mutation-Induced Phase Transition of FUS Liquid Droplets and Reversible Hydrogels into Irreversible Hydrogels Impairs RNP Granule Function. Neuron. 2015 Nov 18;88(4):678–690.

333. Hofweber M, Dormann D. Friend or foe-Post-translational modifications as regulators of phase separation and RNP granule dynamics. J Biol Chem. 2019 May 3;294(18):7137–7150.

334. Suárez-Calvet M, Neumann M, Arzberger T, Abou-Ajram C, Funk E, Hartmann H, et al. Monomethylated and unmethylated FUS exhibit increased binding to Transportin and distinguish FTLD-FUS from ALS-FUS. Acta Neuropathol. 2016 Apr;131(4):587–604.

335. Qamar S, Wang G, Randle SJ, Ruggeri FS, Varela JA, Lin JQ, et al. FUS Phase Separation Is Modulated by a Molecular Chaperone and Methylation of Arginine Cation-π Interactions. Cell. 2018 Apr 19;173(3):720–734.e15.

336. Babinchak WM, Haider R, Dumm BK, Sarkar P, Surewicz K, Choi J-K, et al. The role of liquid-liquid phase separation in aggregation of the TDP-43 low-complexity domain. J Biol Chem. 2019 Apr 19;294(16):6306–6317.

337. Conicella AE, Dignon GL, Zerze GH, Schmidt HB, D'Ordine AM, Kim YC, et al. TDP-43 α-helical structure tunes liquid-liquid phase separation and function. Proc Natl Acad Sci USA. 2020 Mar 17;117(11):5883–5894.

338. Murthy AC, Dignon GL, Kan Y, Zerze GH, Parekh SH, Mittal J, et al. Molecular interactions underlying liquid-liquid phase separation of the FUS low-complexity domain. Nat Struct Mol Biol. 2019 Jul 1;26(7):637–648.

339. Wegmann S, Eftekharzadeh B, Tepper K, Zoltowska KM, Bennett RE, Dujardin S, et al. Tau protein liquid-liquid phase separation can initiate tau aggregation. EMBO J. 2018 Apr 3;37(7).

340. Ambadipudi S, Biernat J, Riedel D, Mandelkow E, Zweckstetter M. Liquid-liquid phase separation of the microtubule-binding repeats of the Alzheimer-related protein Tau. Nat Commun. 2017 Aug 17;8(1):275.

341. Ray S, Singh N, Kumar R, Patel K, Pandey S, Datta D, et al. α-Synuclein aggregation nucleates through liquid-liquid phase separation. Nat Chem. 2020 Aug;12(8):705–716.

342. Jain A, Vale RD. RNA phase transitions in repeat expansion disorders. Nature. 2017 Jun 8;546(7657):243–247.

343. Zu T, Pattamatta A, Ranum LPW. Repeat-Associated Non-ATG Translation in Neurological Diseases. Cold Spring Harb Perspect Biol. 2018 Dec 3;10(12).

344. Narita T, Weinert BT, Choudhary C. Functions and mechanisms of non-histone protein acetylation. Nat Rev Mol Cell Biol. 2019;20(3):156–174.

345. Allfrey VG, Faulkner R, Mirsky AE. Acetylation and methylation of histones and their possible role in the regulation of RNA synthesis. Proc Natl Acad Sci USA. 1964 May;51:786–794.

346. Choudhary C, Kumar C, Gnad F, Nielsen ML, Rehman M, Walther TC, et al. Lysine acetylation targets protein complexes and co-regulates major cellular functions. Science. 2009 Aug 14;325(5942):834–840.

347. Weinert BT, Narita T, Satpathy S, Srinivasan B, Hansen BK, Schölz C, et al. Time-Resolved Analysis Reveals Rapid Dynamics and Broad Scope of the CBP/p300 Acetylome. Cell. 2018 Jun 28;174(1):231–244.e12.

348. Zhao S, Xu W, Jiang W, Yu W, Lin Y, Zhang T, et al. Regulation of cellular metabolism by protein lysine acetylation. Science. 2010 Feb 19;327(5968):1000–1004.

349. Lundby A, Lage K, Weinert BT, Bekker-Jensen DB, Secher A, Skovgaard T, et al. Proteomic analysis of lysine acetylation sites in rat tissues reveals organ specificity and subcellular patterns. Cell Rep. 2012 Aug 30;2(2):419–431.

350. Sivanand S, Viney I, Wellen KE. Spatiotemporal Control of Acetyl-CoA Metabolism in Chromatin Regulation. Trends Biochem Sci. 2018 Jan;43(1):61–74.

351. Paik WK, Pearson D, Lee HW, Kim S. Nonenzymatic acetylation of histones with acetyl-CoA. Biochim Biophys Acta. 1970 Aug 8;213(2):513–522.

352. Weinert BT, Iesmantavicius V, Moustafa T, Schölz C, Wagner SA, Magnes C, et al. Acetylation dynamics and stoichiometry in Saccharomyces cerevisiae. Mol Syst Biol. 2014 Jan 30;10:716.

353. Wagner GR, Hirschey MD. Nonenzymatic protein acylation as a carbon stress regulated by sirtuin deacylases. Mol Cell. 2014 Apr 10;54(1):5–16.

354. Baeza J, Smallegan MJ, Denu JM. Site-specific reactivity of nonenzymatic lysine acetylation. ACS Chem Biol. 2015 Jan 16;10(1):122–128.

355. Newman JC, He W, Verdin E. Mitochondrial protein acylation and intermediary metabolism: regulation by sirtuins and implications for metabolic disease. J Biol Chem. 2012 Dec 14;287(51):42436–42443.

356. Weinert BT, Moustafa T, Iesmantavicius V, Zechner R, Choudhary C. Analysis of acetylation stoichiometry suggests that SIRT3 repairs nonenzymatic acetylation lesions. EMBO J. 2015 Nov 3;34(21):2620–2632.

357. Drazic A, Myklebust LM, Ree R, Arnesen T. The world of protein acetylation. Biochim Biophys Acta. 2016 Oct;1864(10):1372–1401.

358. Shahbazian MD, Grunstein M. Functions of site-specific histone acetylation and deacetylation. Annu Rev Biochem. 2007;76:75–100.

359. Berndsen CE, Denu JM. Catalysis and substrate selection by histone/protein lysine acetyltransferases. Curr Opin Struct Biol. 2008 Dec;18(6):682–689.

360. Jin Q, Yu L-R, Wang L, Zhang Z, Kasper LH, Lee J-E, et al. Distinct roles of GCN5/PCAF-mediated H3K9ac and CBP/p300-mediated H3K18/27ac in nuclear receptor transactivation. EMBO J. 2011 Jan 19;30(2):249–262.

361. Filippakopoulos P, Picaud S, Mangos M, Keates T, Lambert J-P, Barsyte-Lovejoy D, et al. Histone recognition and large-scale structural analysis of the human bromodomain family. Cell. 2012 Mar 30;149(1):214–231.

362. Fujisawa T, Filippakopoulos P. Functions of bromodomain-containing proteins and their roles in homeostasis and cancer. Nat Rev Mol Cell Biol. 2017 Apr;18(4):246–262.

363. Tessarz P, Kouzarides T. Histone core modifications regulating nucleosome structure and dynamics. Nat Rev Mol Cell Biol. 2014 Nov;15(11):703–708.

364. Westerheide SD, Anckar J, Stevens SM, Sistonen L, Morimoto RI. Stress-inducible regulation of heat shock factor 1 by the deacetylase SIRT1. Science. 2009 Feb 20;323(5917):1063–1066.

365. Reed SM, Quelle DE. p53 acetylation: regulation and consequences. Cancers (Basel). 2014 Dec 23;7(1):30–69.

366. Sun Y, Jiang X, Chen S, Fernandes N, Price BD. A role for the Tip60 histone acetyltransferase in the acetylation and activation of ATM. Proc Natl Acad Sci USA. 2005 Sep 13;102(37):13182–13187.

367. Yamamori T, DeRicco J, Naqvi A, Hoffman TA, Mattagajasingh I, Kasuno K, et al. SIRT1 deacetylates APE1 and regulates cellular base excision repair. Nucleic Acids Res. 2010 Jan;38(3):832–845.

368. Akella JS, Wloga D, Kim J, Starostina NG, Lyons-Abbott S, Morrissette NS, et al. MEC-17 is an alpha-tubulin acetyltransferase. Nature. 2010 Sep 9;467(7312):218–222.

369. Hubbert C, Guardiola A, Shao R, Kawaguchi Y, Ito A, Nixon A, et al. HDAC6 is a microtubule-associated deacetylase. Nature. 2002 May 23;417(6887):455–458.

370. Portran D, Schaedel L, Xu Z, Théry M, Nachury MV. Tubulin acetylation protects long-lived microtubules against mechanical ageing. Nat Cell Biol. 2017 Apr;19(4):391–398.

371. Even A, Morelli G, Broix L, Scaramuzzino C, Turchetto S, Gladwyn-Ng I, et al. ATAT1-enriched vesicles promote microtubule acetylation via axonal transport. Sci Adv. 2019 Dec 18;5(12):eaax2705.

372. D Ydewalle C, Krishnan J, Chiheb DM, Van Damme P, Irobi J, Kozikowski AP, et al. HDAC6 inhibitors reverse axonal loss in a mouse model of mutant HSPB1-induced Charcot-Marie-Tooth disease. Nat Med. 2011 Jul 24;17(8):968–974.

373. Godena VK, Brookes-Hocking N, Moller A, Shaw G, Oswald M, Sancho RM, et al. Increasing microtubule acetylation rescues axonal transport and locomotor deficits caused by LRRK2 Roc-COR domain mutations. Nat Commun. 2014 Oct 15;5:5245.

374. Sharma S, Poetz F, Bruer M, Ly-Hartig TBN, Schott J, Séraphin B, et al. Acetylation-Dependent Control of Global Poly(A) RNA Degradation by CBP/p300 and HDAC1/2. Mol Cell. 2016 Sep 15;63(6):927–938.

375. Kovacs JJ, Murphy PJM, Gaillard S, Zhao X, Wu J-T, Nicchitta CV, et al. HDAC6 regulates Hsp90 acetylation and chaperone-dependent activation of glucocorticoid receptor. Mol Cell. 2005 May 27;18(5):601–607.

376. Kawaguchi Y, Kovacs JJ, McLaurin A, Vance JM, Ito A, Yao TP. The deacetylase HDAC6 regulates aggresome formation and cell viability in response to misfolded protein stress. Cell. 2003 Dec 12;115(6):727–738.

377. Lin S-Y, Li TY, Liu Q, Zhang C, Li X, Chen Y, et al. GSK3-TIP60-ULK1 signaling pathway links growth factor deprivation to autophagy. Science. 2012 Apr 27;336(6080):477–481.

378. Lee IH, Finkel T. Regulation of autophagy by the p300 acetyltransferase. J Biol Chem. 2009 Mar 6;284(10):6322–6328.

379. Oanh NTK, Park Y-Y, Cho H. Mitochondria elongation is mediated through SIRT1-mediated MFN1 stabilization. Cell Signal. 2017 Oct;38:67–75.

380. Inuzuka H, Gao D, Finley LWS, Yang W, Wan L, Fukushima H, et al. Acetylation-dependent regulation of Skp2 function. Cell. 2012 Jul 6;150(1):179–193.

381. Vikram A, Lewarchik CM, Yoon J-Y, Naqvi A, Kumar S, Morgan GM, et al. Sirtuin 1 regulates cardiac electrical activity by deacetylating the cardiac sodium channel. Nat Med. 2017 Mar;23(3):361–367.

382. Timmermann S, Lehrmann H, Polesskaya A, Harel-Bellan A. Histone acetylation and disease. Cell Mol Life Sci. 2001 May;58(5-6):728–736.

383. Iyer A, Fairlie DP, Brown L. Lysine acetylation in obesity, diabetes and metabolic disease. Immunol Cell Biol. 2012 Jan;90(1):39–46.

384. Peleg S, Feller C, Ladurner AG, Imhof A. The metabolic impact on histone acetylation and transcription in ageing. Trends Biochem Sci. 2016 Aug;41(8):700–711.

385. Sharma S, Sarathlal KC, Taliyan R. Epigenetics in neurodegenerative diseases: the role of histone deacetylases. CNS Neurol Disord Drug Targets. 2019;18(1):11–18.

386. Walker MP, LaFerla FM, Oddo SS, Brewer GJ. Reversible epigenetic histone modifications and Bdnf expression in neurons with aging and from a mouse model of Alzheimer's disease. Age (Omaha). 2013 Jun;35(3):519–531.

387. Cohen TJ, Guo JL, Hurtado DE, Kwong LK, Mills IP, Trojanowski JQ, et al. The acetylation of tau inhibits its function and promotes pathological tau aggregation. Nat Commun. 2011;2:252.

388. Gorsky MK, Burnouf S, Dols J, Mandelkow E, Partridge L. Acetylation mimic of lysine 280 exacerbates human Tau neurotoxicity in vivo. Sci Rep. 2016 Mar 4;6:22685.

389. Carlomagno Y, Chung D-EC, Yue M, Castanedes-Casey M, Madden BJ, Dunmore J, et al. An acetylation-phosphorylation switch that regulates tau aggregation propensity and function. J Biol Chem. 2017 Sep 15;292(37):15277–15286.

390. Rossaert E, Pollari E, Jaspers T, Van Helleputte L, Jarpe M, Van Damme P, et al. Restoration of histone acetylation ameliorates disease and metabolic abnormalities in a FUS mouse model. Acta Neuropathol Commun. 2019 Jul 5;7(1):107.

391. Elsässer SJ, Ernst RJ, Walker OS, Chin JW. Genetic code expansion in stable cell lines enables encoded chromatin modification. Nat Methods. 2016 Feb;13(2):158–164.

392. Bryson DI, Fan C, Guo L-T, Miller C, Söll D, Liu DR. Continuous directed evolution of aminoacyl-tRNA synthetases. Nat Chem Biol. 2017 Dec;13(12):1253–1260.

393. North BJ, Marshall BL, Borra MT, Denu JM, Verdin E. The human Sir2 ortholog, SIRT2, is an NAD+-dependent tubulin deacetylase. Mol Cell. 2003 Feb;11(2):437–444.

394. Reyon D, Tsai SQ, Khayter C, Foden JA, Sander JD, Joung JK. FLASH assembly of TALENs for high-throughput genome editing. Nat Biotechnol. 2012 May;30(5):460–465.

395. Emiliani S, Fischle W, Van Lint C, Al-Abed Y, Verdin E. Characterization of a human RPD3 ortholog, HDAC3. Proc Natl Acad Sci USA. 1998 Mar 17;95(6):2795–2800.

396. Fischle W, Emiliani S, Hendzel MJ, Nagase T, Nomura N, Voelter W, et al. A new family of human histone deacetylases related to Saccharomyces cerevisiae HDA1p. J Biol Chem. 1999 Apr 23;274(17):11713–11720.

397. Warnecke A, Sandalova T, Achour A, Harris RA. PyTMs: a useful PyMOL plugin for modeling common post-translational modifications. BMC Bioinformatics. 2014 Nov 28;15:370.

398. Ayala YM, Pantano S, D'Ambrogio A, Buratti E, Brindisi A, Marchetti C, et al. Human, Drosophila, and C.elegans TDP43: nucleic acid binding properties and splicing regulatory function. J Mol Biol. 2005 May 6;348(3):575–588.

399. Kamieniarz K, Schneider R. Tools to tackle protein acetylation. Chem Biol. 2009 Oct 30;16(10):1027–1029.

400. Haggarty SJ, Koeller KM, Wong JC, Grozinger CM, Schreiber SL. Domain-selective small-molecule inhibitor of histone deacetylase 6 (HDAC6)-mediated tubulin deacetylation. Proc Natl Acad Sci USA. 2003 Apr 15;100(8):4389–4394.

401. Schölz C, Weinert BT, Wagner SA, Beli P, Miyake Y, Qi J, et al. Acetylation site specificities of lysine deacetylase inhibitors in human cells. Nat Biotechnol. 2015 Apr;33(4):415–423.

402. Yau R, Rape M. The increasing complexity of the ubiquitin code. Nat Cell Biol. 2016 May 27;18(6):579–586.

403. Winton MJ, Igaz LM, Wong MM, Kwong LK, Trojanowski JQ, Lee VM-Y. Disturbance of nuclear and cytoplasmic TAR DNA-binding protein (TDP-43) induces disease-like redistribution, sequestration, and aggregate formation. J Biol Chem. 2008 May 9;283(19):13302–13309.

404. Mann JR, Gleixner AM, Mauna JC, Gomes E, DeChellis-Marks MR, Needham PG, et al. RNA Binding Antagonizes Neurotoxic Phase Transitions of TDP-43. Neuron. 2019 Apr 17;102(2):321–338.e8.

405. Gal J, Chen J, Katsumata Y, Fardo DW, Wang W-X, Artiushin S, et al. Detergent Insoluble Proteins and Inclusion Body-Like Structures Immunoreactive for PRKDC/DNA-PK/DNA-PKcs, FTL, NNT, and AIFM1 in the Amygdala of Cognitively Impaired Elderly Persons. J Neuropathol Exp Neurol. 2018 Jan 1;77(1):21–39.

406. Liao SE, Regev O. Splicing at the phase-separated nuclear speckle interface: a model. Nucleic Acids Res. 2021 Jan 25;49(2):636–645.

407. Alberti S, Gladfelter A, Mittag T. Considerations and Challenges in Studying Liquid-Liquid Phase Separation and Biomolecular Condensates. Cell. 2019 Jan 24;176(3):419–434.

408. Gomes E, Shorter J. The molecular language of membraneless organelles. J Biol Chem. 2019 May 3;294(18):7115–7127.

409. François-Moutal L, Perez-Miller S, Scott DD, Miranda VG, Mollasalehi N, Khanna M. Structural Insights Into TDP-43 and Effects of Post-translational Modifications. Front Mol Neurosci. 2019 Dec 17;12:301.

410. Hans F, Glasebach H, Kahle PJ. Multiple distinct pathways lead to hyperubiquitylated insoluble TDP-43 protein independent of its translocation into stress granules. J Biol Chem. 2020 Jan 17;295(3):673–689.

411. Gasset-Rosa F, Lu S, Yu H, Chen C, Melamed Z, Guo L, et al. Cytoplasmic TDP-43 De-mixing Independent of Stress Granules Drives Inhibition of Nuclear Import, Loss of Nuclear TDP-43, and Cell Death. Neuron. 2019 Apr 17;102(2):339–357.e7.

412. Nonaka T, Suzuki G, Tanaka Y, Kametani F, Hirai S, Okado H, et al. Phosphorylation of TAR DNA-binding Protein of 43 kDa (TDP-43) by Truncated Casein Kinase 1δ Triggers Mislocalization and Accumulation of TDP-43. J Biol Chem. 2016 Mar 11;291(11):5473–5483.

413. Jumper J, Evans R, Pritzel A, Green T, Figurnov M, Ronneberger O, et al. Highly accurate protein structure prediction with AlphaFold. Nature. 2021 Jul 15;

414. Maraschi A, Gumina V, Dragotto J, Colombrita C, Monpeán M, Buratti E, et al. SUMOylation Regulates TDP-43 Splicing Activity and Nucleocytoplasmic Distribution. Res Sq. 2021 Mar 24;

415. Elia AEH, Boardman AP, Wang DC, Huttlin EL, Everley RA, Dephoure N, et al. Quantitative proteomic atlas of ubiquitination and acetylation in the DNA damage response. Mol Cell. 2015 Sep 3;59(5):867–881.

416. Svinkina T, Gu H, Silva JC, Mertins P, Qiao J, Fereshetian S, et al. Deep, Quantitative Coverage of the Lysine Acetylome Using Novel Anti-acetyl-lysine Antibodies and an Optimized Proteomic Workflow. Mol Cell Proteomics. 2015 Sep;14(9):2429–2440.

417. Deng W, Wang C, Zhang Y, Xu Y, Zhang S, Liu Z, et al. GPS-PAIL: prediction of lysine acetyltransferase-specific modification sites from protein sequences. Sci Rep. 2016 Dec 22;6:39787.

418. Lee S, Kwon Y, Kim S, Jo M, Jeon Y-M, Cheon M, et al. The Role of HDAC6 in TDP-43-Induced Neurotoxicity and UPS Impairment. Front Cell Dev Biol. 2020 Nov 17;8:581942.

419. Fiesel FC, Schurr C, Weber SS, Kahle PJ. TDP-43 knockdown impairs neurite outgrowth dependent on its target histone deacetylase 6. Mol Neurodegener. 2011 Aug 30;6:64.

420. Fazal R, Boeynaems S, Swijsen A, De Decker M, Fumagalli L, Moisse M, et al. HDAC6 inhibition restores TDP-43 pathology and axonal transport defects in human motor neurons with TARDBP mutations. EMBO J. 2021 Oct 3;

421. Pulya S, Amin SA, Adhikari N, Biswas S, Jha T, Ghosh B. HDAC6 as privileged target in drug discovery: A perspective. Pharmacol Res. 2021 Jan;163:105274.

422. Boyault C, Sadoul K, Pabion M, Khochbin S. HDAC6, at the crossroads between cytoskeleton and cell signaling by acetylation and ubiquitination. Oncogene. 2007 Aug 13;26(37):5468–5476.

423. Hu J, Jing H, Lin H. Sirtuin inhibitors as anticancer agents. Future Med Chem. 2014 May;6(8):945–966.

424. Tang BL. Could sirtuin activities modify ALS onset and progression? Cell Mol Neurobiol. 2017 Oct;37(7):1147–1160.

425. McClure JJ, Li X, Chou CJ. Advances and challenges of HDAC inhibitors in cancer therapeutics. Adv Cancer Res. 2018 Mar 1;138:183–211.

426. Dietz KC, Casaccia P. HDAC inhibitors and neurodegeneration: at the edge between protection and damage. Pharmacol Res. 2010 Jul;62(1):11–17.

427. Haberland M, Montgomery RL, Olson EN. The many roles of histone deacetylases in development and physiology: implications for disease and therapy. Nat Rev Genet. 2009 Jan;10(1):32–42.

428. Onishi T, Maeda R, Terada M, Sato S, Fujii T, Ito M, et al. A novel orally active HDAC6 inhibitor T-518 shows a therapeutic potential for Alzheimer's disease and tauopathy in mice. Sci Rep. 2021 Jul 29;11(1):15423.

429. Nikić-Spiegel I. Expanding the genetic code for neuronal studies. Chembiochem. 2020 Nov 16;21(22):3169–3179.

430. Wang W, Takimoto JK, Louie GV, Baiga TJ, Noel JP, Lee K-F, et al. Genetically encoding unnatural amino acids for cellular and neuronal studies. Nat Neurosci. 2007 Aug;10(8):1063–1072.

431. Tseng J-H, Ajit A, Tabassum Z, Patel N, Tian X, Chen Y, et al. Tau seeds are subject to aberrant modifications resulting in distinct signatures. Cell Rep. 2021 Apr 27;35(4):109037.

432. Elsässer SJ. Generation of stable amber suppression cell lines. Methods Mol Biol. 2018;1728:237–245.

433. Stepanenko AA, Dmitrenko VV. HEK293 in cell biology and cancer research: phenotype, karyotype, tumorigenicity, and stress-induced genome-phenotype evolution. Gene. 2015 Sep 15;569(2):182–190.

434. Lin Y-C, Boone M, Meuris L, Lemmens I, Van Roy N, Soete A, et al. Genome dynamics of the human embryonic kidney 293 lineage in response to cell biology manipulations. Nat Commun. 2014 Sep 3;5:4767.

435. Hendriks IA, Lyon D, Young C, Jensen LJ, Vertegaal ACO, Nielsen ML. Site-specific mapping of the human SUMO proteome reveals co-modification with phosphorylation. Nat Struct Mol Biol. 2017 Mar;24(3):325–336.

436. Morato JG, Hans F, von Zweydorf F, Feederle R, Elsässer SJ, Skodras AA, et al. Lysine acetylation of TDP-43 drives phase separation and pathological aggregation. BioRxiv. 2020 May 26;

437. Tammsalu T, Matic I, Jaffray EG, Ibrahim AFM, Tatham MH, Hay RT. Proteome-wide identification of SUMO2 modification sites. Sci Signal. 2014 Apr 29;7(323):rs2.

438. Hendriks IA, D'Souza RCJ, Yang B, Verlaan-de Vries M, Mann M, Vertegaal ACO. Uncovering global SUMOylation signaling networks in a site-specific manner. Nat Struct Mol Biol. 2014 Oct;21(10):927–936.

439. Lamoliatte F, Caron D, Durette C, Mahrouche L, Maroui MA, Caron-Lizotte O, et al. Large-scale analysis of lysine SUMOylation by SUMO remnant immunoaffinity profiling. Nat Commun. 2014 Nov 13;5:5409.

440. Endo R, Takashima N, Nekooki-Machida Y, Komi Y, Hui KK-W, Takao M, et al. TAR DNA-Binding Protein 43 and Disrupted in Schizophrenia 1 Coaggregation Disrupts Dendritic

Local Translation and Mental Function in Frontotemporal Lobar Degeneration. Biol Psychiatry. 2018 Oct 1;84(7):509–521.

441. Liu-Yesucevitz L, Lin AY, Ebata A, Boon JY, Reid W, Xu Y-F, et al. ALS-linked mutations enlarge TDP-43-enriched neuronal RNA granules in the dendritic arbor. J Neurosci. 2014 Mar 19;34(12):4167–4174.

442. Dyer MS, Woodhouse A, Blizzard CA. Cytoplasmic Human TDP-43 Mislocalization Induces Widespread Dendritic Spine Loss in Mouse Upper Motor Neurons. Brain Sci. 2021 Jun 30;11(7).

443. Charif SE, Luchelli L, Vila A, Blaustein M, Igaz LM. Cytoplasmic Expression of the ALS/FTD-Related Protein TDP-43 Decreases Global Translation Both in vitro and in vivo. Front Cell Neurosci. 2020 Dec 8;14:594561.

444. Russo A, Scardigli R, La Regina F, Murray ME, Romano N, Dickson DW, et al. Increased cytoplasmic TDP-43 reduces global protein synthesis by interacting with RACK1 on polyribosomes. Hum Mol Genet. 2017 Apr 15;26(8):1407–1418.

445. Hergesheimer RC, Chami AA, de Assis DR, Vourc'h P, Andres CR, Corcia P, et al. The debated toxic role of aggregated TDP-43 in amyotrophic lateral sclerosis: a resolution in sight? Brain. 2019 May 1;142(5):1176–1194.

446. Sasaguri H, Chew J, Xu Y-F, Gendron TF, Garrett A, Lee CW, et al. The extreme N-terminus of TDP-43 mediates the cytoplasmic aggregation of TDP-43 and associated toxicity in vivo. Brain Res. 2016 Sep 15;1647:57–64.

447. Mitsumoto H, Santella RM, Liu X, Bogdanov M, Zipprich J, Wu H-C, et al. Oxidative stress biomarkers in sporadic ALS. Amyotroph Lateral Scler. 2008 Jun;9(3):177–183.

448. Yang C, Tan W, Whittle C, Qiu L, Cao L, Akbarian S, et al. The C-terminal TDP-43 fragments have a high aggregation propensity and harm neurons by a dominant-negative mechanism. PLoS One. 2010 Dec 31;5(12):e15878.

449. Aarum J, Cabrera CP, Jones TA, Rajendran S, Adiutori R, Giovannoni G, et al. Enzymatic degradation of RNA causes widespread protein aggregation in cell and tissue lysates. EMBO Rep. 2020 Oct 5;21(10):e49585.

450. Mann JR, Donnelly CJ. RNA modulates physiological and neuropathological protein phase transitions. Neuron. 2021 Jul 22;

451. Deryusheva S, Gall JG. Small Cajal body-specific RNAs of Drosophila function in the absence of Cajal bodies. Mol Biol Cell. 2009 Dec;20(24):5250–5259.

452. Ryan VH, Fawzi NL. Physiological, pathological, and targetable membraneless organelles in neurons. Trends Neurosci. 2019 Oct;42(10):693–708.

453. Wu C-C, Jin L-W, Wang I-F, Wei W-Y, Ho P-C, Liu Y-C, et al. HDAC1 dysregulation induces aberrant cell cycle and DNA damage in progress of TDP-43 proteinopathies. EMBO Mol Med. 2020 Jun 8;12(6):e10622.

454. Mo Z, Zhao X, Liu H, Hu Q, Chen X-Q, Pham J, et al. Aberrant GlyRS-HDAC6 interaction linked to axonal transport deficits in Charcot-Marie-Tooth neuropathy. Nat Commun. 2018 Mar 8;9(1):1007.

455. Yu Z, Fan D, Gui B, Shi L, Xuan C, Shan L, et al. Neurodegeneration-associated TDP-43 interacts with fragile X mental retardation protein (FMRP)/Staufen (STAU1) and regulates SIRT1 expression in neuronal cells. J Biol Chem. 2012 Jun 29;287(27):22560–22572.

456. Jiao F, Gong Z. The Beneficial Roles of SIRT1 in Neuroinflammation-Related Diseases. Oxid Med Cell Longev. 2020 Sep 14;2020:6782872.

457. Cashman NR, Durham HD, Blusztajn JK, Oda K, Tabira T, Shaw IT, et al. Neuroblastoma x spinal cord (NSC) hybrid cell lines resemble developing motor neurons. Dev Dyn. 1992 Jul;194(3):209–221.

458. Hawrot J, Imhof S, Wainger BJ. Modeling cell-autonomous motor neuron phenotypes in ALS using iPSCs. Neurobiol Dis. 2020 Feb;134:104680.

459. Maury Y, Côme J, Piskorowski RA, Salah-Mohellibi N, Chevaleyre V, Peschanski M, et al. Combinatorial analysis of developmental cues efficiently converts human pluripotent stem cells into multiple neuronal subtypes. Nat Biotechnol. 2015 Jan;33(1):89–96.

460. Fujimori K, Ishikawa M, Otomo A, Atsuta N, Nakamura R, Akiyama T, et al. Modeling sporadic ALS in iPSC-derived motor neurons identifies a potential therapeutic agent. Nat Med. 2018 Oct;24(10):1579–1589.

461. Imamura K, Izumi Y, Watanabe A, Tsukita K, Woltjen K, Yamamoto T, et al. The Src/c-Abl pathway is a potential therapeutic target in amyotrophic lateral sclerosis. Sci Transl Med. 2017 May 24;9(391).

462. Shi Y, Lin S, Staats KA, Li Y, Chang W-H, Hung S-T, et al. Haploinsufficiency leads to neurodegeneration in C9ORF72 ALS/FTD human induced motor neurons. Nat Med. 2018 Mar;24(3):313–325.

463. Egawa N, Kitaoka S, Tsukita K, Naitoh M, Takahashi K, Yamamoto T, et al. Drug screening for ALS using patient-specific induced pluripotent stem cells. Sci Transl Med. 2012 Aug 1;4(145):145ra104.

464. Kuhle J, Barro C, Andreasson U, Derfuss T, Lindberg R, Sandelius Å, et al. Comparison of three analytical platforms for quantification of the neurofilament light chain in blood samples: ELISA, electrochemiluminescence immunoassay and Simoa. Clin Chem Lab Med. 2016 Oct 1;54(10):1655–1661.

465. Disanto G, Barro C, Benkert P, Naegelin Y, Schädelin S, Giardiello A, et al. Serum Neurofilament light: A biomarker of neuronal damage in multiple sclerosis. Ann Neurol. 2017 Jun;81(6):857–870.

466. Sugimoto K, Han Y, Song Y, Gao Y. Correlational analysis of ALS progression and serum nfl measured by simoa assay in chinese patients. Front Neurol. 2020 Dec 3;11:579094.

467. Li D, Mielke MM. An Update on Blood-Based Markers of Alzheimer's Disease Using the SiMoA Platform. Neurol Ther. 2019 Dec 12;8(Suppl 2):73–82.

7.- Appendix

7. 1.- List of abbreviations

DTT	1,4-dithiothreitol
aa	Aminoacid
Ac. Tub	Acetylated (K40) Tubulin
Ac.K	Acetylated lysine
AcKRS	Acetylated lysine RNA synthetase
ALS	Amyotrophyc lateral sclerosis
APS	Ammoniun persulfate
ATP	Adenosine tri-phosphate
BCA	Bicinchoninic acid
BSA	Bovine Serum Albumin
bvFTD	Behavioural frontotemporal dementia
C. elegans	*Caenorhabditis elegans*
CBP	Cap binding protein
cDNA	Coding DNA
CFTR	Cystic fibrosis transmembrane conductance regulator
C-ter	Carboxil terminal
D. melanogaster	*Drosophila melanogaster*
DMEM	Dulbecco's modified Eagle medium
DMSO	Dimethyl sulfoxide
DPR	Dipeptide repeat
DSBR	Double strand break repair
EDTA	Ethylenediaminetetraacetic acid
EGFP	Enhanced green fluorescent protein
ER	Endoplasmatic reticulum
EWS	Ewing's sarcoma
FACS	Fluorescence assisted cell sorting
fALS	Familiar ALS
FBS	Fetal bovine serum
FFLL	F147L/F149L
FMRP	Fragile X mental retardation protein 1
FRAP	Fluorescence recovery after photobleaching
FTD	Frontotemporal dementia
FTLD	Frontotemporal lobar degeneration
FTLD -FET	Frontotemporal lobal degeneration with FET protein accumulation
FTLD-Tau	Frontotemporal lobar degeneration with Tau-positive inclusions
FTLD-TDP	Frontotemporal lobar degeneration with TDP-43-positive inclusions
FTLD-UPS	Frontotemporal lobal degeneration with ubiquitin/proteasomal markers accumulation
FUS	Fused in sarcoma
FUS/TLS	Human gene encoding FUS

GAPDH	Glyceraldehyde 3-phosphate dehydrogenase
GaRoS	Glycine-Aromatic-Serine-Rich domain
GEM	Gemini bodies
GRN	Granulin
Gt	Goat
GWAS	Genome wide association study
HEK	Human embryonic kidney
His	Histidine
hnRNP	Hetereogeneous nuclear ribonucleoprotein family
HRP	Horseradish peroxidase
IDRs	Intrinsically disordered regions
IF	Immunofluoresnce
iPSCs	Induced pluripotent stem cells
KAT	Lysine acetyl transferase
kDa	kilo Dalton
KDAC	Lysine deacetylase
LARKS	Low aromatic-rich structures
LB	Lysogeny Broth
LC-MS	Liquid chromatography mass spectrometry
LLPS	Liquid-liquid phase separation
MAPT	Microtubule associated protein tau
Mfn2	Mitofusin-2
miRNA	MicroRNA
MND	Motor neuron disease
mRNA	Messenger RNA
Ms	Mouse
mut	Mutated
NaArs	Sodium Arsenite
NES	Nuclear export signal
nfvPPA	Nonfluent progressive aphasia dementia
NGS	Normal Goat Serum
Ni-NTA	nickel-nitrilotriacetic acid
NLS	Nuclear localisation signal
NMR	Nuclear magnetic resonance
NP-40	Nonident P-40
OXPHOS	Oxidative phosphorylation
p	p-value
PAGE	Polyacrylamide gel electrophoresis
PAR	Poly ADP-ribosylation
PBD	Protein data bank identifier
P-bodies	Processing bodies
PBS	Phosphate saline buffer
PCR	Polymerase chain reaction
PDL	Poly-D-lysine
PEG	Plyethylene glycol
pERK	phosphorylated ERK
PODs	Product oncogene domains

Poly-GA	Poly-guanidine-adenosine
pTDP-43	Phosphorylated S409/410 TDP-43
PTMs	Posttranslational modifications
PVDF	Polyvinyllidene difluoride
QGSY	Glutamine -Glycine-Serine-Tyrosine domain
Rb	Rabbit
RBP	RNA-binding protein
RIPA	Radio immunoprecipitation assay
RISC	RNA-induced silencing complex
ROS	Reactive oxigen species
RRM	RNA recognition motif
rtPCR	Reverse transcription PCR
sALS	Sporadic ALS
SAP	Shrimp alkaline phosphatase
SDS	Sodium dodecyl sulphate
SG	Stress granules
sh^{TDP-43}	shRNA directed against TDP-43
sh^{TDP-43}-HEK293E	Stable KD TDP-43 HEK293E cells
SINE	Short interspersed nuclear elements
SMN	Survival of motor neuron protein
SOD1	Superoxide dismutase 1
Sp	Species
STS	Staurosporine
SUMO	Small Ubiquitin-like molecule
svPPA	Semantic progressive aphasia
TAF15	TATA-binding protein associated factor
TARDBP	Human gene encoding TDP-43
TBS	Tris buffered saline buffer
TEMED	N,N,N',N'-tetramethylethylendiamine
ThT	Thioflavin positive
tRNA	Transfer RNA
TSA	Trichostatin A
UBQLN	Ubiquilin
UTR	Untranslated region
UV	Ultraviolet
W.O.	Washout
WB	Western blot
Wt	Wild type
Δ	Deletion

7. 2.- List of figures

7. 3.- List of tables

Acknowledgements

First and foremost, I would like to thank Prof. Dr. Philipp J. Kahle for giving me the opportunity of joining as a PhD student to his group. Here I had the chance of researching a fascinating project and grow as a scientist more than I could imagine. I am very grateful for all the supervision and guidance during this project.

I thank Prof. Dr. Dirk Schwarzer from the Interfaculty Institute for Biochemistry in Tübingen for reading and give a second opinion about this work. In addition, thanks to Prof. Dr. Manuela Neumann from the Neuropathology Department at the University Tubingen for the help and guidance along the whole PhD and manuscript editing process.

I would like to thank Dr. Simon Elsässer from the Chemical and Synthetic Systems Biology laboratory at the Karolinska Institute in Stockholm for providing the materials and support regarding the amber suppression system. His contribution truly helped with the project and opened many research opportunities. Additionally, I would like to thank Prof. Dr. Christian Johannes Gloeckner from the Tubingen DZNE site who provided the seminal data for this work and who patiently explained the intricacies of Mass Spectrometry to me.

I want to thank all the past and present colleagues from the functional neurogenetics group who welcome me and guided me through my PhD, teaching me so much during all these years. I specially thank Dr. Friederike Hans and Dr. Sven Geisler for being patient with me and support me through my first PhD years, helping me to feel at home in this little swabian village. Additionally, I would like to thank Anna Lechado Terradas and Bernadette Dahl for enduring my internal debates about the pettiest purchases and for making the laboratory and the office a lively, fun place.

Por último, quiero dar las gracias a mis padres, sin los cuales nunca podría haber terminado este proyecto. Realmente son ellos los gigantes sobre cuyos hombros me apoyo.

Publications

At the time of submission, part of this work has been accepted for publication and the preliminary manuscript is available at Biorxiv.

Original manuscript

Sirtuin-1 Sensitive Lysine-136 Acetylation Drives Phase Separation and Pathological Aggregation of TDP-43. **Jorge Garcia Morato**, Friederike Hans, Felix von Zweydorf, Regina Feederle, Simon J. Elsässer, Angelos A. Skodras, Christian Johannes Gloeckner, Emanuele Buratti, Manuela Neumann, Philipp J. Kahle. *Nat Commun* **13,** 1223 (2022). https://doi.org/10.1038/s41467-022-28822-7

Statement of contributions

- J Garcia Morato contributed with the experimental design, performance and analysis of the data and wrote the manuscript.
- F Hans contributed with the experimental design, performed the original mass spectrometry analysis, supervised J Garcia Morato and edited the manuscript.
- F von Zewydorf and CJ Gloeckner performed the original mass spectrometry analysis and edited the manuscript.
- R Feederle immunised and tested the specific acK84 and acK136 TDP-43 antibodies.
- SJ Elsässer cloned, tested and provided the plasmids containing the amber suppression elements.
- AA Skodras provided technical support regarding FRAP experiments and analysis.
- E Buratti provided technical support regarding Filter binding assays.
- M Neumann provided technical support and edited the manuscript
- PJ Kahle supervised J Garcia Morato, conceived and coordinated the study and wrote the manuscript